Direct Oxidation of Benzene to Phenol:

Investigation of the active iron species in [Fe,Al]MFI catalysts by ^{57}Fe Mössbauer spectroscopy

The research described in this thesis was performed at the section Fundamental Aspects of Materials and Energy, Department of Radiation, Radionuclides and Reactors,[†] the section Biocatalysis and Organic Chemistry, Department of Biotechnology,[‡] and the section Catalysis Engineering, DelftChemTech,[‡] Faculty of Applied Sciences, Delft University of Technology

[†] *Mekelweg 15, 2629 JB Delft, The Netherlands*
[‡] *Julianalaan 136, 2628 BL Delft, The Netherlands*

Direct Oxidation of Benzene to Phenol:

Investigation of the active iron species in [Fe,Al]MFI catalysts by ^{57}Fe Mössbauer spectroscopy

PROEFSCHRIFT

ter verkrijging van de graad van doctor
aan de Technische Universiteit Delft,
op gezag van de Rector Magnificus prof. dr. ir. J. T. Fokkema,
voorzitter van het College voor Promoties,
in het openbaar te verdedigen
op maandag 6 november te 15:00 uur
door

Jerome Bolabola TABOADA

scheikundig ingenieur
geboren te Cebu City, Philippines

Dit proefschrift is goedgekeurd door de promotor:
Prof.dr. I.M. de Schepper

Toegevoegd promotor
Dr. I.W.C.E. Arends

Samenstelling promotiecommissie:

Rector Magnificus	Technische Universiteit Delft, voorzitter
Prof. dr. I.M. de Schepper	Technische Universiteit Delft, promotor
Dr. I.W.C.E. Arends	Technische Universiteit Delft, toegevoegd promotor
Prof. dr. F. Kapteijn	Technische Universiteit Delft
Prof. dr. R.A. Sheldon	Technische Universiteit Delft
Prof. dr. G.I. Panov	Boreskov Institute of Catalysis
Prof. dr. R.A. van Santen	Technische Universiteit Eindhoven
Dr. A.R. Overweg	Technische Universiteit Delft

Dr. G. Mul and most notably Dr. A.R. Overweg have provided substantial guidance and support in the preparation of this thesis.

ISBN 1-58603-691-2

Keywords: [Fe,Al]MFI zeolites, isomorphous substitution, steam-treatment, benzene to phenol, extra-framework iron species, ^{57}Fe Mössbauer spectroscopy.

Published and distributed by IOS Press under the imprint Delft University Press

Publisher
IOS Press
Nieuwe Hemweg 6b
1013 BG Amsterdam
The Netherlands
tel: +31-20-688 3355
fax: +31-20-687 0019
email: info@iospress.nl

For my wife Eve,
our daughter Venise, and son Nico

Contents

Chapter 1

General Introduction

Abstract

The opening chapter of this thesis is structured to give a general background in the direct oxidation of benzene to phenol, using nitrous oxide as oxidant (BTOP). [Fe,Al]MFI zeolite catalyst, which exhibits superior performance in terms of activity and selectivity in the BTOP reaction, is described. Furthermore, a literature overview of several propositions on the nature of the active sites in the [Fe,Al]MFI catalyst for the BTOP reaction is presented. However, recent investigations have shown strong indication that extra-framework iron species in the [Fe,Al]MFI catalyst are the catalytically active constituents in the BTOP reaction. These developments form the backbone of this study, which utilizes ^{57}Fe Mössbauer spectroscopy as the primary characterization technique to investigate the active iron species in the direct oxidation of benzene to phenol.

1.1. Background

Over the past decades, the development of catalytic oxidation processes has rapidly increased. The advancement in oxidation catalysis has been fueled by the development of efficient catalysts that has led to cleaner processes and has provided high product yields, high selectivity, and less energy requirements.[1,2] In fact, the contribution of oxidation catalysis in specialized catalysis journals has increased significantly over the last decade.[3] This indicates that oxidation catalysis is one of the most dynamic and productive fields in catalysis. However, despite the advancement, there are areas that still remain a challenge; such is the case concerning the direct oxidation of benzene to phenol.

Phenol, C_6H_5OH, is an aromatic alcohol. It is a colorless crystalline solid at room temperature, which exhibits weak acidic properties and is corrosive and poisonous. It is sometimes called carbolic acid, especially when in water solution and reacts with strong bases to form phenolates. Phenol is often used as a base compound in the chemical industry to produce intermediate chemicals for a wide range of applications such as plastics, pharmaceuticals and agricultural chemicals (*see figure 1.1 for typical examples*). About 6.5 million metric tons of phenol is produced worldwide annually,[4] and has been increasing over the years. The increase in demand, therefore, prompted the research towards a more efficient and economical production of phenol.

Figure 1.1. *Examples of products made from phenol derivatives. They are* [top left] *nylon-6 (fishing net) from caprolactam,* [top right] *surfactants and emulsifiers from alkylphenols,* [bottom right] *aspirin and other pharmaceuticals from salicylic acid, and* [bottom left] *polycarbonate plastics (CDs) from bisphenol A.*

At present, the most widely used industrial process for the synthesis of phenol is the multi-step cumene process.[5] This process is shown in figure 1.2, and includes the alkylation (using propylene) of benzene to cumene (*eqn.*1.1), followed by the oxidation of cumene to cumene hydroperoxide (*eqn.*1.2), and finally an acid-catalyzed cleavage of the cumene hydroperoxide to yield phenol and acetone (*eqn.*1.3).

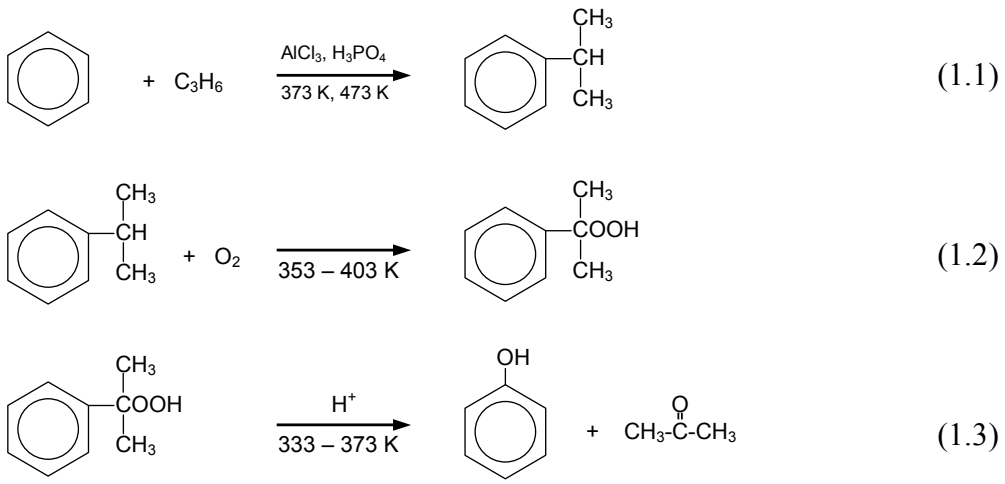

Figure 1.2. *Synthesis of phenol via the cumene process.*

However, in spite of its success, there are several disadvantages that are inherent to this process. First, the multi-step nature of this process entails that a high phenol yield is difficult to achieve. Second, this process involves the production of an explosive intermediate (i.e. cumene hydroperoxide) that presents a serious risk hazard to the industrial plant as well as to the environment. Third, and most notable, is the formation of the by-product acetone in a one to one molar ratio. Unlike phenol, acetone has a smaller market demand. Recycling acetone by converting it to propylene is possible but this would require additional complicated steps in the process, which makes it economically unattractive. Therefore, for obvious reasons, a direct oxidation of benzene to phenol that is acetone-free is highly desired.

1.2. Direct oxidation of benzene to phenol

1.2.1. Early attempts

In a published report by Marek and Hahn,[6] it was stated that the first attempt to oxidize benzene directly to phenol, by using molecular oxygen, can be traced back to 1865 even before the structure of benzene was known. Many attempts have been tried thereafter to oxidize benzene directly to phenol in the presence of molecular oxygen, both in gas and liquid phases, in low and high-pressure, with and without catalysts. Nevertheless, the results are still far from leading to practical developments.[3] Because it remains difficult to directly oxidize benzene to phenol using molecular oxygen, research in this field has since been

directed towards the use of *monooxygen* donors as alternative oxidants for the conversion of benzene to phenol. Among them are hydrogen peroxide, H_2O_2 (*eqn.*1.4),[7] nitric acid, HNO_3 (*eqn.*1.5),[8] salts and oxides of transition metals, e.g. Cu (*eqn.*1.6),[9] and even water (*eqn.*1.7).[10] Nevertheless, the benzene conversion as well as the selectivity towards phenol in these reactions are still relatively low.

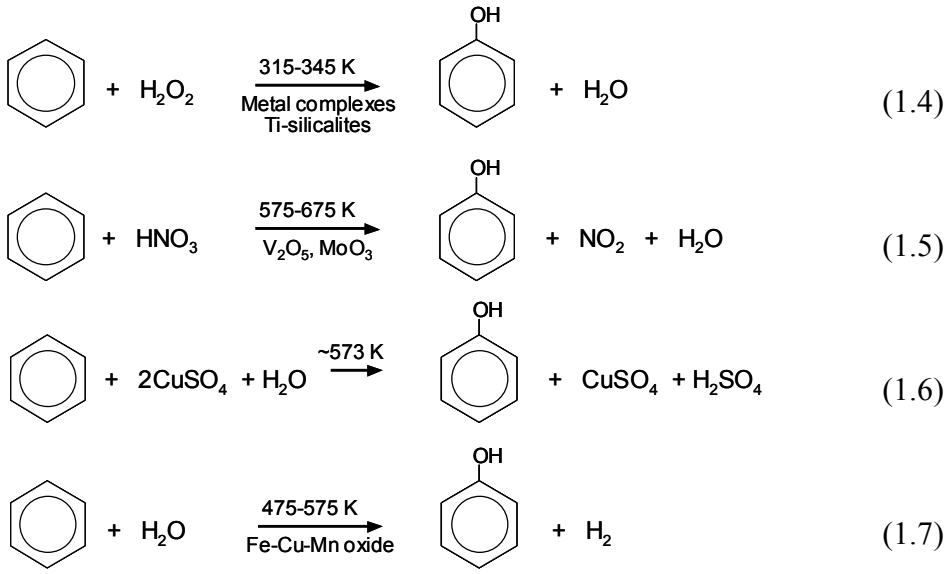

Figure 1.3. *Direct oxidation of benzene to phenol using monooxygen donors.*

1.2.2. Benzene oxidation to phenol with N_2O as oxidant

Progress in the direct oxidation of benzene to phenol took a significant step upon the discovery of using nitrous oxide as oxidant. Nitrous oxide, N_2O, is a colorless non-flammable gas, with a pleasant, slightly sweet odor. It is commonly known as *laughing gas* due to the exhilarating effects of inhaling it. Nowadays, N_2O is also used in surgery and dentistry for its anesthetic and analgesic effects. However, it was discovered only a couple of decades ago that N_2O is also a powerful greenhouse gas [11,12] when present in the atmosphere and has the potential to deplete the ozone layer.[13] Therefore, the consumption of N_2O as reagent for the oxidation of benzene to phenol is environmentally attractive since (i) the oxidation reaction decomposes N_2O and (ii) the BTOP reaction involving N_2O is very clean as the sole by-product is molecular nitrogen. This offers an attractive alternative especially to chemical industries that are producing highly concentrated N_2O, such as adipic acid plants.[14,15] In addition, N_2O has a wider range in terms of process safety compared to molecular oxygen.

The use of N_2O as oxidant for the direct oxidation of benzene to phenol was first reported in 1983 by Iwamoto *et al*.[16] Applying a V_2O_5/SiO_2 catalyst, temperatures as high as 823 K were necessary to carry out the BTOP reaction, obtaining about 11% benzene conversion with 45%

selectivity towards phenol. Although this reaction appears to be promising, the selectivity towards phenol proved to be too low to be translated into a commercial process. Nevertheless, this work stimulated further efforts in the development of new and effective catalytic systems for the BTOP reaction.

1.2.3. Discovery of MFI zeolite as BTOP catalyst

In 1988, it was discovered that MFI [‡] zeolites are excellent catalysts for the direct oxidation of benzene to phenol using nitrous oxide as oxidant.[17-19] Using this catalyst, BTOP reaction can be carried out at lower temperatures (575-675 K) compared to that using a V_2O_5/SiO_2 catalyst, and more importantly, the selectivity to phenol approaches 100%. Panov *et al*.,[20-28] have further developed this system and, over the last decade, have reported that iron containing ZSM-5, or [Fe,Al]MFI, zeolites exhibit excellent catalytic performance for the direct oxidation of benzene to phenol (*eqn.* 1.8), achieving high selectivity of over 95 %, in all cases. This reaction is not only superior to that using molecular oxygen as oxidant,[3] but is also far better in performance compared to other promising *monooxygen* donors and catalysts illustrated in figure 1.3.[29,30]

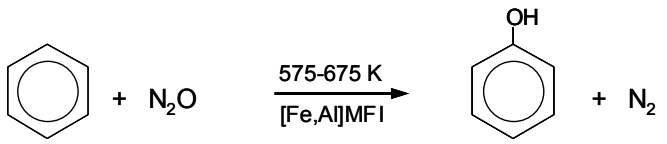

(1.8)

Figure 1.4. *Direct oxidation of benzene to phenol using N_2O as oxidant.*

However, despite extensive effort, the nature of the active site present in the [Fe,Al]MFI catalyst for the BTOP reaction is still largely unknown. In the following discussion, an overview of several proposals on the identity of the active site is presented. But in order to understand and elucidate the potential active site, it is essential to first describe the [Fe,Al]MFI zeolite.

1.3. [Fe,Al]MFI Zeolite

Zeolites belong to a class of minerals consisting of hydrated aluminosilicates. These minerals contain micropores, which provide an inherently large surface area. They are generally classified according to structural types. To date, there are 40 known natural zeolites and in excess of 140 synthetic zeolites;[31,32] among them is the MFI zeolite.

[‡] MFI is a code derived from Mobil Five.

MFI is a class of zeolites that are highly porous materials having an intersecting two-dimensional pore system throughout its structure created by the 10-membered oxygen-bridged rings (*see figure 1.5, lower right*). The MFI zeolite has two types of pores, both formed by 10-membered rings. The first of these pores is straight and slightly elliptical in cross section, while the second type of pores intersect the straight pores at right angles, in a zig-zag pattern and are circular in cross section (*see figure 1.5, upper left*). The channels have an average diameter of about 5.5 Å.[32] MFI zeolites are constructed of tetrahedral SiO_4 and AlO_4 structural units, normally with Si/Al ratio ≥ 10. Two special forms of MFI zeolites that have attained commercial significance are: (1) the high silica to alumina ratio of ZSM-5, and (2) the aluminum-free silicalite.

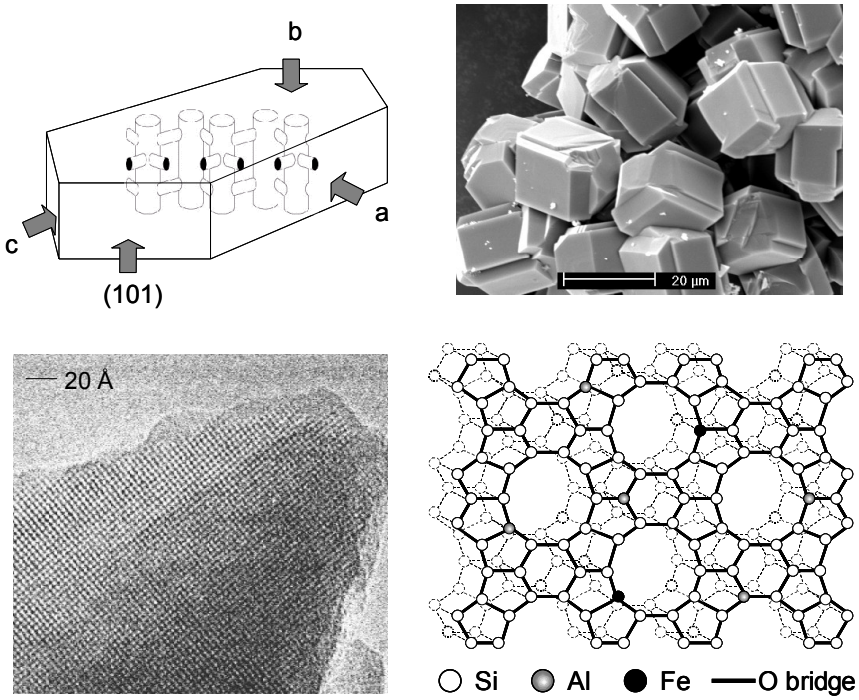

Figure 1.5. [top left] *representation of the* [Fe,Al]MFI *crystal illustrating the 2 channel types,* [top right] *a scanning electron micrograph showing a typical* MFI *crystal morphology,* [bottom right] *a scheme of the* [Fe,Al]MFI *structure viewed along* [010]*, and* [bottom left] *a transmission electron micrograph showing the channels created by the 10-membered oxygen-bridged rings.*

In this study, the initial state of the zeolite contains trivalent iron and aluminum ions that are incorporated in the framework of the MFI crystal. These materials are hereafter referred to as [Fe,Al]MFI zeolites. The incorporation of an aluminum ion and/or iron ion (charge 3^+) in the MFI framework by isomorphous substitution of a silicon ion (charge 4^+) entails that the zeolite lattice acquires a negative charge. To obtain electroneutrality, the excess negative charge is compensated by the presence of a dynamic cation, or by a bound proton as illustrated in figure 1.6. In the *as*-synthesized material, the original charge-compensating cation may come from the organic template [$(CH_3CH_2CH_2)_4N^+$] and/or alkaline metal

(e.g. Na^+). However, after the removal of the organic template by calcination, and its subsequent transformation into the H-form, the charge-compensating cation becomes the proton of the so-called bridging OH group.

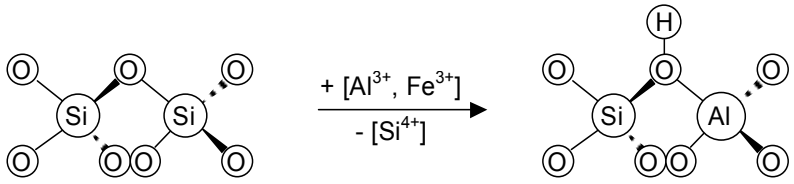

Figure 1.6. *Isomorphous substitution of silicon by aluminum and/or iron.*

Typically, the [Fe,Al]MFI zeolite is activated into a versatile catalyst through high-temperature calcination (up to 1175 K),[24] or by steam-treatment.[30] Apart from the selective oxidation of benzene to phenol using N_2O as oxidant, [Fe,Al]MFI zeolite has attracted increasing attention due to its ability to catalyse various reactions, such as the isomerization and oxidative dehydrogenation of alkanes,[33,34] the reduction of NO_x and N_2O with hydrocarbons (HC-SCR) or ammonia (NH_3-SCR),[35-42] direct N_2O decomposition,[43,44] and the selective oxidation of NH_3 to N_2 with O_2.[45]

1.4. Overview of the Proposed Active Sites

1.4.1. Brønsted acid sites

One of the pioneering works on the MFI catalysed oxidation of benzene to phenol, using N_2O as oxidant, was performed by Suzuki *et al*.[17] In that study, which used ZSM-5 (or [Al]MFI) zeolite as catalyst, Brønsted acid site was suggested to take part in the activation of the N_2O molecule. It was proposed,[17,46] that the N_2O molecule undergoes protonation on a Brønsted acid site to form hydroxy diazonium ion $(N{=}N{-}OH)^+$ that yields a hydroxyl cation $(OH)^+$, which reacts with the benzene molecule to form phenol.

The formation of Brønsted acid sites is traced from the presence of trivalent ions, in this case aluminum, in framework of the MFI lattice. As discussed above, the incorporation of a trivalent ion in the zeolite framework creates a negative charge. The presence of protons as charge-compensating cations therefore gives the MFI zeolite a high level of acidity. The amount of Brønsted acidity in the MFI zeolite can be quantified using a method based on the double adsorption of isopropylamine (IPA),[47] or derived from the infrared absorption band at 3610 cm^{-1}.[48-50] However, the proposal on Brønsted acid site being the catalytically active center for the oxidation of benzene to phenol with N_2O is largely debatable. For instance, infrared spectroscopic studies [24] do not support the hypothesis of Suzuki *et al*.[17]

1.4.2. Lewis acid sites

Another type of acidity in the MFI zeolite that is proposed by several authors [51-54] to be the catalytic center in the BTOP reaction is the Lewis acid site. By definition, Lewis acids are electron pair acceptors. In the case of ZSM-5 zeolites, the presence of extra-framework aluminum, which acts as an electron pair acceptor, creates the Lewis acid center. These sites are reported to form even upon the removal of the organic template in the zeolite during calcination, which could potentially create structural defects and thereby removing framework aluminum to extra-framework position.[51,55]

The effect of high extra-framework aluminum concentration created by thermal hydrolysis of the Al-O-Si bonds in the zeolite upon steam-treatment was studied by Motz *et al*.[52]. In that study, they claimed that the activity of ZSM-5 catalyst for the BTOP reaction is related to the harshness of the steaming conditions. These authors suggested that the effect of prolonged catalyst steam treatment increases the amount of extra-framework aluminum species and thus increases the catalytic activity of the ZSM-5 in the benzene to phenol conversion. Furthermore, under severe steam-treatment a reduction of catalyst activity was observed. They attributed this reduction to agglomeration of extra-framework aluminum species, thus reducing the amount of exposed Lewis acid sites.

Similar effects were also observed for the [Ga]MFI system, where extra-framework gallium was suggested to be the active site in the direct oxidation of benzene to phenol using N_2O as oxidant.[54] In general, the degree of post-synthesis treatments (i.e. high-temperature calcination and/or steam treatment) has been shown to affect the catalytic activity of the MFI zeolite in the BTOP reaction. However, up to date, there is still no concrete evidence that correlates the amount of Lewis acid sites to the BTOP activity.

1.4.3. Extra-framework iron species

Both propositions on Brønsted and Lewis acid sites as catalytic centers are based on the notion that the active centers in the Al or Ga MFI catalysts are acidic in nature. However, the presence of transition metal impurities, which are most often observed in ppm levels in commercial zeolites, can in principle form active *redox* centers. The presence of impurities can sometimes lead to unexpected results. For example, intensive studies on hydrocarbon transformations, such as alkylation, isomerization and cracking, with [B]MFI zeolites often yielded contradictory results. It was later realized that borosilicates by themselves are inactive in these reactions, and that the catalytic activity was attributed to the presence of aluminum impurities in ppm levels.[56]

For the BTOP reaction, Panov *et al*.[3,20-28] identified iron, which is present in practically all commercial MFI zeolites as an impurity at a level of a few hundred ppm (table 1.1), as the active *redox* constituent. They reported that 'pure' [Al] MFI (containing 20-30 ppm Fe) proved to be inactive,[27] while the presence of iron (as low as 300-500 ppm) in the MFI appeared to be adequate to obtain catalytically active materials.[20] Thus, the presence of iron impurity in commercial MFI zeolites at a few hundred ppm level could be sufficient to explain a high benzene to phenol reaction rate without assuming any catalytic activity of Al or Ga.

Table 1.1. Some commercial ZSM-5 (or [Al]MFI) zeolites and their Fe impurity

Commercial Sample	ppm Fe	Ref.
Degussa	210	57
Uetikon	530	55
Zeolyst International	250	15

Panov *et al*. [3,20-28] conditionally called the active iron centers for the conversion of benzene to phenol with N_2O as oxidant as *α-sites*. They suggested that the reaction mechanism involves the steps illustrated in figure 1.7. The key step in this reaction is the decomposition of nitrous oxide on an *α-site*, producing specific surface oxygen (*eqn.* 1.9), which in turn reacts with benzene (*eqn.* 1.10). Finally, desorption of the product phenol leaving a free active *α-site* completes the catalytic cycle (*eqn.* 1.11).

$$N_2O + (\ )_\alpha \rightarrow (O)_\alpha + N_2 \qquad (1.9)$$

$$C_6H_6 + (O)_\alpha \rightarrow (C_6H_5OH)_\alpha \qquad (1.10)$$

$$(C_6H_5OH)_\alpha \leftrightarrow C_6H_5OH + (\ )_\alpha \qquad (1.11)$$

Figure 1.7. *Benzene to phenol reaction mechanism involving α-sites.*

It has been proposed that *α-sites* are extra-framework iron species stabilized on the micropore channels of the MFI-type zeolite.[3] They are formed when iron is extracted from framework to extra-framework position during high temperature activation of [Fe,Al]MFI zeolites. This can be carried out by high-temperature calcination in air at 875-1125 K,[3,23] in vacuum at 1100-1175 K,[24] or by steam-treatment at 825-975 K.[24,27,30] Although there are other methods to introduce extra-framework iron species in the MFI zeolite,[58-60] such as post-synthesis impregnation with $FeCl_3$ followed by a high temperature treatment, recent developments have shown that steam-treatment of isomorphously substituted [Fe,Al]MFI zeolites provides outstanding properties conducive for the selective oxidation of benzene to phenol using N_2O as oxidant.[3,30]

According to a Mössbauer data, iron atoms forming the *α-sites* are in bivalent state having a special affinity to nitrous oxide.[21,22] The decomposition of N_2O over an *α-site* produces the so-called atomic *α*-oxygen (*eqn.* 1.9), which exhibits unique oxidation features. This particular oxygen species is considered important in playing a role in the direct catalytic oxidation of benzene to phenol by nitrous oxide. Many studies have been conducted [3,61] to describe the *α*-oxygen and even theoretical quantum-chemical calculations of this species were performed.[62,63] Nevertheless, the specificity of N_2O to form this active oxygen over an *α-site* is still a subject that is not clear at present. It should be noted that *α*-oxygen is not formed if molecular oxygen is used as oxidant. With N_2O, the benzene conversion reaches 27% and selectivity of 98% at 623 K, compared to 0.3% benzene conversion and no selectivity with molecular oxygen.[3]

1.5. On the Role of Iron and Aluminum on Catalyst Activity

The main propositions on the nature of the active sites for the catalytic oxidation of benzene to phenol using N_2O as oxidant have been the Brønsted acid sites, the Lewis acid sites, and the *redox* sites associated to extra-framework iron species. However, recent developments seem to have gravitated towards the notion that extra-framework iron species constitute the catalytically active centers, both in the N_2O decomposition and benzene to phenol reactions.[3,30,64-67] Although many important aspects of the active extra-framework iron species such as the structure and nuclearity are still unclear, recent studies employing Fe *K* edge HR-XANES and EXAFS,[68,69] and ESR,[70,71] have considered binuclear iron complexes as a probable structure of the active iron species. This is further substantiated by the presence of a high-spin Fe^{2+} component in the Mössbauer spectrum, which Panov *et al.*[21,22] have attributed to binuclear iron complexes similar to those present in the enzyme methane *monooxygenase* (MMO). For these enzymatic complexes, almost equal Mössbauer parameters have been obtained.[72] MMO is well known to activate molecular oxygen for incorporation into methane and other hydrocarbons.[73] Therefore, these zeolite samples have been ascribed to as having a bio-mimetic capability. However, it should be stressed that the active oxygen in the [Fe,Al]MFI catalyst originates from nitrous oxide and not from molecular oxygen. Oxygen treatment only leaves the catalyst unchanged. Therefore, it remains doubtful whether the structure of the active iron species for BTOP reaction is similar to that of MMO.

Likewise, isolated extra-framework iron ions have also been proposed to be capable of forming the active oxygen from N_2O.[74,75] [Fe,Al]MFI catalysts containing highly dispersed extra-framework iron ions has been shown to be more active in mediating the transfer of

atomic oxygen to CO or C_3H_8 at lower temperature than in the case when iron clusters are more dominant.[76] The formation of a particular form of extra-framework iron species has been reported to be strongly influenced by the activation condition.[77] Thus, in principle the formation of a preferred iron site can be modulated for instance by tuning the steaming temperature during activation.

However, there is still no agreement in literature that extra-framework iron species is solely responsible for the BTOP activity. Admixtures of Brønsted acid sites,[15] or extra-framework aluminum,[78,79] together with extra-framework iron species have also been proposed. Particularly since [Fe,Al]MFI and [Fe,Ga]MFI have often yielded superior performance in the direct oxidation of benzene to phenol compared to [Fe,B]MFI and silicalites.[20] Because of this, the study presented here aims to elucidate the roles of iron and aluminum in the [Fe,Al]MFI catalyst, and their importance in the BTOP reaction.

1.6. Rationale of the study

As presented in sections 1.4 and 1.5, much of the fundamental aspects, i.e. the nature, identity, locality, and nuclearity, of the active site for the direct oxidation of benzene to phenol using N_2O as oxidant, are still largely unknown. Much of these uncertainties stem from diversities in preparation method, activation conditions, elemental composition, and activity of the [Fe,Al]MFI catalyst, leading to various interpretations. Nevertheless, there seems to be a consensus regarding the role of iron and to some extent aluminum (at least not excluded explicitly) in the formation of the active species. A better understanding of the structure-activity relationship is essential for catalyst development, leading to a more economical route in preparing efficient and highly selective catalysts. This leaves great potential for improvement in the oxidation catalysis in general.

Although extra-framework iron species appear to be the leading candidate as the primary constituent of the active site, finding a common relationship from various interpretations is still extremely complicated due to the intrinsic heterogeneous nature of the iron species formed in the zeolite.[80,81] Therefore it is crucial to have a consistent basis for comparative analysis of the catalytic activity as a function of iron and aluminum content. This can be achieved by: (i) carrying out a systematic variation of the iron and aluminum concentrations in the [Fe,Al]MFI zeolite, synthesized *via* hydrothermal treatment; (ii) activating the zeolite samples under the same conditions; and (iii) performing benzene to phenol activity measurements as a function of iron and aluminum concentrations.

Working according to these requirements, this study investigates the structure-activity relationship of the [Fe,Al]MFI catalyst in the BTOP reaction. To characterize the various iron species in the [Fe,Al]MFI zeolite catalyst, ^{57}Fe Mössbauer spectroscopy – which is available in house – will be used as the primary technique to (i) obtain a better understanding on the evolution of iron from framework to extra-framework position during zeolite activation, (ii) elucidate the various iron species after steam-treatment, and (iii) identify the active iron species, through *in-situ* studies, under oxidizing and reducing environments.

1.7. Interest in Mössbauer spectroscopy

^{57}Fe Mössbauer spectroscopy is an ideal method to characterize iron-containing solids, such as the various iron species present in the steam-treated [Fe,Al]MFI catalysts. Unlike electron paramagnetic resonance (EPR), there is no form of iron that is Mössbauer-silent. Moreover, the observed spectrum is the sum of different sub-spectra corresponding to iron in different environments, thus providing richer information compared to bulk-averaging techniques such as magnetic susceptibility.

One of the many advantages that ^{57}Fe Mössbauer spectroscopy offers, particularly to iron-containing zeolites, is the ability to discriminate between framework iron (i.e. isomorphously substituted Fe^{3+} ions in the zeolite lattice) and extra-framework iron (i.e. Fe^{3+} ions in cationic position, or Fe^{3+} ions in oxidic compounds precipitated on the zeolite surface, such as iron oxide clusters).[82,83] Furthermore, ^{57}Fe Mössbauer spectroscopy provides information regarding the oxidation and coordination states of various iron species in the zeolite,[84] and distinguishes different iron species present through relaxation behavior (*see chapter 2*). This is important in evaluating the reactivity of different forms of iron species – for instance, isolated iron ions and oligonuclear iron clusters – in the direct oxidation of benzene to phenol, using N_2O as oxidant, through *in-situ* studies.

1.8. Contents of the thesis

A general background of the subject in the direct oxidation of benzene to phenol, using N_2O as oxidant, has been presented in this chapter. In the following chapter, the basic concept of ^{57}Fe Mössbauer spectroscopy is discussed. The information given in chapter 2 is important to readers (non-experts), particularly since ^{57}Fe Mössbauer spectroscopy is not a common technique in catalyst characterization, to follow and understand the interpretation of the ^{57}Fe Mössbauer spectra presented throughout this thesis.

In this study, the concentration of iron introduced during hydrothermal synthesis of isomorphously substituted [Fe,Al]MFI zeolites is very low (i.e. 0.075 – 0.6 wt.% Fe). Therefore, to enhance the Mössbauer effect, all samples were enriched with ^{57}Fe isotope, since normal iron contains only 2% of the ^{57}Fe Mössbauer isotope. This implies a slight modification in the preparation of the solution gel, i.e. starting from ^{57}Fe foil instead of the usual iron salts, for the hydrothermal synthesis. The *as*-synthesized zeolites were characterized by inductively coupled plasma optical emission spectroscopy (ICP-OES) for elemental analysis, high-resolution x-ray diffraction (HR-XRD), scanning electron microscopy (SEM), and ^{57}Fe Mössbauer spectroscopy. The representative results of this novel synthesis route are presented in chapter 3.

To gain better understanding particularly on the role of iron and aluminum in the formation of various iron species, the evolution of iron from framework ions to extra-framework species during zeolite activation was studied by ^{57}Fe Mössbauer spectroscopy and transmission electron microscopy (TEM). Results of this study are presented in chapter 4. The *redox* properties as deduced from Fe *K* edge XANES (x-ray absorption near edge spectroscopy) and ^{57}Fe Mössbauer spectroscopy of different steam-treated [Fe,Al]MFI zeolite catalysts are evaluated in chapter 5. Their corresponding activities in both N_2O decomposition and in the direct oxidation of benzene to phenol as a function of iron and aluminium concentrations are discussed in chapter 6.

The important *in-situ* ^{57}Fe Mössbauer spectroscopy results are presented in chapter 7. In this chapter, various active iron species are proposed based on the observed reactivity of the different iron species under oxidizing and reducing environments at different temperatures.

Finally, from these data, the author's thoughts concerning the direction of the study in this field will serve as a concluding chapter of this highly provocative and much debated area in oxidation catalysis. This is followed by a summary of the important aspects achieved in this scientific study on the direct oxidation of benzene to phenol using N_2O as oxidant.

REFERENCES

1. F. Cavani and F. Trifirò, *Catal. Today*, 34 (1997) 269.
2. R.A. Sheldon and J. Dakka, *Catal. Today*, 19 (1994) 215.
3. G.I. Panov, *Cattech*, 4 (2000) 18.
4. http://www.greener-industry.org/pages/phenol/1PhenolAnnualProd.htm
5. A.M. Brownstain, *Chemtech*, Sept. (1994) 58.

6. L.F. Marek and D.A. Hahn, *The Catalytic Oxidation of Organic Compounds in the Vapour Phase*, The Chemical Catalog Company Inc., N.Y., 1932.
7. B. Notari, *Adv. in Catal.*, 41 (1996) 253.
8. F. Matsuda and K. Kato, *Jpn. Kokai Tokkyo Koho* JP 62 67, 038 (Chem. Abstract, 107 (1987) No. 17, p. 674, No. 154068t).
9. M. Mori, T. Nakai, H. Jahiro, M. Nata, K. Sasaki, *Bull. Chem. Soc. Jpn*, 68 (1995) 1747.
10. Shengchun Cao *et al.*, *Chin. J. Petrochem. Tech*., 10 (1995) 708 [Chem. Abstracts, 123 (1995)].
11. L. Donner, V. Rantanen, *J. Atmos. Sci.*, 37 (1980) 119.
12. V. Ramanathan, R.J. Cicerone, H.H. Singh, J.T. Kiel, *J. Geophys. Res.*, 90 (1985) 5547.
13. J.T. Houghton, B.A. Callander, S.K. Verney (Eds.), *Climate Change 1992: The Supplementary Report to the IPCC Scientific Assessment*, IPCC, Cambridge, 1992.
14. A.K. Uriarte, M.A. Rodkin, M.J. Gross, A.S. Kharitonov, G.I. Panov, *Stud. Surf. Sci. Catal.*, 110 (1997) 857.
15. P.P. Notte, *Top. Catal.*, 13 (2000) 387.
16. M. Iwamoto, K. Matsukami, S. Kagawa, *J. Phys. Chem*., 87 (1983) 903.
17. E. Suzuki, K. Makashiro, and Y. Ono, *Chem. Soc. Jap. Chem. Commun.*, (1988) 953.
18. M.H. Gubelmann and P.J. Tirel, Fr. Pat.2.630.735 (1988).
19. A.S. Kharitonov, T.N. Alexandrova, L.A. Vostrikova, K.G. Ione, and G.I. Panov, Russ. Patent 4.445.646, (1988).
20. L.V. Pirutko, V.S. Chernyavsky, A.K. Uriarte, and G.I. Panov, *Appl. Catal. A,* 227 (2002) 143.
21. K.A. Dubkov, N.S. Ovanesyan, A.A. Shteinman, E.V. Starokon, and G.I. Panov, *J. Catal.*, 207 (2002) 341.
22. N.S. Ovanesyan, A.A. Shteinman, V.I. Sobolev, K.A. Dubkov, and G.I. Panov, *Kinet. Katal.*, 39 (1998) 863.
23. G.I. Panov, A.K. Uriarte, M.A. Rodkin, and V.I. Sobolev, *Catal. Today*, 41 (1998) 365.
24. V.I. Sobolev, K.A. Dubkov, E.A. Paukshtis, L.V. Pirutko, M.A. Rodkin, A.S. Kharitonov, and G.I. Panov, *Appl. Catal. A*, 141 (1996) 185.
25. G.I. Panov, A.S. Kharitonov, and V.I. Sobolev, *Appl. Catal. A*, 98 (1993) 1.
26. G.I. Panov, A.S. Kharitonov, and V.I. Sobolev, *Appl. Catal. A*, 98 (1993) 117.
27. G.I. Panov, G.A. Sheveleva, A.S. Kharitonov, V.N. Romannikov, and L.A. Vostrikova, *Appl. Catal. A*, 82 (1992) 31.
28. G.I. Panov, V.I. Sobolev, and A.S. Kharitonov, *J. Mol. Catal.*, 61, 85 (1990).
29. J. Pérez-Ramírez, *Catalyzed N_2O Activation: Promising (New) Catalysts for Abatement and Utilization*, Ph.D. Thesis, Delft University of Technology, The Netherlands, 2002.
30. A. Ribera, I.W.C.E. Arends, S. de Vries, J. Pérez-Ramírez, and R.A. Sheldon, *J. Catal.*, 195 (2000) 287.

31. R. Szostak, *Molecular sieves; principles of synthesis and identification, 2nd Ed.*, London : Blackie, 1998.
32. http://topaz.ethz.ch/IZA-SC/StdAtlas.htm
33. P.B. Venuto, *Microporous Mesoporous Mater*., 2 (1994) 297.
34. Md. Uddin, T. Komatsu, and T. Kashima, *J. Catal*., 150 (1994) 439.
35. X. Feng and W.K. Hall, *Catal. Lett.*, 41 (1996) 45.
36. H-Y. Chen and W.M.H. Sachtler, *Catal. Today*, 42 (1998) 73.
37. A.Z. Ma and W. Grünert, *Chem. Commun*., 71 (1999).
38. R.Q. Long and R.T. Yang, *J. Catal.*, 188 (1999) 332.
39. M. Kögel, R. Mönnig, W. Schwieger, A. Tissler, and T. Turek, *J. Catal.*, 182 (1999) 470.
40. C. Pophal, T. Yogo, K. Yamada, and K. Segawa, *Appl. Catal. B*, 16 (1998) 177.
41. G. Centi, F. Vazanna, *Catal. Today*, 53 (1999) 683.
42. M. Mauvezin, G. Delahay, F. Kiβlich, B. Coq, and S. Kieger, *Catal. Lett*., 62 (1999) 41.
43. F. Kapteijn, G. Márban, J. Rodríguez-Mirasol, and J.A. Moulijn, *J. Catal.*, 167 (1997) 256.
44. E.M. El-Malki, R.A. van Santen, and W.M.H. Sachtler, *J. Catal.*, 196 (2000) 212.
45. R.Q. Long and R.T. Yang, *Chem. Commun.*, 1651 (2000).
46. P.J. Tirel, M.H. Gubelmann, and J.M. Popa, *Extended abstracts of the 9th International Zeolite Conference*, J.B. Higgins, R. von Ballmoos and M.M.J. Treacy (Eds.), Montreal, July 5-10, 1992, p. 61.
47. R.J. Gorte, *Catal. Lett.*, 62 (1999) 1.
48. J.C. Vedrine, A. Auroux, V. Bolis, P. Bejaifve, C. Naccache, P. Wierchowski, E.G. Deroune, J.B. Nagy, J.P. Gilson, J.H.C. van Hooff, J.P. van der Berg , and J. Wolthuizen, *J. Catal.*, 59 (1979) 248.
49. J. Datka and Z. Piwowarska, *Zeolites*, 8 (1988) 30.
50. Y.A. Paukshtis, *Infrared Spectroscopy in Heterogeneous Acid-Base Catalysis*, Nauka Publishers, Novosibirsk, (1992).
51. V.L. Zholobenko, I.N. Senchenya, L.M. Kustov, and V.B. Kanzansky, *Kinet. Katal.*, 32 (1991) 132.
52. J.L. Motz, H. Heinichen, and W.F. Hölderich, *Stud. Surf. Sci. Catal.*, 105 (1997) 1053.
53. V.I. Bogdan, L.M. Kustov, D.B. Batizat, A.M. Sakharov, V.B. Kazansky, *Stud. Surf. Sci. Catal.*, 94 (1995) 635.
54. M. Häfele, A. Reitzmann, D. Roppelt, G. Emig, *Appl. Catal. A*, 150 (1997) 153.
55. V. Zholobenko, *Mendeleev Commun.*, 28 (1993).
56. C.T.-W. Chu, G.H. Kuehl, R.M. Lago, C.D. Chang, *J. Catal.*, 93 (1985) 451.
57. J.L. Motz, H. Heinichen, and W.F. Hölderich, *J. Mol. Catal. A*: *Chem*., 136 (1998) 175.
58. X. Feng, W.K. Hall, *J. Catal.*, 166 (1997) 368.

59. C. Plog, F. Schueth, V. Goeman, R. Andorf, *Preparation of a Fe- or Mn-exchanged zeolite*, EP 0867406, 1998.
60. M. Kögel, V.H. Sandoval, W. Schwieger, A. Tissler, T. Turek, *Catal. Lett.,* 51 (1998) 23.
61. K. Lazar, A.N. Kotasthane, and R. Fejes, *Catal. Lett.*, 57 (1999) 171.
62. M.J. Filatov, A.G. Pelmenschikov, and G.M. Zhidomirov, *J. Mol. Catal.*, 8 (1993) 243.
63. K. Yoshizawa, Y. Shiota, T. Yumura, and T. Yamabe, *J. Phys. Chem. B*, 104 (2000) 734.
64. Q. Zhu, R.M. van Teeffelen, R.A. van Santen, E.J.M. Hensen, *J. Catal.*, 221 (2004) 575.
65. E.J.M. Hensen, Q. Zhu, M.M.R.M. Hendrix, A.R. Overweg, P.J. Kooyman, M.V. Sychev, R.A. van Santen, *J. Catal.*, 221 (2004) 560.
66. E.J.M. Hensen, Q. Zhu, R.A. van Santen, *J. Catal.*, 220 (2003) 260.
67. G. Berlier, G. Spoto, S. Bordiga, G. Ricchiardi, P. Fisicaro, A. Zecchina, I. Rossetti, E. Selli, L. Forni, E. Giamello, C. Lamberti, *J. Catal.*, 208 (2002) 169.
68. A.A. Battiston, J.H. Bitter, D.C. Koningsberger, *J. Catal.*, 218 (2003) 163.
69. A.A. Battiston, J.H. Bitter, W.M. Heijboer, F.M.F. de Groot, D.C. Koningsberger, *J. Catal.*, 215 (2003) 279.
70. P. Fejes, J.B. Nagy, K. Lazar, and J. Halasz, *Appl. Catal. A*, 190 (2000) 117.
71. E.M. El-Malki, R.A. van Santen, and W.M.H. Sachtler, *J. Phys. Chem. B*, 103 (1999) 4611.
72. J.G. DeWitt, J.G. Bentsen, A.C. Rosenzweig, B. Hedman, J. Green, S. Pilkington, G.C. Papaeftymiou, H. Datlton, K.O. Hodgson, S.J. Lippard, *J. Am. Chem. Soc.*, 113 (1991) 9219.
73. B.G. Fox, J.G. Borneman, L.P. Wackett, and J.D. Lipscomb, *Biochemistry*, 29 (1990) 6419.
74. P.K. Roy and G.D. Pirngruber, *J. Catal.*, 227 (2004) 164.
75. J.A. Ryder, A.K. Chakraborty, and A.T. Bell, *J. Catal.*, 220 (2003) 84.
76. J. Pérez-Ramírez, F. Kapteijn, and A. Brückner, *J. Catal.*, 218 (2003) 234.
77. J. Pérez-Ramírez, *J. Catal.*, 227 (2004) 512.
78. E.J.M. Hensen, Q. Zhu, R.A.J. Janssen, P.C.M.M. Magusin, P.J. Kooyman, and R.A. van Santen, *J. Catal.*, 233 (2005) 123.
79. E.J.M. Hensen, Q. Zhu, R.A. van Santen, *J. Catal.*, 233 (2005) 136.
80. J. Pérez-Ramírez, G. Mul, F. Kapteijn, J.A. Moulijn, A.R. Overweg, A. Doménech, A. Ribera, I.W.C.E. Arends, *J. Catal.*, 207 (2002) 113.
81. J. Pérez-Ramírez, F. Kapteijn, J.C. Groen, A. Doménech, G. Mul, and J.A. Moulijn, *J. Catal.*, 214 (2003) 33.
82. A. Meager, V. Nair, and R. Szostak, *Zeolites*, 8 (1988) 3.
83. G. Calis and P. Frenken, *Zeolites*, 7 (1987) 319.
84. N.N. Greenwood and T.C. Gibb, *Mössbauer Spectroscopy*, Chapman and Hall Ltd., London, 1971, chap. 3.

Chapter 2

^{57}Fe Mössbauer Spectroscopy: General Concept

Abstract

This chapter is devoted to the general concept of ^{57}Fe Mössbauer spectroscopy. It starts from the basic theory of the Mössbauer effect and how this nuclear resonance technique is used to extract chemical information and physical properties of a particular sample. In addition, as the bulk of the investigation contained in this thesis deals with iron ions, which show magnetic behavior, focus will be given to the relaxation phenomena and the concept of paramagnetic hyperfine splitting and superparamagnetism observed in ^{57}Fe Mössbauer spectroscopy.

2.1. Introduction

Mössbauer spectroscopy is a local technique that provides detailed information on the chemical, structural, and magnetic properties of a material. This nuclear resonance technique is based on the recoil-free emission and absorption of gamma (γ) radiation in solids.[1] This is referred to as the 'Mössbauer effect' after its discoverer Rudolf L. Mössbauer, who first observed the effect in 1957. For this work, he was awarded with the Nobel Price in physics in 1961. Nowadays, Mössbauer spectroscopy is widely used to provide information in various disciplines of science such as physics, chemistry, biology, metallurgy, geology, and catalysis to name a few.

A unique feature of this technique is that the effect is isotope specific, as resonance only occurs when the transition energy of the emitting and absorbing nucleus are identical. A total of 46 different elements have been identified in which the Mössbauer effect has been detected. Fifteen of these elements have known isotopes that are widely used in Mössbauer spectroscopy (*see figure 2.1.*). An isotope needs to meet two requirements in order to be suitable for Mössbauer spectroscopy. First, the number of recoil-free events should be high. Since the number of recoil-free events is strongly dependent upon the gamma-ray energy, the Mössbauer effect is only detected in isotopes with very low lying excited states. Second, the isotope should have a relatively long-lived excited state, as the resolution is dependent on the lifetime of the excited state. Because of these factors, the number of isotopes in which the Mössbauer effect can be detected is limited.

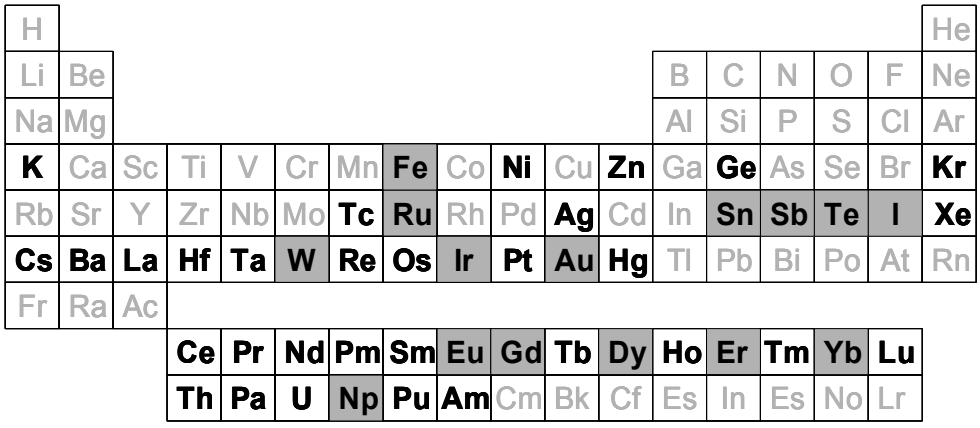

Figure 2.1. *The periodic table highlighting the known Mössbauer isotopes (shown in bold font) and those that are used most (in shaded background).*

Among all known Mössbauer isotopes, ^{57}Fe has an almost ideal combination of physical properties for Mössbauer spectroscopy, i.e. possessing very low energy γ-ray and a long-lived

excited state. In fact, 75% of all papers on experimental Mössbauer spectroscopy deal with the first excited state decay of ^{57}Fe.[2]

In this chapter, the general concept of ^{57}Fe Mössbauer spectroscopy is presented and divided into 3 sections. The first section deals with the fundamental background of ^{57}Fe Mössbauer spectroscopy. The second section introduces the hyperfine interactions, and the last section deals with the theory behind relaxation phenomena, and discusses paramagnetic hyperfine splitting and superparamagnetism. For more detailed information and discussion on ^{57}Fe Mössbauer spectroscopy and the applications of the Mössbauer effect, the books by Greenwood and Gibb,[2] and Wertheim,[3] are recommended.

2.2. ^{57}Fe Mössbauer spectroscopy: basic concept

2.2.1. γ-ray transition

^{57}Fe Mössbauer spectroscopy refers to the resonant and recoil-free emission and absorption of the 14.4 keV γ-ray transition in the nucleus of the ^{57}Fe isotope. The 14.4 keV gamma ray is produced with 91% efficiency from the decay of a radioactive ^{57}Co source *via* electron capture to the ground state of the ^{57}Fe isotope according to the scheme illustrated in figure 2.2. The ^{57}Co source has a half-life of 270 days, which makes ^{57}Fe ideal for Mössbauer spectroscopy compared to other Mössbauer isotopes. In addition, ^{57}Fe has a relatively long-lived exited state, as mentioned earlier, with a half-life of about 99 ns. The absorption of 14.4 keV γ-ray energy by a sample containing ^{57}Fe allows a transition to occur from the ground state with a nuclear spin quantum number I = ½ to the first excited state of ^{57}Fe of spin I = 3/2.

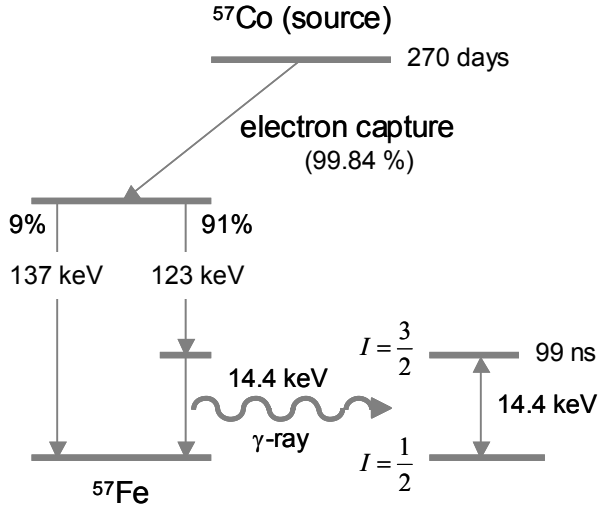

Figure 2.2. *The γ-decay scheme of ^{57}Co and the 14.4 keV transition used in ^{57}Fe Mössbauer Spectroscopy.*

The energy levels of the ground state and the first excited state are influenced by the surrounding environment of the nuclei, both electronic and magnetic, which can split or, in other words, remove the degeneracy of the energy levels. Therefore, the changes in energy levels provide information on the chemical and physical properties of an investigated sample. However, in order to obtain this information, there are two conditions that need to be fulfilled. First, a recoil-free event during emission and absorption of the gamma ray must be achieved in order to obtain resonance. Second, the energy resolution must be extremely high since the hyperfine interactions between the nucleus and its environment are extremely small.

2.2.2. Recoil-free event

During emission of a gamma ray, the nucleus of a free atom recoils. This is analogous to firing a bullet, where a gun experiences a counter force called recoil. Conservation of energy requires that the emitted γ-ray energy (E_γ) is equal to the energy of the nuclear transition (E_0), which is broadened by the Doppler effect (E_D) resulting from the translational thermal motion of the nucleus, minus the recoil energy (E_R). Thus, $E_\gamma = E_0 + E_D - E_R$. Likewise, for the absorbing process, the gamma ray must have the energy necessary to excite and overcome the effect of recoil in the absorbing nucleus. In this case, a photon energy of $E_\gamma = E_0 + E_D + E_R$ is required. The recoil energy is described by the equation:

$$E_R = \frac{E_\gamma^{\,2}}{2Mc^2} \tag{2.1}$$

where M is the mass of the emitting or absorbing body, and c is the speed of light. For a free ^{57}Fe atom, the mass is small, resulting in large recoil energy of about $2 \cdot 10^{-3}$ eV. This is much larger than the typical natural linewidth of the exited nuclear state ($\Gamma = 5 \cdot 10^{-9}$ eV) of the ^{57}Fe atom. Therefore, for free atoms, i.e. in a liquid or in a gas phase, resonant absorption does not occur. However, if the atom is bound in a solid, the recoil energy may be taken up by a large number of atoms in the solid, resulting in a much higher mass M and therefore a much lower recoil energy loss (*eqn. 2.1*).

Due to the fundamental quantum nature of solids, atoms bound in solids are restricted to a specific set of vibrational energies called phonon energies. If the recoil energy is smaller than the phonon energy, there is insufficient energy to excite the lattice to the next vibrational state. The probability f for the lattice to be in the same state before and after the decay of the nucleus corresponds to a certain fraction of the nuclear events such that the entire crystal acts as the recoiling body, rather than just the single atom. Since the mass of the crystal is very large compared to that of a single atom, these events can be considered recoil-free.

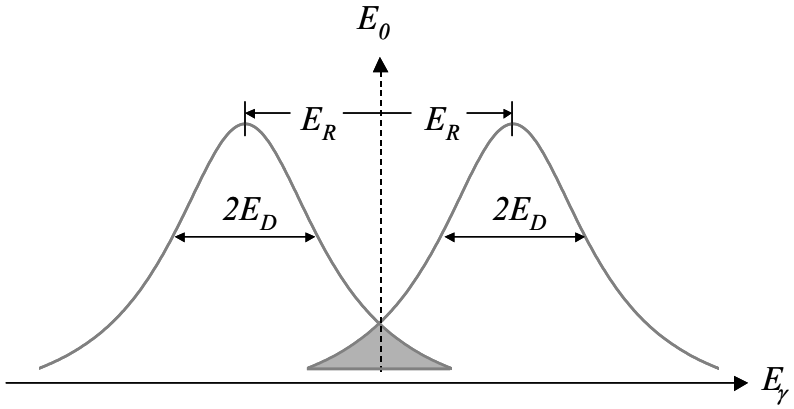

Figure 2.3. *Distribution of energies of the emitted and absorbed γ-rays. The resonant overlap shown as shaded area is the recoil-free fraction exhibiting the Mössbauer effect.*

In general, the probability f for recoil-free absorption and emission of gamma radiation can be described by the Debye model. Here, f is given as a function of temperature and of a parameter θ_D, called the Debye temperature:

$$f = \exp\left[-\frac{3}{2}\frac{E_R}{k_B\theta_D}\left(1+4\frac{T^2}{\theta_D{}^2}\int_0^{\theta_D/T}\frac{x\,dx}{e^x-1}\right)\right] \tag{2.2}$$

where k_B is Boltzmann's constant. By approximation, the Debye temperature, θ_D, can be used as an indication of the bonding strength of the Mössbauer active nucleus to its environment, i.e. the stronger the bond, the larger the θ_D value. Equation 2.2 indicates that the recoil-free fraction f is high for large θ_D values and increases when the temperature is decreased. Therefore, for most Mössbauer experiments, measurements are carried out under cryogenic conditions (i.e. 77 and 4.2 K) in addition to room temperature measurements.

2.2.3. Energy resolution

With negligible recoil energy and the Doppler broadening suppressed as the resonant atom is bound to a rigid lattice, the limiting resolution is now the natural linewidth of the ^{57}Fe isotope, which is related to the average lifetime of the excited state. As mentioned earlier, ^{57}Fe isotope has a natural linewidth of about $5\cdot10^{-9}$ eV. This corresponds to 0.19 mm·s^{-1} in a Mössbauer spectrum. Compared to the Mössbauer γ-ray energy of 14.4 keV, this gives a resolution of 1 in 10^{12}. This very high resolution makes it possible to detect the hyperfine interactions in the nucleus.

2.2.4. Typical Mössbauer experiment

The energy changes within the nuclear levels caused by the hyperfine interactions are extremely small. To observe and measure these small energy changes, it is necessary to modulate the energy of the emitted 14.4 keV gamma ray energy. Because the energy changes are so minute, it is simply sufficient to move the source towards and away from the absorber, creating a Doppler broadening of the γ-ray energy.

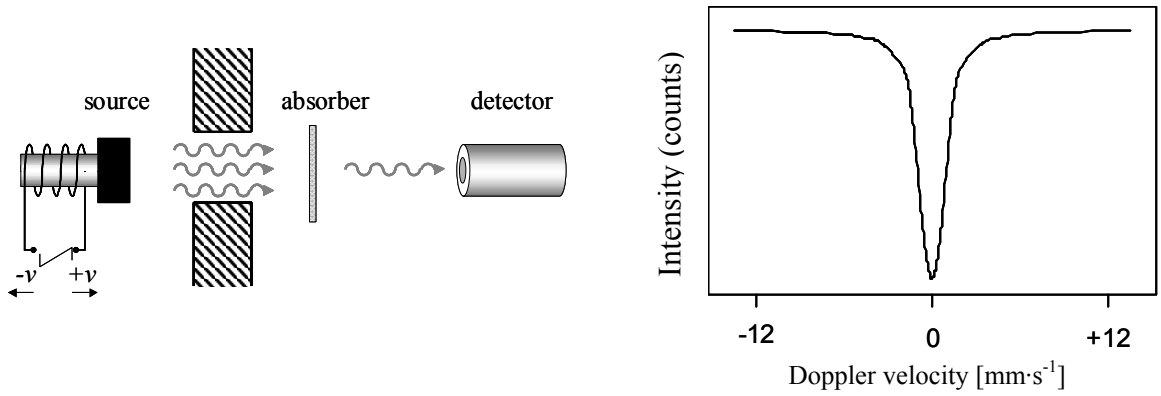

Figure 2.4. *Schematic illustration of Mössbauer spectroscopy*

A typical Mössbauer experiment, containing an oscillating source, an absorber (i.e. the sample) and detector, is illustrated in figure 2.4. A spectrum is obtained by plotting the intensity of the gamma ray as a function of the Doppler velocity (v) of the source, which is expressed in mm·s^{-1}. The Doppler velocity is related to the energy by:

$$E(v) = E_0 \cdot \left(1 + \frac{v}{c}\right) \tag{2.3}$$

At velocities that guarantee matching of the resonant energy levels, some of the gamma rays are absorbed, resulting in a change in intensity and a corresponding peak in the Mössbauer spectrum. The number, position, and intensity of the peaks provide information about the chemical environment of the absorbing nuclei. The generated spectrum given in figure 2.4 shows a single absorption line or a singlet centered at 0 mm·s^{-1}. This spectrum is characteristic when the source and absorber are in identical cubic or spherical environments. In the next section, the three hyperfine interactions are discussed that contain information on the chemical and structural parameters of a sample: the isomer shift (**IS**), the quadrupole splitting (**QS**), and the magnetic splitting expressed by the magnetic hyperfine field (**HF**).

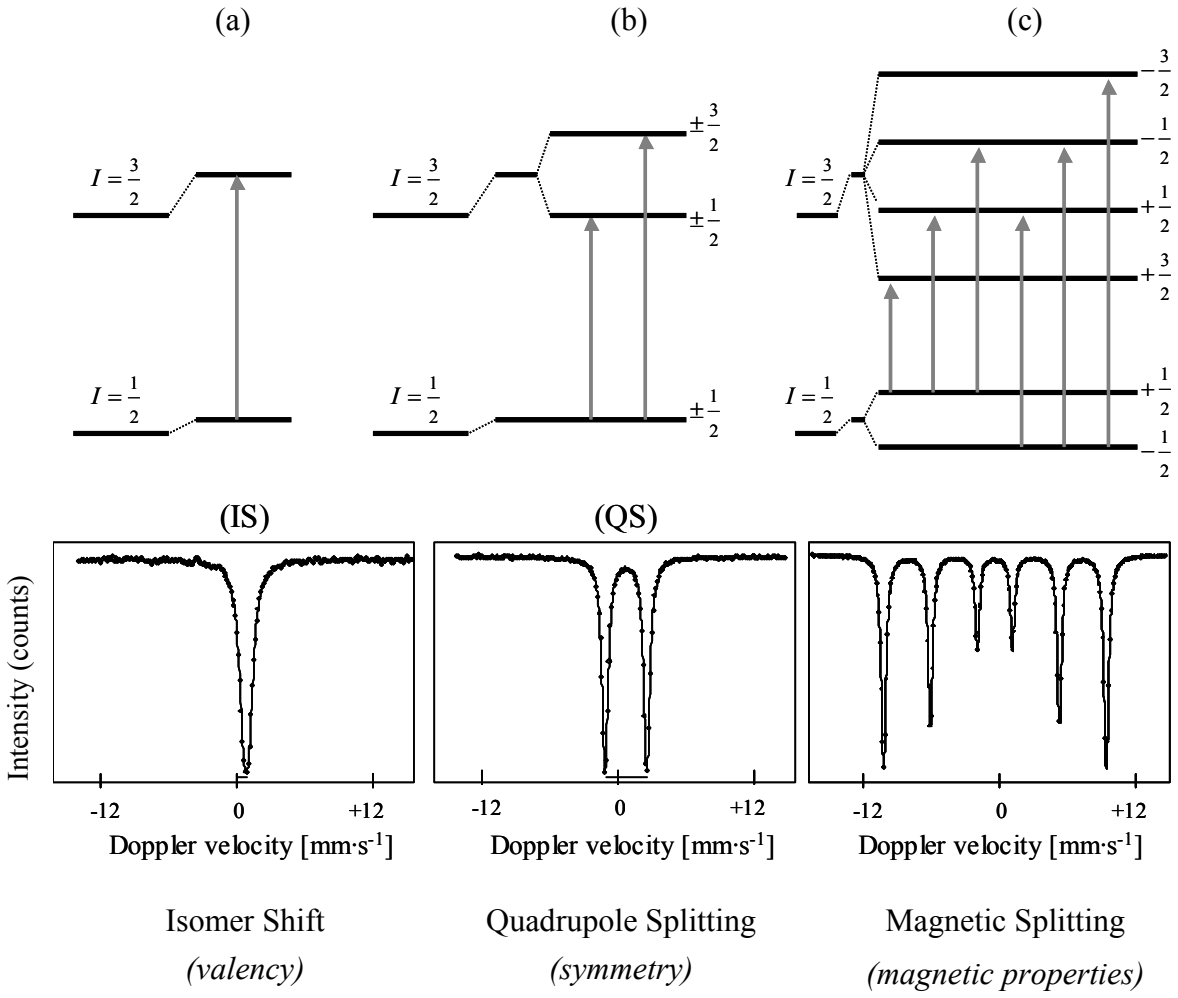

Figure 2.5. *The nuclear level schemes showing the* 3/2 → 1/2 *transitions in* ^{57}*Fe nuclei and the removal of the degenerate energy levels in the presence of the different hyperfine interactions giving:* (a) *isomer shift*, (b) *quadrupole splitting, and* (c) *magnetic splitting*.

2.3. Hyperfine Interactions

2.3.1. Isomer Shift

The isomer shift, IS, is a measure for the *s*-electron density at the nucleus of an atom. The IS arises from the Coulomb interaction which alters the energy separation between the ground state and the excited state of the nucleus as shown in figure 2.5(a). The energy shift of the nuclear levels is dependent on the size of the nuclear radius and the electronic charge density of the nucleus, and is given by:

$$\delta = \Delta E_a - \Delta E_s = \frac{2\pi}{5} Ze^2 \left(R_e^{\,2} - R_g^{\,2} \right) \left[\left| \psi_a(0) \right|^2 - \left| \psi_s(0) \right|^2 \right] \tag{2.4}$$

where Ze is the nuclear charge; $|\psi(0)|^2$ is the electronic charge density of the nucleus, which is given by the *s*-electron density since only *s*-electrons have a finite density at the nuclear site; the subscripts *a* and *s* refer to absorber and source, respectively; and R_e^2 and R_g^2 are the mean square radii of the nucleus in the excited and the ground states, respectively.

Since the isomer shift is a measure of the *s*-electron density at the nucleus, which is affected by the valence electrons, it yields information on the oxidation states of the Mössbauer isotope in the sample under investigation. Because, one can not directly obtain or measure this shift, in practice, the isomer shift is plotted relative to a standard or reference material. For ^{57}Fe Mössbauer spectroscopy, spectra will often be quoted relative to alpha-iron or sodium nitroprusside (or SNP), i.e. $Na_2[Fe(CN)_5NO].2H_2O$, at room temperature.

The expression of the Doppler shift (*eqn.* 2.3) however does not incorporate the effect brought about by the thermal motion of atoms in a solid or lattice vibrations. The presence of vibrational velocity leads to a second line shift in the Mössbauer spectrum that is unrelated to the isomer shift. This phenomenon is called the *second-order Doppler shift*. Since the kinetic energy of the atoms depends on the temperature, the second-order Doppler shift is a function of temperature. Due to this effect, isomer shifts increase as the temperature is lowered. For instance, in the case of tetrahedral ferric iron, an increase of 0.35 mm·s^{-1} in the isomer shift at 4.2 K has been reported,[4] whereas octahedral ferric iron gives even larger second-order Doppler shifts, for example 0.47 mm·s^{-1} for α-Fe_2O_3.[5]

2.3.2. Quadrupole Splitting

When a nucleus is in a state where the spin quantum number is greater than 1/2, its nuclear charge distribution is said to be non-spherical. In this case, the nucleus possesses a quadrupole moment eQ, where e is the electrostatic charge and Q is the magnitude of the nuclear charge distribution. In the presence of an asymmetrical electric field, arising from asymmetric electronic charge distribution in the incompletely filled valence shells of the atom itself and to charges on neighboring ions or ligand arrangement, an electric field gradient (EFG) is produced. The EFG partially lifts the degeneracy and a splitting of energy at the nuclear level is observed. For the first excited state of the ^{57}Fe isotope, the spin $I_e = 3/2$ is split into two substates $I = \pm 1/2$ and $I = \pm 3/2$. This produces two transitions, resulting in a two-line spectrum called ‘doublet’ as shown in figure 2.5(b). The center of the doublet corresponds to the IS. The energy separation between the sublevels, called the **quadrupole splitting** or QS, is proportional to the magnitude of the EFG.

2.3.3. Magnetic Splitting

In the presence of a magnetic field, B_{eff}, the nuclear spin moment experiences a dipolar interaction with the magnetic field and a **magnetic hyperfine splitting** or nuclear Zeeman splitting occurs. This interaction removes the degeneracy of the nuclear levels completely and splits the nuclear energies into $(2I+1)$ substates. For the ^{57}Fe isotope, the excited state, $I_e = 3/2$, splits into 4 substates and the ground state, $I_g = ½$, splits into 2 substates as illustrated in figure 2.5(c). As the 14.4 keV transition of ^{57}Fe is a magnetic dipole transition, only transitions in which the magnetic quantum number changes by $\Delta m = 0, \pm 1$ are allowed. This leads to six possible transitions for the 3/2 → 1/2 transition, giving a six-line pattern or 'sextuplet' in the Mössbauer spectrum, as shown in figure 2.5(c), with the line spacing being proportional to B_{eff}.

The line positions are related to the splitting of the energy levels, whereas, the line intensities are related to the angle θ between the Mössbauer gamma-ray and the nuclear spin moment. The intensities of the outer lines (+3/2 → +1/2 and -3/2 → -1/2 transitions), middle lines (+1/2 → +1/2 and -1/2 → -1/2 transitions), and inner lines (-1/2 → +1/2 and +1/2 → -1/2 transitions) are related by:

$$3 : \frac{4\sin^2\theta}{1+\cos^2\theta} : 1 \tag{2.5}$$

This indicates that the outer and inner lines are always in the same proportion but the middle lines can vary in relative intensity between 0 and 4 depending upon the angle the nuclear spin moments make to the γ-ray. In polycrystalline samples (such as the ones used in this study) with no applied field, this value averages to 2 as is shown in figure 2.5(c).

The presence of a magnetic field at the nucleus can come from a variety of sources. The total effective magnetic field at the nucleus, B_{eff}, is given by:

$$B_{eff} = (B_{contact} + B_{orbital} + B_{dipolar}) + B_{applied} \tag{2.6}$$

where the first three terms being due to the atom's own partially filled valence electron shells. $B_{contact}$ is the dominant term and is due to the polarized *s*-electron spin density at the nucleus. $B_{orbital}$ is due to the orbital magnetic moment on those electrons, and $B_{dipolar}$ is the dipolar interaction of the nucleus with the spin moment of the atom. $B_{applied}$ is the value of the magnetic field at the nucleus generated by an external magnet.

2.3.4. Combined quadrupole and magnetic interaction

When both quadrupole and magnetic interactions are present, a complex spectrum is created since these interactions are direction dependent effects. Only IS is unaffected. The combined presence of a magnetic field and an electric field gradient causes the four levels of the excited state to obtain an extra shift in energy due to the interaction of the nuclear quadrupole moment with the EFG.

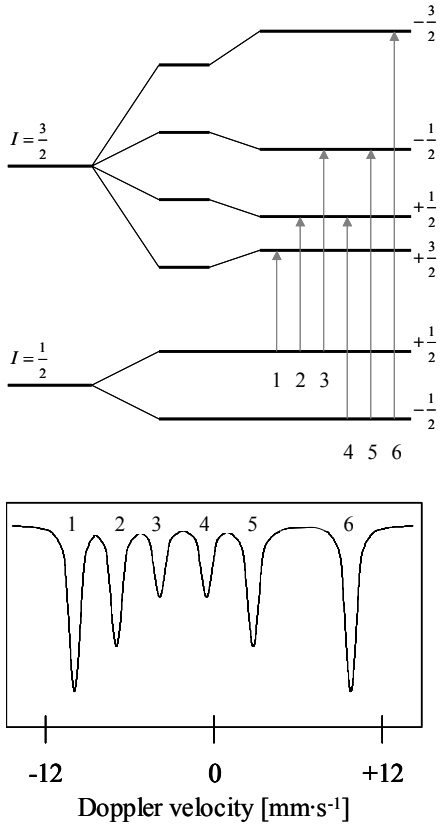

Figure 2.6. *Effect of a first-order quadrupole perturbation on a magnetic hyperfine spectrum for a* 3/2 → 1/2 *transition and its hypothetical spectrum.*

If the electric field gradient tensor is axially symmetric and the magnetic interaction is much greater than the quadrupole interaction, then the quadrupole interaction can be treated as a first-order perturbation to the magnetic interaction. Under these conditions, the level splitting for a 3/2 → 1/2 transition is characterized by a shift of the $m_I = \pm 3/2$ by an energy $+\varepsilon'$ and the $m_I = \pm 1/2$ by an energy $-\varepsilon'$ as illustrated in figure 2.6.

The quadrupole shift ε' is proportional to the magnitude of EFG and is dependent on the angle θ between the EFG and the magnetic field. The relationship of ε' to the quadrupole splitting can be expressed by:

$$\varepsilon' = \frac{1}{2}\Delta E_Q \frac{\left(3\cos^2\theta - 1\right)}{2} \tag{2.7}$$

where ΔE_Q is the magnitude of the electric quadrupole splitting.

2.4. Relaxation Phenomena

As briefly mentioned above, the polarizing effects of the unpaired electron spins generate a magnetic hyperfine field. However, this magnetic field at the nucleus varies in time due to the fact that the electronic spin direction is not invariant and can change or 'flip' after a period of time τ. This process of spin flipping is called the **relaxation phenomenon**, and is important in the interpretation of Mössbauer spectra involving paramagnetic (i.e. containing partially filled electron shell) ions and superparamagnetic (*vide infra*) particles.

There are two main processes that can cause spin flipping:

1. electronic *spin-spin* relaxation; and
2. electronic *spin-lattice* relaxation.

The *spin-spin* relaxation involves the energy transfer between neighboring ions via the magnetic dipole and exchange interaction. This interaction is basically related to the proximity of interacting spins, and the *spin-spin* relaxation time τ_{ss} is independent of temperature. On the other hand, the *spin-lattice* relaxation involves the energy transfer between the electron spins and lattice phonons mostly via spin-orbit interaction but also weakly through dipolar interactions. Unlike τ_{ss}, the *spin-lattice* relaxation time τ_{sl} is dependent of temperature. For this relaxation process, τ_{sl} becomes longer when the temperature is lowered.

2.4.1. Effect of Relaxation Time on Mössbauer Spectrum

When the relaxation time, $\tau = \tau_{ss} + \tau_{sl}$, is comparable to the nuclear Larmor precession period, which is characteristic of the measuring time in Mössbauer spectroscopy, the lineshape is strongly influenced by the relaxation behavior. For paramagnetic Fe^{3+}, when $\tau \geq 25$ ns, resolved magnetic hyperfine split spectra are observed with a linewidth decreasing with increasing τ. This is usually referred to as the slow relaxation rate limit. In the range between 1 and 25 ns, the splitting is unresolved and identification of individual lines is difficult. In the fast limit, where $\tau \leq 1$ ns, the magnetic hyperfine splitting collapses to a singlet or a doublet.

The relaxation phenomena reflected in the Mössbauer spectra can be used to obtain information on the properties of the investigated material and therefore it is important to

know the relative contribution of the *spin-spin* relaxation and the *spin-lattice* relaxation. In general, the coupling between the lattice and the spin of the ion is weak since the ^6S ground state of the high-spin Fe^{3+} ion is spherically symmetric. This usually favors a long *spin-lattice* relaxation time. When the spin-lattice relaxation time is much longer compared to the spin-spin relaxation time, its contribution becomes negligible. Only when the *spin-spin* relaxation time is longer, such as in the case when the Mössbauer ion concentration is low, the influence of the *spin-lattice* relaxation becomes significant.

2.4.2. Special Case for High Spin Fe^{3+} ion

In cases when the spin-lattice relaxation term is dominant, the Mössbauer spectra can become more complicated. For Fe^{3+} $3d^5$ ion, the ^6S ground state (S = 5/2, L = 0) has a spherically symmetric distribution of electronic charge. Therefore, the crystal field interaction is relatively small even when the ion is found in a non-cubic environment. However, the spin-orbit coupling can cause crystal field splitting by introducing small admixtures of excited states with an asymmetric electronic charge distribution into the ground state.

Since the spin state S_z of Fe^{3+} has three eigenstates ($S_z = \pm 5/2, \pm 3/2, \pm 1/2$), the crystal field interaction gives rise to a splitting of the electronic ground state into three Kramer's doublets. This can, in principle, result in a complicated Mössbauer spectrum that is generated by three hyperfine components since the *spin-lattice* relaxation times of these different spin states are not identical. The ±5/2 states have long relaxation times, while the ±1/2 and ±3/2 states are usually relaxed in a Mössbauer experiment.

2.5. Magnetic behavior and Application to zeolites

The importance of using ^{57}Fe Mössbauer spectroscopy to characterize Fe-containing zeolites has been briefly discussed in section 1.7. In particular is its suitability to discriminate between framework ions and extra-framework iron species. Iron in the framework position is essentially in tetrahedral oxygen coordination, while iron in the extra-framework position is probably present in oxidic iron clusters, in which they are most likely in octahedral coordination. Therefore by distinguishing between iron in tetrahedral and octahedral coordination using the isomer shift values, the discrimination between framework and extra-framework iron is facilitated. Garten *et al*.[6] reported that at room temperature, IS ≤ 0.56 $mm \cdot s^{-1}$ is indicative of tetrahedral ferric iron, while octahedral ferric ions have IS > 0.56 $mm \cdot s^{-1}$, relative to SNP.

The presence of ferrous ions is an extra indication of the presence of extra-framework iron.[7,8] Particularly since iron in framework positions can only be present in the trivalent state.[9] Ferrous iron species normally have larger IS than their ferric iron counterpart due to the shielding effect on the *s*-electron density of the additional valence electron in the *d*-orbital. Isomer values of ca. 1.6 $mm \cdot s^{-1}$ have been reported for high-spin Fe^{2+} ions.[10]

In the present study, where the main focus is on extra-framework iron species created after steam-treatment, the interest in ^{57}Fe Mössbauer spectroscopy is also in its potential to discriminate between the different extra-framework iron species present in the [Fe,Al]MFI catalyst. It has been shown that steam-treatment of [Fe,Al]MFI causes extraction of framework iron to extra-framework positions ranging from isolated iron ions to large iron oxide particles (ca. 2 nm in diameter).[11] Thus, in this study, the types of magnetic behavior that can be expected are paramagnetic behavior from isolated ferric ions, and superparamagnetic behavior from oxidic (magnetically ordered) iron clusters. These are discussed in detail in the sections below.

2.5.1. Paramagnetic hyperfine splitting

Mössbauer spectra of isolated or dilute paramagnetic ferric iron ions often show **paramagnetic hyperfine splitting** (PHS). When the average spacing between the Fe^{3+} ions is larger than about 15 Å, corresponding to an ion concentration of about 0.5 mol/liter, the *spin-spin* relaxation is so slow that well-resolved magnetically hyperfine splitting is observed.[12] This results in an apparent sextuplet in the Mössbauer spectrum at low temperatures, where the electronic relaxation times become longer than the Mössbauer measuring time. However, at higher temperatures, the spins are rapidly fluctuating resulting in a zero net magnetic moment. This causes a collapse of the absorption lines in the Mössbauer spectra into a broad singlet or unresolved doublet. In addition, an increase in iron concentration resulting in a faster *spin-spin* relaxation rate also leads to reduction of the magnetic component (sextuplet) contribution in favor of a central singlet or doublet.

This (PHS) behavior has been observed in zeolites with low iron concentration.[13,14] In these cases, ferric ions are typically highly dispersed whether they are located in the framework (*see chapter 3*), or extra-framework positions (*see chapter 4*).

2.5.2. Superparamagnetism

Another kind of magnetic relaxation behavior, i.e. superparamagnetism, occurs in samples containing microcrystals of magnetically ordered compounds. **Superparamagnetism** is a phenomenon by which magnetic materials may exhibit a behavior similar to paramagnetism

at temperatures below the Curie[†] or the Néel[‡] temperature. In general, coupling forces in ferromagnetic materials cause the magnetic moments of neighboring atoms to align, resulting in very large internal magnetic fields. At temperatures above the Curie temperature (or the Néel temperature for antiferromagnetic materials), the thermal energy is sufficient to overcome the coupling forces. This causes the atomic magnetic moments to fluctuate randomly cancelling out the magnetic ordering. Since the internal magnetic field no longer exists, the material exhibits paramagnetic behavior.

Superparamagnetism has been observed when the absorber material is composed of very small crystallites (1-10 nm). In this case, the thermal energy is sufficient to change the direction of magnetization of the entire crystallite, even though the temperature is below the Curie or Néel temperature. In this event, the small crystallites behave as one fluctuating spin entity in a manner similar to paramagnetic ions. In MFI zeolites, superparamagnetism has been observed when very small iron oxide nanoparticles are formed after steam-treatment.[11] From the hyperfine field it was determined that the iron-oxide (α-Fe_2O_3) particles have a diameter of ca. 2nm.

The energy required to change the direction of magnetization of a crystallite is called the crystalline anisotropy energy and depends both on the material properties and the crystallite size. As the crystallite size decreases, so does the crystalline anisotropy energy, resulting in a decrease of the temperature at which the material becomes superparamagnetic. This temperature is usually referred to as the superparamagnetic blocking temperature, T_B. In addition to the superparamagnetic behavior, small crystalline particles exhibit a smaller hyperfine field (HF) at non-zero temperatures compared to when it is present in the bulk. This effect is known as collective magnetic excitations,[15] and can be used together with the superparamagnetic behavior to estimate the crystal size of small particles in catalyst systems.[16]

It is therefore clear that two different magnetic behavior, i.e. highly dispersed, isolated Fe^{3+} ions (paramagnetic) and small iron oxide particles (superparamagnetic), give rise to rather similar Mössbauer spectra. Normally, applying a strong external magnetic field often differentiates these two different cases (*see chapter 3*). However, as will be illustrated in chapters 4 and 5, it is also possible to attribute a Mössbauer spectrum only to paramagnetic

[†] Curie temperature is the temperature above which it loses its characteristic ferromagnetic ability to possess a net (spontaneous) magnetization in the absence of an external magnetic field – i.e. from ferromagnetic to paramagnetic material.
[‡] The Néel temperature is the temperature at which an antiferromagnetic material becomes paramagnetic.

ions when other technique, such as TEM, does not support the presence of superparamagnetic iron-oxide clusters.

Figure 2.7. *The Reactor Institute Delft where the department of radiation, radionuclides and reactors, of the faculty of applied sciences, of Delft University of Technology is located.*

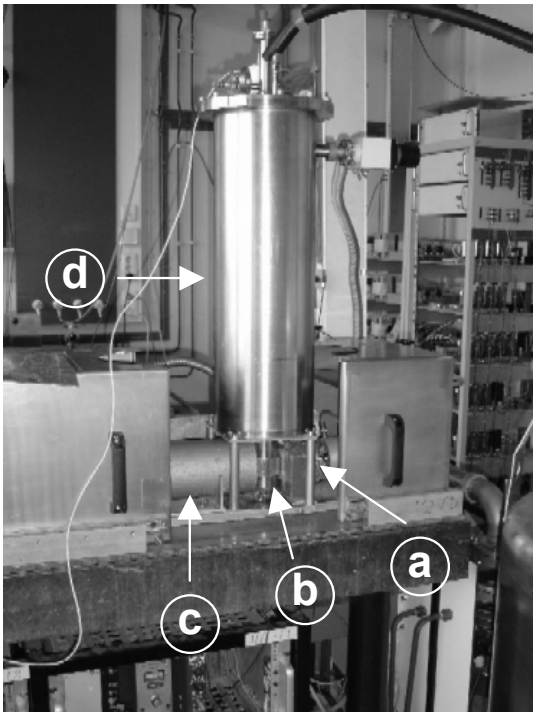

Figure 2.8. *A typical Mössbauer spectroscope showing* a) *source,* b) *sample/absorber,* c) *detector and* d) *the helium bath cryostat.*

2.6. Mössbauer experimental Facility

Mössbauer spectroscopy is a technique that is not commonly applied in catalysis research, even though it is a powerful characterization tool. This is mainly because the technique

requires a laboratory that is capable of handling radioactive materials. This laboratory is present at the department of radiation, radionuclides and reactors, of the faculty of applied sciences, Delft University of Technology – the only location presently in the Netherlands where Mössbauer studies are performed (*see figure 2.7*).

Within this Mössbauer laboratory, Mössbauer spectroscopes (*see figure 2.8 for example*) can be equipped with a helium bath cryostat for low temperature measurements (i.e. at 77 K and 4.2 K).

REFERENCES

1. R.L. Mössbauer, Z. Physik, 151 (1958) 124, R.L. Mössbauer, *Naturwissenschaften*, 45 (1958) 538.
2. N.N. Greenwood and T.C. Gibb, *Mössbauer Spectroscopy*, Chapman and Hall, London, 1971.
3. G.K. Wertheim, *Mössbauer Effect: Principles and Applications*, Academic Press, New York, 1964.
4. J.M.D. Coey, *Mössbauer Spectroscopy Applied to Inorganic Chemistry*, Vol. 1, ed. G.J. Long, Plenum, New York and London, (1984) Chap.14.
5. D.D. Amarasiriwardena, *Clays Clay Miner.*, 34 (1986), 250.
6. R.L. Garten, W.N. Delgass, and M. Boudart, *J. Catal.*, 18 (1970) 90.
7. K. Lázár, G. Lejeune, R.K. Ahedi, S.S. Shevade, and A.N. Kotasthane, *J. Phys. Chem. B*, 102 (1998) 102.
8. K.A. Dubkov, N.S. Ovanesyan, A.A. Shteinman, E.V. Starokon, and G.I. Panov, *J. Catal.*, 207 (2002) 341.
9. S. Bordiga, R. Buzzoni, F. Geobaldo, C. Lamberti, E. Giamello, A. Zecchina, G. Leofanti, G. Petrini, G. Tozzola, *J. Catal*., 158 (1996) 486.
10. N.S. Ovanesyan, A.A. Shteinman, V.I. Sobolev, K.A. Dubkov, and G.I. Panov, *Kinet. Katal.*, 39 (1998) 863.
11. J. Pérez-Ramírez, G. Mul, F. Kapteijn, J.A. Moulijn, A.R. Overweg, A. Doménech, A. Ribera, I.W.C.E. Arends, *J. Catal.*, 207 (2002) 113.
12. S. Mørup, J.E. Knudsen, M.K. Nielsen, and G. Trumpy, *J. Chem. Phys*, 65 (1976) 536.
13. A. Meagher, V. Nair, and R. Szostak, *Zeolites*, 8 (1988) 3.
14. J.B. Taboada, A.R. Overweg, M.W.J. Crajé, I.W.C.E. Arends, G. Mul, and A.M. van der Kraan, *Microporous Mesoporous Mater.*, 75 (2004) 237.
15. S. Mørup, and H. Topsøe, *Appl. Phys.*, 11 (1976) 63.
16. L.N. Mulay, and T. Pannaparayil, in: *Catalyst Characterization Science: Surface and Solid State Chemistry*, ACS Symp. Ser. 288 (1985) 498.

Chapter 3

[Fe,Al]MFI Zeolite Synthesis and Characterization[†]

Abstract

The synthesis of isomorphously substituted [Fe,Al]MFI zeolites, enriched with ^{57}Fe isotope, is described. Several [Fe,Al]MFI zeolites varying in iron (0.075-0.6 wt.%) and aluminum (0.0-1.1 wt.%) concentrations were successfully synthesized. These samples were characterized by X-ray diffraction (XRD), scanning electron microscopy (SEM) and ^{57}Fe Mössbauer spectroscopy. Although XRD data indicate that zeolites prepared under *static* hydrothermal treatment are crystalline with an MFI zeolite structure, other characterization studies suggest the occurrence of phase segregation. The formation of different phases (i.e. the iron-rich and iron-poor phases) and the difficulty to incorporate all silicon, aluminum, and iron in the solution gel to the zeolite crystal are attributed to the presence of a concentration gradient during *static* hydrothermal treatment. The homogeneity of the synthesis gel was improved by rotating the autoclaves during hydrothermal treatment. In doing so, highly crystalline white samples with the expected Si/Fe and Si/Al molar ratios were obtained. Mössbauer spectra of all *as*-synthesized [Fe,Al]MFI zeolite samples reveal the presence of isolated, tetrahedrally coordinated paramagnetic Fe^{3+} ions. This implies that in all [Fe,Al]MFI zeolites, iron is incorporated in the zeolite framework.

[†] *Parts of this chapter have appeared in two publications:*

- *J.B. Taboada, A.R. Overweg, M.W.J. Crajé, I.W.C.E. Arends, G. Mul,and A.M. van der Kraan, Micropor. Mesopor. Mater., 75 (2004) 237-246; and*
- *J.B. Taboada, A.R. Overweg, and P.J. Kooyman, Stud. Surf. Sci. Catal., 158 (2005) 27-34.*

3.1. Introduction

[Fe,Al]MFI zeolite has been widely investigated for reactions such as the selective catalytic reduction (SCR) of NO_x,[1-4] and the direct decomposition of N_2O.[5,6] Recently, [Fe,Al]MFI has gained increasing attention in the one-step selective oxidation of benzene to phenol using N_2O as oxidant (BTOP).[7-10] Its remarkable catalytic performance has been associated to iron species stabilized in the [Fe,Al]MFI zeolite, generating a new form of surface oxygen (α-oxygen) from N_2O.[7,11] At ambient temperature and pressure, α-oxygen exhibits high reactivity similar to the active oxygen of monooxygenases,[12] which is a type of enzyme that mediate the selective oxidation of hydrocarbons.

There are several methods in preparing the [Fe,Al]MFI catalyst. Conventionally, [Fe,Al]MFI zeolites are loaded with iron using ion-exchange methods.[4,13,14] However, these methods are often not reproducible,[15,16] and calcination of these materials often leads to the formation of significant amount of large iron oxide particles, which are inactive in the benzene to phenol,[7] and other reactions catalysed by [Fe,Al]MFI.[17,18] An efficient and reproducible method in obtaining the highest possible dispersion of extra-framework iron at the exchange position of the MFI lattice is the use of $FeCl_3$ in the gaseous form through chemical vapor deposition (CVD).[18] However, post-treatment steps after CVD strongly affects the state of iron, and calcination leads to the formation of large haematite and α-goethite particles.[19-21]

One particular method of interest to prepare an active catalyst for the direct oxidation of benzene to phenol is the hydrothermal synthesis of isomorphously substituted [Fe,Al]MFI zeolite, followed by calcination and subsequent treatment by steam at 873 K.[10] An extensive physicochemical characterization of the [Fe,Al]MFI catalyst, prepared using this method, indicated that after the post-activation treatments a broad distribution of extra-framework iron species was created ranging from isolated mononuclear iron ions to large iron oxide particles of 2 nm in diameter.[22] Due to the heterogeneous nature of the extra-framework iron species formed, it is difficult to identify the iron species that is active in the catalytic oxidation of benzene to phenol.

In order to gain insight of the active species, two sets of [Fe,Al]MFI zeolites were prepared in which the amount of iron and aluminum were systematically varied. Keeping the aluminium content constant (1.1 wt.%), iron concentration in the first set of [Fe,Al]MFI zeolites was systematically decreased from 0.6 wt.% to ppm levels to emulate the iron concentration in commercial ZSM-5 zeolites. For the second set of samples, aluminum concentration was varied from 1.1 wt.%, which is typical of ZSM-5 (or [Al]MFI) zeolite, to the aluminum-free

MFI (or silicalite); while keeping the iron content constant at 0.6 wt.%. All isomorphously substituted [Fe,Al]MFI zeolite samples were synthesized *via* hydrothermal treatment. All *as*-synthesized [Fe,Al]MFI zeolites were enriched with ^{57}Fe isotope to enhance the Mössbauer effect, and thus providing an excellent signal-to-noise ratio.

In this chapter, the synthesis and characterization of [Fe,Al]MFI zeolites varying in iron and aluminium concentrations are presented. In particular, this study focuses on the effects of iron and aluminum variation on the properties of the *as*-synthesized [Fe,Al]MFI zeolites.

3.2. Experimental

3.2.1. Preparation of [Fe,Al]MFI zeolites

Isomorphously substituted [Fe,Al]MFI zeolites, enriched with ^{57}Fe isotope, were prepared by hydrothermal treatment. In this synthesis method, a solution gel is first prepared by adding in a drop-wise manner a mixture of silica source, organic template, and sodium hydroxide (NaOH, Merck, 98%) to a stirred aqueous solution containing iron and aluminum ions. This aqueous solution was prepared by dissolving solid ^{57}Fe foil (95% ^{57}Fe) in excess concentrated nitric acid. The amount of nitric acid used was determined stoichiometrically with an excess ratio of 2. The ^{57}Fe solution was diluted in 20 ml water and titrated with ammonium hydroxide (NH_4OH, Aldrich, 28 wt.% in H_2O) until it reached the pH (2.3) comparable to that of iron nitrate ($Fe(NO_3)_3.9H_2O$, Merck, 99%) in 20 ml water having the same ^{57}Fe equivalent. After which, aluminum nitrate ($Al(NO_3)_3.9H_2O$, Merck, 98.5%) was added. Tetraethylorthosilicate (TEOS, Acros, 98%) was used as silica source, and tetrapropylammonium hydroxide (TPAOH, Alfa Aesar, 40 wt.% in H_2O) as organic template.

Various solution gels were prepared having different Si/Al and Si/Fe molar ratios as shown in tables 3.1 and 3.2, while keeping the nominal molar ratios of TPAOH/Si and NaOH/Si constant at 0.1 and 0.2 respectively. Hydrothermal synthesis proceeded by placing the solution gel in an autoclave lined with Teflon and heating it to 448 K for 5 days. For the synthesis of [Fe,Al]MFI $(1s)_{as}$ and [Fe,Al]MFI $(2s)_{as}$, hydrothermal treatment was carried out under *static* condition. Hydrothermal synthesis under this mode implies that the autoclaves were left standing in the oven during hydrothermal synthesis. For the preparation of [Fe,Al]MFI in which iron and aluminum concentrations were varied, hydrothermal synthesis was performed under *rotated* hydrothermal condition. This means that the autoclaves were rotated (ca. 25 rpm) through an external motor to maintain well mixing of the solution gel during hydrothermal synthesis. The resulting *as*-synthesized materials were washed and filtered several times with demineralised water until the pH was neutral. Finally, the materials were dried at 353 K overnight.

3.2.2. Characterization techniques

The analysis on elemental composition of the *as*-synthesized zeolites was carried out by inductively coupled plasma optical emission spectroscopy (Perkin-Elmer Plasma 40 (Si) and Optima 3000DV (axial)).

Powder X-ray diffraction analysis of the *as*-synthesized [Fe,Al]MFI zeolites were performed on a Bruker-Nonius D5005 diffractometer with an incident beam Huber monochromator and a Braun Position Sensitive Detector. The wavelength used was Cu Kα1 (λ=0.1541 nm). Data were collected in the 2θ range of 5 to 50^{o} at a scan rate of 0.2325^{o}min^{-1}.

Scanning electron microscopy (SEM) was carried out using a Philips XL 20 electron microscope. All samples were coated with gold before placing the sample under the microscope to achieve contrast.

Transmission electron microscopy (TEM) was performed using either a Philips CM30T or CM30UT electron microscope with a LaB_6 filament or FEG as the source of electrons respectively, operated at 300 kV. Samples were mounted on Quantifoil® microgrid carbon polymer supported on a copper grid by placing a few droplets of a suspension of ground sample in ethanol on the grid, followed by drying at ambient conditions.

^{57}Fe Mössbauer spectra were measured on a constant acceleration spectrometer in a triangular mode with a ^{57}Co:Rh source. Spectra of *as*-synthesized [Fe,Al]MFI samples were taken at 300 K in air and in hv (i.e. high vacuum at 10^{-6} mbar), 77 K in hv, and 4.2 K in hv. The overall spectra were fitted with calculated Mössbauer spectra that consisted of Lorentzian-shaped lines. Isomer shift values are reported relative to sodium nitroprusside (SNP).

3.3. Results

3.3.1. On *static* hydrothermal synthesis

For sample identity, 1s and 2s denotes first and second *static* batches, respectively. The subscript '*as*' hereafter refers to the sample in the *as*-synthesized state. Elemental analysis of [Fe,Al]MFI $(1s)_{as}$ shows that the Si/Al and Si/Fe molar ratios are twice as low as compared to the original composition of the synthesis gel (*see table 3.1*). This suggests that about half of the silicon present in the solution gel is not incorporated in the *as*-synthesized zeolite crystal. Furthermore, the synthesis of [Fe,Al]MFI $(2s)_{as}$, which is a reproduction of [Fe,Al]MFI $(1s)_{as}$ in a larger batch (i.e. with twice the volume) has resulted in the formation of 2 solid phases, which can be physically segregated by color. One is a white precipitate, hereafter referred to

as [Fe,Al]MFI (2s)$^{a}_{as}$, and the other is a brownish denser phase, denoted as [Fe,Al]MFI (2s)$^{b}_{as}$. Elemental analysis of these phases indicates that [Fe,Al]MFI (2s)$^{a}_{as}$ contains about 10 times less iron than [Fe,Al]MFI (2s)$^{b}_{as}$. Although they differ in iron content, X-ray diffraction results (not shown for brevity) reveal that both have the MFI-type topology as the only crystalline phase. Analysis of the iron species in both samples with ^{57}Fe Mössbauer spectroscopy (not shown for brevity) shows that the iron-poor phase contains homogeneously distributed Fe^{3+} ions throughout the zeolite framework, while in the iron-rich phase iron is present mainly as iron oxide particles.

Table 3.1. ICP-OES results of the *as*-synthesized [Fe,Al]MFI zeolites prepared under *static* condition.

Sample	Si (w%)[a]	Al (w%)[a]	Fe (w%)[a]	Si/Al (mol/mol)[b]	Si/Fe (mol/mol)[b]	Si/Al (mol/mol)[c]	Si/Fe (mol/mol)[c]
[Fe,Al]MFI (1s)$_{as}$	35.5	2.20	1.05	15	70	36	152
[Fe,Al]MFI (2s)$^{a}_{as}$	37.1	1.30	0.11	27.5	673	36	152
[Fe,Al]MFI (2s)$^{b}_{as}$	37.6	1.39	1.02	25.9	73.4	36	152

[a] weight percent in the crystalline samples

[b] molar ratio of the crystalline samples

[c] molar ratio of the solution gel

In addition, SEM images of the iron-poor phase exhibit twinned prismatic crystals of about 15-20 microns typical for MFI crystals (*see figure 3.1, left*). On the other hand, the iron-rich phase is formed by agglomeration of small crystals into spheres with an average diameter of about 15 microns (*see figure 3.1, right*). These differences in crystal shape indicate that the two phases differ in growth kinetics during hydrothermal synthesis.

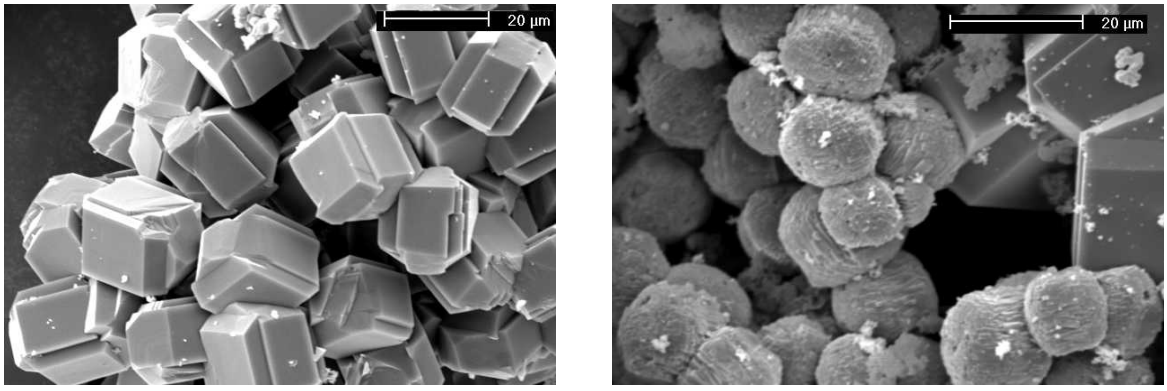

Figure 3.1. *Scanning electron micrographs of the two phases formed. Left picture shows the white, iron-poor phase* [Fe,Al]MFI (2s)$^{a}_{as}$, *and right picture shows the brownish, iron-rich phase* [Fe,Al]MFI (2s)$^{b}_{as}$.

Table 3.2. ICP-OES results of the *as*-synthesized [Fe,Al]MFI zeolites prepared under *rotated* condition.

Sample	Si (w%)[a]	Al (w%)[a]	Fe (w%)[a]	Si/Al (mol/mol)[b]	Si/Fe (mol/mol)[b]	Si/Al (mol/mol)[c]	Si/Fe (mol/mol)[c]
[Fe,Al]MFI (0.12:4)$_{as}$	39.0	1.20	0.08	31	1018	36	1200
[Fe,Al]MFI (0.17:4)$_{as}$	39.0	1.10	0.10	34	794	36	900
[Fe,Al]MFI (0.25:4)$_{as}$	39.0	1.15	0.14	33	567	36	600
[Fe,Al]MFI (0.5:4)$_{as}$	39.0	1.16	0.28	33	284	36	300
[Fe,Al]MFI (1:4)$_{as}$	39.0	1.10	0.56	34	142	36	152
[Fe,Al]MFI (1:2)$_{as}$	40.0	0.63	0.60	62	136	70	152
[Fe,Al]MFI (1:1)$_{as}$	41.0	0.22	0.47	179	178	152	152
[Fe,Al]MFI (1:0.5)$_{as}$	40.0	0.14	0.54	276	151	300	152
[Fe,Al]MFI (1:0)$_{as}$	39.7	--	0.5	--	161	--	152

[a] *weight percent in the crystalline samples*
[b] *molar ratio of the crystalline samples*
[c] *molar ratio of the solution gel*

3.3.2. On *rotated* hydrothermal synthesis

Elemental analysis of the *as*-synthesized [Fe,Al]MFI zeolites varying in iron and aluminum concentrations, prepared under *rotated* hydrothermal condition, is summarized in table 3.2. Comparison of the elemental composition of the *as*-synthesized samples to their corresponding solution gels indicates that most silicon, iron and aluminum are incorporated in the [Fe,Al]MFI crystal. X-ray diffractograms of these samples, plotted in figure 3.2, show only MFI-type structure with a high degree of crystallinity.

It is also observed that for samples with varying iron content (i.e. figures 3.2A-E), the diffractograms exhibit additional Bragg peaks particularly visible around 23.05, 23.65 and 44.90 *2θ*. These small differences in the XRD pattern (*see insets of figure 3.2 as example*) can be attributed to the variation of unit cell sizes, which is believed to be caused by the disparity of the amount of iron present in the [Fe,Al]MFI zeolite crystals. This is because the length of Fe-O bond (1.86 ± 0.1 Å) [23] is larger than that of the Al-O bond (1.73 Å) and Si-O bond (1.63 Å).[24] Thus, a crystal containing more iron atoms could in principle induce small shifts of the Bragg peaks.

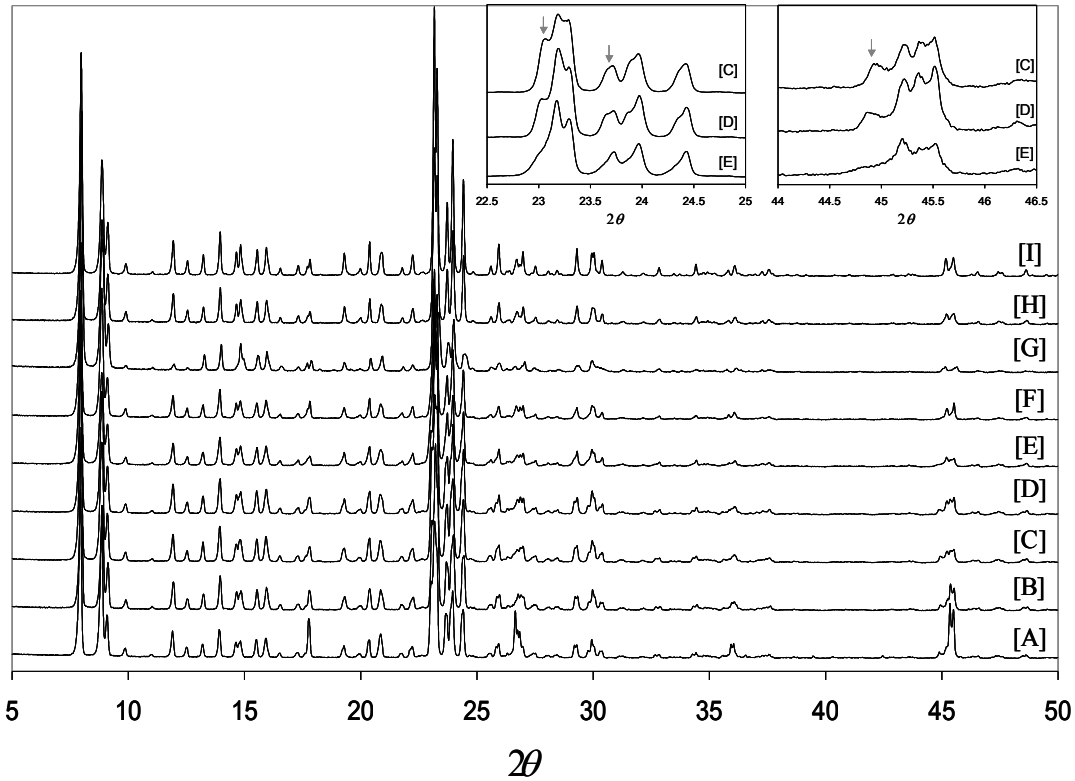

Figure 3.2. *X-ray diffractograms of as-synthesized* [Fe,Al]MFI *zeolites with different Fe:Al molar ratio:* [A] [Fe,Al]MFI (0.12:4) $_{as}$, [B] [Fe,Al]MFI (0.17:4) $_{as}$, [C] [Fe,Al]MFI (0.25:4) $_{as}$, [D] [Fe,Al]MFI (0.5:4) $_{as}$, [E] [Fe,Al]MFI (1:4) $_{as}$, [F] [Fe,Al]MFI (1:2)$_{as}$, [G] [Fe,Al]MFI (1:1) $_{as}$, [H] [Fe,Al]MFI (1:0.5) $_{as}$, *and* [I] [Fe,Al]MFI (1:0) $_{as}$,

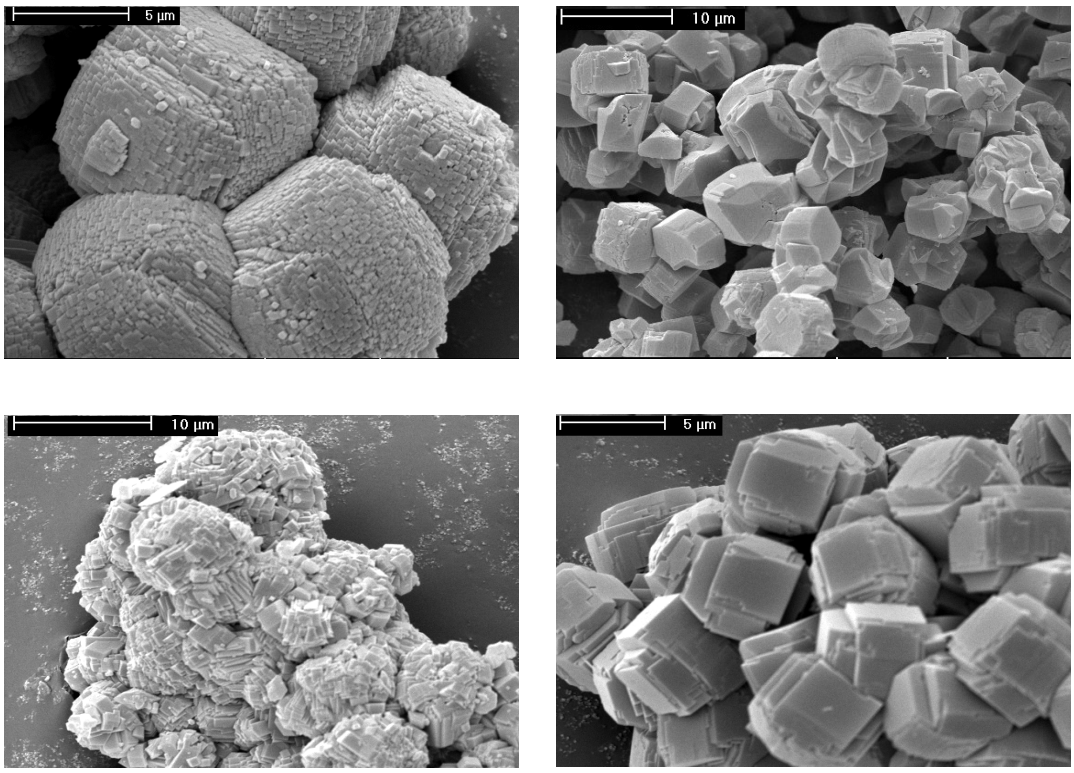

Figure 3.3. *Scanning electron micrographs of* (top left) [Fe,Al]MFI (1:4) $_{as}$, (top right) [Fe,Al]MFI (0.5:4) $_{as}$, (bottom left) [Fe,Al]MFI (1:2) $_{as}$ *and* (bottom right) [Fe,Al]MFI (1:0) $_{as}$

SEM images of the *as*-synthesized materials show morphologies as expected for MFI-type zeolites, i.e. almost spherical clusters of small rods and large twinned or multiple-twinned crystals. Typical SEM images for some samples are shown in figure 3.3. In general, the micrographs seem to indicate that the higher the concentration of trivalent ions (i.e. both Al^{3+} and Fe^{3+}), the smaller the crystal size is produced. This trend is observed to be much stronger in the case when the aluminium concentration is varied (from 0 to 1.1 wt.% Al, keeping Fe constant at 0.6 wt.%) than in the case where iron concentration is varied (from 0.075 to 0.6 wt.% Fe, keeping Al constant at 1.1 wt.%). This seems to suggest that the amount of trivalent ions present in the solution gel during hydrothermal synthesis influences the rate of crystal nucleation.

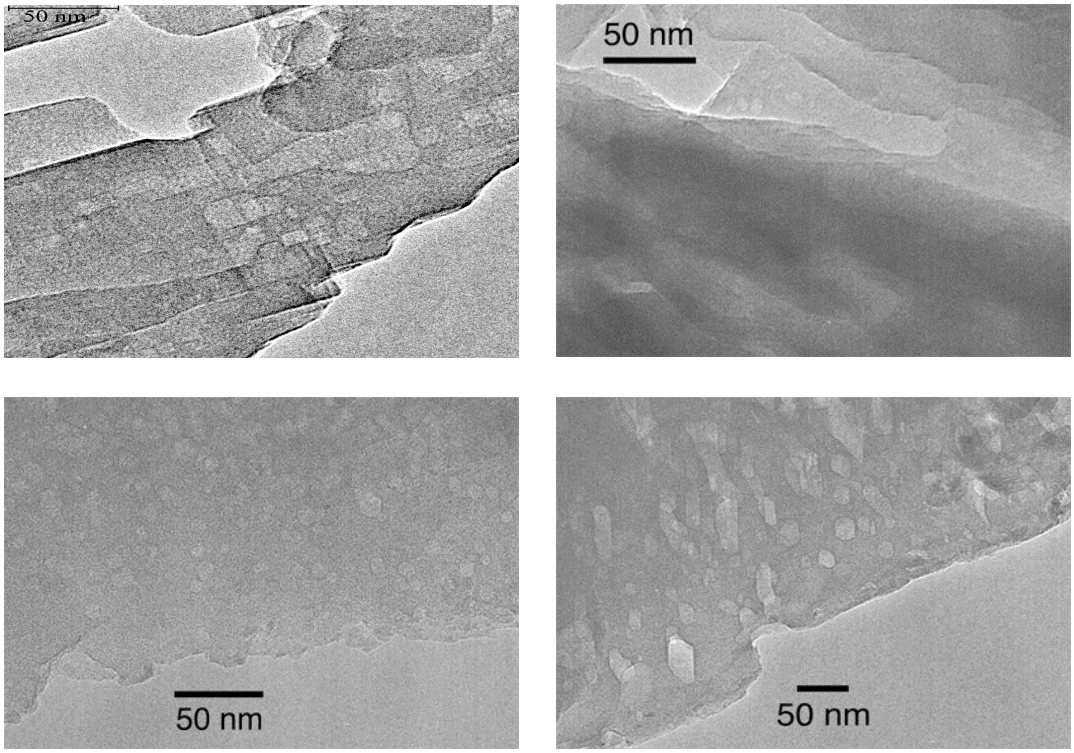

Figure 3.4. *Transmission electron micrographs of* (top left) [Fe,Al]MFI (1:4)$_{as}$, (top right) [Fe,Al]MFI (0.5:4)$_{as}$, (bottom left) [Fe,Al]MFI (0.25:4)$_{as}$ *and* (bottom right) [Fe,Al]MFI (1:0)$_{as}$

TEM shows that all *as*-synthesized [Fe,Al]MFI samples contain a substantial amount of mesopores with a broad pore size distribution in addition to the ordinary MFI pore system. Next to zeolitic material, no amorphous debris is observed either in TEM or SEM investigations. Figure 3.4 shows representative TEM images of some *as*-synthesized [Fe,Al]MFI samples. These micrographs show well-formed mesopores throughout the zeolite crystals. Even the Fe-silicalite (i.e. Al-free) material contains many well-formed mesopores. The mesopore size distribution is very broad for all samples, with pore sizes ranging up to 100 nm.

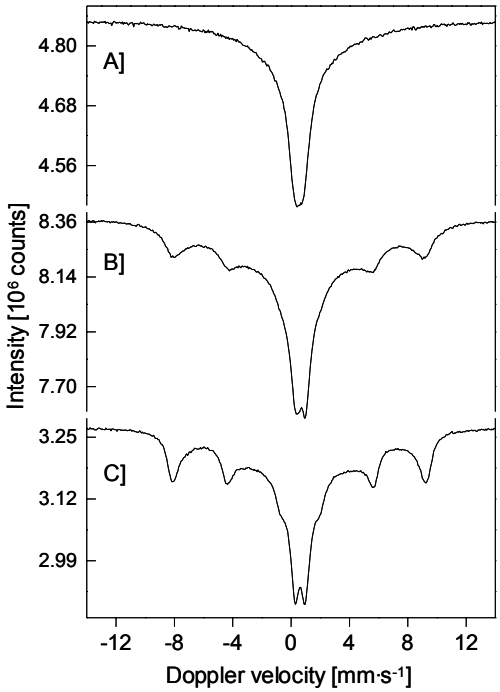

Figure 3.5. *[57]Mossbauer spectra of as-synthesized* [Fe,Al]MFI (1:4) *zeolite taken at* A] *300 K in air,* B] *77 K in hv, and* C] *4.2 K in hv. hv = high vacuum (10^{-6} mbar).*

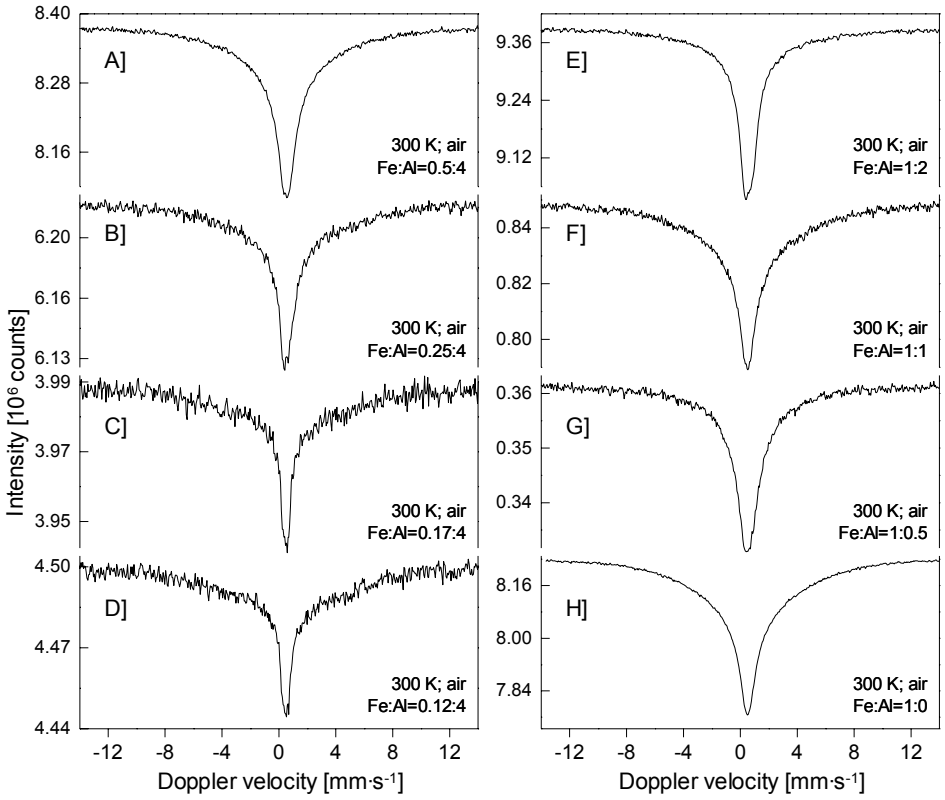

Figure 3.6. *[57]Fe Mossbauer spectra of as-synthesized* [Fe,Al]MFI *zeolites varying in iron* (left) *and aluminum* (right) *concentrations, taken at room temperature in air.*

3.3.2.1. ^{57}Fe Mössbauer spectroscopy of [Fe,Al]MFI *zeolites varying in iron content.*

The Mössbauer spectrum of [Fe,Al]MFI (1:4)$_{as}$ taken at 300 K in air (figure 3.5A) shows a broad singlet with an isomer shift of 0.52 mm·s^{-1} relative to SNP. This confirms that iron is in the high-spin Fe^{3+} state and is present in tetrahedral coordination.[25-27] At low temperatures (figure 3.5B-C), the broad component resolves into a six-line pattern (sextuplet) with a maximum hyperfine field of 53.1 T at 77 K and 53.7 T at 4.2 K (*see table 3.3*). These spectral changes are typical for paramagnetic hyperfine splitting,[28] see chapter 2. This implies that the Fe-Fe distances are larger than 15 Å (*see section 2.5 on dilute paramagnetic iron*). For [Fe,Al]MFI (1:4)$_{as}$, which has a Si/Fe ratio of 142, if a random distribution of Fe^{3+} ions throughout the MFI lattice is assumed, Fe-Fe distances of about 21 Å is obtained. This result therefore affirms the presence of paramagnetic isolated high-spin Fe^{3+} ions with slow electron spin relaxation.

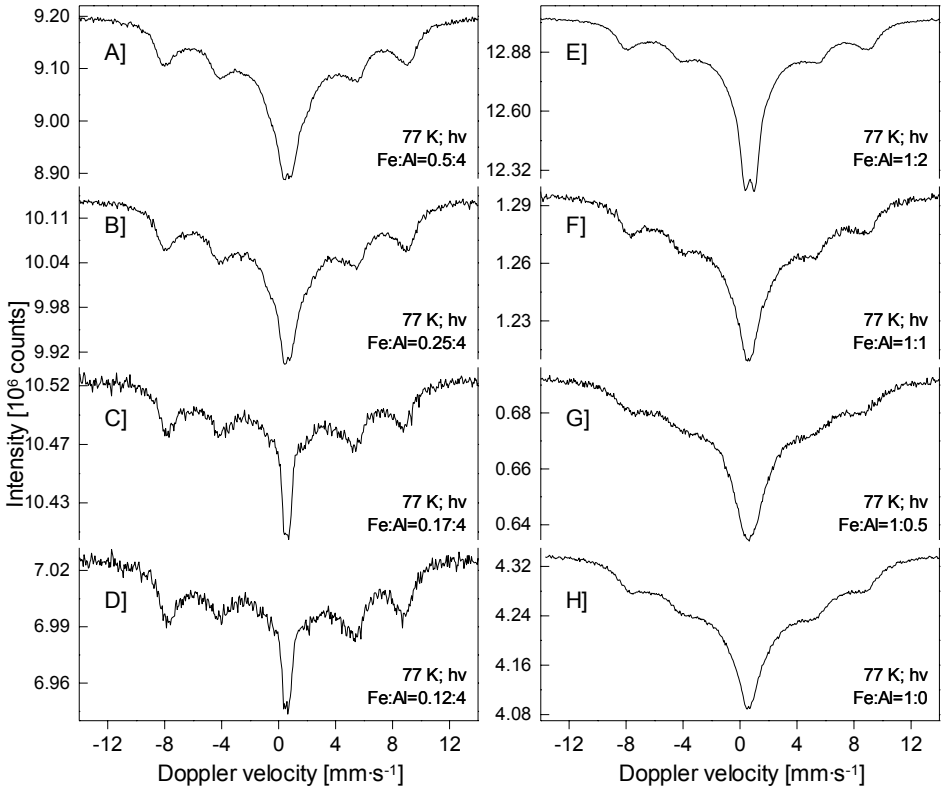

Figure 3.7. *^{57}Fe Mossbauer spectra of as-synthesized* [Fe,Al]MFI *zeolites varying in iron* (left) *and aluminum* (right) *concentrations, taken at 77 K in high vacuum (hv = 10^{-6} mbar).*

Mössbauer spectra, taken at 300 K in air, of the samples varying in iron content are plotted in figure 3.6A-D. All spectra exhibit an IS values of 0.52 mm·s^{-1} indicating tetrahedrally coordinated Fe^{3+} ions, regardless of iron concentration. In addition, all spectra show a broad singlet, similar to that of the spectrum of [Fe,Al]MFI (1:4)$_{as}$ in figure 3.5A, which is typical for paramagnetic Fe^{3+} ions with slow spin-relaxation rate. For these spectra, it is difficult to

fit with only one Lorentian line. The spectral line-shape is most likely complicated by the presence of crystal field splitting that forms the Kramer's doublets (*see section 2.4.2, Chapter 2*). In this case, an iron species could in principle generate 3 components with different relaxation behavior. Therefore, only the IS values are reported in table 3.3. In addition, a narrowing of the central lines is observed for samples with low iron concentration. This can be attributed to a more uniform distribution of relaxation behavior since Fe-Fe distances are larger in dilute samples (e.g. 40 Å for [Fe,Al]MFI $(1:32)_{as}$).

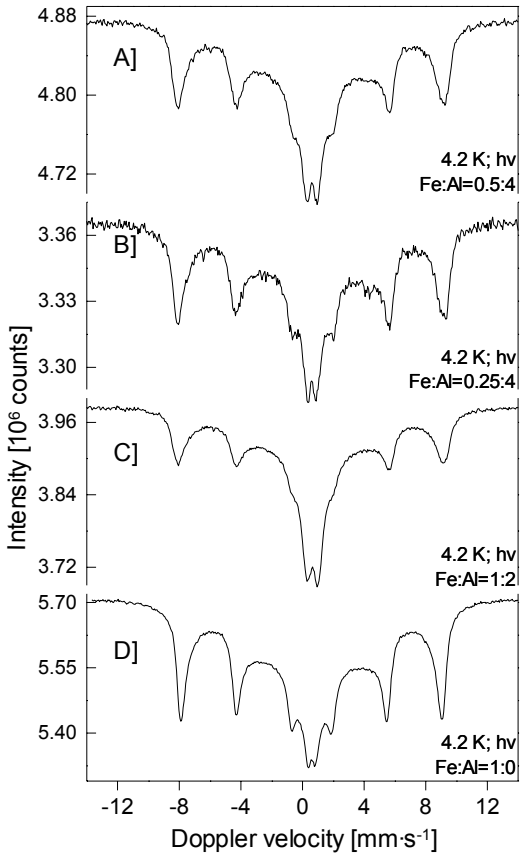

Figure 3.8. *^{57}Mossbauer spectra of as-synthesized* [Fe,Al]MFI *zeolites, varying in iron and aluminum concentrations, taken at 4.2 K in high vacuum. (hv = 10^{-6} mbar)*

At low temperatures (77 K and 4.2 K), small differences in spectral contributions from the different components become visible. At 77 K, shown in figures 3.7A-D, a quadrupole doublet together with a broad sextuplet with a maximum hyperfine field of 53.1 T is present in all samples. However the quadrupole doublet, with a small quadrupole splitting (QS≈0.7 mm·s^{-1}), is more pronounced with increasing iron loading. This indicates that with a higher iron concentration, an increase of spin relaxation rate is observed resulting in a stronger contribution of the quadrupole doublet. At 4.2 K (figures 3.5C, 3.8A and 3.8B), a more-resolved doublet is observed together with a sextuplet with a maximum hyperfine field of 53.7 T in all samples.

Table 3.3. ^{57}Fe Mössbauer Hyperfine Parameters and Relative Intensities of iron species in [Fe,Al]MFI zeolites varying in iron content.†

sample	spectrum no.	condition	IS ($mm \cdot s^{-1}$)	QS ($mm \cdot s^{-1}$)	HF (T)	RI (%)	oxidation state
[Fe,Al]MFI	**3.5A**	300K in air	0.52	--	--	100	Fe^{3+}
$(1:4)_{as}$	**3.5B**	77K in hv	0.59	0.69	--	11	Fe^{3+}
			0.59	--	--	34	Fe^{3+}
			0.59	--	53.1	55	Fe^{3+}
	3.5C	4.2K in hv	0.61	0.72	--	10	Fe^{3+}
			0.61	--	--	29	Fe^{3+}
			0.61	--	53.7	61	Fe^{3+}
[Fe,Al]MFI	**3.6A**	300K in air	0.52	--	--	100	Fe^{3+}
$(0.5:4)_{as}$	**3.7A**	77K in hv	0.62	0.66	--	2	Fe^{3+}
			0.62	--	--	35	Fe^{3+}
			0.62	--	52.7	63	Fe^{3+}
	3.8A	4.2K in hv	0.61	0.75	--	6	Fe^{3+}
			0.61	--	--	26	Fe^{3+}
			0.61	--	53.7	68	Fe^{3+}
[Fe,Al]MFI	**3.6B**	300K in air	0.52	--	--	100	Fe^{3+}
$(0.25:4)_{as}$	**3.7B**	77K in hv	0.62	0.50	--	4	Fe^{3+}
			0.62	--	--	28	Fe^{3+}
			0.62	--	52.4	68	Fe^{3+}
	3.8B	4.2K in hv	0.62	0.60	--	6	Fe^{3+}
			0.62	--	--	22	Fe^{3+}
			0.62	--	53.7	72	Fe^{3+}
[Fe,Al]MFI	**3.6C**	300K in air	0.52	--	--	100	Fe^{3+}
$(0.17:4)_{as}$	**3.7C**	77K in hv	0.60	0.40	--	8	Fe^{3+}
			0.60	--	--	67	Fe^{3+}
			0.60	--	51.0	25	Fe^{3+}
[Fe,Al]MFI	**3.6D**	300K in air	0.52	--	--	100	Fe^{3+}
$(0.12:4)_{as}$	**3.7D**	77K in hv	0.60	0.40	--	7	Fe^{3+}
			0.60	--	--	59	Fe^{3+}
			0.60	--	50.9	34	

IS(isomer shift), QS(quadrupole splitting), HF(hyperfine field), RI(relative intensity);
hv(high vacuum at 10^{-6} mbar)

† In tables 3.3 and 3.4, the spectra at 77 K and 4.2 K were fitted with 3 components in order to extract the three distributions resulting from the three Kramer's doublets. At room temperature this proved to be impossible. The IS of these contributions should be the same. The magnetic contributions of these components differ due to differences in their relaxation rates.

Table 3.4. ^{57}Fe Mössbauer Hyperfine Parameters and Relative Intensities of iron species in [Fe,Al]MFI zeolites varying in aluminum content.

sample	spectrum no.	condition	IS (mm·s^{-1})	QS (mm·s^{-1})	HF (T)	RI (%)	oxidation state
[Fe,Al]MFI	**3.6E**	300K in air	0.52	--	--	100	Fe^{3+}
$(1:2)_{as}$	**3.7E**	77K in hv	0.60	0.74	--	10	Fe^{3+}
			0.60	--	--	34	Fe^{3+}
			0.60	--	52.6	56	Fe^{3+}
	3.8C	4.2K in hv	0.62	0.76	--	10	Fe^{3+}
			0.62	--	--	33	Fe^{3+}
			0.62	--	53.1	57	Fe^{3+}
[Fe,Al]MFI	**3.6F**	300K in air	0.52	--	--	100	Fe^{3+}
$(1:1)_{as}$	**3.7F**	77K in hv	0.61	0.40	--	13	Fe^{3+}
			0.61	--	--	74	Fe^{3+}
			0.61	--	51.0	13	Fe^{3+}
[Fe,Al]MFI	**3.6G**	300K in air	0.52	--	--	100	Fe^{3+}
$(1:0.5)_{as}$	**3.7G**	77K in hv	0.61	0.40	--	19	Fe^{3+}
			0.61	--	--	65	Fe^{3+}
			0.61	--	50.0	16	Fe^{3+}
[Fe,Al]MFI	**3.6H**	300K in air	0.52	--	--	100	Fe^{3+}
$(1:0)_{as}$	**3.7H**	77K in hv	0.56	--	--	6	Fe^{3+}
			0.56			36	Fe^{3+}
			0.56	--	51.7	58	Fe^{3+}
	3.8D	4.2K in hv	0.60	0.49	--	2	Fe^{3+}
			0.60	--	--	24	Fe^{3+}
			0.60	--	52.9	74	Fe^{3+}

IS(isomer shift), QS(quadrupole splitting), HF(hyperfine field), RI(relative intensity); hv(high vacuum at 10^{-6} mbar)

3.3.2.2. ^{57}Fe Mössbauer spectroscopy of [Fe,Al]MFI *zeolites varying in aluminum content.*

Mössbauer spectra taken at 300 K in air for the samples with varying aluminum concentration are shown in figures 3.6E-H. All spectra exhibit a broad singlet with an average IS of 0.52 mm·s^{-1}, which is comparable to that of [Fe,Al]MFI $(1:4)_{as}$, indicating tetrahedrally coordinated Fe^{3+} ions regardless of aluminum concentration. At 77 K (figures 3.7E-H), all spectra contain a broad magnetic component that resolves into a sextuplet at 4.2 K (figures 3.8C and 3.8D), which is more pronounced in [Fe,Al]MFI $(1:0)_{as}$, and is typical for paramagnetic Fe^{3+} ions with large Fe-Fe distances.

3.4. Discussion

For the synthesis of [Fe,Al]MFI zeolites, enriched ^{57}Fe isotope, it is apparent that under *static* hydrothermal conditions the resulting zeolite exhibits significant heterogeneity with respect to the iron concentration. In extreme cases, this discrepancy in iron distribution can lead to the formation of iron-rich and iron-poor crystalline phases as seen from the results of [Fe,Al]MFI $(2s)^{a}_{as}$ and [Fe,Al]MFI $(2s)^{b}_{as}$. The formation of two phases with different iron content is most likely explained by the presence of a concentration gradient in the solution gel during hydrothermal synthesis. Due to the *static* nature of the synthesis method, it is presumed that during the nucleation stage of zeolite formation, phase segregation takes place thereby separating the denser iron-rich nuclei in the solution gel. Consequently, the iron-rich phase is formed at the bottom of the solution gel, while the iron-poor phase is formed on top of it. In addition, the presence of a concentration gradient in the solution gel possibly affects the nucleation and crystal growth process of the zeolite formation. Derouane *et al*.[29,30] have postulated that depending on the aluminum content in the ZSM-5, or [Al]MFI, different mechanisms in nucleation and crystal growth occur. It is therefore assumed that this phenomenon can take place in iron containing systems as well. The occurrence of different iron and aluminum concentrations within the solution gel, leads to the formation of zeolites with different nucleation and growth kinetics as evident by the observed difference in crystal morphology of the two phases formed as illustrated in figure 3.1.

The results presented in this study confirmed that by rotating the autoclave during hydrothermal treatment, a potential concentration gradient in the solution gel during hydrothermal synthesis was eliminated. SEM and XRD studies showed that this synthesis method successfully prepared highly crystalline zeolites with MFI structure containing the expected iron and aluminum concentrations. Therefore, subsequent synthesis of [Fe,Al]MFI zeolites, particularly in the systematic variation of iron and aluminum concentrations, had been carried out under *rotated* hydrothermal condition.

Several factors indicate that iron in all *as*-synthesized [Fe,Al]MFI zeolites is incorporated in the framework of the [Fe,Al]MFI zeolite. First, the white color of the *as*-synthesized material suggests the absence of large iron oxide particles.[31] Second, the average isomer shift in the Mössbauer spectra suggests that Fe^{3+} is present in tetrahedral coordination. The Mössbauer spectra of all samples, regardless of iron and aluminum concentrations, have an isomer shift close to 0.52 $mm \cdot s^{-1}$ that is attributed to tetrahedrally coordinated Fe^{3+} ions. Iron in the framework sites is essentially in tetrahedral coordination. On the other hand, iron in the extra-framework sites is most likely present as iron oxide clusters, which are octahedrally coordinated such as those observed in the bulk phases of α-FeOOH (goethite) and α-Fe_2O_3

(haematite).[32] Therefore, it is inferred that iron ions in all samples, independent of iron and aluminium concentrations, are paramagnetic high spin Fe^{3+} ions which are tetrahedrally coordinated in the framework of the MFI lattice.

Moreover, the trends that have been observed in the Mössbauer spectra are consistent with the systematic variation. Meaning that for an increase in iron loading, a decrease in Fe-Fe distances is expected. In this case, an enhanced spin interaction with the neighboring Fe^{3+} ions, i.e. spin-spin relaxation, is produced resulting in a faster relaxation rate. The progressive increase of spin-spin relaxation contribution, as iron concentration is systematically increased, produces the line broadening that is observed in samples with varying iron. This is probably due to the overlap of the spin-spin contribution and the central relaxed component of Kramer's doublets, arising from spin-lattice relaxation. The presence of spin-spin relaxation behavior, which is more apparent in the samples with high iron concentration, suggests that some Fe-Fe distances, either inter- or intra-crystals, are less than 15 Å. This indicates that iron in the [Fe,Al]MFI zeolite samples is not as homogeneously well distributed as earlier assumed. This is further confirmed by XRD, which indicates a distribution of unit cell sizes within the crystals evidenced by the presence of additional Bragg peaks, assigned to MFI structure, around 23.05, 23.65 and 44.9 2θ in the diffractogram. This illustrates that iron is indeed incorporated in the MFI lattice and its concentration almost certainly varies from crystal to crystal.

For [Fe,Al]MFI zeolites varying in aluminum content, there are no substantial differences in their Mössbauer spectra taken at 300 K in air apart from a small narrowing of the central lines for the samples with increasing aluminium content. At cryogenic temperatures (i.e. at 77 K and 4.2 K) a broad magnetic component (± 10 mm·s^{-1}) is more profound for samples with low aluminium, especially for [Fe,Al]MFI $(1{:}0)_{as}$ that contains no aluminium at all. These spectral differences indicate that a more homogeneous iron distribution is achieved (i.e. with large Fe-Fe distances) for samples with low and no aluminum content. In addition, a less asymmetric iron ion is obtained, in terms of charge distribution of the iron tetrahedral coordination, as indicated by the lowering of QS. This asymmetry in the iron tetrahedron has been reported by other authors,[25,33] and they have associated this to the presence of aluminum. Therefore, for the aluminum-free [Fe,Al]MFI $(1{:}0)_{as}$, the tetrahedral coordination of the framework Fe^{3+} ions is less distorted resulting in a strongly narrowed quadrupole doublet in the Mössbauer spectrum recorded at 4.2 K.

Further evidence for homogeneous, well distribution of paramagnetic Fe^{3+} ions, especially for samples with low or no aluminium, can be obtained from the Mössbauer results with applied external magnetic field. As indicated in chapter 2, two different types of magnetic behavior,

i.e. paramagnetic hyperfine splitting by isolated Fe^{3+} ions and superparamagnetism through iron oxide particles give rise to similar Mössbauer spectra – i.e. a broad singlet or doublet at room temperature resolving to magnetically split component at cryogenic temperatures. By applying a strong external magnetic field (in this case, 4 T), these two different cases can be further differentiated as illustrated in figure 3.9. For an Fe-impregnated sample (figure 3.9 1A and 2A), application of 4 T results in the broadening of linewidths as well as an apparent increase in intensity of lines 2 and 5 (*see arrows in figure 3.9 2A*). These spectral changes are typical for superparamagnetic iron oxide particles. On the other hand, for [Fe,Al]MFI $(1:0)_{as}$, a narrowing of linewidth is observed accompanied by the decrease of lines 2 and 5, which is typical for well isolated paramagnetic Fe^{3+} ions. These results, therefore, corroborate very well with the analysis that has been presented in the above discussions.

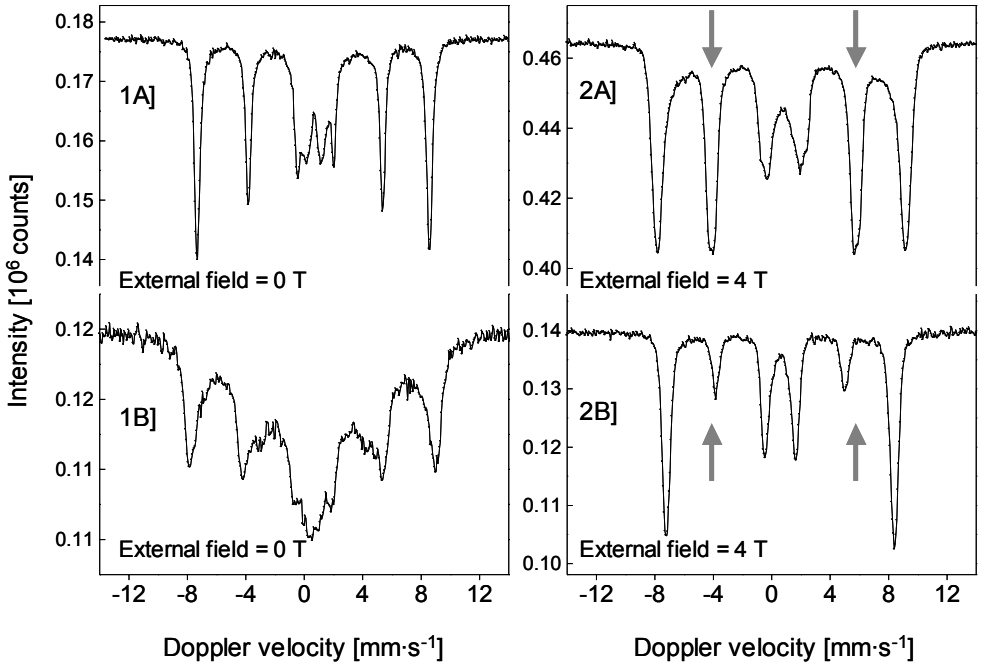

Figure 3.9. *^{57}Mossbauer spectra of* 1A] *Fe-impregnated* ZSM-5 *sample and its corresponding spectrum,* 2A] *under applied external magnetic field; and* 1B] [Fe,Al]MFI $(1:0)_{as}$, *and its spectrum,* 2B] *under applied external magnetic field. All spectra were taken at 4.2 K in high*

In addition, TEM micrographs of all *as*-synthesized [Fe,Al]MFI zeolites show a substantial amount of mesopores with a broad pore size distribution. This finding is unexpected since conventional synthesis of [Fe,Al]MFI zeolites has never mentioned any mesopore formation. Mesopores are normally introduced in the zeolite crystal by dealumination,[34] or desilication.[35] The presence of mesopores improves the efficiency of zeolite-based catalysts by minimising diffusion-related problems. As mesopores are already present in the *as*-synthesized materials, standard calcination to remove the template followed by mild steaming to activate the isolated iron species would be sufficient to obtain catalytically active materials. The

previously required severe steaming in order to create mesopores to overcome diffusion limitations during catalytic processes is no longer necessary and thus sintering of iron species into iron oxide crystalline nanoparticles can be prevented.

3.5. Conclusion

The occurrence of phase segregation and the heterogeneity of the trivalent (iron and aluminum) ion distribution in the [Fe,Al]MFI zeolite pose a problem to the reproducibility of the results, and therefore a lack of control over the synthesis parameters. To circumvent these synthesis problems, a method has been adopted to enhance the homogeneity of the solution gel during hydrothermal treatment to prevent the presence of concentration gradient. By rotating the autoclave, a zeolite with MFI structure and enriched with ^{57}Fe isotope can be prepared with varying elemental composition. A remarkable feature in using the synthesis method described in this chapter is the formation of mesopores as evidenced by TEM. SEM images indicate that the amount of trivalent ions present in the solution gel probably influences the rate of nucleation during hydrothermal synthesis. A high trivalent ion concentration leads to a fast nucleation rate resulting in small MFI crystals agglomerating into large spheres.

^{57}Fe Mössbauer spectroscopy reveals that iron can be incorporated in the zeolite framework with ^{57}Fe loading of 0.6 wt.% or less. Iron in the framework position is present as Fe^{3+} ions that are mostly well distributed in the zeolite framework. On varying the iron content, the decrease in iron concentration in the zeolite lattice leads to the lowering of spin relaxation rates, which indicates highly dispersed iron ions. On the other hand, the increase of aluminum content enhances spin relaxation among neighboring iron ions, which implies that these ions are much closer to each other for samples with high aluminum content.

Acknowledgements

N.M.van der Pers, of the X-Ray Diffraction group at the Laboratory of Materials Science, Delft University of Technology (TUDelft), is gratefully acknowledged for the HR-XRD measurements. Thanks to Dr. J.C. Jansen, of the Pore group at DelftChemTech, TUDelft, for his valuable suggestions particularly in zeolite synthesis. Thanks also to Ing. M.P. Steenvoorden, of the Radiation, Radionuclides & Reactors (R^3) department, TUDelft, for his assistance during Mössbauer measurements, and to Prof. Dr. G. J. Kearley, R^3, TUDelft, for his input

REFERENCES

1. A.A. Battiston, J.H. Bitter, and D.C. Koningsberger, *Catal.Lett.*, 66 (2000) 75.
2. L.J. Lobree, I. Hwang, J.A. Reimer, and A.T. Bell, *Catal.Lett.*, 63 (1999) 233.
3. H.-Y. Chen, T. Voskoboinikov, and W.M.H. Sachtler, *J. Catal.*, 180 (1998) 171.
4. X. Feng and W.K. Hall, *J. Catal.*, 166 (1997) 368.
5. E.M. El-Malki, R.A. van Santen, and W.M.H. Sachtler, *J. Catal.*, 196 (2000) 212.
6. F. Kapteijn, G. Marbán, J. Rodríguez-Mirasol, and J.A. Moulijn, *J. Catal.*, 167 (1997) 256.
7. G.I. Panov, A.K. Uriarte, M.A. Rodkin, and V.I. Sobolev, *Catal. Today*, 41 (1998) 365.
8. G.I. Panov, *Cattech*, 4 (2000) 18.
9. P.P. Notté, *Topics in Catalysis*, 13 (2000) 387.
10. A. Ribera, I.W.C.E. Arends, S. de Vries, J. Pérez-Ramírez, and R.A. Sheldon, *J. Catal.*, 195 (2000) 287.
11. G.I. Panov, V.I. Sobolev, and A.S. Kharitonov, *J. Mol. Catal.*, 61 (1990) 85.
12. B.J. Waller and J.D. Lipscomb, *Chem. Rev.*, 96 (1996) 2625.
13. C. Plog, F. Schueth, V. Goeman, and R. Andorf, *Preparation of a Fe- or Mn-exchanged zeolite*, EP 0867406 (1998).
14. M. Kögel, V.H. Sandoval, W. Schwieger, A. Tissler, and T. Turek, *Catal. Lett.*, 51 (1998) 23.
15. P. Marturano, A. Kogelbauer, and R. Prins, *Stud. Surf. Sci. Catal.*, 125 (1999) 619.
16. R. Joyner and M. Stockenhuber, *J. Phys. Chem. B*, 103 (1999) 5963.
17. M. Kögel, R. Mönnig, W. Schwieger, A. Tissler, and T. Turek, *J. Catal.*, 182 (1999) 470.
18. H.-Y. Chen and W.M.H. Sachtler, *Catal. Today*, 42 (1998) 73.
19. P. Marturano, L. Drozdová, A. Kogelbauer, and R. Prins, *J. Catal.*, 192 (2000) 236.
20. A.A. Battiston, J.H. Bitter, F.M.F. de Groot, A.R. Overweg, O. Stephan, J.A. van Bokhoven, P.J. Kooyman, C.v.d. Spek, G. Vankó, and D.C. Koningsberger, *J. Catal.*, 213 (2003) 251.
21. J. Pérez-Ramírez, F. Kapteijn, G. Mul, and J.A. Moulijn, *Chem. Commun.,* (2001) 693.
22. J. Pérez-Ramírez, G. Mul, F. Kapteijn, J.A. Moulijn, A.R. Overweg, A. Doménech, A. Ribera, and I.W.C.E. Arends, *J. Catal.*, 207 (2002) 113.
23. G. Berlier, G. Spoto, S. Bordiga, G. Ricchiardi, P. Fisicaro, A. Zecchina, I. Rossetti, E. Selli, L. Forni, E. Giamello, and C. Lamberti, *J. Catal.*, 208 (2002) 64.
24. H. van Bekkum, E.M. Flaningen, P.A. Jacobs, and J.C. Jansen, (eds), *Introduction to Zeolite Science and Practice, 2nd Ed.*, Elsevier, Amsterdam (2001).

25. D.M. Kurts, Jr., *Chem. Rev.*, 90 (1990) 585.
26. A. Meagher, V. Nair, and R. Szostak, *Zeolites*, 8 (1988) 3.
27. R.L. Garten, W.N. Delgass, and M. Boudart, *J. Catal.*, 19 (1970) 90.
28. S. Mørup, J.E. Knudsen, M.K. Nielsen, and G. Trumpy, *J. Chem. Phys.*, 76 (1976) 65.
29. E.G. Derouane, S. Detremmerie, Z. Gabelica, and N. Blom, *Appl. Catal.*, 1 (1981) 101.
30. Z. Gabelica, E.G. Derouane, and N. Blom, in: T.E. Whyte, Jr., R.A. Dalla Betta, E.G. Derouane, and Baker, R.T.K. (eds) *Catalytic Materials: Relationship between Structure and Reactivity*, ACS Symp. Ser. No. 248, American Chemical Society, Washington DC (1984) p. 219.
31. G.R. Rossman, *Am. Mineral*, 60 (1975) 698.
32. R.M. Cornell, U. Schwertmann, *The Iron Oxides*, VCH Verlagsgesellschaft mbH, Weinheim, Germany (1996).
33. K.I. Segawa, Y. Chen, J.E. Kubsh, W.N. Delgass, J.A. Dumesic, and W.K. Hall, *J. Catal.*, 76 (1982) 112.
34. M. Müller, G. Harvey, R. Prins, *Micropor. Mesopor. Mater.*, 34 (2000) 135.
35. J.C. Groen, J.C. Jansen, J.A. Moulijn, J. Pérez-Ramírez, *J. Phys. Chem. B*, 108 (2004) 13062.

Chapter 4

Evolution of Iron from Framework Ions to Extra-framework Species in [Fe,Al]MFI Zeolites†

Abstract

The evolution of iron in isomorphously substituted [Fe,Al]MFI zeolites, from framework ions to extra-framework species after a sequence of post-treatment activation, is investigated as a function of iron and aluminum concentrations. Various *as*-synthesized [Fe,Al]MFI zeolites varying in iron (i.e. 0.075 – 0.6 wt.% Fe, while Al was kept constant at 1.1 wt.%) and aluminum (i.e. 0 – 1.1 wt.% Al, while Fe was kept constant at 0.6 wt.%) concentrations were used in the study. Post-treatment activation steps consist of calcination, transformation to H-form, and steam-treatment of the [Fe,Al]MFI zeolites to make them active catalysts in the direct oxidation of benzene to phenol using N_2O as oxidant (BTOP). The physico-chemical state of iron after each post-treatment step was characterized by ^{57}Fe Mössbauer spectroscopy and transmission electron microscopy (TEM), as a complementary technique. In general, the extraction of framework iron to extra-framework position during calcination and transformation to H-form is observed to be more extensive in [Fe,Al]MFI zeolites containing high iron and aluminum concentrations. For [Fe,Al]MFI zeolites varying in iron concentration, steam-treatment leads to complete removal of framework iron to extra-framework positions. Moreover, extra-framework iron is predominantly in the high-spin Fe^{2+} state (ca. 90% based on spectral contribution). On the other hand, for [Fe,Al]MFI zeolites varying in aluminum concentration, removal of framework iron to extra-framework position after steam-treatment appears to be dependent on the aluminum concentration.

† *Parts of this chapter have appeared in:*

- *J.B. Taboada, A.R. Overweg, P.J Kooyman, I.W.C.E. Arends, and G. Mul, J. Catal., 231 (2005) 56-66.*

4.1. Introduction

Iron containing ZSM-5 zeolite, or [Fe,Al]MFI, is widely used for many catalytic reactions.[1-6] Recently, it has attracted attention in the direct oxidation of benzene to phenol using N_2O as oxidant (BTOP).[7-10] Panov *et al.*[7,8] were among the first to report the remarkable catalytic activity and selectivity of [Fe,Al]MFI for the BTOP reaction. They later ascribed the presence of extra-framework iron species stabilized in the zeolite channels to be the catalytically active constituents for the BTOP reaction. It has been proposed that these iron species form *redox* centers that generate a new form of surface oxygen (α-oxygen) from N_2O.[11]

Following the pioneering work of Panov *et al.*,[7,8] Ribera *et al.*[10] studied the BTOP activity of the [Fe,Al]MFI catalyst, which was prepared *via* hydrothermal treatment of isomorphously substituted [Fe,Al]MFI zeolite, followed by calcination and subsequent treatment by steam at 873 K. This catalyst proved to be active in the direct oxidation of benzene to phenol with selectivity >99% and a phenol yield of 27%. A physico-chemical characterization of this catalyst reveals a broad distribution of extra-framework iron species ranging from isolated mononuclear iron to large iron oxide nanoparticles of ca. 2 nm in diameter.[12]

Due to the broad range of extra-framework iron species that is formed after steam-treatment, it is rather difficult to identify which species of extra-framework iron is participating in the BTOP reaction. Thus, to gain insight into the structure-activity relationship of the [Fe,Al]MFI catalyst in the BTOP reaction, it is important to understand the factors affecting the formation of various extra-framework iron species. From isomorphously substituted [Fe,Al]MFI zeolites, the evolution of iron in a sequential post-treatment activation (i.e. (i) calcination, (ii) transformation to H-form, and (iii) steam-treatment) is followed. In this chapter, the migration of iron from framework to extra-framework species after each post-treatment activation of *as*-synthesized [Fe,Al]MFI zeolites is investigated with ^{57}Fe Mössbauer spectroscopy and TEM. In particular, this study focuses on the effect of varying the iron and aluminum concentrations on the formation of iron species in the [Fe,Al]MFI zeolite.

As discussed in the previous chapter, the iron concentration was systematically decreased down to ppm levels to simulate not only the iron impurity in commercial zeolites, but also to prevent the formation of iron oxide nanoparticles, which are known to be inactive in the BTOP reaction.[8] For this, TEM provides an excellent complementary tool to assess the presence of iron oxide nanoparticles. Apart from iron, aluminum was also systematically decreased to low Al and Al-free MFI zeolites to study the influence of aluminum on the state of iron after each post-treatment step.

In figure 4.1 a schematic representation of the sample variation and the post-treatment steps is shown. ^{57}Fe Mössbauer spectroscopy is used as the primary characterization technique to probe the evolution of the physico-chemical state of iron. Thus, all [Fe,Al]MFI zeolites were enriched with ^{57}Fe isotope to enhance the Mössbauer effect.

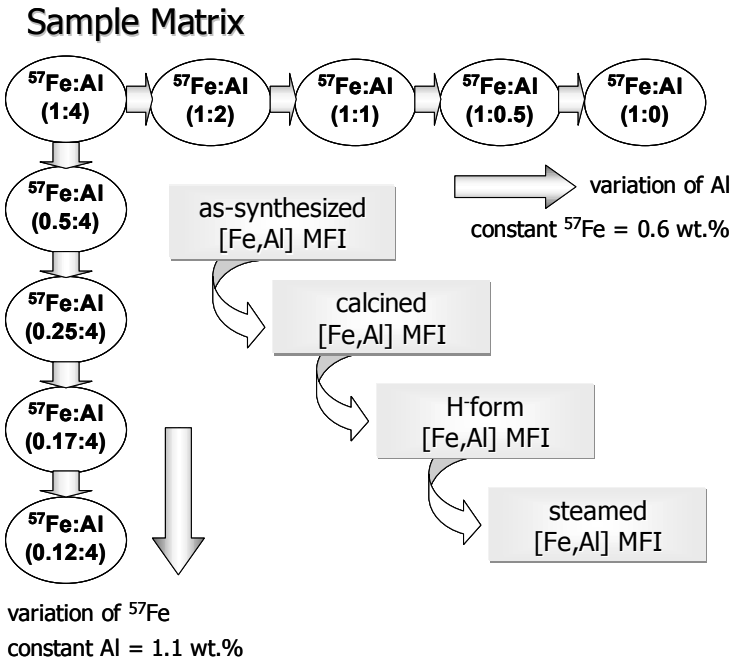

Figure 4.1. *Systematic variation of iron and aluminum concentrations, and the schematic representation of the sequential post-treatment steps to activate the catalyst.*

4.2. Experimental

4.2.1. Activation of [Fe,Al]MFI zeolites

Isomorphously substituted [Fe,Al]MFI zeolites enriched with ^{57}Fe isotope were prepared by hydrothermal synthesis. The iron (0.075 – 0.6 wt.%) and aluminum (0 – 1.1 wt.%) concentrations were varied as described in the previous chapter. To remove the organic template in the *as*-synthesized zeolites, the samples were calcined in air at 823 K for 10 h. The calcined zeolites were then transformed into their H-form by three consecutive overnight exchanges with 0.1 M ammonium nitrate and subsequent calcination at 823 K for 5 h. Afterwards, the samples were heated to 873 K in 30 ml·min^{-1} of He and steam-treated at that temperature for 5 h. For this step, the activation set-up was equipped with a water-filled saturator that was kept at 343 K to obtain a water partial pressure of 300 mbar in 30 ml·min^{-1} flow of He. After steam-treatment, the samples were cooled to room temperature in 30 ml·min^{-1} flow of He. For all samples, calcination and steam-treatment steps were carried out using a temperature ramp of 5 K/min.

4.2.2. Characterization techniques

^{57}Fe Mössbauer spectra were measured on a constant acceleration spectrometer in a triangular mode with a ^{57}Co:Rh source. Spectra for the different [Fe,Al]MFI samples were obtained at 300 K (both in air and in high vacuum, 10^{-6} mbar), and 77 K and 4.2 K in high vacuum. The spectra were fitted with Lorentzian-shaped lines to obtain the Mössbauer parameters (i.e. isomer shift [IS], quadrupole splitting [QS], and hyperfine field [HF]). Isomer shift values are reported relative to sodium nitroprusside (SNP). The magnetically split lines were fitted with several components to simulate a distribution of hyperfine fields. Thus, the hyperfine field reported here is the average value.

Transmission electron microscopy (TEM) was performed using a Philips CM30UT electron microscope with a field emission gun as the source of electrons operated at 300 kV. Samples were mounted on Quantifoil® carbon polymer supported on a copper or gold grid by placing a few droplets of a suspension of ground sample in ethanol on the grid, followed by drying at ambient conditions.

4.3. Results

For discussion purposes, the *as*-synthesized, calcined, H-form, and steam-treated [Fe,Al]MFI samples are denoted by the subscripts '*as*', '*cal*', '*H*', and '*stm*', respectively. The given ratio in parenthesis indicates the relative molar iron to aluminum (Fe:Al) ratio (*see table 3.2, Chapter 3 for details*).

4.3.1. Calcination of [Fe,Al]MFI zeolites

Calcination of the [Fe,Al]MFI $(1{:}4)_{as}$ to remove the template results in small but significant changes in the zeolite material as illustrated in the Mössbauer spectra (figures 4.2A-C). The Mössbauer spectrum of [Fe,Al]MFI $(1{:}4)_{cal}$ taken at 300 K in air (figure 4.2A) exhibits a slightly wider quadrupole splitting compared to the spectrum of the *as*-synthesized sample recorded under the same conditions (*refer to figure 3.5A, chapter 3*). This is most likely due to an enhanced spin-spin interaction between Fe-ions as a result of reduced Fe-Fe ion distances. Therefore, this suggests that a small fraction of framework iron has already migrated to extra-framework positions during calcination, allowing it to move freely and closer to other iron ions, both in the framework and extra-framework positions.

Under high-vacuum (10^{-6} mbar) condition, figure 4.2B, the high-spin Fe^{3+} doublet exhibits an increase in the quadrupole splitting and an asymmetry in line shape is observed. These changes can be interpreted as an increase in interaction between the extra-framework Fe^{3+} ions and the zeolite lattice. It should be noted that all samples under investigation were

unavoidably exposed to air after calcination for considerable time, i.e. days to weeks. Thus, evacuation to high-vacuum leads to the removal of physisorbed water from the zeolite pores which gives rise to an increased electrostatic interaction between the positively charged ferric ions and the negatively charged zeolite lattice.

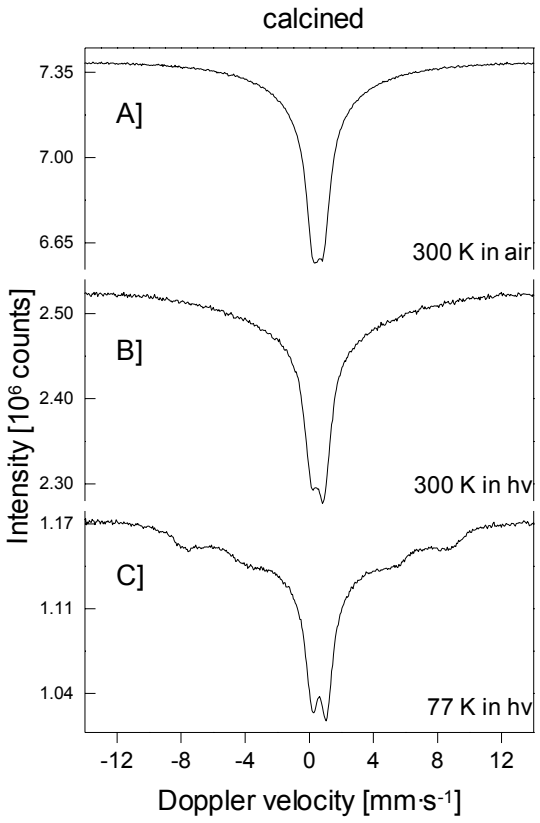

Figure 4.2. *^{57}Fe Mössbauer Spectra of* [Fe,Al]MFI (1:4)$_{cal}$ *taken at different conditions. hv (high vacuum = 10^{-6} mbar)*

At 77 K (figure 4.2C), the Mössbauer spectrum exhibits a well-resolved doublet together with a broad magnetically split component. Compared to the spectrum of [Fe,Al]MFI (1:4)$_{as}$ taken at the same condition (*refer to figure 3.5C, chapter 3*), the linewidth of the doublet in the calcined sample is broader and the quadrupole splitting is higher (i.e. 0.91 mm·s^{-1}, which is typical for octahedrally coordinated extra-framework Fe^{3+} ions in the high-spin state)[13,14]. The presence of the broad magnetic feature at 77 K is attributed to paramagnetic hyperfine splitting of isolated Fe^{3+} ions. The other possibility, that of the presence of very small iron oxide particles just below the superparamagnetic blocking temperature,[15] was ruled out since no trace of any iron oxide related phase was observed with TEM (i.e. for [Fe,Al]MFI (1:4)$_{cal}$ and also for the other calcined samples, see figure 4.3).

In addition, the broad magnetic component has a hyperfine field of 49.2T, which is lower compared to the value obtained for the *as*-synthesized zeolite (53.1T). This lowering of hyperfine field, which was also observed by Meagher *et al*.[13] after calcination, can be attributed to reduced paramagnetic Fe-Fe ion distances, further affirming the removal of a fraction of the paramagnetic ferric ions from framework to extra-framework positions.

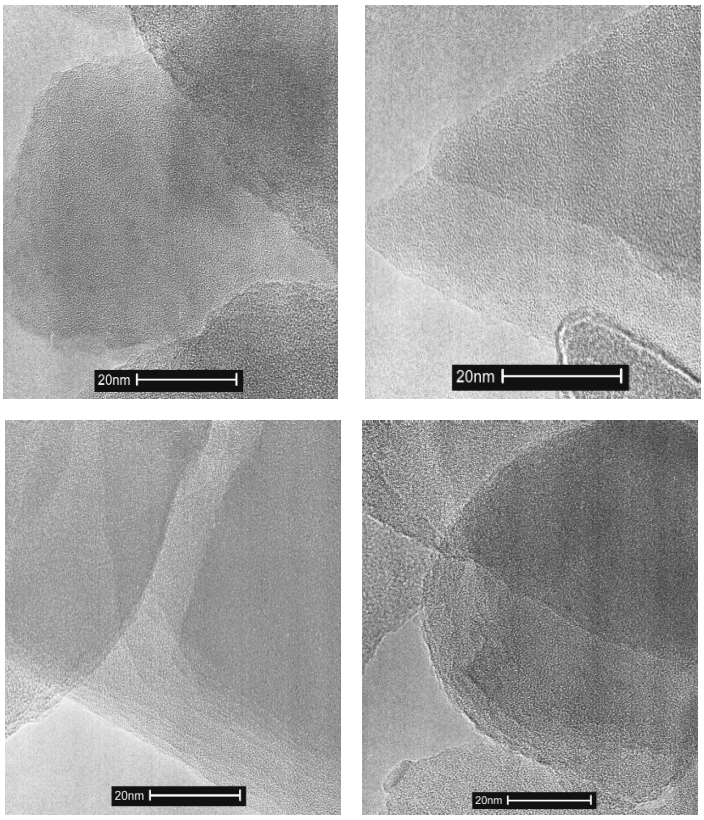

Figure 4.3. *Typical TEM micrographs of the calcined* [Fe,Al]MFI *zeolites taken at high magnification:* (top left) [Fe,Al]MFI $(1:4)_{cal}$, (top right) [Fe,Al]MFI $(0.5:4)_{cal}$, (bottom left) [Fe,Al]MFI $(1:2)_{cal}$, *and* (bottom right) [Fe,Al]MFI $(1:0)_{cal}$.

These spectral changes due to a partial removal of framework iron to extra-framework positions upon calcination are also observed for other samples with different iron and aluminum concentrations. However, when the 77 K spectra of the different calcined samples are plotted together (figure 4.4), the increase in intensity of the central line relative to that of the broad magnetic component is observed to be more prominent for samples with high iron and aluminum concentrations. Figure 4.5 illustrates the increase in intensity ratio – i.e. the ratio of the central line to the broad magnetic component (based on spectral contribution) as a function of iron (figure 4.5A) and aluminum (figure 4.5B) concentrations. The increase in intensity ratio with the increase in both iron and aluminum content suggest that iron is most likely to migrate from framework to extra-framework positions during calcination if the framework iron concentration is high, and in the presence of aluminum.

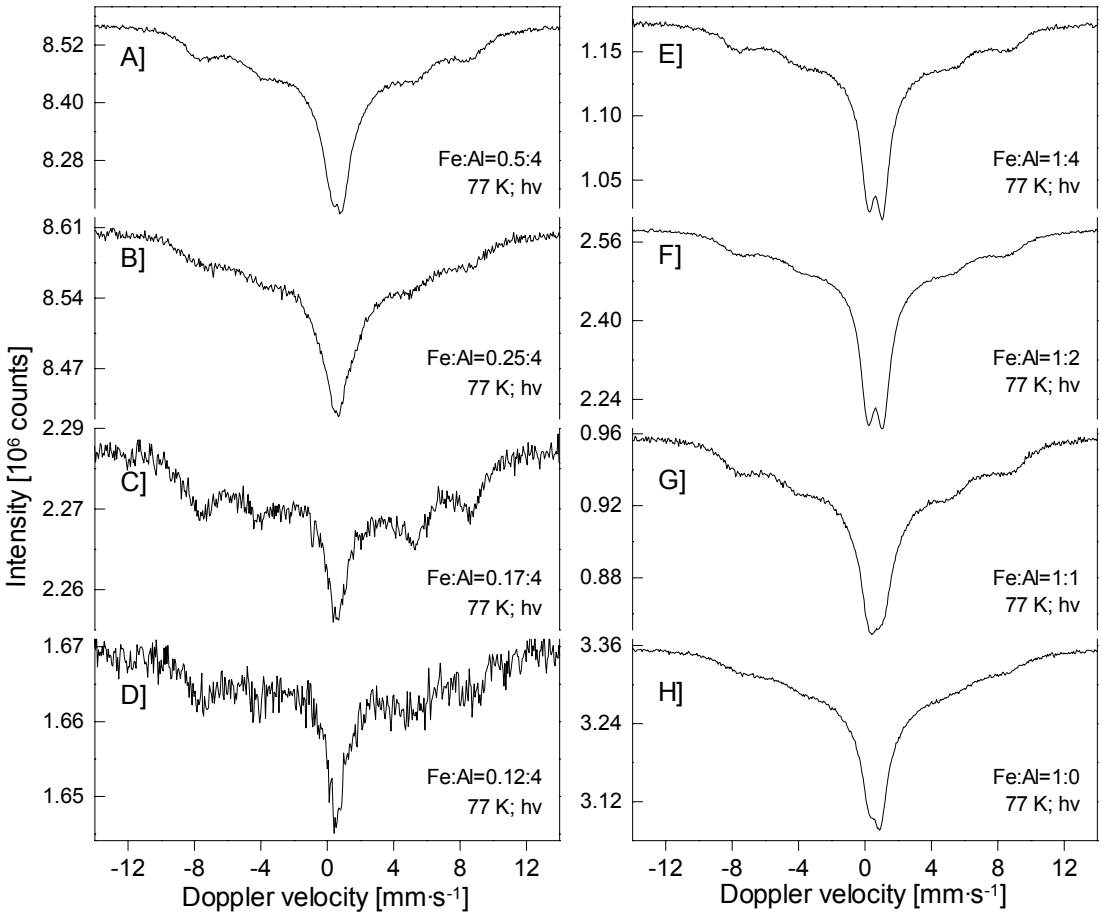

Figure 4.4. *^{57}Fe Mössbauer spectra of calcined* [Fe,Al]MFI *zeolites of varying iron* (A-E) *and aluminum* (E-H) *concentrations taken at 77 K in hv* (*high vacuum = 10^{-6} mbar*).

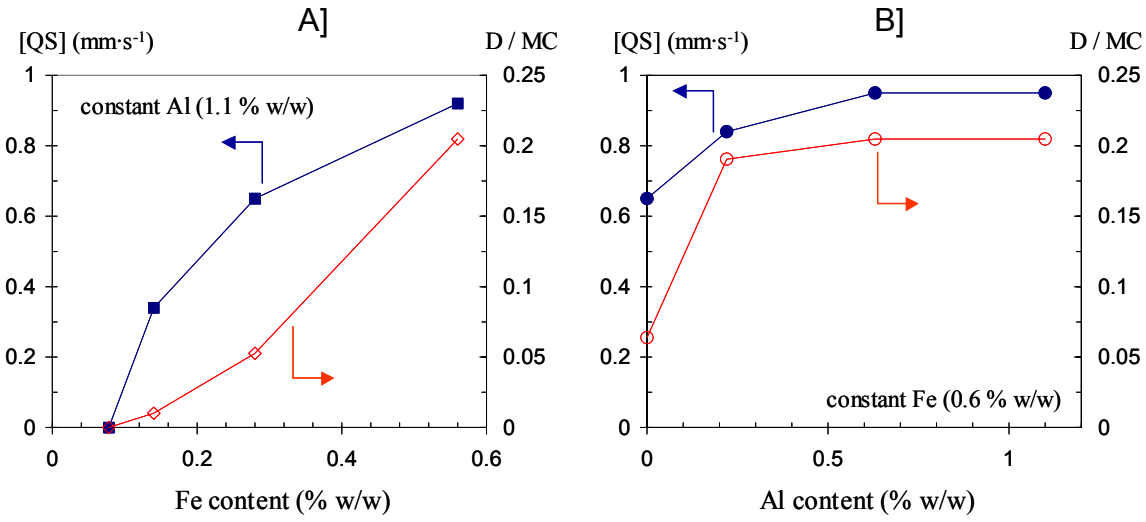

Figure 4.5. *Relative increase in quadrupole splitting* (■ and ●) *and the intensity ratio* (◊ and ○) *of the quadrupole doublet to the magnetic component* (D/MC) *as a function of* A] *iron and* B] *aluminum concentrations in the calcined* [Fe,Al]MFI *zeolites taken at 77 K in 10^{-6} mbar.*

Table 4.1. ^{57}Fe Mössbauer hyperfine parameters and relative intensities of the iron species in [Fe,Al]MFI (1:4) after different post-treatments.

sample	spectrum no.	condition	IS **(mm·s^{-1})**	QS **(mm·s^{-1})**	HF **(T)**	RI **(%)**	oxidation state
[Fe,Al]MFI	**4.2 A**	300K in air	0.54	--	--	59	Fe^{3+}
$(1:4)_{cal}$	**4.2 B**	300K in hv	0.58	--	--	66	Fe^{3+}
			0.54	0.87	--	34	Fe^{3+}
	4.2 C	77K in hv	0.67	0.91		17	Fe^{3+}
			0.66	--	49.2	83	Fe^{3+}
[Fe,Al]MFI	**4.6 A**	300K in air	0.54	--	--	76	Fe^{3+}
$(1:4)_{H}$			0.67	0.96		24	Fe^{3+}
	4.6 B	300K in hv	0.54	--	--	44	Fe^{3+}
			0.61	1.09	--	56	Fe^{3+}
	4.6 C	77K in hv	0.69	1.26	--	44	Fe^{3+}
			1.68	2.95	--	7	Fe^{2+}
			0.77	--	49.8	49	Fe^{3+}
[Fe,Al]MFI	**4.9 A**	300K in air	0.56	0.80	--	23	Fe^{3+}
$(1:4)_{stm}$			1.48	1.92	--	77	Fe^{2+}
	4.9 B	300K in hv	0.56	0.80	--	17	Fe^{3+}
			1.46	2.21	--	83	Fe^{2+}
	4.9 B	77K in hv	0.75	1.0	--	9	Fe^{3+}
			1.61	3.04	--	88	Fe^{2+}
			1.16	--	51.1	3	Fe^{3+}

IS*(isomer shift),* QS*(quadrupole splitting),* HF*(hyperfine field),* RI*(relative intensity);*
all IS values are relative to SNP
hv*(high vacuum at 10^{-6} mbar)*

4.3.2. H-form [Fe,Al]MFI zeolites

For [Fe,Al]MFI $(1:4)_H$, the Mössbauer spectrum taken at 300 K in air (figure 4.6 A) shows a broad asymmetric doublet that is fitted with two components – a quadrupole doublet and a broad component. Based on spectral parameters (table 4.1), the quadrupole doublet is attributed to octahedrally coordinated Fe^{3+} ions. The spectral parameters also indicate that at least a quarter of the iron in the [Fe,Al]MFI $(1:4)_H$ have migrated from tetrahedrally coordinated framework to octahedrally coordinated extra-framework positions. The broad component, which partially resolves into a magnetically split feature at low temperature (77 K), is attributed to paramagnetic isolated Fe^{3+} ions that are most likely in both framework and extra-framework positions. The presence of superparamagnetic iron oxide nanoparticles, which can generate similar spectral characteristics, was ruled out, as these nanoparticles were not detected by TEM (figure 4.7).

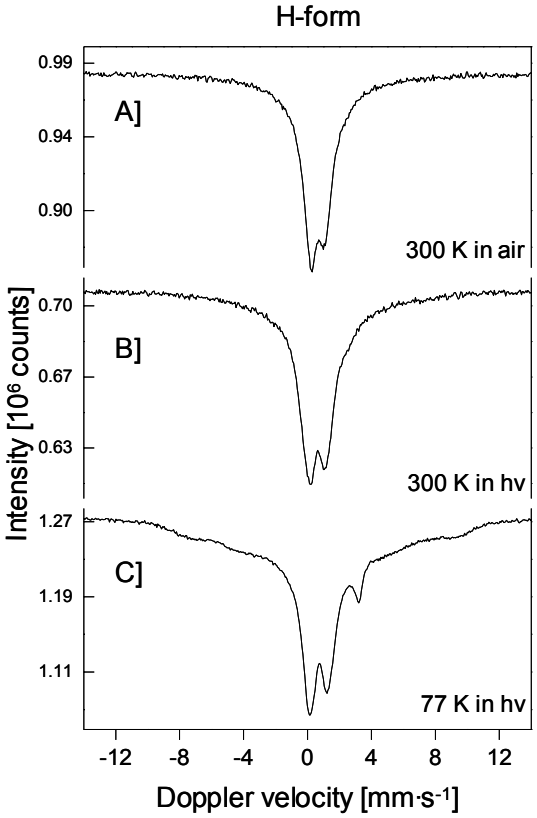

Figure 4.6. *^{57}Fe Mössbauer Spectra of* [Fe,Al]MFI (1:4)$_H$ *taken at different conditions. hv (high vacuum = 10^{-6} mbar)*

At 300 K under high vacuum (figure 4.6B), the Mössbauer spectrum shows a well-resolved doublet with an increased quadrupole splitting. Similar to the situation of the calcined zeolites (*vide supra*), but much more prominent here, evacuation to high vacuum leads to an increase in recoilfree fraction of the extra-framework Fe^{3+} ions. This is due to the removal of physisorbed water (as evident by the increase in total resonant absorption area from 6.45 to 8.49 units).

At 77 K (figure 4.6C), the spectrum is composed of a well-resolved high-spin Fe^{2+} doublet (IS = 1.68 mm·s^{-1}; QS = 2.95 mm·s^{-1}) together with the high-spin Fe^{3+} doublet and a broad magnetically split feature. Due to low Debye temperature of the high-spin Fe^{2+} component, its contribution is usually not observed at room temperature measurements. Since it is known that framework iron is difficult to reduce,[16] therefore the presence of Fe^{2+} ions are attributed to extra-framework species.

For samples with varying iron concentration (figures 4.8E,A-D), the spectral contribution of the high-spin Fe^{3+} doublet is observed to be largest for [Fe,Al]MFI (1:4)$_H$. This indicates that for samples with high iron concentration, a significant removal of framework iron ions to

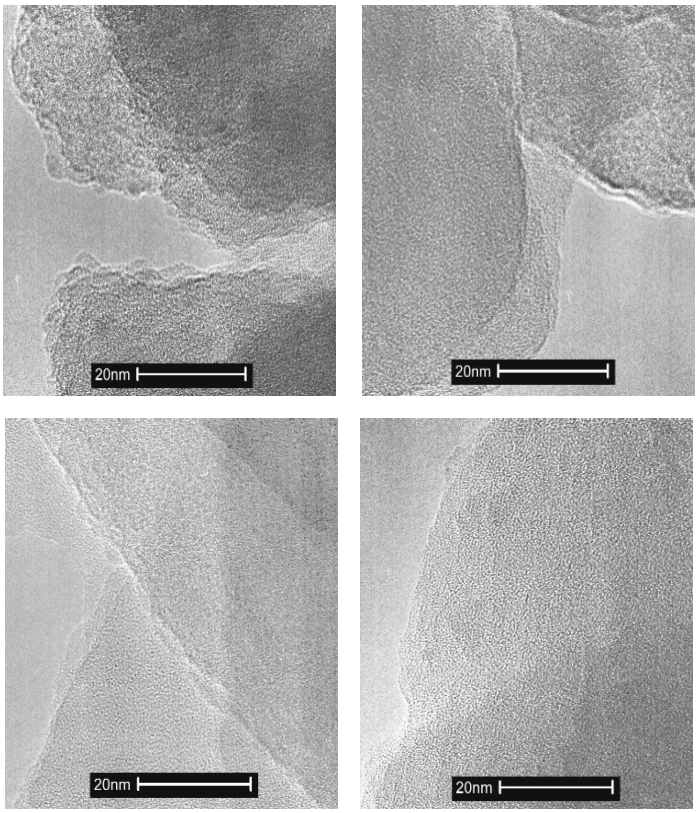

Figure 4.7. *Typical TEM micrographs of the H-form* [Fe,Al]MFI *zeolites taken at high magnification: (top left)* [Fe,Al]MFI $(1:4)_{cal}$, *(top right)* [Fe,Al]MFI $(0.25:4)_{cal}$, *(bottom left)* [Fe,Al]MFI $(1:2)_{cal}$, *and (bottom right)* [Fe,Al]MFI $(1:0)_{cal}$,

extra-framework positions is obtained. On the other hand, for samples with low iron concentrations (i.e., Fe:Al = 0.17:4 and Fe:Al = 0.12:4, figures 4.8C-D, respectively) the spectral contribution of the high-spin Fe^{3+} doublet (i.e. the doublet with a quadrupole splitting close to 1 $mm \cdot s^{-1}$) decreased significantly such that only a narrow central line is observed. The decrease in ratio between the extra-framework high-spin Fe^{3+} doublet to the framework Fe^{3+} broad singlet in the Mössbauer spectrum indicates that iron is likely to remain in the framework position for samples with low iron concentration. For Fe^{2+} ions, the relative intensity of the high-spin Fe^{2+} doublet compared to the high-spin Fe^{3+} doublet appears to increase with the decrease in iron concentration (table 4.2). This suggests that a high concentration of iron would likely lead to clustering of extra-framework iron species, whereas, a low concentration of iron would lead to highly dispersed extra-framework iron species that are easily reduced to their Fe^{2+} state.

For the set of samples with varying aluminum, the spectral intensity of the high-spin Fe^{2+} doublet diminishes with the decrease in aluminum concentration (figures 4.8E-H), and is not

observed in the [Fe,Al]MFI $(1:0)_H$ sample that does not contain aluminum at all. It seems, therefore, that aluminum plays a role in the formation of extra-framework Fe^{2+} species.

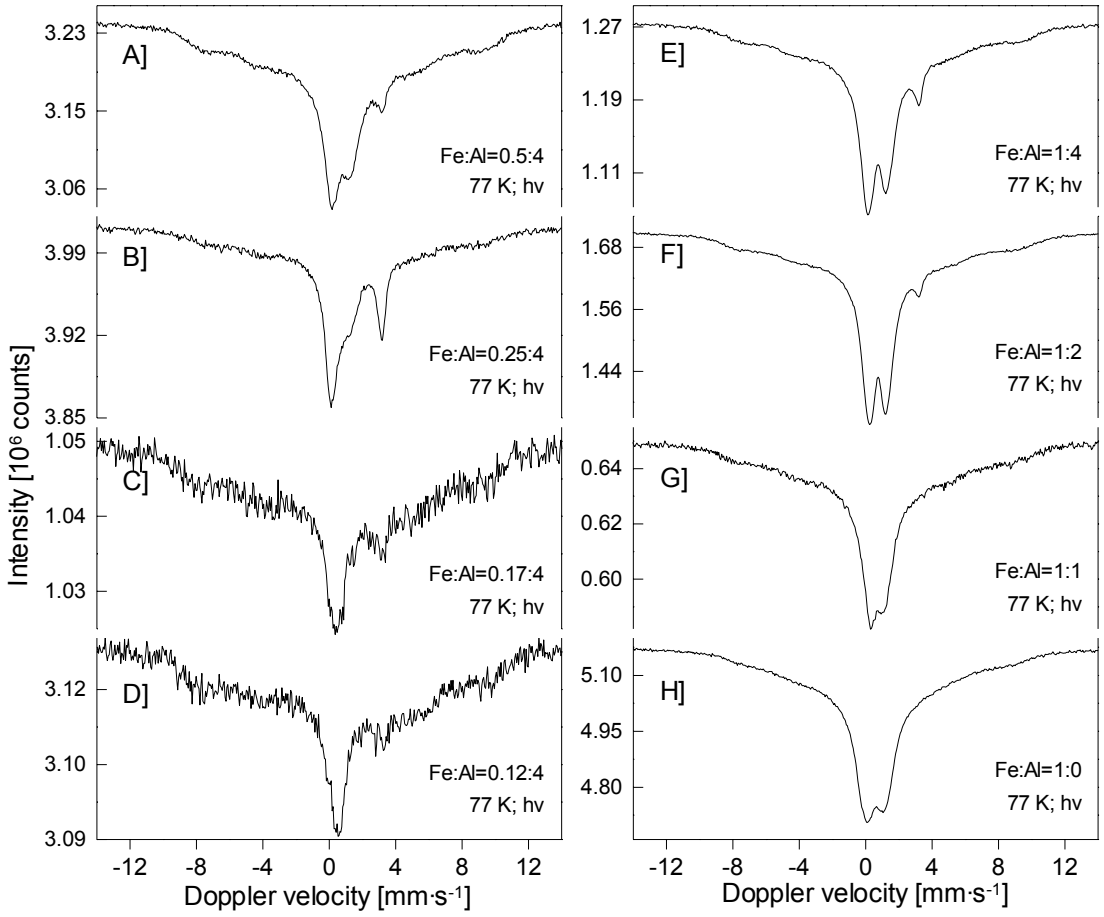

Figure 4.8. *^{57}Fe Mössbauer spectra of* [Fe,Al]MFI *zeolites in H-form with varying iron* (A-E) *and aluminum* (E-H) *concentrations taken at 77 K in hv* (*high vacuum = 10^{-6} mbar*).

Table 4.2. ^{57}Fe Mössbauer hyperfine parameters and relative intensities of the iron species in H-form [Fe,Al]MFI zeolites.

sample	spectrum no.	condition	IS **(mm·s^{-1})**	QS **(mm·s^{-1})**	HF **(T)**	RI **(%)**	oxidation state
[Fe,Al]MFI	**4.8 E**	77 K in hv	0.69	1.26	--	44	Fe^{3+}
$(1:4)_H$			1.68	2.95	--	7	Fe^{2+}
			0.77	--	49.8	49	Fe^{3+}
[Fe,Al]MFI	**4.8 A**	77 K in hv	0.72	1.17	--	34	Fe^{3+}
$(1:8)_H$			1.64	2.99	--	8	Fe^{2+}
			0.85	--	51.4	58	Fe^{3+}
[Fe,Al]MFI	**4.8 B**	77 K in hv	0.70	1.00	--	35	Fe^{3+}
$(1:16)_H$			1.62	3.06	--	20	Fe^{2+}
			0.87	--	49.6	45	Fe^{3+}
[Fe,Al]MFI	**4.8 C**	77 K in hv	0.52	--	--	7	Fe^{3+}
$(1:24)_H$			1.56	3.05	--	11	Fe^{2+}
			0.60	--	52.0	82	Fe^{3+}
[Fe,Al]MFI	**4.8 D**	77 K in hv	0.54	--	--	15	Fe^{3+}
$(1:32)_H$			1.60	3.20	--	5	Fe^{2+}
			0.77	--	52.2	80	Fe^{3+}
[Fe,Al]MFI	**4.8 F**	77 K in hv	0.71	1.14	--	45	Fe^{3+}
$(1:2)_H$			1.75	2.82	--	5	Fe^{2+}
			0.72	--	51.0	50	Fe^{3+}
[Fe,Al]MFI	**4.8 G**	77 K in hv	0.56	--	--	30	Fe^{3+}
$(1:1)_H$			0.75	0.95	--	18	Fe^{3+}
			0.68	--	47.7	52	Fe^{3+}
[Fe,Al]MFI	**4.8 H**	77 K in hv	0.57	1.24	--	51	Fe^{3+}
$(1:0)_H$			0.66	--	--	49	Fe^{3+}

IS*(isomer shift),* QS*(quadrupole splitting),* HF*(hyperfine field),* RI*(relative intensity);*
all IS values are relative to SNP
hv*(high vacuum at 10^{-6} mbar)*

4.3.3. Steam-treated [Fe,Al]MFI zeolites

For the samples varying in iron content, steam-treatment leads to [Fe,Al]MFI catalysts that contain almost exclusively Fe^{2+} ions (figures 4.9A-D). All spectra were fitted with a high-spin Fe^{2+} doublet (IS =1.67 mm·s^{-1}, QS = 3.19 mm·s^{-1}), ca. 90% based on spectral contribution (table 4.3).

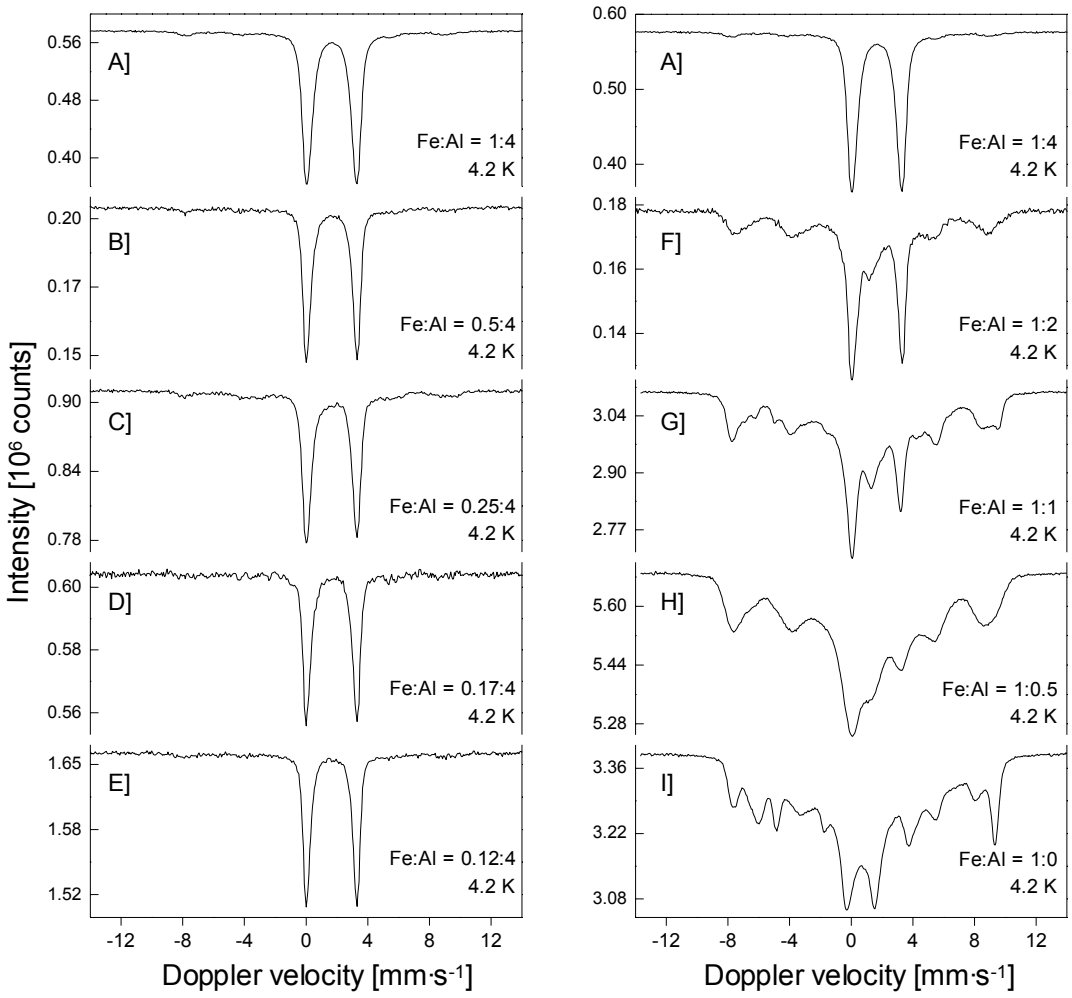

Figure 4.9. *^{57}Fe Mössbauer spectra of steam-treated [Fe,Al]MFI zeolites of varying iron* (A-E) *and aluminum* (A,F-I) *concentrations taken at 4.2 K in hv* (*high vacuum = 10^{-6} mbar*).

Although steam-treatment of [Fe,Al]MFI zeolites varying in iron concentration leads to the formation of extra-framework iron in divalent state, steam-treatment of [Fe,Al]MFI zeolites varying in aluminum concentration reveals a distinct influence of aluminum on the oxidation state of iron. Figures 4.9A,F-I show the spectra of steam-treated [Fe,Al]MFI samples varying in aluminum concentration taken at 4.2 K. For [Fe,Al]MFI (1:2)$_{stm}$, containing roughly 50% less aluminum, the spectrum is a mixture of a high-spin Fe^{2+} doublet (IS =1.66 mm·s^{-1}, QS = 3.26 mm·s^{-1}), a high-spin Fe^{3+} doublet (IS = 0.88 mm·s^{-1}, QS = 0.92 mm·s^{-1}), and a broad magnetic feature with a hyperfine field of 50.1 T that is attributed to iron species in the trivalent state. The spectral contribution of the divalent iron decreases further upon lowering the aluminum content in [Fe,Al]MFI (1:1)$_{stm}$ and [Fe,Al]MFI (1:0.5)$_{stm}$, respectively. However, it is noteworthy to mention that the spectra particularly of low to no aluminum samples (figures 4.9G-I) generate a complicated magnetic part of the spectrum that is not fully understood at the moment, and fitting them proves to be very difficult.

Table 4.3. ^{57}Fe Mössbauer hyperfine parameters and relative intensities of the iron species in steam-treated [Fe,Al]MFI zeolites.

sample	spectrum no.	condition	IS **(mm·s^{-1})**	QS **(mm·s^{-1})**	HF **(T)**	RI **(%)**	oxidation state
[Fe,Al]MFI	**4.9 A**	4.2 K in hv	1.67	3.19	--	92	Fe^{2+}
$(1:4)_{stm}$			0.96	--	52.1	8	Fe^{3+}
[Fe,Al]MFI	**4.9 B**	4.2 K in hv	1.67	3.24	--	90	Fe^{2+}
$(0.5:4)_{stm}$			0.98	--	52.0	10	Fe^{3+}
[Fe,Al]MFI	**4.9 C**	4.2 K in hv	1.67	3.23	--	83	Fe^{2+}
$(0.25:4)_{stm}$			0.92	--	52.0	17	Fe^{3+}
[Fe,Al]MFI	**4.9 D**	4.2 K in hv	1.66	3.23	--	94	Fe^{2+}
$(0.17:4)_{stm}$			0.92	--	49.5	6	Fe^{3+}
[Fe,Al]MFI	**4.9 E**	4.2 K in hv	1.65	3.24	--	95	Fe^{2+}
$(0.12:4)_{stm}$			0.92	--	52.0	5	Fe^{3+}
[Fe,Al]MFI	**4.9 F**	4.2 K in hv	0.88	0.92	--	16	Fe^{3+}
$(1:2)_{stm}$			1.66	3.26	--	37	Fe^{2+}
			0.66	--	50.1	47	Fe^{3+}

IS*(isomer shift),* QS*(quadrupole splitting),* HF*(hyperfine field),* RI*(relative intensity);*
all IS values are relative to SNP
hv*(high vacuum at 10^{-6} mbar)*

To further investigate the different iron species formed in steam-treated [Fe,Al]MFI zeolites varying in aluminum concentration without the presence of the complex magnetic contributions, we take a look at their spectra recorded at room temperature. Figure 4.10 shows the measurements taken at ambient pressure and under high vacuum conditions. A summary of the spectral parameters is reported in table 4.4. At room temperature in air, the spectrum of [Fe,Al]MFI $(1:4)_{stm}$ is dominated by a doublet with a high quadrupole splitting typical of high-spin Fe^{2+} species. The quadrupole splitting of this high-spin Fe^{2+} doublet is small compared to its corresponding quadrupole splitting at 4.2 K (*see table 4.3*). This temperature dependence of the quadrupole splitting of high-spin Fe^{2+} doublets is often observed due to Jahn-Teller distortion to lower symmetry and lower energy, thereby removing the degeneracy of t_{2g} and e_g orbitals.[17]

The high-spin Fe^{2+} doublet taken at room temperature is observed to progressively decrease in contribution for samples with decreasing aluminum concentration, similar to the trend observed for the spectra taken at 4.2 K. The decrease in contribution of the high-spin Fe^{2+}

doublet as the iron concentration is systematically lowered is accompanied by the presence of a high-spin Fe^{3+} doublet that further translates into a broad singlet-like line for samples with very low iron loadings. This broad singlet is most likely a summation of quadrupole doublets with small quadrupole splitting. In addition, a broad component in these spectra ($\pm$ 10 mm·s^{-1}), which is not observed in samples with high aluminum content, is attributed to paramagnetic high-spin Fe^{3+} ions both in the framework and extra-framework positions.

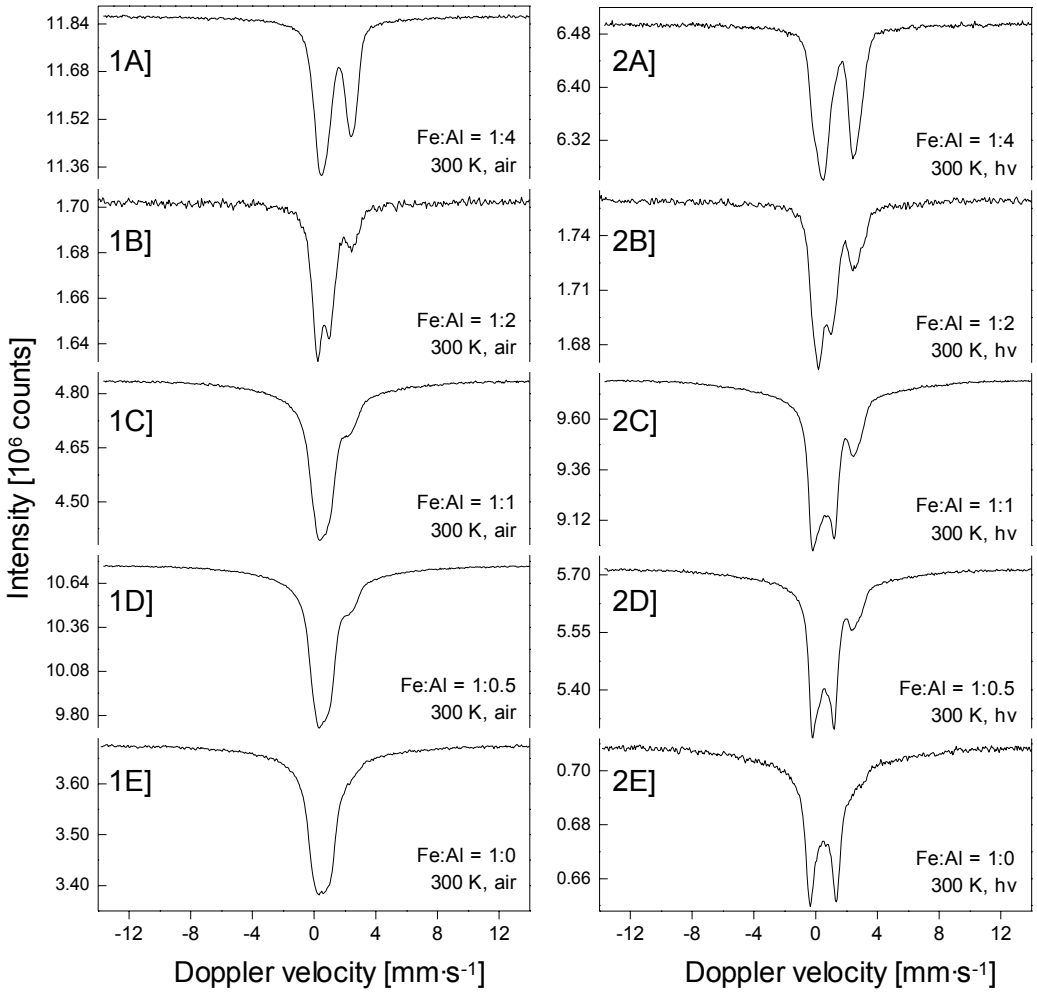

Figure 4.10. *^{57}Fe Mössbauer spectra of steam-treated* [Fe,Al]MFI *zeolites varying in aluminum concentration:* (left column) *taken at 300 K in air, and* (right column) *taken at 300 K in hv (high vacuum = 10^{-6} mbar).*

Table 4.4. ^{57}Fe Mössbauer hyperfine parameters and relative intensities of iron species in steam-treated [Fe,Al]MFI zeolites with varying aluminum concentration.

sample	spectrum no.	condition	IS ($mm \cdot s^{-1}$)	QS ($mm \cdot s^{-1}$)	RI (%)	oxidation state
[Fe,Al]MFI $(1:4)_{stm}$	**4.10 1A**	300 K in air	1.38	2.12	77	Fe^{2+}
			0.83	0.32	23	Fe^{3+}
	4.10 2A	300 K in hv	1.46	1.85	47	Fe^{2+}
			1.50	2.70	36	Fe^{2+}
			0.40	1.11	17	Fe^{3+}
[Fe,Al]MFI $(1:2)_{stm}$	**4.10 1B**	300 K in air	1.43	2.15	29	Fe^{2+}
			0.61	0.85	71	Fe^{3+}
	4.10 2B	300 K in hv	1.46	2.30	42	Fe^{2+}
			0.56	1.03	58	Fe^{3+}
[Fe,Al]MFI $(1:1)_{stm}$	**4.10 1C**	300 K in air	1.43	1.98	13	Fe^{2+}
			0.56	0.80	57	Fe^{3+}
			0.60†		30	Fe^{3+}
	4.10 2C	300 K in hv	1.50	2.21	25	Fe^{2+}
			0.50	1.31	49	Fe^{3+}
			0.60†		26	Fe^{3+}
[Fe,Al]MFI $(1:0.5)_{stm}$	**4.10 1D**	300 K in air	1.45	2.04	11	Fe^{2+}
			0.55	0.82	63	Fe^{3+}
			0.60†		26	Fe^{3+}
	4.10 2D	300 K in hv	1.50	2.19	21	Fe^{2+}
			0.50	1.28	53	Fe^{3+}
			0.60†		26	Fe^{3+}
[Fe,Al]MFI $(1:0)_{stm}$	**4.10 1E**	300 K in air	1.48	2.03	4	Fe^{2+}
			0.53	0.88	71	Fe^{3+}
			0.60†		25	Fe^{3+}
	4.10 2E	300 K in hv	1.48	2.99	5	Fe^{2+}
			0.50	1.71	56	Fe^{3+}
			0.60†		39	Fe^{3+}

IS*(isomer shift),* QS*(quadrupole splitting),* HF*(hyperfine field),* RI*(relative intensity);*
†*broad component (± 10 $mm \cdot s^{-1}$)*
all IS values are relative to SNP
hv*(high vacuum at 10^{-6} mbar)*

Under high vacuum condition, this singlet changes into a doublet with an isomer shift typical of high-spin Fe^{3+} species. The quadrupole splitting is unusually large (ca. 1.7 $mm \cdot s^{-1}$) for a high-spin Fe^{3+} doublet, and indicates that these extra-framework Fe^{3+} species are in highly asymmetric environment. The change in the Mössbauer spectra upon high vacuum treatment is attributed to the removal of weakly adsorbed ligands (e.g. H_2O), which results in coordinatedly highly unsaturated extra-framework ferric ions. This implies that these ferric ions are probably surface species that are highly dispersed.

Furthermore, a weak shoulder is observed for [Fe,Al]MFI $(1:0)_{stm}$ which can be fitted with a second doublet that is typical for high-spin Fe^{2+} species. Interestingly, this high-spin Fe^{2+} doublet is not observed in the spectrum measured at 4.2 K (figure 4.9I). This suggests that the high-spin Fe^{2+} species in the aluminum-free [Fe,Al]MFI $(1:0)_{stm}$ zeolites could be magnetically coupled with the high-spin Fe^{3+} species at 4.2 K. However, due to the complexity of the magnetic part of the spectrum at 4.2 K, we were not able to deconvolute the spectrum.

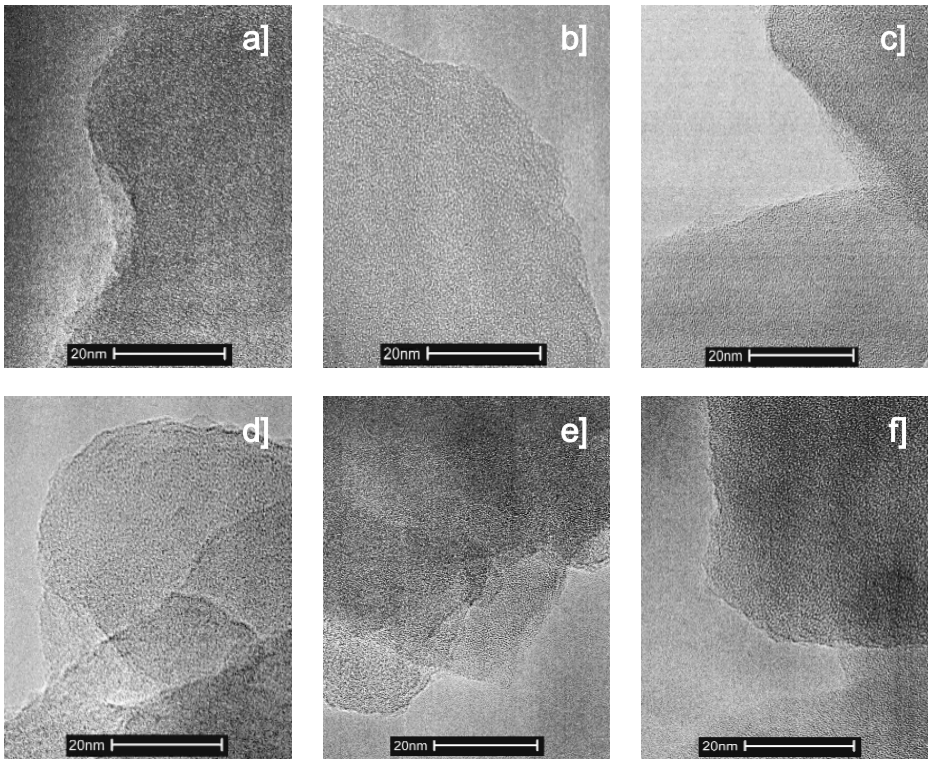

Figure 4.11. *TEM micrographs of steam-treated* [Fe,Al]MFI *zeolites:* a) [Fe,Al]MFI $(0.12:4)_{stm}$, b) [Fe,Al]MFI $(0.25:4)_{stm}$, c) [Fe,Al]MFI $(0.5:4)_{stm}$, d) [Fe,Al]MFI $(1:4)_{stm}$, e) [Fe,Al]MFI $(1:2)_{stm}$, *and* f) [Fe,Al]MFI $(1:0)_{stm}$.

Transmission Electron Microscopy (TEM) shows that no large Fe-oxide particles are present in all steamed samples, evident by the absence of any iron-related phase at high-magnification (figure 4.11). This confirms the notion that the type of magnetic behavior observed in Mössbauer spectroscopy in this study is due to paramagnetic hyperfine splitting and not of ferromagnetism exhibited by iron oxide nanoparticles.

4.4. Discussion

4.4.1. Evolution of Iron

Detailed Mössbauer study of the starting *as*-synthesized [Fe,Al]MFI zeolites is described in the previous chapter and confirms that iron in the zeolite is present as ferric ions that are tetrahedrally coordinated in isolated framework position in the zeolite lattice. From the changes observed in the Mössbauer spectra, it can be inferred that calcination of the *as*-synthesized zeolite at 823 K induces a small fraction of framework iron to migrate to extra-framework positions. The extraction of iron upon calcination was also observed by Pérez-Ramírez *et al*.[12] However, since the average isomer shift (0.54 $mm \cdot s^{-1}$) of the calcined sample recorded at room temperature in air is close to the isomer shift of the *as*-synthesized sample (0.52 $mm \cdot s^{-1}$), majority of the iron ions (i.e. >80%, based on 77 K spectra of [Fe,Al]MFI $(1{:}4)_{cal}$) are still tetrahedrally coordinated in isolated framework positions.

Comparison of the spectral contribution of the high-spin Fe^{3+} doublets and quadrupole splittings obtained from the calcined samples varying in iron content, it is apparent that framework iron is inclined to migrate to extra-framework position during calcination if the molar Fe:Al ratio is relatively low. The Si-O-Al framework bonds have been reported to be stronger than that of the Si-O-Fe.[18] Thus, framework iron in low Fe:Al configuration is likely to destabilize upon calcination. On the other hand, the migration of iron is suppressed if the molar Fe:Al ratio is relatively high. This has been observed in the samples varying in aluminum content. Framework iron has been shown to be more stable from migration in Fe-silicalite (i.e. aluminum-free MFI) than in ZSM-5 (i.e. aluminum-containing MFI) zeolites.[12] Thus, a decrease in aluminum content would likely approach the properties of the Fe-silicalite, and therefore less extraction of iron is observed.

Transformation of the calcined zeolites to their H-form induces further changes in the Fe-species in the zeolite. It is evident in the Mössbauer spectra and in the increase in total resonant absorption that the transformation leads to an additional migration of Fe^{3+} framework ions to extra-framework positions, of which some are present in the reduced Fe^{2+} state. These changes are likely induced during the second calcination treatment following three consecutive ion exchanges, which transforms the Na-form MFI zeolites to its H-form.

The additional calcination treatment, thus, destabilizes the framework iron leading to extraction and clustering of extra-framework species.

The final activation step involves the steam-treatment of [Fe,Al]MFI zeolites. This treatment has proven to be crucial since it has shown to have a profound influence on the [Fe,Al]MFI catalyst activity in the selective oxidation of benzene to phenol and N_2O decomposition.[19,20] Steam-treatment is known to cause the hydrolysis of the SiO_2 framework of the [Fe,Al]MFI zeolite and thus an extensive migration of framework iron to extra-framework positions take place. For the set of [Fe,Al]MFI samples varying in iron content, Mössbauer spectra reveals a complete removal of Fe^{3+} ions from the zeolite framework. It is remarkable that for this set of samples, extra-framework iron species are predominantly in the Fe^{2+} state after steam-treatment. This emphasizes the importance of the steaming conditions on the final state of the catalyst, since hardly any divalent iron was observed in previous studies.[12]

For the set of samples varying in aluminum concentration, Mössbauer spectra of the steam-treated samples recorded in ambient and high-vacuum conditions show changes that strongly indicate the presence of extra-framework iron species. However, the quantity of Fe^{2+} species formed after steam-treatment is found to be relative to the amount of aluminum present in the sample. This suggests that the presence of aluminum seems to enhance the formation of extra-framework Fe^{2+} species (*vide infra*). In addition, for [Fe,Al]MFI samples with decreasing aluminum content, substantial amount of iron is still in the zeolite framework. This is evidenced by the broad line component that exhibits paramagnetic hyperfine splitting at low temperatures. Therefore, this affirms that the presence of framework aluminum promotes the removal of framework iron to extra-framework position, and that the lack thereof enhances the stability of framework iron from migrating to extra-framework positions on steam-treatment.

4.4.2. Autoreduction process

It has been shown that extra-framework iron can undergo a transition from Fe^{3+} to Fe^{2+} on heat treatment in inert or vacuum, which is known as an autoreduction process.[21-25] The occurrence of this phenomenon in the H-form [Fe,Al]MFI zeolites explains the substantial presence of extra-framework iron in the Fe^{2+} state. However, the extent at which extra-framework iron undergoes autoreduction appears to be a function of the iron loading as well as the aluminum concentration.

For [Fe,Al]MFI zeolites with relatively high iron content, figures 4.8A-B, the spectral contribution of the high-spin Fe^{2+} doublet appears to increase with the decrease in iron concentration (*see also table 4.2*). This can be attributed to the nature of the extra-framework

iron species formed upon extraction. Overweg *et al*.[26] have shown that highly dispersed extra-framework iron species in the MFI zeolites readily undergoes autoreduction. An increase in the iron content only enhances the extra-framework iron species to form clusters as evidenced by the increase in high-spin Fe^{3+} doublet spectral contribution.

On the contrary, for [Fe,Al]MFI zeolites with relatively low iron content, figures 4.8B-D, the spectral contribution of the high-spin Fe^{2+} doublet appears to decrease with the decrease in iron concentration (*see also table 4.2*). For [Fe,Al]MFI $(0.17:4)_H$ and [Fe,Al]MFI $(0.12:4)_H$, most extra-framework iron species are likely to be isolated Fe^{3+} ions, based on spectral parameters. Thus, a decrease in Fe^{2+} species in this case substantiates an autoreduction mechanism where a ferric ion requires at least one neighboring ferric ion to undergo reduction during heat treatment in the presence of inert gas, similar to the reaction proposed by Lobree *et al*.[27]:

$$2[Fe(OH)_2]^+Z^- \rightarrow 2[Fe(OH)]^+Z^- + H_2O + \tfrac{1}{2}\,O_2 \qquad (4.1)$$

where Z *is the zeolite lattice*.

The reducing equivalents are thus delivered by two-electron oxidation of OH^- to oxygen. A similar autoreduction mechanism has also been suggested for Cu^{2+} ions.[28,29]

For the steam-treated [Fe,Al]MFI varying in iron concentration, Mössbauer spectra indicates that a complete removal of iron from framework to extra-framework positions occurred. Furthermore, the extra-framework iron species formed after steam-treatment were predominantly in the high-spin Fe^{2+} state. Since a considerable portion of iron ions in bulk or large clusters would be difficult to reduce *via* an autoreduction process, this suggests that extra-framework iron species are likely to be highly dispersed surface species. This is supported by transmission electron microscopy (TEM), which shows no traces of Fe-oxide nanoparticles after steam-treatment. However, since extra-framework Fe^{3+} clusters have been observed in the H-form [Fe,Al]MFI zeolites, particularly for samples with high iron content, the presence of highly dispersed surface iron species would therefore imply that a reconstitution of the extra-framework iron species possibly takes place during steam-treatment.

Mössbauer spectra of the steam-treated samples with varying aluminum concentration indicate that the presence of aluminum enhances the removal of framework iron to extra-framework positions. Therefore, the observed increase in high-spin Fe^{2+} is mainly attributed to the increase in the extraction of framework iron to extra-framework positions. However,

for [Fe,Al]MFI (1:4)$_{stm}$ and [Fe,Al]MFI (1:2)$_{stm}$, Mössbauer spectra of both samples show indications that almost all framework iron has been completely removed. Despite the removal of most framework iron, the high-spin Fe^{2+} contribution in [Fe,Al]MFI (1:2)$_{stm}$ is only about half as much compared to that of [Fe,Al]MFI (1:4)$_{stm}$, which contains twice the amount of aluminum. This strongly indicates that the presence of aluminum enhances the formation of extra-framework Fe^{2+} species. One probable role of aluminum is the stabilization of extra-framework iron species that are most likely in cationic positions (e.g. as charge compensating binuclear complex)[1,30-32], similar to the one that is illustrated in figure 4.12 A. On the other hand, a decrease in aluminum would increase the formation of extra-framework iron clusters (figure 4.12 B).

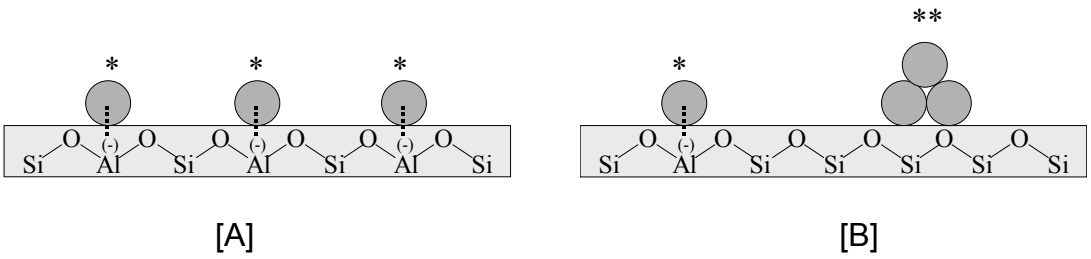

Figure 4.12. *Schematic representation of extra-framework iron species formed in the H-form* [Fe,Al]MFI *zeolites, showing cationic iron species (*) and extra-framework iron clusters (**).* A] *in high* Al [Fe,Al]MFI *and* B] *in low* Al [Fe,Al]MFI *zeolites.*

4.5. Conclusion

From Mössbauer data, it is shown that iron in the *as*-synthesized [Fe,Al]MFI zeolites is present as paramagnetic Fe^{3+} ions that are tetrahedrally coordinated in the MFI framework regardless of iron and aluminum concentrations. Calcination of the *as*-synthesized [Fe,Al]MFI zeolites causes part of the framework iron to migrate into extra-framework positions. The extent of migration is more pronounced in samples with high iron and aluminum concentrations. Transformation to H-form of the calcined [Fe,Al]MFI induces further migration of iron from framework to extra-framework positions. [Fe,Al]MFI with relatively low iron content (< 0.6 wt%) tends to have Fe^{3+} ions in isolated extra-framework positions that are easily reduced to its divalent state. In addition, the presence of aluminum enhances the formation of Fe^{2+} ions. Finally, steam treatment of [Fe,Al]MFI completely removes iron from framework to extra-framework positions in [Fe,Al]MFI samples with ca. 1.1 wt% aluminum. In these zeolite samples, all extra-framework iron is almost exclusively in the divalent state. In the steam-treated [Fe,Al]MFI however with low aluminum contents, the quantity of the trivalent iron increases.

Furthermore, the absence of iron-oxide particles (which are known to be spectator species in the direct oxidation of benzene to phenol with N_2O), in the steamed and specifically in the calcined and H-form samples, affirms that the relaxation behavior of iron at low temperatures (77 and 4.2 K) in the Mössbauer spectra is caused by paramagnetic hyperfine splitting rather than superparamagnetic iron-oxide nanoparticles. This illustrates very well the complementary nature of TEM and Mössbauer spectroscopy.

Acknowledgments

The author would like to acknowledge Ing. M.P. Steenvoorden, Radiation, Radionuclides and Reactiors, Delft University of Technology, for his assistance during Mössbauer measurements and to Dr. P.J. Kooyman, DelftChemTech, Delft University of Technology, for the TEM images.

REFERENCES

1. A.A. Battiston, J.H. Bitter, and D.C. Koningsberger, *Catal.Lett.,* 66 (2000) 75.
2. L.J. Lobree, I. Hwang, J.A. Reimer, and A.T. Bell, *Catal.Lett.,* 63 (1999) 233.
3. H.-Y. Chen, T. Voskoboinikov, and W.M.H. Sachtler, *J. Catal.,* 180 (1998) 171.
4. X. Feng and W.K. Hall, *J. Catal.* 166 (1997) 368.
5. E.M. El-Malki, R.A. van Santen, and W.M.H. Sachtler, *J. Catal.,* 196 (2000) 212.
6. F. Kapteijn, G. Marbán, J. Rodríguez-Mirasol, and J.A. Moulijn, *J. Catal.,* 167 (1997) 256.
7. G.I. Panov, *Cattech* 4 (2000) 18.
8. G.I. Panov, A.K. Uriarte, M.A. Rodkin, and V.I. Sobolev, *Catal. Today,* 41 (1998) 365.
9. P.P. Notté, *Topics in Catalysis* 13 (2000) 387.
10. A. Ribera, I.W.C.E. Arends, S. de Vries, J. Pérez-Ramírez, and R.A. Sheldon, *J. Catal.,* 195 (2000) 287.
11. G.I. Panov, V.I. Sobolev, and A.S. Kharitonov, *J. Mol. Catal.,* 61 (1990) 85.
12. J. Pérez-Ramírez, G. Mul, F. Kapteijn, J.A. Moulijn, A.R. Overweg, A. Doménech, A. Ribera, and I.W.C.E. Arends, *J. Catal.,* 207 (2002) 113.
13. A. Meagher, V. Nair, and R. Szostak, *Zeolites,* 8 (1988) 3.
14. R.L. Garten, W.N. Delgass, and M. Boudart, *J. Catal.,* 19 (1970) 90.
15. S. Yuen, Y. Chen, J.E. Kubsh, J.A. Dumesic, N. Topsøe, and H. Topsøe, *J. Phys. Chem.,* 86 (1982) 3022.
16. S. Bordiga, R. Buzzoni, F. Geobaldo, C. Lamberti, E. Giamello, A. Zecchina, G. Leofanti, G. Petrini, and G. Tozzola, *J. Catal.,* 158 (1996) 486.
17. H. R. Leider and D. N. Pipkorn, *Phys. Rev.*, 165 (1968) 494.
18. R. Szostak, N. Nair, D.K. Simmons, T.L. Thomas, R. Kuvadia, B. Dunsion, and D.C. Shieh, *in "Innovations in Zeolite Materials Science"* (P.J. Grobet, *et al*., Eds), p. 403. Elsevier, Amsterdam (1998).
19. A.S. Kharitonov, G.I. Panov, G.A. Sheveleva, L.V. Pirutko, T.P. Voskresenskaya, V.I. Sobolev, US Patent 5,672,777, 1997, assigned to Monsanto.
20. L.V. Pirutko, V.S. Chernyavsky, A.K. Uriarte, G.I. Panov, *Appl. Catal., A* 227 (2002) 143.
21. R. Joyner and M. Stockenhuber, *J. Phys. Chem. B,* 103 (1999) 5963.
22. L.J. Lobree, I. Hwang, J.A. Reimer, and A.T. Bell, *J. Catal.,* 186 (1999) 242.
23. G. Spoto, A. Zecchina, G. Berlier, S. Bordiag, M.G. Clerici, and L. Basini, *J. Mol. Catal. A,* 158 (2000) 107.
24. K. Lázár, A.N. Kotasthane, and R. Fejes, *Catal. Lett.,* 57 (1999) 171.

25. T.V. Voskoboinikov, H.-Y. Chen, and W.M.H. Sachtler, *Appl. Catal. B,* 19 (1998) 279.
26. A.R. Overweg, M.W.J. Crajé, A.M. van der Kraan, I.W.C.E. Arends, A. Ribera, and R.A. Sheldon, *J. Catal.,* 223 (2004) 262.
27. L.J. Lobree, I. Hwang, J.A. Reimer, and A.T. Bell, *J. Catal.*, 186 (1999) 242.
28. M. Iwamoto, H. Yahiro, K. Tanda, N. Mizuno, Y. Mine, and S. Kagawa, *J. Phys. Chem.,* 95 (1991) 3727.
29. H.-J. Jang, W.K. Hall, J.L. d'Itri, *J. Phys. Chem.* 100 (1996) 9416.
30. K.A. Dubkov, N.S. Ovanesyan, A.A. Shteinman, E.V. Starokon, G.I. Panov, *J. Catal.,* 207 (2002) 341.
31. P. Marturano, L. Drozdova, A. Kogelbauer, and R. Prins, *J. Catal.*, 192 (2000) 236.
32. T.V. Voskoboinikov, H.-Y. Chen, and W.M.H. Sachtler, *Appl. Catal. B*, 19 (1998) 279.

Chapter 5

Role of Aluminum in the Formation of *Redox*-Active Iron Species in Steam-treated [Fe,Al]MFI Catalysts

Abstract

In situ Fe *K*-edge XANES measurements were performed to study the *redox* properties of extra-framework iron species in steam-treated [Fe,Al]MFI zeolites. Three steam-treated [Fe,Al]MFI zeolites, varying in aluminum concentration, were subjected to heat-treatments in nitrogen and nitrous oxide environments. From the Fe *K*-edge energy position, extensive autoreduction of iron in the steam-treated [Fe,Al]MFI zeolite is observed particularly in the sample containing the most aluminum. On the contrary, minimal autoreduction of iron is exhibited in the sample with the lowest aluminum concentration. This illustrates that (upon steam-treatment) the presence of aluminum in the MFI zeolite enhances the formation of extra-framework ferric species that are prone to autoreduction under thermal treatment in inert gas. In addition, *in situ* Fe *K*-edge XANES spectra reveal that autoreduction of the iron species takes place almost instantaneously during thermal treatment in N_2 from room temperature to 398 K. On the other hand, re-oxidation of the iron species in the presence of N_2O occurs only above 498 K. This indicates the need for *in-situ* measurement as the actual state of the *redox*-active extra-framework iron can change at low temperature due to autoreduction.

5.1. Introduction

Extra-framework iron species that are stabilized in the intracrystalline micropore channels of the MFI zeolite often exhibit unusual catalytic properties.[1] In particular, extra-framework iron species formed after steam-treatment of isomorphously substituted [Fe,Al]MFI zeolites have been reported to exhibit superior catalytic performance in the direct oxidation of benzene to phenol, using N_2O as oxidant (BTOP).[2,3] Panov *et al*.,[4] suggested that these extra-framework iron species, or the so-called *α-sites*,[5,6] are able to generate surface active oxygen through the dissociation of N_2O. The formation of these active oxygen species is considered a vital step in the direct oxidation of benzene to phenol.[2,7,8]

According to ^{57}Fe Mössbauer spectroscopic studies,[4,9] extra-framework iron species forming the *α-sites* are in the ferrous state. These species are usually formed upon high-temperature activation of the MFI zeolite in inert gas or high vacuum.[10] Due to the absence of reducing agents involved during thermal treatment, the reduction of ferric to ferrous ion phenomenon is usually referred to as an autoreduction process.[11,12] However, for the steam-treated [Fe,Al]MFI zeolites varying in iron concentration (0.075-0.6 wt.% Fe), almost all extra-framework iron species are already in the high-spin ferrous state as presented in the previous chapter – i.e. ca. 90%, based on Mössbauer spectral contribution, independent of the iron concentration.[13] This is most likely due to the presence of a substantial amount of aluminum in all samples.

Interestingly, for the samples with relatively low aluminum content, the amount of the high-spin ferrous species formed after steam-treatment appears to be a function of the aluminum content.[9] This was also observed by several authors,[14-16] and they proposed that the presence of aluminum facilitates the removal of framework iron to extra-framework positions during post-treatment catalyst activation by destabilization of the zeolite framework. Thus, the presence of Fe^{2+} species is related to the amount of extra-framework iron. However, as discussed in chapter 4, Mössbauer spectra give indications of an almost complete removal of framework iron to extra-framework position after steam-treatment, particularly for the samples with relatively high aluminum concentration. Nevertheless, the quantity of Fe^{2+} species is observed to be dependent of aluminum content. This clearly indicates that the presence of aluminum has also an influence in the formation of ferrous species in the [Fe,Al]MFI catalysts.

The role of aluminum in the catalytic BTOP reaction, if there is one, is not clear at the moment, based on open literature. Nevertheless, it has gained substantial interest since aluminum-containing [Fe,Al]MFI catalyst has often yielded superior catalytic performance in

the BTOP reaction compared to that of aluminum-free [Fe]MFI catalyst.[17] Since the presence of Fe^{2+} species, which has been correlated to the formation of the *α-sites*,[9] appears to be a function of aluminum content, it is therefore important to study the role of aluminum particularly in the formation of *redox*-active iron species in the [Fe,Al]MFI catalyst.

In this study, representative steam-treated [Fe,Al]MFI zeolites varying in Al concentration are subjected to (i) thermal treatment in N_2 and (ii) N_2O oxidation. The effect on the valence and coordination states of the extra-framework iron species in steam-treated [Fe,Al]MFI zeolites under these treatments is investigated using Fe *K*-edge X-ray Absorption Near Edge Spectroscopy (XANES). The advantage of Fe *K*-edge XANES is that it enables one to perform a *quasi*-transient study on the *redox* properties of iron in the zeolite sample as a function of temperature and different gas treatments. In principle, analysis of the features well above the Fe *K*-edge (i.e. EXAFS) provides information on the type of coordinating atoms and first-shell iron-ligand distances, but this has proven to be difficult for zeolites with dilute iron concentration.[18,19] Therefore, the interest in this study will focus on the edge region and the feature prior to the pre-edge jump. These features provide chemical information regarding the oxidation state and coordination of the iron atoms, respectively.[19-22]

5.2. Experimental

5.2.1. [Fe,Al]MFI zeolites

Three steam-treated [Fe,Al]MFI zeolite samples, i.e. [Fe,Al]MFI $(1:4)_{stm}$, [Fe,Al]MFI $(1:2)_{stm}$, and [Fe,Al]MFI $(1:1)_{stm}$, varying in aluminum concentration were characterized using *in situ* Fe *K*-edge XANES. These samples were obtained from the same batch of steam-treated zeolites that was mentioned in chapter 4. Therefore, for experimental details and discussion regarding hydrothermal synthesis of these zeolites and their post-treatment activation steps, the readers are refered to chapters 3 and 4, respectively.

5.2.2. Fe K-edge XANES

Fe *K*-edge XANES measurements were performed at beamline 26 (BM26A) of the European Synchrotron Radiation Facility in Grenoble, France. The storage ring was operating at 6 GeV electron energy and ~60 mA electron current. A Si(111) monochromator with an energy resolution of ~0.5 eV at the Fe *K*-edge was used.

The zeolite samples were pressed into self-supporting wafers and placed in a heat-and-gas flow controlled cell to allow *in situ* measurements (*see figure 5.1 for details*). XANES spectra were recorded in fluorescence mode during a temperature-programmed heating from room

temperature to 623 K, following a temperature ramp rate of 5 K/min, under N_2 or N_2O flow of 30 ml/min.

Fe foil, recorded in transmission mode, was used for internal energy calibration of the monochromator in all spectra. All spectra were normalized according to standard procedures. To extract the pre-edge feature, the contribution of the edge jump (fitted using a cubic-spline function) was subtracted from the spectra. The obtained pre-edge peaks were fitted with pseudo-Voigt functions using 1:1 ratio of Lorentzian to Guassian lines.

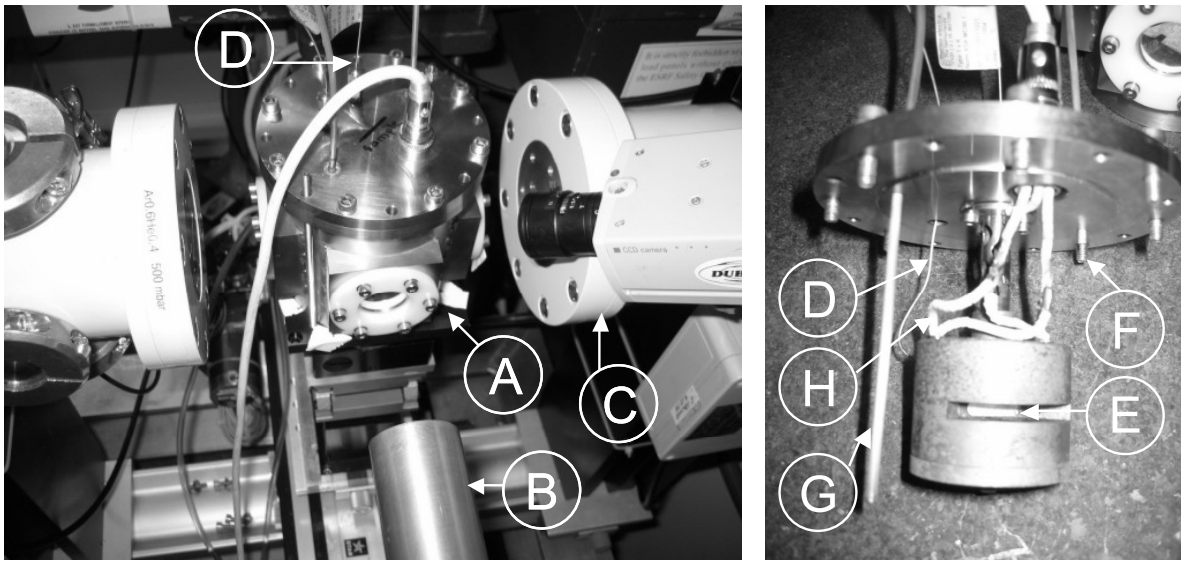

Figure 5.1. (Left photo) *In situ Fe XANES setup, which consists of:* (A) *In situ cell equipped with Mylar (aluminized) windows,* (B) *nine channel monolithic Ge detector,* (C) *Ion chamber,* (D) *thermocouple.* (Right photo) *Inside features of the in situ cell, which includes:* (D) *thermocouple,* (E) *sample holder with wide angle slit designed to allow X-ray beam detection in both fluorescence and transmission mode,* (F) *gas inlet,* (G) *gas outlet, and* (H) *heating elements*.

5.3. Results

5.3.1. Heat treatment in N_2

Figure 5.2 shows the normalized Fe *K*-edge XANES spectra of the [Fe,Al]MFI $(1{:}4)_{stm}$ sample taken at increasing temperatures (i.e. 300 K, 300-398 K, 398-498 K, 498-598 K, and 623 K) during thermal treatment in N_2. Two important features in these spectra are the Fe *K*-edge energy and the pre-edge peak. These spectral features reveal chemical information – i.e. valency (*via* the edge energy) and coordination symmetry (*via* the pre-edge intensity) – of iron in the sample under investigation. The edge energy is defined as the first inflection point in the edge jump, while the pre-edge peak is the spectral feature prior to the edge jump.

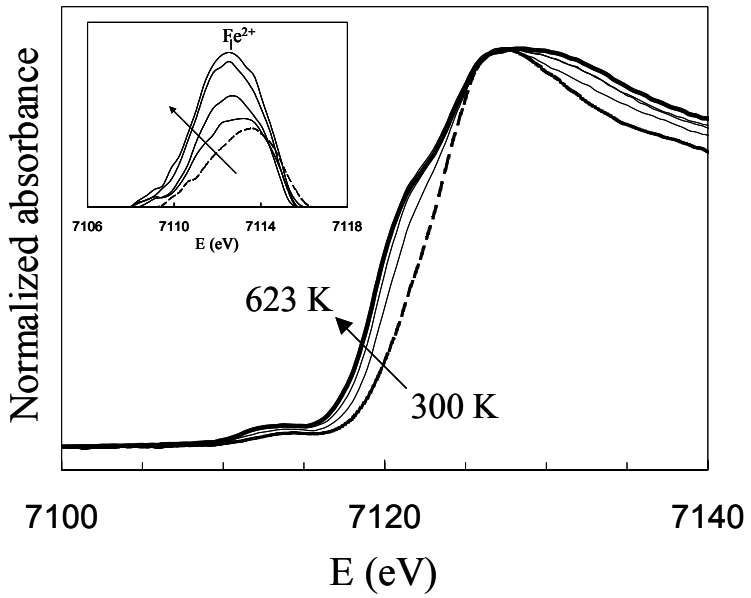

Figure 5.2. Fe *K*-edge XANES *spectra of* [Fe,Al]MFI (1:4)$_{stm}$ *taken at increasing heat treatment temperatures – i.e. at 300 K (indicated by bold-broken line), 300-398 K, 398-498 K, 498-598 K and 623 K (indicated by bold-solid line) – in* N_2*. The inset shows the corresponding background-subtracted pre-edge peaks. The arrow indicates the increase in temperature.*

Upon thermal treatment of the [Fe,Al]MFI (1:4)$_{stm}$ sample in N_2 from room temperature to 623 K, a large shift to lower edge energy is observed, as shown in figure 5.2. The shift to lower energy (7122.20 $\rightarrow$ 7120.27 eV) of the Fe *K*-edge is attributed to an autoreduction process, in which Fe^{3+} ions are reduced to their Fe^{2+} state. This is consistent with the changes observed in the pre-edge peak positions. The background-subtracted pre-edge peaks are shown as inset in figure 5.2. At room temperature, the pre-edge peak can be roughly fitted by two pseudo-Voigt functions with peak positions corresponding to that of Fe^{3+} and Fe^{2+} ions, i.e. at 7114.00 and 7112.40 eV, respectively.[19-22] Nevertheless, a predominant contribution of the Fe^{2+} is already observed, which fits with the Mössbauer result (*see chapter 4*). At 623 K, the pre-edge peak strongly indicates the presence of mostly Fe^{2+} ions. This is substantiated by a centroid at 7112.4 eV, which is close to the value reported for ferrous compounds.

In addition, the intensity of the pre-edge peak increases with the increase in thermal treatment temperature. This is most likely due to the changes in coordination number and geometry around the iron atom. In a centrosymmetric coordination environment (e.g. octahedral symmetry), the pre-edge peak is normally very weak since the 1*s* to 3*d* transition is electric dipole forbidden.[21,23] Its intensity is only gained in a weak electric quadrupole coupling.[21] However, in the case where there is an absence of inversion center, e.g. in tetrahedral coordination, the dipole-allowed 1*s* to 4*p* transition is enhanced due to mixing of 3*d* and 4*p*

orbitals of the transition metal. This results in a more intense pre-edge feature.[21,24] Thus, a higher pre-edge peak intensity suggests an average coordination geometry that is less centrosymmetric.

These spectral changes are also observed in the other samples with lower aluminum concentrations, albeit to a lesser degree. It is therefore clear that thermal treatment in N_2 of steam-treated [Fe,Al]MFI zeolites induces particular ferric species to undergo an autoreduction process. Furthermore, the increase in pre-edge intensity indicates that thermal treatment leads to a coordinatively unsaturated metal atom. This is most likely due to the removal of coordinating water ligands during thermal treatment.[22]

To compare the relative extent of autoreduction of different steam-treated [Fe,Al]MFI zeolite samples, their normalized *in situ* Fe *K*-edge XANES spectra recorded at 623 K in N_2 are plotted in figure 5.3. By visual inspection, the sample with the highest aluminum concentration exhibits an extensive reduction compared to that of the sample with the least aluminum. This is confirmed by the Fe *K*-edge energy position of the different samples, which is lowest for [Fe,Al]MFI $(1:4)_{stm}$ (i.e. 7120.27 eV) and increases in edge energy with the decrease in aluminum concentration.

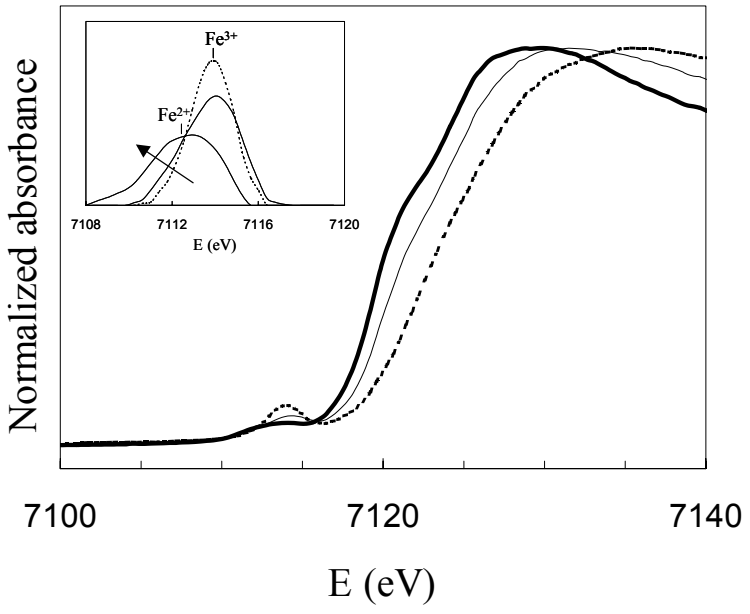

Figure 5.3. Fe *K*-edge XANES *spectra of* [Fe,Al]MFI $(1:4)_{stm}$ (thick solid line), [Fe,Al]MFI $(1:2)_{stm}$ (thin solid line)*, and* [Fe,Al]MFI $(1:1)_{stm}$ (broken line) *recorded at 623 K in* N_2*. The inset shows the corresponding background-subtracted pre-edge peaks (arrow indicate an increasing aluminum content).*

The extent of reduction is more apparent when the Fe *K*-edge energy position is plotted as a function of heat treatment temperature of the different samples. Figure 5.4 illustrates a large shift to lower edge energy from 300 K to 623 K (i.e. 7122.20 → 7120.27 eV) for [Fe,Al]MFI (1:4)$_{stm}$, while a moderate Fe *K*-edge energy shift (i.e. 7122.98 → 7121.82 eV) is observed in [Fe,Al]MFI (1:2)$_{stm}$, and hardly a shift to lower energy (i.e. 7124.52 → 7124.14 eV) in [Fe,Al]MFI (1:1)$_{stm}$. These changes in edge energy position as a function of thermal treatment temperature in N_2 imply that extensive autoreduction occurred in the sample with high aluminum concentration and, in contrast, hardly any autoreduction was observed for the sample with low aluminum concentration.

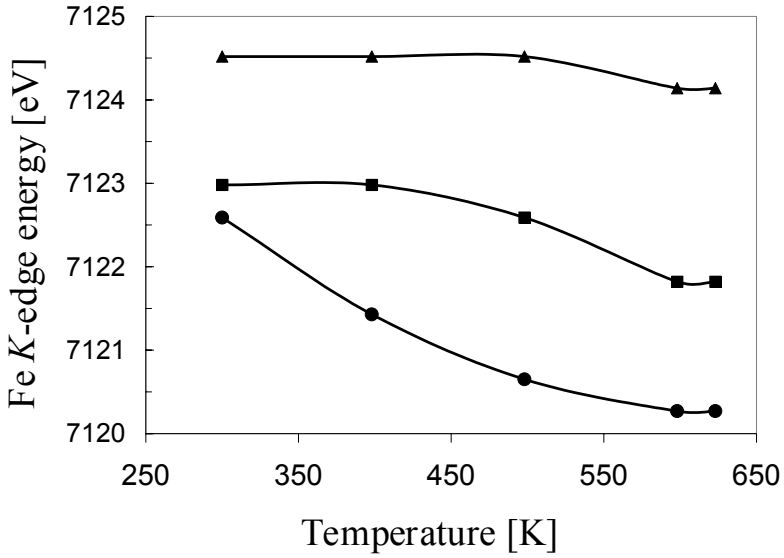

Figure 5.4. *Plot of* Fe *K*-edge *energy position of samples* [Fe,Al]MFI (1:4)$_{stm}$ (●), [Fe,Al]MFI (1:2)$_{stm}$ (■), *and* [Fe,Al]MFI (1:1)$_{stm}$ (▲) *as a function of heat treatment temperatures.*

In addition, the trend observed in the edge energy position as a function of aluminum concentration is again consistent with the changes in centroid position and shape of the pre-edge peaks. The background-subtracted pre-edges that were extracted from the XANES spectra recorded at 623 K of the samples with varying aluminum concentration are shown in the inset of figure 5.3. The corresponding fit parameters (intensity and centroid position) of the extracted pre-edge peaks are summarized in table 5.1. The pre-edge position clearly indicate a shift from a predominant Fe^{2+} centroid in the [Fe,Al]MFI (1:4)$_{stm}$ sample, to a more dominant Fe^{3+} centroid position at 7114.1 eV in the [Fe,Al]MFI (1:1)$_{stm}$ sample. This indicates that most iron ions in the [Fe,Al]MFI (1:1)$_{stm}$ sample, hardly undergoes autoreduction upon heat treatment in N_2 at high temperatures.

5.3.2. N_2O treatment

Figure 5.5 shows the normalized Fe *K*-edge XANES spectra of [Fe,Al]MFI (1:4)$_{stm}$ sample recorded at increasing temperatures from 300 K to 623 K during N_2O treatment. It is evident that N_2O treatment of [Fe,Al]MFI (1:4)$_{stm}$ at high-temperatures leads to a shift of the Fe *K*-edge position to higher energy (i.e. 7122.20 $\rightarrow$ 7123.97 eV, from 300 K to 623 K). This shift to high Fe *K*-edge energy is attributed to oxidation of Fe^{2+} to Fe^{3+} ions during N_2O treatment. However, it should be worthy to note that the shift to higher energy during N_2O treatment occurs only when the temperature is above 498 K. This indicates that oxidation of ferrous to ferric ions takes place only above this temperature. This information is important to consider as the actual state of iron can change at low temperature due to autoreduction. This points to the need for conduction measurements *in-situ* or in well-controlled environment.

Fe *K*-edge XANES spectra of the samples with different aluminum concentrations after heat treatment in N_2O at 623 K are illustrated in figure 5.6. In all samples, the Fe *K*-edge energy positions, *vis-à-vis* after thermal treatment in N_2 at 623 K (figure 5.3), shift to higher energy. The shift is observed to be extensive in samples with high aluminum concentrations. This indicates that much of the Fe^{2+} species in [Fe,Al]MFI (1:4)$_{stm}$ and [Fe,Al]MFI (1:2)$_{stm}$ after autoreduction are oxidized to Fe^{3+} in the presence of N_2O. For [Fe,Al]MFI (1:1)$_{stm}$, the edge position slightly shifts (i.e. 7123.75 $\rightarrow$ 7124.14 eV), further affirming that iron is already present predominantly as Fe^{3+} ions. The normalized background-subtracted pre-edges extracted from the XANES spectra of the oxidized samples are shown in figure 5.6 inset. In all samples, the pre-edge peaks exhibit a centroid position that is close to 7114 eV, indicating the presence of predominantly Fe^{3+} species.[21] This indicates that almost all reduced iron ions were oxidized upon N_2O treatment at 623 K.

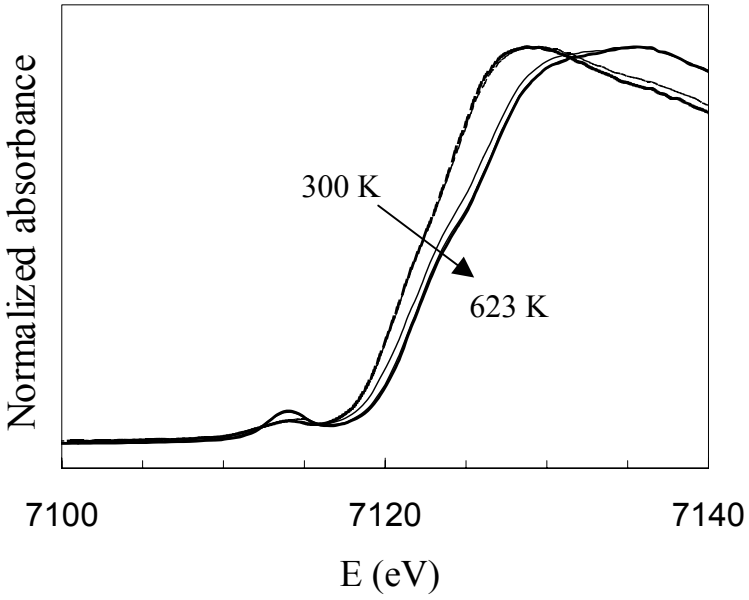

Figure 5.5. Fe *K*-edge XANES *spectra of* [Fe,Al]MFI $(1{:}4)_{stm}$ *taken at increasing oxidation temperatures– i.e. from 300 K* (indicated by bold-broken line) *to 623 K* (indicated by bold-solid line) – *in* N_2O.

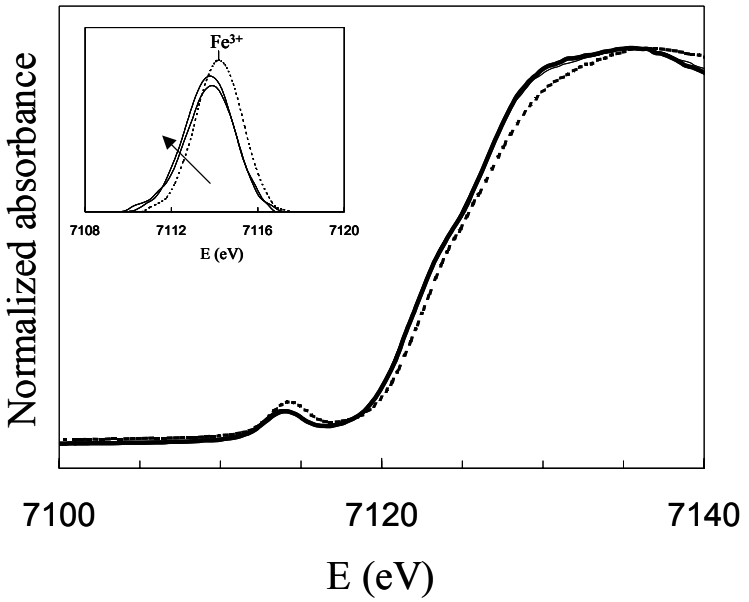

Figure 5.6. Fe *K*-edge XANES *spectra of* [Fe,Al]MFI $(1{:}4)_{stm}$ (thick solid line), [Fe,Al]MFI $(1{:}2)_{stm}$ (thin solid line)*, and* [Fe,Al]MFI $(1{:}1)_{stm}$ (broken line) *recorded at 623 K in* N_2O*. The inset shows the corresponding background-subtracted pre-edge peaks (arrow indicate an increasing aluminum content)*.

Table 5.1. Pre-edge parameters of steam-treated [Fe,Al]MFI zeolites varying in Al content under *in situ* heat-treatments.

Sample	*In situ* condition	edge energy (eV)	ferrous state *I* (centroid)[a]	ferric state *I* (centroid)[a]
[Fe,Al]MFI (1:4)$_{stm}$	623 K in N_2	7120.27	0.119 (7112.40)	0.012 (7114.00)
	623 K in N_2O	7123.97	0.031 (7112.60)	0.129 (7114.01)
[Fe,Al]MFI (1:2)$_{stm}$	623 K in N_2	7121.82	0.041 (7112.55)	0.098 (7114.00)
	623 K in N_2O	7123.97	0.029 (7112.60)	0.132 (7113.90)
[Fe,Al]MFI (1:1)$_{stm}$	623 K in N_2	7123.75	0.031(7112.94)	0.969 (7114.10)
	623 K in N_2O	7124.14	--	0.181 (7114.10)

[a] Integrated intensities (*I*) ± 10%; centroid position (eV) ± 0.5 eV.

5.4. Discussion

In situ Fe *K*-edge XANES measurements were performed to study the *redox* properties of extra-framework iron species formed after steam-treatment of the [Fe,Al]MFI zeolites. In particular, this study investigates the effect of aluminum on the *redox* state of the iron ions. Thus, three representative steam-treated [Fe,Al]MFI samples varying in aluminum content were probed. *In situ* Fe *K*-edge XANES is a suitable technique to follow the changes in the chemical state of iron under reducing and oxidizing conditions at different temperatures. Most importantly, it allows a *quasi*-transient study of the *redox* changes with increasing temperatures. This is useful information in complement to other spectroscopic techniques, such as Mössbauer spectroscopy – which is not capable of performing *quasi*-transient studies.

5.4.1. Autoreduction process

For the [Fe,Al]MFI zeolites under investigation, all samples contain iron that amounts to ca. 0.6% by weight. Mössbauer spectra taken at room temperature in high vacuum of these samples approximate that around 83%, 49%, and 21% of iron is reduced to its ferrous state in the [Fe,Al]MFI (1:4), [Fe,Al]MFI (1:2), and [Fe,Al]MFI (1:1) samples, respectively, after steam-treatment (*see table 4.4, chapter 4*). The observed increase in ferrous species, as a function of aluminum concentration has led to a proposition in the previous chapter that aluminum also has an influence in the formation of these extra-framework ferrous species, as it is the only parameter varied in this set of samples.

To confirm this notion, three steam-treated [Fe,Al]MFI samples with varying aluminum concentration were subjected to heat treatment at 623 K in N_2 to induce an autoreduction of the ferric ions in the zeolite. *In situ* Fe *K*-edge XANES results confirmed that upon heat treatment extra-framework ferric ions in [Fe,Al]MFI zeolites were reduced. This is illustrated by the shift of the Fe *K*-edge energy position to lower values (*see figures 5.3 and 5.4*). The lowest edge energy attained is 7120.27 eV, which is indicative of extra-framework iron that is predominantly in the ferrous state. This was obtained by the steam-treated [Fe,Al]MFI (1:4) zeolite, which contains the most aluminum amongst the samples investigated. Furthermore, heat treatment of the samples above 623 K (i.e. up to 823 K) exhibits no further shift in the Fe *K*-edge position to lower energies. This implies that autoreduction only involves the ferric to ferrous transition.

The plot of the Fe *K*-edge values at increasing heat treatment temperatures of the different samples is shown in figure 5.4. It shows that for the sample with the least amount of aluminum, heat treatment only leads to a small shift in Fe *K*-edge energy position. Whereas, for the sample with the highest aluminum loading, an extensive shift to lower Fe *K*-edge energy is observed. This clearly illustrates the differences in the potential of various extra-framework iron species to undergo autoreduction. From these observations, it is therefore apparent that the presence of aluminum in steam-treated [Fe,Al]MFI zeolites enhances the formation of extra-framework iron species that readily go through an autoreduction process upon heat treatment in inert gas.

5.4.2. Framework *vs* extra-framework aluminum

In the previous chapter, it has been proposed that *redox*-active extra-framework iron species are most likely surface species exhibiting at least a binuclear structure. It can be envisaged that the presence of framework aluminum could stabilize these extra-framework iron species in cationic positions. This would suppress an agglomeration of extra-framework iron ions into large iron oxide particles that are inactive to *redox* changes at these conditions.[25] As heat treatment of [Fe,Al]MFI $(1:4)_{stm}$ in N_2 leads to a coordinatively unsaturated and disordered metal atom (*see inset of figure 5.2*), which is not typical for iron ions in the bulk material, this substantiates the proposition that extra-framework iron species in the sample with relatively high aluminum concentration are surface species.

However, based on the current data, it is not possible to conclude whether aluminum is located in the framework or extra-framework of the zeolite lattice after steam-treatment. Conventional steaming has been reported to cause dealumination,[26] which consequently alters various properties of the zeolites. Recent works of Hensen *et al.*[18,27-29] have shown that extra-framework aluminum could play an important role in the formation of active Fe^{2+} sites.

Nevertheless, quantitative analysis of framework and extra-framework aluminum in iron containing ZSM-5 zeolites (or [Fe,Al]MFI) using ^{27}Al NMR is difficult since the intensity of the signal is generally affected by the paramagnetism of neighboring iron ions. This is due to the unpaired electrons of the iron ions, which generate a local magnetic field that strongly perturbs the resonance of the ^{27}Al nuclei. However, qualitatively, it has been proposed by Pérez-Ramírez *et al*,[30] that using the same steam-treatment conditions a considerable amount of framework aluminum in [Fe,Al]MFI zeolite is dislodged to extra-framework positions.

Evidence of extra-framework aluminum having an influence on the *redox* properties of extra-framework iron in the [Fe,Al]MFI zeolites is manifested by the fact that extensive autoreduction of ferric to ferrous ions is only observed for samples with relatively high aluminum concentration after steam-treatment (*see chapter 4*). Mössbauer spectrum of the [Fe,Al]MFI (1:4) sample suggests that a substantial amount of framework iron is already removed after transformation to H-form (*see figure 4.8 E, chapter 4*). Furthermore, the large contribution of the high-spin Fe^{3+} doublet indicates a strong contribution of clustered extra-framework iron species. However, after steam-treatment, the Mössbauer spectrum exhibits a predominant high-spin Fe^{2+} doublet (*see figure 4.9 A, chapter 4*). This can only be attributed to a certain re-dispersion of the extra-framework iron clusters to highly dispersed surface species. This re-dispersion is most likely induced by the presence of extra-framework aluminum formed on steam-treatment.

The notion of a reconstitution of extra-framework iron clusters due to the presence of extra-framework aluminum upon steam-treatment is further supported by the results of Hensen *et al*.[27,29] They reported that the benzene oxidation activity of sublimed Fe/ZSM-5 increases in activity after steam-treatment, despite the fact that virtually all iron species are introduced in extra-framework positions. Most likely, *redox* active extra-framework iron species are stabilized on extra-framework aluminum created on steam-treatment. This has led to their speculation that extra-framework Fe-Al-O species are active in the BTOP reaction.[18,28]

It is, therefore, more likely that a zeolite lattice containing aluminum (either as framework or extra-framework species) is able to stabilize highly dispersed surface iron species that exhibit autoreduction during thermal treatment, causing the $Fe^{3+} \rightarrow Fe^{2+}$ transition.

5.4.3. Oxidation in N_2O

Upon N_2O treatment of the steam-treated [Fe,Al]MFI samples at high temperatures, almost all ferrous ions are shown to be oxidized to their ferric state. The formation of these *redox*-active extra-framework Fe^{2+} species, which are easily oxidized by N_2O above 498 K, have been shown to be influenced by the presence of aluminium. However, although these Fe^{2+}

species appear to be active *redox* centers, it is important to determine whether these species are catalytically active particularly in the direct oxidation of benzene to phenol, as well as in the decomposition of N_2O. These will be presented and discussed separately in the next chapter.

Finally, comparison of the pre-edge peak intensities upon oxidation of the samples by exposure with N_2O at 623 K reveals that samples with low aluminum concentration exhibit high peak intensities of the ferric component. As mentioned, a pre-edge peak with high intensity suggests an average coordination geometry that is not centrosymmetric. Therefore a strong pre-edge intensity for samples with low aluminum concentration may in principle result from the presence of tetrahedral ferric ions.[19] This is strong indication that part of the iron ions are still in the framework positions, which is in agreement with the Mössbauer spectroscopy results.[13]

5.5. Conclusion

In situ Fe *K*-edge XANES measurements performed on three [Fe,Al]MFI zeolites varying in aluminum concentration reveal that the presence of aluminum enhances the stabilization of specific extra-framework iron species that undergo autoreduction upon thermal treatment in N_2 at 623 K. Extensive autoreduction was observed for [Fe,Al]MFI $(1{:}4)_{stm}$, which contains the highest amount of aluminum among the samples under investigation. On the other hand, the extent of autoreduction progressively decreased upon the decrease in aluminum concentration.

Autoreduction of iron is shown to occur already at low heat-treatment temperatures (i.e. between 300 K and 398 K) in N_2. On the other hand, ferrous species were easily oxidized to its ferric form in the presence of N_2O only above 498 K. This illustrates that *redox*-active extraframework iron species can change at low temperature as a result of autoreduction.

In situ Fe *K*-edge XANES spectra after oxidation with nitrous oxide strongly indicates that the presence of aluminum promotes the removal of framework iron to extra-framework position, which is in agreement with the ^{57}Fe Mössbauer result.

Finally, it is evident from *in situ* Fe *K*-edge XANES results that the presence of aluminum influences the *redox* properties of extra-framework iron in steam-treated [Fe,Al]MFI zeolites. However, it remains to be seen whether this influence on the *redox* property of iron has catalytic implications both in N_2O decomposition, as well as, in the BTOP reaction.

Acknowledgements

The author would like to thank Dr. A.R. Overweg and Ing. M.P. Steenvoorden, of the department of Radiation, Radionuclides and Reactors, Delft University of Technology, and to Dr. E.J.M. Hensen, of Schuit Institute of Catalysis, Eindhoven University of Technology, for their assistance during X-ray Absorption Spectroscopy experiments. Dr. S. Nikitenko, beamline scientist, Dutch-Belgian Station, European Synchrotron Radiation Facility, is gratefully acknowledged for his technical support.

REFERENCES

1. G. Centi, B. Wichterlova, A.T. Bell (Eds.), *Catalysis by Unique Metal Ion Structures in Solid Matrices*, in: NATO Science Series, Kluwer Academic, Dordrecht, 2001.
2. G.I. Panov, *Cattech*, 4 (2000) 18.
3. A. Ribera, I.W.C.E. Arends, S. de Vries, J. Pérez-Ramírez, R.A. Sheldon, *J. Catal.*, 195 (2000) 287.
4. N.S. Ovanesyan, A.A. Shteinman, V.I. Sobolev, K.A. Dubkov, and G.I. Panov, *Kinet. Katal*., 39 (1998) 863.
5. G.I. Panov, A.S. Kharitonov, and V.I. Sobolev, *Appl. Catal*., 98 (1993) 1.
6. G.I. Panov, V.I. Sobolev, K.A. Dubkov, V.N. Parmon, N.S. Ovanesyan, A.E. Shilov, and A.A. Shteinman, *React. Kinet. Catal. Lett*., 61 (1997) 251.
7. P.P. Notté, *Topics in Catalysis*, 13 (2000) 387.
8. G.I. Panov, A.K. Uriarte, M.A. Rodkin, and V.I. Sobolev, *Catal. Today*, 41 (1998) 365.
9. K.A. Dubkov, N.S. Ovanesyan, A.A. Shteinman, E.V. Starokon, G.I. Panov, *J. Catal.*, 207 (2002) 341.
10. G.I. Panov, A.S. Kharitonov, and V.I. Sobolev, *Appl. Catal. A*, 98 (1993) 1.
11. D. Meloni, R. Monaci, V. Solinas, G. Berlier, S. Bordiga, I. Rossetti, C. Oliva, and L. Forni, *J. Catal.*, 214 (2003) 169.
12. L.J. Lobree, I. Hwang, J.A. Reimer, and A.T. Bell, *J. Catal.*, 186 (1999) 242.
13. J.B. Taboada, A.R. Overweg, P.J. Kooyman, I.W.C.E. Arends, G. Mul, *J. Catal*., 231 (2005) 56.
14. P. Kubánek, B. Wichterlová, and Z. Sobalík, *J. Catal*., 211 (2002) 109.
15. V.I. Sobolev, G.I. Panov, A.S. Kharitonov, V.N. Romannikov, A.M. Vologin, and K.G. Ione, *J. Catal.*, 139 (1993) 435.
16. J. Pérez-Ramírez, F. Kapteijn, and A. Brückner, *J. Catal*., 218 (2003) 234.
17. L.V. Pirutko, V.S. Chernyavsky, A.K. Uriarte, and G.I. Panov, *Appl. Catal. A*, 227 (2002) 143.

18. E. Hensen, Q. Zhu, P.-H. Liu, K.-J. Chao, and R. van Santen, *J. Catal.*, 226 (2004) 466.
19. S. Bordiga, R. Buzzoni, F. Geobaldo, C. Lamberti, E. Giamello, A. Zecchina, G. Leofanti, G. Petrini, G. Tozzola, and G. Vlaic, *J. Catal.*, 158 (1996) 486.
20. G. Berlier, G. Spoto, S. Bordiga, G. Ricchiardi, P. Fisicaro, A. Zecchina, I. Rossetti, E. Selli, L. Forni, E. Giamello, and C. Lamberti, *J. Catal*., 208 (2002)64.
21. M. Wilke, F. Fargas, P.-E. Petit, G.E. Brown Jr., and F. Martin, *Am. Miner*., 86 (2001) 714.
22. A.A. Battiston, J.H. Bitter, W.M. Heijboer, F.M.F. de Groot, and D.C. Koningsberger, *J. Catal*., 215 (2003) 279.
23. D.C. Koningsberger and R. Prins (Eds.) *X-ray Absorption: Principles, Applications, Techniques of EXAFS, SEXAFS, and XANES* (Wiley, 1988), Chemical Analysis Vol. 92, p. 87.
24. T.E. Westre, P. Kennepohl, J.G. DeWitt, B. Hedmann, K.O. Hodgson, and E.I. Solomon, *J. Am. Chem. Soc.*, 119 (1997) 6297.
25. A.A. Battiston, J.H. Bitter, F.M.F. de Groot, A.R. Overweg, O. Stephan, J.A. van Bokhoven, P.J. Kooyman, C. van der Spec, G. Vankó and D.C. Koningsberger, *J. Catal*. 213 (2003) 251.
26. M. Müller, G. Harvey, and R. Prins, *Micropor. Mesopor. Mater.*, 34 (2000) 135.
27. Q. Zhu, R.M. van Teeffelen, R.A. van Santen, and E.J.M. Hensen, *J. Catal.*, 221 (2004) 575.
28. E.J.M. Hensen, Q. Zhu, and R.A. van Santen, *J. Catal.*, 220 (2003) 260.
29. E.J.M. Hensen, Q. Zhu, M.M.R.M. Hendrix, A.R. Overweg, P.J. Kooyman, M. Sychev, and R.A. van Santen, *J. Catal.*, 221 (2004) 560.
30. J. Pérez-Ramírez, G. Mul, F. Kapteijn, J.A. Moulijn, A.R. Overweg, A. Doménech, A. Ribera, and I.W.C.E. Arends, *J. Catal.*, 207 (2002) 113.

Chapter 6

Catalytic Performance of Steam-treated [Fe,Al]MFI Zeolites in the Direct Oxidation of Benzene to Phenol and Decomposition of N_2O †

Abstract

Various steam-treated [Fe,Al]MFI zeolites were evaluated for their catalytic performance in the direct oxidation of benzene to phenol, using N_2O as oxidant (BTOP), and in the decomposition of N_2O. For [Fe,Al]MFI catalysts varying in iron content (i.e. 0.075-0.6 wt.% Fe), the results suggest that only a fraction of extra-framework iron species are active in the BTOP reaction. On the other hand, the apparent increase in activity with the increase of iron in the [Fe,Al]MFI catalyst indicates that most extra-framework iron species are active in N_2O decomposition. For the set of [Fe,Al]MFI catalysts varying in aluminum concentration (0.0-1.1 wt.% Al), BTOP activity after 2 h time-on-stream is observed to decrease significantly for catalysts with higher aluminum loading. This implies that the occurrence of catalyst deactivation, most likely due to coke formation, is more favorable in the presence of aluminum. On the other hand, N_2O decomposition data reveals that catalysts with higher aluminum concentration exhibit superior performance compared to the samples with lower or without aluminum.

† *Parts of this chapter have appeared in:*

- *J.B. Taboada, E.J.M. Hensen, I.W.C.E. Arends, G. Mul, and A.R. Overweg, Catalysis Today, 110 (2005) 221-227.*

6.1. Introduction

[Fe,Al]MFI zeolites have attracted increasing attention due to their ability to catalyse different reactions.[1-5] One particular reaction of interest nowadays is the direct oxidation of benzene to phenol using N_2O as oxidant (BTOP),[6-8] which could potentially replace the three-step cumene process for the production of phenol. However, despite extensive efforts, there is still no agreement in open literature as to the nature and identity of the active site. Nevertheless, recent studies are directing towards extra-framework iron species, stabilized in the micropore channels of the MFI (or ZSM-5) zeolite, as the catalytically active centers.[9-14]

To gain insight into the structure-activity relationship of the extra-framework iron species in the [Fe,Al]MFI catalyst in the direct oxidation of benzene to phenol reaction, various [Fe,Al]MFI zeolites were prepared with varying iron and aluminum concentrations. In one set of [Fe,Al]MFI zeolites, the concentration of iron was systematically varied down to ppm levels (6000-750 ppm Fe, while aluminum content was kept constant at 1.1 wt.%). Iron in few hundred ppm level simulates the concentration of iron – present as an impurity – in commercial zeolites, and has been proposed to be the active *redox* center in the catalytic oxidation of benzene to phenol.[15] In addition, another set of [Fe,Al]MFI catalysts varying in aluminum concentration (0.0-1.1 wt.% Al, while iron content was kept constant at 0.6 wt.%) was prepared to investigate the influence of aluminum in the formation of active iron species. The interest in varying the aluminum content in [Fe,Al]MFI catalysts stems from recent works in this field, which propose the involvement of aluminum as an acid site[7] or a necessary constituent[16-18] of the active site in the BTOP reaction.

Although there are several methods to prepare [Fe,Al]MFI catalysts,[19-21] the hydrothermal synthesis of isomorphously substituted [Fe,Al]MFI zeolite, followed by calcination, conversion to H-form, and finally steam-treatment appears to be the most promising route to form the active sites in the direct oxidation of benzene to phenol.[6,8,22] In an effort to elucidate the iron species present in the catalysts using Mössbauer spectroscopy as the primary technique, all catalysts were enriched with ^{57}Fe isotope to enhance the Mössbauer absorption. Detailed characterization of the catalyst activation (*presented in chapter 4*) showed that calcination followed by steam-treatment causes extensive migration of framework iron to extra-framework position.

Panov *et al*,[23] proposed that extra-framework iron species stabilized in the MFI matrix, which are active in the BTOP reaction, called *α-sites*,[24,25] are in a bivalent state having a special affinity to nitrous oxide. They suggested that N_2O dissociation causes Fe^{2+} transition to Fe^{3+}, forming active surface oxygen species for the BTOP reaction. Furthermore, Dubkov *et al.*, [9]

showed that a linear correlation exists between the Fe^{2+} concentration and the number of *α-sites*. Nonetheless, no actual BTOP experiments were reported to support such correlation.

In this study, the catalytic activity of various steam-treated [Fe,Al]MFI zeolites varying in iron and aluminum concentrations is evaluated in the direct oxidation of benzene to phenol. For [Fe,Al]MFI catalysts varying in iron content, extra-framework iron species were found predominantly in the high-spin Fe^{2+} state as deduced from Mössbauer spectroscopic studies presented in chapter 4. It is therefore of primary interest to investigate if the amount of Fe^{2+} species present in the [Fe,Al]MFI samples shows a correlation to the BTOP activity of the catalyst. Similar activity measurement is also performed on [Fe,Al]MFI catalysts containing different aluminum concentrations. The amount of Fe^{2+} species in these samples has been shown (in previous chapters) to be dependent on the aluminum concentration.

In addition, the catalytic performance of steam-treated [Fe,Al]MFI zeolites, varying in iron and aluminum concentrations, is investigated in the decomposition of N_2O. Information regarding the catalytic activity of steam-treated [Fe,Al]MFI zeolites in N_2O decomposition is equally important in BTOP studies. This is because the generation of active oxygen species for the BTOP reaction has been shown to be directly related to the dissociation of N_2O.[6,7,26] Thus, the catalytic performance of steam-treated [Fe,Al]MFI zeolites in N_2O decomposition could prove essential in optimising the design of the [Fe,Al]MFI catalyst in the direct oxidation of benzene to phenol and its reaction conditions.

6.2. Experimental

6.2.1. BTOP activity measurements

The experimental setup for evaluating the catalytic performance of various steam-treated [Fe,Al]MFI samples in the direct oxidation of benzene to phenol, using N_2O as oxidant, is schematically illustrated in figure 6.1. The setup consists of a gas mixing section, a reactor and a gas analysis section.

Catalytic reaction is carried out in a single-pass atmospheric plug flow reactor. In a typical BTOP experiment, 100 mg of catalyst particles with a size range of 180-220 μm is placed in a quartz tube reactor (ca. 4mm in diameter) and diluted with SiC to obtain a catalyst bed of 2 cm in height. Prior to BTOP reaction, the catalyst was pre-treated in a flow of 100 ml/min of He for 2 h at 823 K (using a heating rate of 1 K/min). Pre-treatment in inert is normally carried out to remove organic impurities and adsorbed H_2O in the zeolite catalyst, at the same time opens up the zeolite pores and improves accessibility of active sites. Benzene oxidation was carried out by feeding a mixture of C_6H_6/N_2O/He (volume ratio = 1/4/95) at a flow rate

of 100 ml/min at a reaction temperature of 623 K. Gas-phase product analysis was performed by a well-calibrated combination of GC and MS.

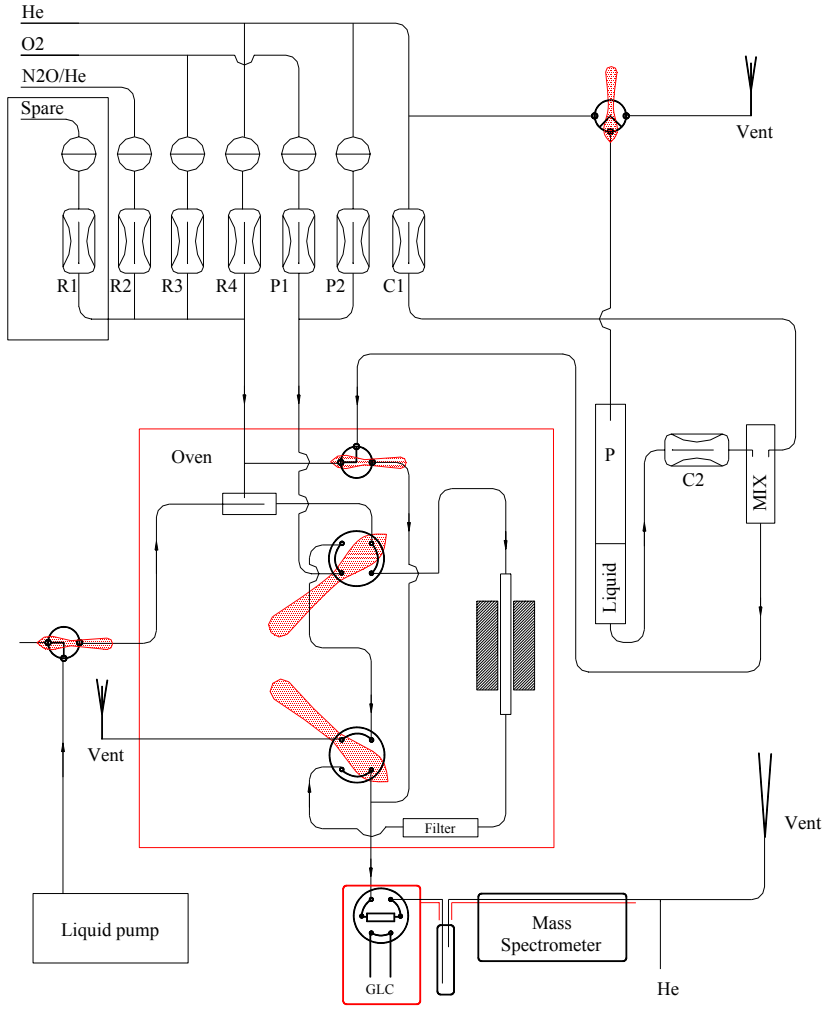

Figure 6.1. *Schematic layout of the single-pass plug flow reactor setup for BTOP reaction.*

6.2.2. N_2O decomposition measurements

N_2O decomposition was carried out in a six-flow reactor set-up,[27] for fast catalyst screening. A basic schematic drawing of the set-up is illustrated in figure 6.2. For the reaction, 50 mg of the catalyst particles with a size range of 180-220 μm and a space-time of $8.65 \cdot 10^5$ g·s·mol^{-1} were used. The space time is defined as the ratio $W / F(N_2O)$, where W is the mass of the catalyst and $F(N_2O)$ is the molar flow of N_2O at the reactor inlet. The feed composition was 1500 ppm N_2O in He at atmospheric condition. Before reaction, the catalysts were pre-treated in He at 823 K for 2 hours and cooled in the same gas flow to the initial reaction temperature.

N_2O, N_2, and O_2 were analysed with a GC (Chrompack CP 9001) equipped with a thermal conductivity detector, using a Poraplot Q column (for N_2O separation) and Molsieve 5A column (for N_2 and O_2 separation). Online product gas analysis was taken every after 30 min of stabilization time.

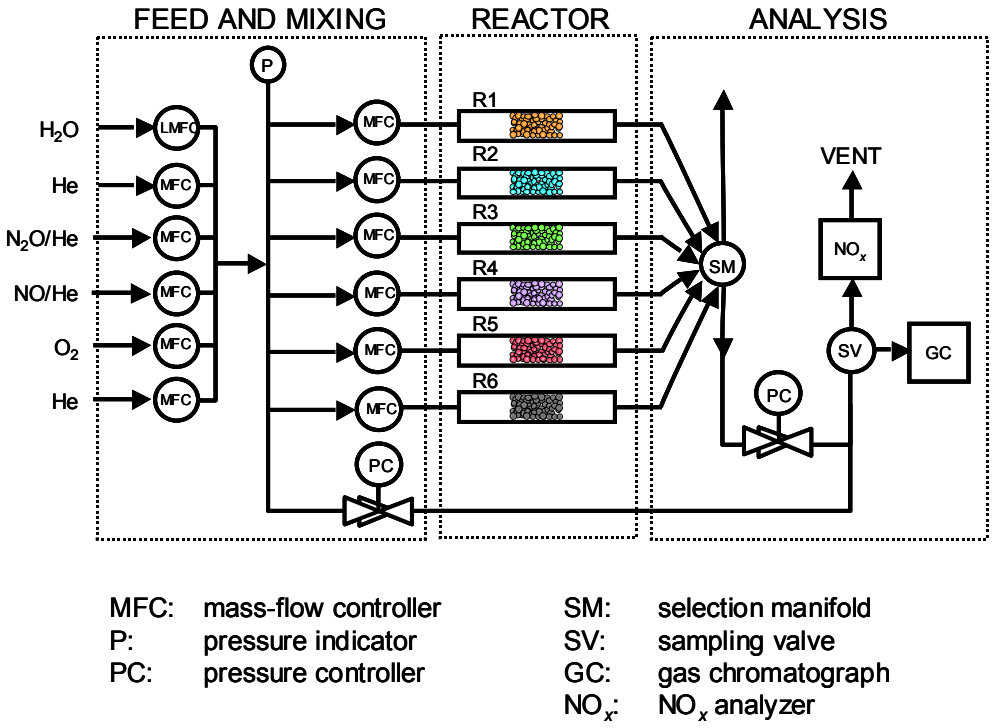

Figure 6.2. *Basic scheme of the six-flow reactor set-up for fast catalyst screening.*[27]

6.3. Results

6.3.1. Catalytic BTOP activity of [Fe,Al]MFI catalysts

6.3.1.1. Effect of iron concentration

[Fe,Al]MFI catalysts varying in iron concentration (0.075-0.6 wt.% Fe, while aluminum content was kept constant at 1.1 wt.%) were tested in the direct oxidation of benzene to phenol, using N_2O as oxidant. Descriptions of the catalyst preparation and activation methods are presented in chapters 3 and 4, respectively. In all activity measurements, BTOP reactions were carried out at the reaction temperature of 623 K.[6,8] The catalytic performance of these catalysts in the BTOP reaction is shown in figure 6.3 and their corresponding reaction data are condensed in table 6.1.

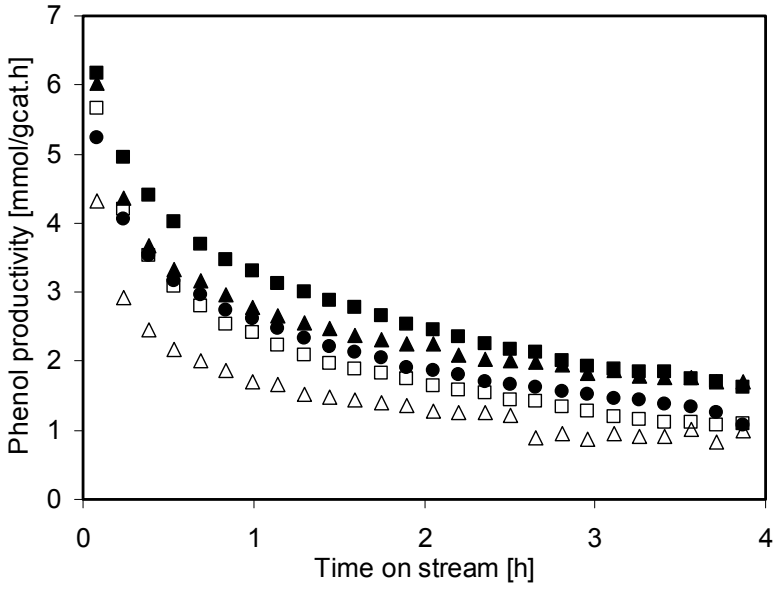

Figure 6.3. *Phenol productivity per gram catalyst of* (Δ) [Fe,Al]MFI $(1:4)_{stm}$, (▲) [Fe,Al]MFI $(0.5:4)_{stm}$, (□) [Fe,Al]MFI $(0.25:4)_{stm}$, (■) [Fe,Al]MFI $(0.17:4)_{stm}$, *and* (●) [Fe,Al]MFI $(0.12:4)_{stm}$ *as a function of reaction time.*

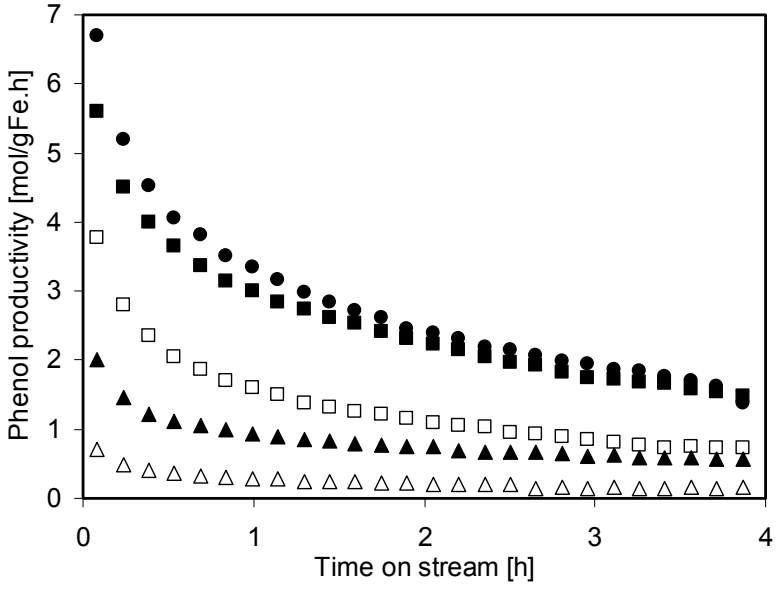

Figure 6.4. *Phenol productivity per gram Fe of* (Δ) [Fe,Al]MFI $(1:4)_{stm}$, (▲) [Fe,Al]MFI $(0.5:4)_{stm}$, (□) [Fe,Al]MFI $(0.25:4)_{stm}$, (■) [Fe,Al]MFI $(0.17:4)_{stm}$, *and* (●) [Fe,Al]MFI $(0.12:4)_{stm}$ *as a function of reaction time.*

Table 6.1. *Reaction data of the* [Fe,Al]MFI *samples with varying iron concentration*.

Sample	t_R = 5 min				t_R = 4 h			
	$X_{C_6H_6}$	$S_{C_6H_6}$	X_{N_2O}	S_{N_2O}	$X_{C_6H_6}$	$S_{C_6H_6}$	X_{N_2O}	S_{N_2O}
[Fe,Al]MFI $(0.12{:}4)_{stm}$	0.22	0.80	0.10	0.50	0.07	0.70	0.01	0.80
[Fe,Al]MFI $(0.17{:}4)_{stm}$	0.29	0.92	0.11	0.65	0.07	>.99	0.02	>.99
[Fe,Al]MFI $(0.25{:}4)_{stm}$	0.27	0.90	0.10	0.60	0.07	0.80	0.02	0.60
[Fe,Al]MFI $(0.5{:}4)_{stm}$	0.37	0.70	0.12	0.54	0.10	>.99	0.03	0.70
[Fe,Al]MFI $(1{:}4)_{stm}$	0.26	0.70	0.14	0.31	0.11	0.50	0.15	0.07
[Fe,Al]MFI $(1{:}2)_{stm}$	0.23	0.76	0.09	0.48	0.07	0.60	0.02	0.60
[Fe,Al]MFI $(1{:}1)_{stm}$	0.22	0.85	0.10	0.48	0.07	>.95	0.03	0.45
[Fe,Al]MFI $(1{:}0.5)_{stm}$	0.27	0.87	0.11	0.51	0.04	>.99	0.03	0.50
[Fe,Al]MFI $(1{:}0)_{stm}$	0.23	0.86	0.08	0.66	0.11	0.90	0.03	0.75

Data contains benzene conversion ($X_{C_6H_6}$)*, benzene selectivity to phenol* ($S_{C_6H_6}$)*, nitrous oxide conversion* (X_{N_2O})*, and nitrous oxide selectivity to phenol* (S_{N_2O}) *after reaction times* (t_R) *of 5 min and 4 h.*

Figure 6.3 shows the rates of phenol formation expressed per gram of catalyst as a function of the reaction time for various [Fe,Al]MFI catalysts varying in iron concentration. This plot illustrates that no apparent trend is observed in relation to the iron content of the catalyst, which is the only parameter varied in this set of samples. However, if the rates of phenol production are compared per gram of iron (figure 6.4), it is evident that the BTOP activity of the steam-treated [Fe,Al]MFI catalysts increases with a decrease in iron concentration. This would imply that active species in the BTOP reaction are favorably formed in samples with dilute iron concentration.

In general, the phenol productivity per gram of iron is observed to increase by about a factor of two, which is similar to the decrement in iron content of the catalyst sample. This would suggest that the number of active sites in the BTOP reaction is more or less comparable in all catalysts, particularly in the first five minutes of reaction time, regardless of iron concentration. Thus, the fraction of active species relative to the iron concentration increases with decreasing iron loading. However, at some point, it will reach an optimum as indicated by (■) [Fe,Al]MFI $(0.17{:}4)_{stm}$, and (●) [Fe,Al]MFI $(0.12{:}4)_{stm}$ in figure 6.4.

Although [Fe,Al]MFI (0.12:4)$_{stm}$, which contains the least iron, exhibits a slightly higher activity than [Fe,Al]MFI (0.17:4)$_{stm}$ (*see figure 6.4*) during the initial stage (i.e. after 5 min time-on-stream) of the BTOP reaction, in essence both samples have a comparable phenol productivity profile when expressed per gram of iron. This indicates that the amount of active species for the BTOP reaction in the [Fe,Al]MFI (0.17:4)$_{stm}$ sample is higher than that in the [Fe,Al]MFI (0.12:4)$_{stm}$. Therefore, amongst the [Fe,Al]MFI catalysts with varying iron concentration, [Fe,Al]MFI (0.17:4)$_{stm}$ contains the most active species. This explains the apparent high catalytic activity exhibited by the [Fe,Al]MFI (0.17:4)$_{stm}$ sample when it is expressed per gram of catalyst as shown in figure 6.3.

6.3.1.2. Effect of aluminum concentration

The rates of phenol formation at 623 K expressed per gram of catalyst as a function of the reaction time for [Fe,Al]MFI catalysts varying in aluminum concentration (0.0-1.1 wt.% Al, while iron content was kept constant at 0.6 wt.%) are shown in figure 6.5. Description of the preparation and activation methods of these catalysts is presented in chapters 3 and 4, respectively. A summary of the reaction data is condensed in table 6.1.

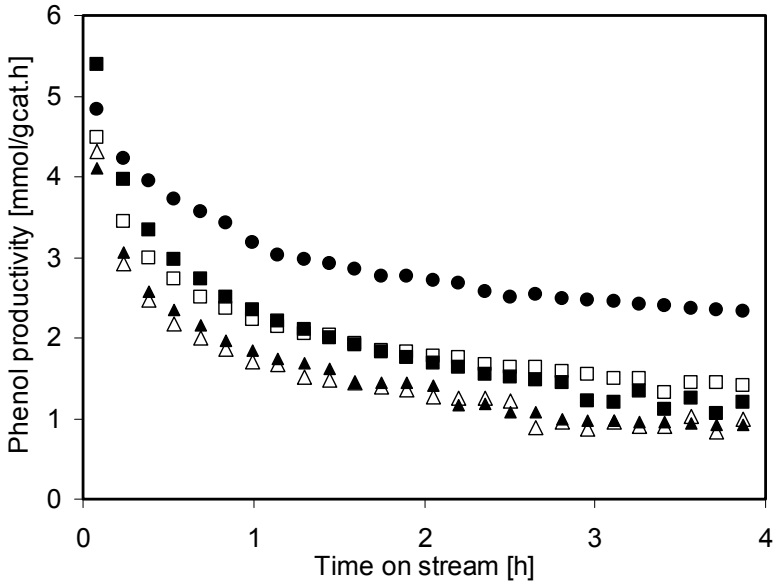

Figure 6.5. *Phenol productivity per gram catalyst of* (Δ) [Fe,Al]MFI (1:4)$_{stm}$, (▲) [Fe,Al]MFI (1:2)$_{stm}$, (□) [Fe,Al]MFI (1:1)$_{stm}$, (■) [Fe,Al]MFI (1:0.5)$_{stm}$, *and* (●) [Fe,Al]MFI (1:0)$_{stm}$ *as a function of reaction time.*

The results show that after a two-hour BTOP time-on-stream, which is close to a steady state condition, the phenol productivity expressed per gram catalyst is observed to increase with the decrease in aluminum concentration. Surprisingly, at this stage of the reaction, the aluminum-free sample exhibits the highest BTOP activity. This is contrary to the recent

works of Hensen *et al*.,[16-18] which advocate the need for aluminum to create the active iron species for the BTOP reaction. The results presented here clearly indicate that active sites for BTOP can be formed without the presence of aluminum. In fact, the presence of aluminum is observed to even deter the conversion of benzene towards phenol. Table 6.1 shows that aluminum-containing samples suffer from an inferior selectivity in both benzene and N_2O conversions towards phenol. This is attributed to (i) coke formation that is evidenced by the change in catalyst color from white (before reaction) to brownish-black in the spent catalyst, and (ii) overoxidation to CO_2 and H_2O. The later products of combustion were detected by online mass spectroscopy particularly for the [Fe,Al]MFI $(1:4)_{stm}$ sample that contains the highest aluminum concentration amongst the samples investigated.

6.3.2. N_2O decomposition activity of [Fe,Al]MFI catalysts

Figure 6.6 shows the N_2O conversion of the steam-treated [Fe,Al]MFI catalysts, varying in iron concentration, as a function of reaction temperature. It is evident from the N_2O conversion *vs* temperature profile that the activity is highest for [Fe,Al]MFI $(1:4)_{stm}$, which contains most iron. Furthermore, the activity progressively decreases with the decrease in iron concentration. Therefore, a straightforward relationship between the activity and the amount of iron is observed. Figure 6.7 illustrates the linear correlation of the N_2O activity and the amount of iron in the [Fe,Al]catalyst at different reaction temperatures.

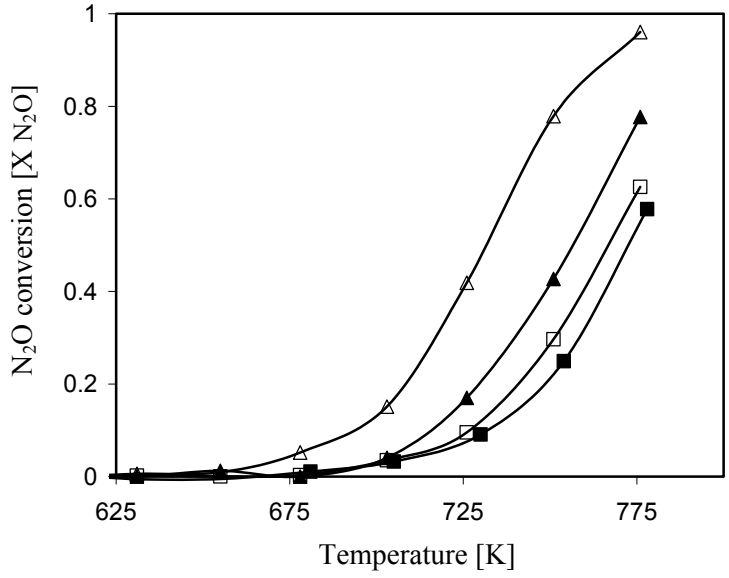

Figure 6.6. *Plot of the N_2O conversion vs temperature of variou steam-treated* [Fe,Al]MFI *catalysts varying in iron concentration. The activity of the catalyst is indicated by*: (Δ) *for* [Fe,Al]MFI $(1:4)_{stm}$, (▲) *for* [Fe,Al]MFI $(0.5:4)_{stm}$, (□) *for* [Fe,Al]MFI $(0.25:4)_{stm}$, *and* (■) [Fe,Al]MFI $(0.17:4)_{stm}$.

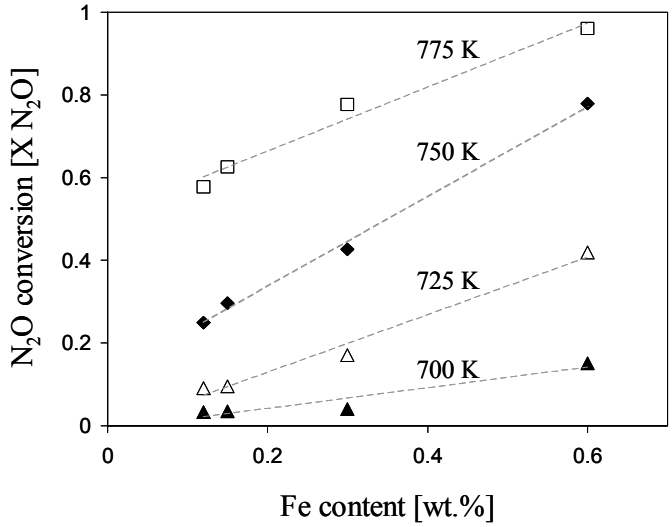

Figure 6.7. *N_2O conversion as a function of iron content taken at different reaction temperatures.*

However for the samples varying in aluminum concentration, figure 6.8 reveals that the activity of [Fe,Al]MFI catalysts in the N_2O decomposition is influenced by the presence of aluminum. Results show that [Fe,Al]MFI $(1:4)_{stm}$, which contains most aluminum, exhibits the highest N_2O decomposition activity. N_2O conversion is observed to decrease as the aluminum concentration in the [Fe,Al]MFI catalyst is decreased. Finally, Fe,Al]MFI $(1:1)_{stm}$, which contains least aluminum, is observed to exhibit a similar N_2O decomposition activity compared to Fe,Al]MFI $(1:0)_{stm}$, which contains no aluminum. These results indicate that although active sites can be formed without aluminum, its presence does enhance the catalytic performance of the [Fe,Al]MFI catalyst in N_2O decomposition.

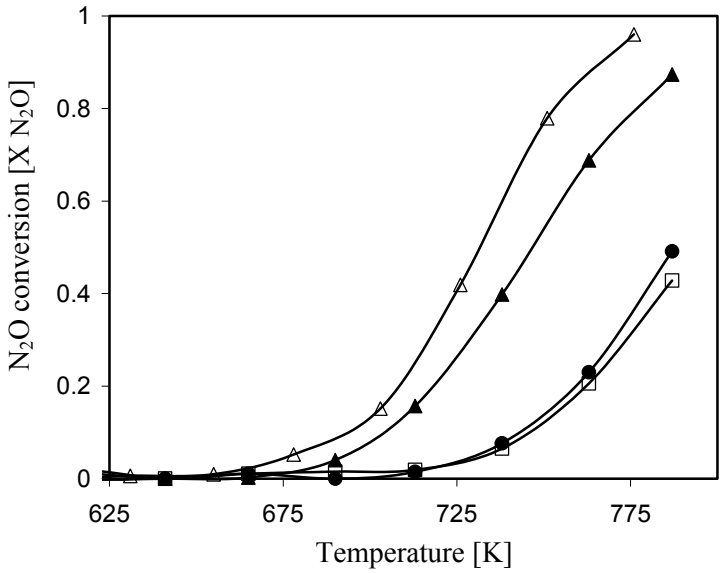

Figure 6.8. *Plot of the N_2O conversion vs temperature of various steam-treated* [Fe,Al]MFI *catalysts varying in aluminum concentration. The activity of the catalyst is indicated by*: (Δ) *for* [Fe,Al]MFI $(1:4)_{stm}$, (▲) *for* [Fe,Al]MFI $(1:2)_{stm}$, (□) *for* [Fe,Al]MFI $(1:1)_{stm}$, *and* (●) *for* [Fe,Al]MFI $(1:0)_{stm}$.

6.4. Discussion

6.4.1. Active species in [Fe,Al]MFI catalysts

Following recent developments in the direct oxidation of benzene to phenol,[9-13] this study also views extra-framework iron species, forming *redox* centers, as the catalytically active species in the BTOP reaction. Brønsted acid sites, which have been proposed as active centers,[30,31] do not play a prominent role. This was substantiated by the BTOP measurement performed on the H-form of [Fe,Al]MFI (1:4) zeolite, i.e. the state of the sample prior to steam-treatment, which did not exhibit any catalytic activity (result is not shown for brevity). Furthermore, the substantial BTOP activity observed in the aluminum-free [Fe,Al]MFI catalyst (figure 6.5) also rules out the possibilities of strong Lewis acid sites,[32-34] created by extra-framework aluminum, and extra-framework (Fe-Al-O) mixed oxide species[16,18] as active centers for BTOP reaction.

For the set of [Fe,Al]MFI samples varying in iron concentration, Mössbauer spectroscopic study (*see chapter 4*) shows that steam-treatment leads to a complete removal of framework iron to extra-framework position. Based on spectral parameters, the extra-framework iron formed is predominantly in the divalent state (ca. 90%). However, although these samples have a prevalent high-spin Fe^{2+} component, the BTOP activity relative to the amount of iron is shown to increase with the decrease in iron concentration.

To recall, XANES (x-ray absorption near-edge spectroscopy) experiments (*see chapter 5*) have shown that most, if not all, Fe^{2+} species present in the steam-treated [Fe,Al]MFI samples are easily oxidized to Fe^{3+} ions in the presence of N_2O at 623 K. The oxidation proceeds by abstracting atomic oxygen from an impinging N_2O molecule, thereby generating an active surface oxygen species.[6,7,26] Since BTOP activity (relative to iron) is higher for samples with lower Fe^{2+} concentration, this suggests that most likely the selectivity of N_2O to form phenol decreases with an increase of Fe^{2+} concentration.

To illustrate the reactivity of the generated oxygen species from N_2O towards benzene oxidation, the initial N_2O consumption during the BTOP reaction is plotted (figure 6.9) together with the initial phenol productivity as a function of Fe^{2+} concentration of the different [Fe,Al]MFI catalysts. In this figure, the amount of converted N_2O increases with the increase in Fe^{2+} ions. This indicates that most Fe^{2+} species were oxidized to Fe^{3+} in the presence of N_2O at 623 K. However in the same figure, the initial phenol productivity hardly changed with the increase in Fe^{2+} concentration. This clearly demonstrates that the selectivity of N_2O towards phenol decreases with the increase in iron concentration.

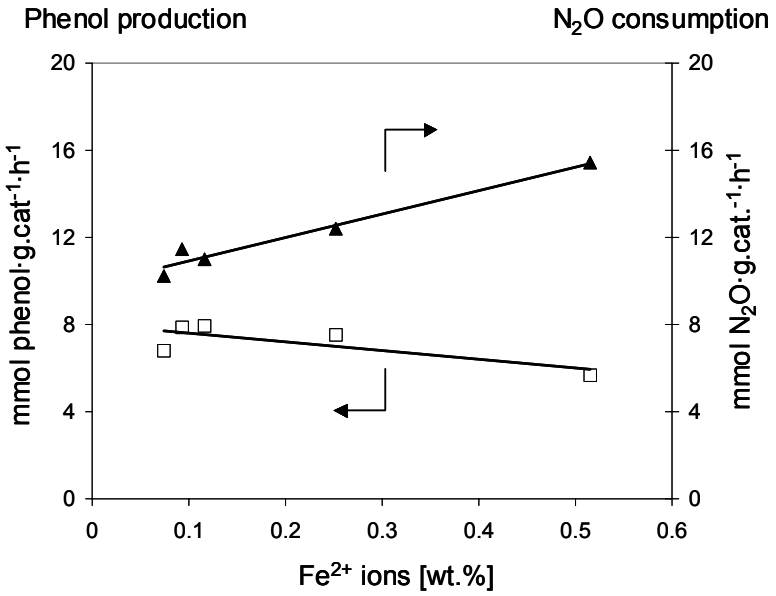

Figure 6.9. (▲) *Initial N_2O consumption during the BTOP reaction and* (□) *initial phenol productivity as a function of Fe^{2+} concentration (wt.%) in steam-treated* [Fe,Al]MFI *samples.*

Since hardly any N_2O decomposition was observed at 623 K (*see figure 6.6*), and furthermore no molecular O_2 was detected by online mass spectroscopy during the BTOP reaction, thus, a competition between the BTOP oxidation and N_2O decomposition for active sites was considered to be highly unlikely to occur. The decrease in selectivity of converted N_2O towards phenol is, therefore, attributed to overoxidation of benzene to condensable products like dihydroxybenzenes[17] as well as coke formation[28] and deep oxidation to CO_2. The latter is confirmed by mass spectroscopy though the presence of CO_2 and H_2O in the product stream. These products were found especially for the catalyst with the highest iron and aluminum concentrations.

On the other hand, the N_2O decomposition shows a straightforward relationship between the activity and the iron concentration. Activity data indicates that the activity is higher for samples with high iron loading, which is in agreement with the study of Pérez-Ramírez *et al.*[12] This confirms that, contrary to the BTOP reaction, most extra-framework iron species present after steam-treatment of the [Fe,Al]MFI zeolite are active in N_2O decomposition.

6.4.2. Role of aluminum

For samples with varying aluminum concentration, and specifically for the aluminum-free [Fe,Al]MFI $(1{:}0)_{stm}$, the BTOP activity after 2 h time-on-stream is observed to be higher for samples with lower aluminum concentration. In fact, at this stage of the reaction, the

aluminum-free [Fe,Al]MFI $(1:0)_{stm}$ exhibits the highest BTOP activity. This is a strong indication that aluminum does not play a role in the BTOP catalysis, and, therefore, is not a necessary constituent of the active species in [Fe,Al]MFI catalysts for the BTOP reaction. To circumvent any doubts of traces of aluminum, which might be present as an impurity, the aluminum-free sample was subjected to INAA (Instrumental Neutron Activation Analysis), in which the detection limit for elemental analysis is up to 10 ppm. This technique confirmed the absence of aluminum. Furthermore, the increase in activity with the decrease in aluminum content is compelling evidence that the presence of aluminum is not crucial at all in the formation of active species for the direct oxidation of benzene to phenol.

On the contrary, the presence of aluminum could bring about deactivation of active sites by coke formation attributed to the presence of acidity (both in the form of Brønsted and Lewis sites) in the zeolite matrix. This could explain the substantial decrease in activity for the samples containing relatively high aluminum over a period of time. Whereas, for the aluminum-free [Fe,Al]MFI sample, deactivation hardly takes place. Thus, due to limited coke formation, the active sites within the microporous voids are still accessible.

For N_2O decomposition, catalytic activity appears to increase as a function of the aluminum content in the [Fe,Al]MFI catalyst. However, the activity observed in the aluminum-free sample would indicate that aluminum *per se* does not play a role in the catalysis. Mössbauer spectroscopic study of the [Fe,Al]MFI zeolites (*chapter 4*) has shown that the presence of aluminum enhances the extraction of framework iron to extra-framework positions. At the same time, it facilitates the stabilization of extra-framework ferric ions that are able to undergo an autoreduction process to form the Fe^{2+} species during heat treatment. These extra-framework Fe^{2+} species have been shown in this study to be readily oxidized in the presence of N_2O, thus, forming *redox* centers that are necessary for N_2O decomposition. Furthermore, this autoreduction process is not restricted to aluminum containing samples only. Extensive studies by Berlier *et al*.[29] have shown that, although limited, a portion of ferric ions in aluminum-free MFI zeolites can also undergo autoreduction to form the active ferrous centers, which would explain the activity in the aluminum-free sample.

These results, therefore, show that a linear correlation between the presence of Fe^{2+} species and the catalytic activity is only applicable to N_2O decomposition. Although N_2O decomposition is directly related to the BTOP reaction, no direct relation between the amount of Fe^{2+} species and the activity in the BTOP reaction can be established. This is mainly due to the fact that the catalyst suffers from deactivation through coke formation and poor selectivity as both iron and aluminum concentrations are increased.

6.5. Conclusion

The performance of various [Fe,Al]MFI catalysts, containing ca. 90% of extra-framework iron in the high-spin Fe^{2+} state, has been evaluated in the direct oxidation of benzene to phenol with N_2O as oxidant. Most, if not all, of these extra-framework iron species are active in N_2O decomposition. However, only a fraction of the Fe^{2+} species is active in the direct oxidation of benzene to phenol. This fraction is observed to increase with deceasing iron concentration. Therefore, the amount of Fe^{2+} species can only be correlated to the activity in the decomposition of N_2O, but not in the BTOP reaction. The increase in iron concentration would lead to the formation of extra-framework iron species that exhibit low selectivity to phenol due to overoxidation of the benzene reactant.

On the other hand, for the [Fe,Al]MFI catalysts varying in aluminum concentration, the BTOP activity appears to increase with the decrease in aluminum loading, after a certain period of reaction time (i.e. >5 minutes time-on-stream). This indicates that the presence of aluminum is not at all crucial as a constituent of the active site in the direct oxidation of benzene to phenol. On the contrary, the decrease in selectivity in both N_2O and benzene towards the formation of phenol, suggests that the presence of aluminum could lead to overoxidation of benzene to condensable products as well as coke formation and deep oxidation to CO_2 and H_2O.

Lastly, the presence of aluminum in the [Fe,Al]MFI catalyst seems to enhance the activity in the decomposition of N_2O. In our view, aluminum *per se* does not participate in the catalysis; rather, it enhances the extraction of framework iron and promotes the stabilization of extra-framework iron species that exhibit *redox* properties, which is necessary for the catalytic decomposition of N_2O.

Acknowledgements

The author would like to thank Dr. E.J.M. Hensen, Schuit Institute of Catalysis, Eindhoven University of Technology, for the dedicated benzene to phenol set-up. Ing. B.van der Linden, Reactor and Catalysis Engineering, DelftChemTech, Delft University of Technology, is gratefully acknowledged for his assistance in the 6-flow reactor set-up.

REFERENCES

1. A.A. Battiston, J.H. Bitter, and D.C. Koningsberger, *Catal. Lett.*, 66 (2000) 75.
2. L.J. Lobree, I. Hwang, J.A. Reimer, and A.T. Bell, *Catal. Lett.*, 63 (1999) 233.
3. H.-Y. Chen, T. Voskoboinikov, and W.M.H. Sachtler, *J. Catal.*, 180 (1998) 171.
4. E.M. El-Malki, R.A. van Santen, and W.M.H. Sachtler, *J. Catal.*, 196 (2000) 212.
5. F. Kapteijn, G. Marbán, J. Rodríguez-Mirasol, and J.A. Moulijn, *J. Catal.*, 167 (1997) 256.
6. G.I. Panov, *Cattech*, 4 (2000) 18.
7. P.P. Notté, *Top. Catal.*, 13 (2000) 387.
8. A. Ribera, I.W.C.E. Arends, S. de Vries, J. Pérez-Ramírez, and R.A. Sheldon, *J. Catal.*, 195 (2000) 287.
9. K.A. Dubkov, N.S. Ovanesyan, A.A. Shteinman, E.V. Starokon, and G.I. Panov, *J. Catal.*, 207 (2002) 341.
10. A.M. Ferretti, C. Oliva, L. Forni, G. Berlier, A. Zecchina, and C. Lamberti, *J. Catal.*, 208 (2002) 83.
11. J.A. Ryder, A.K. Chakraborty, and A.T. Bell, *J. Catal.*, 220 (2003) 84.
12. J. Pérez-Ramírez, F. Kapteijn, and A. Brückner, *J. Catal.*, 218 (2003) 234.
13. P.K. Roy and G.D. Pirngruber, *J. Catal.*, 227 (2004) 164.
14. J. Jia, K.S. Pillai, and W.M.H. Sachtler, *J. Catal.*, 221 (2004) 119.
15. G. Centi, B. Wichterlova, and A.T. Bell (Eds.), *Catalysis by Unique Metal Ion Structures in Solid Matrices*, in: NATO Science Series, Kluwer Academic, Dordrecht, 2001.
16. E. Hensen, Q. Zhu, P.-H. Liu, K.-J. Chao, and R. van Santen, *J. Catal.*, 226 (2004) 466.
17. Q. Zhu, R.M. van Teeffelen, R.A. van Santen, and E.J.M. Hensen, *J. Catal.*, 221 (2004) 575.
18. E.J.M. Hensen, Q. Zhu, and R.A. van Santen, *J. Catal.*, 220 (2003) 260.
19. X. Feng and W.K. Hall, *J. Catal.*, 166 (1997) 368.
20. C. Plog, F. Schueth, V. Goeman, and R. Andorf, *Preparation of a Fe- or Mn-exchanged zeolite*, EP 0867406, 1998.
21. M. Kögel, V.H. Sandoval, W. Schwieger, A. Tissler, and T. Turek, *Catal. Lett.*, 51 (1998) 23.
22. J. Pérez-Ramírez, G. Mul, F. Kapteijn, J.A. Moulijn, A.R. Overweg, A. Doménech, A. Ribera, and I.W.C.E. Arends, *J. Catal.*, 207 (2002) 113.
23. N.S. Ovanesyan, A.A. Shteinman, V.I. Sobolev, K.A. Dubkov, and G.I. Panov, *Kinet. Katal.*, 39 (1998) 863.
24. G.I. Panov, A.S. Kharitonov, and V.I. Sobolev, *Appl. Catal.*, 98 (1993) 1.
25. G.I. Panov, V.I. Sobolev, K.A. Dubkov, V.N. Parmon, N.S. Ovanesyan, A.E. Shilov, and A.A. Shteinman, *React. Kinet. Catal. Lett.*, 61 (1997) 251.

26. G.I. Panov, A.K. Uriarte, M.A. Rodkin, and V.I. Sobolev, *Catal. Today*, 41 (1998) 365.
27. J. Pérez-Ramírez, R.J. Berger, G. Mul, F. Kapteijn, and J.A. Moulijn, *Catal. Today*, 60 (2000) 93.
28. D. Meloni, R. Monaci, V. Solinas, G. Berlier, S. Bordiga, I. Rossetti, C. Oliva, and L. Forni, *J. Catal*., 214 (2003) 169.
29. G. Berlier, G. Spoto, S. Bordiga, G. Ricchiardi, P. Fisicaro, A. Zecchina, I. Rossetti, E. Selli, L. Forni, E. Giamello, and C. Lamberti, *J. Catal*., 208 (2002)64.
30. E. Suzuki, K. Nakashiro, and Y. Ono, *Chem. Lett*., (1988) 953.
31. R. Burch and C. Howitt, *Appl. Catal. A*., 103 (1993) 135.
32. V.L. Zholobenko, I.N. Senchenya, L.M. Kustov, and V.B. Kazansky, *Kinet. Catal.*, 32 (1991) 151.
33. J.L. Motz, H. Heinrichen, and W.F. Hölderich, *J. Mol. Catal.*, 136 (1998) 175.
34. L.M. Kustov, A.L. Tarasov, V.I. Bogdan, A.A. Tyrlov, and J.W. Fulmer, *Catal. Today*, 61 (2000) 123.

Chapter 7

In Situ Studies of [Fe,Al]MFI Catalysts in the Direct Oxidation of Benzene to Phenol

Abstract

In situ Mössbauer studies of the [Fe,Al]MFI catalysts, varying in iron concentration, and that of the aluminum-free [Fe]MFI sample were carried out to facilitate the identification of the catalytically active iron species in the direct oxidation of benzene to phenol (BTOP) reaction. *In situ* treatments were performed in four stages, i.e. (i) He pretreatment, (ii) N_2O oxidation, (iii) C_6H_6 reduction, and (iv) C_6H_6-N_2O reaction. The first 3 treatments simulate a step-wise breakdown of the BTOP reaction, while the last treatment is the BTOP reaction in excess N_2O. Mössbauer spectra were recorded after each *in situ* treatment to monitor the physico-chemical state of iron and its changes. In general, the Mössbauer spectra of the [Fe,Al]MFI catalysts varying in iron concentration recorded after *in situ* treatments reveal the diversity of extra-framework iron species formed. From the trends observed in the Mössbauer spectra, a model is proposed describing the distribution of extra-framework iron species. In addition, it is inferred that the *redox* changes (upon oxidation in N_2O and reduction in benzene) involve a reversible $Fe^{2+}\leftrightarrow Fe^{3+}$ transition. This indicates that at least extra-framework binuclear iron species is required. A reversible $Fe^{2+}\leftrightarrow Fe^{4+}$ transition has not been observed in this study. Finally, although highly dispersed iron species exhibit high sensitivity towards *redox* changes under oxidizing (in N_2O) or reducing (in benzene) environments, results indicate that more than one type of iron species is catalytically active in the BTOP reaction.

7.1. Introduction

Fe-containing ZSM-5 zeolites (or [Fe,Al]MFI) are well-known to catalyse the direct oxidation of benzene to phenol, using N_2O as oxidant (BTOP).[1-4] Nevertheless, identification of the active site in this oxidation reaction continues to be a subject of debate in open literature. Recent studies have shown that extra-framework iron species that are stabilized in the MFI zeolites micropores form the active sites for the BTOP reaction.[5-10] This is confirmed in our previous study on the catalytic performance of various [Fe,Al]MFI with varying iron and aluminum concentrations (*see chapter 6*).

For the [Fe,Al]MFI zeolites varying in iron concentration, extra-framework iron species formed after steam-treatment is predominantly in the high-spin Fe^{2+} state (ca. 90%, based on spectral contribution).[11] From the BTOP activity data of these catalysts, the initial N_2O consumption in the BTOP reaction (*figure 6.9, chapter 6*) shows a straightforward linear relationship with the quantity of extra-framework Fe^{2+} species in the [Fe,Al]MFI zeolite.[4] This indicates that most, if not all, Fe^{2+} species exhibit a high affinity towards N_2O, which forms surface oxygen species necessary for the BTOP reaction.

The generation of active oxygen species on the [Fe,Al]MFI catalyst from the dissociation of N_2O is regarded as a crucial step in the BTOP reaction,[1,12] and has been shown to be a function of extra-framework iron concentration.[4,13] As illustrated in the previous chapter, ca. 90% of extra-framework iron species in the [Fe,Al]MFI catalysts, varying in iron content, is prevalently in the high-spin Fe^{2+} state. However, the direct oxidation of benzene to phenol reaction indicates a decrease in phenol production (relative to iron) with the increase of Fe^{2+} ions in the catalyst. This shows that not all Fe^{2+} species are active in the BTOP reaction. It is therefore evident that we are dealing with various extra-framework iron species.

To discriminate between the different iron species, and to identify the iron species that is catalytically active in the BTOP reaction, ^{57}Fe Mössbauer spectroscopy has been performed on the [Fe,Al]MFI catalysts that have been subjected to controlled treatments. *In situ* ^{57}Fe Mössbauer spectroscopic studies on [Fe,Al]MFI catalysts have been carried out by several authors,[5,14-15] to investigate the reduction/oxidation processes and their relations to catalytic properties. However, these studies did not involve an N_2O-C_6H_6 *redox* cycle. Thus, in this study, the change in the physico-chemical states of iron in the BTOP cycle is investigated. *In situ* ^{57}Fe Mössbauer data were collected at different reduction/oxidation stages that correspond to a breakdown in the BTOP catalytic reaction. The BTOP reaction cycle is based on the reaction mechanism proposed by Panov,[1] and involves the following steps as illustrated in figure 7.1.

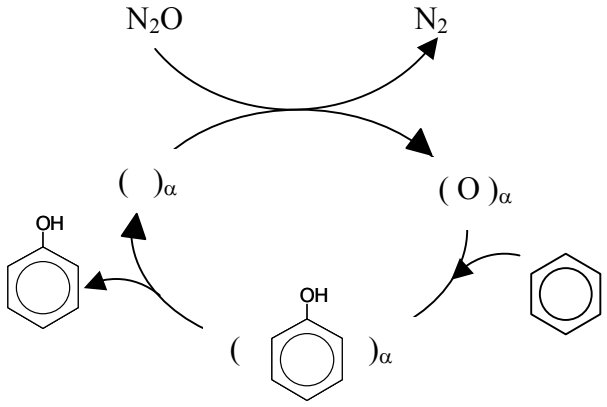

Figure 7.1. *Reaction cycle of benzene oxidation to phenol involving and active site,* $( )_\alpha$.

The first step requires dissociation of nitrous oxide, N_2O, on an active site, $( )_\alpha$, to produce a specific surface α-oxygen, $(O)_\alpha$.[16] This is followed by the oxidation of benzene to form phenol on the active site. Finally, desorption of the product phenol leaves an empty active site, which completes the BTOP reaction cycle.

Each *in situ* treatment in the ^{57}Fe Mössbauer experiment is, therefore, designed to replicate a step in the BTOP reaction cycle – i.e. (i) a pretreatment stage to generate an active site, $( )_\alpha$; (ii) oxidation by N_2O; and (iii) reaction with benzene. Furthermore, Mössbauer measurements were conducted on the catalysts that have been on-stream for 1.5 h under BTOP reaction conditions (i.e. in C_6H_6/N_2O, in excess N_2O, mixture).

In addition to *in situ* studies of the steam-treated [Fe,Al]MFI catalysts varying in iron concentration, *in situ* ^{57}Fe Mössbauer studies were also performed on the aluminum-free [Fe]MFI catalyst (i.e. $[Fe,Al]MFI\ (1:0)_{stm}$). The interest in *in situ* studies of the Al-free sample stems from the fact that it exhibits different spectral characteristics compared to the samples with aluminum (*as illustrated in chapter 4*), and that it shows significant activity and high selectivity in the direct oxidation of benzene to phenol, using N_2O as oxidant (*refer to chapter 6*).

7.2. Experimental

7.2.1. *In situ* ^{57}Fe Mössbauer measurements

[Fe,Al]MFI catalysts used in this study were from the same batch of steam-treated [Fe,Al]MFI zeolites that were described in chapter 4. Their catalytic properties has been presented in chapter 6.

For *in situ* ^{57}Fe Mössbauer studies, a reactor equipped with a stainless steel cell with beryllium windows was used to avoid air exposure (*see figure 7.2*). Description of the reactor and the *in situ* cell is reported elsewhere.[17] A sample of about 160 mg of the catalyst was placed in the *in situ* cell and was subjected to different gas treatments at high temperature. The approach is to have a breakdown of the catalytic cycle and then measure the Mössbauer spectrum after every treatment. That means; (i) after pretreatment with He flow of 30 ml/min at 823 K for about 2 h; (ii) after N_2O loading with 30 ml/min N_2O at 623 K for 1.5 h, and (iii) after flushing with benzene in He using a flow rate of 30 ml/min (4/96 volume ratio of C_6H_6/He) at room temperature and at 473 K for 1.5 h. In addition, Mössbauer measurements were performed after 1.5 h BTOP reaction, in excess N_2O, at 623 K using a flow rate of 30 ml/min (4/96 volume ratio of C_6H_6/N_2O).

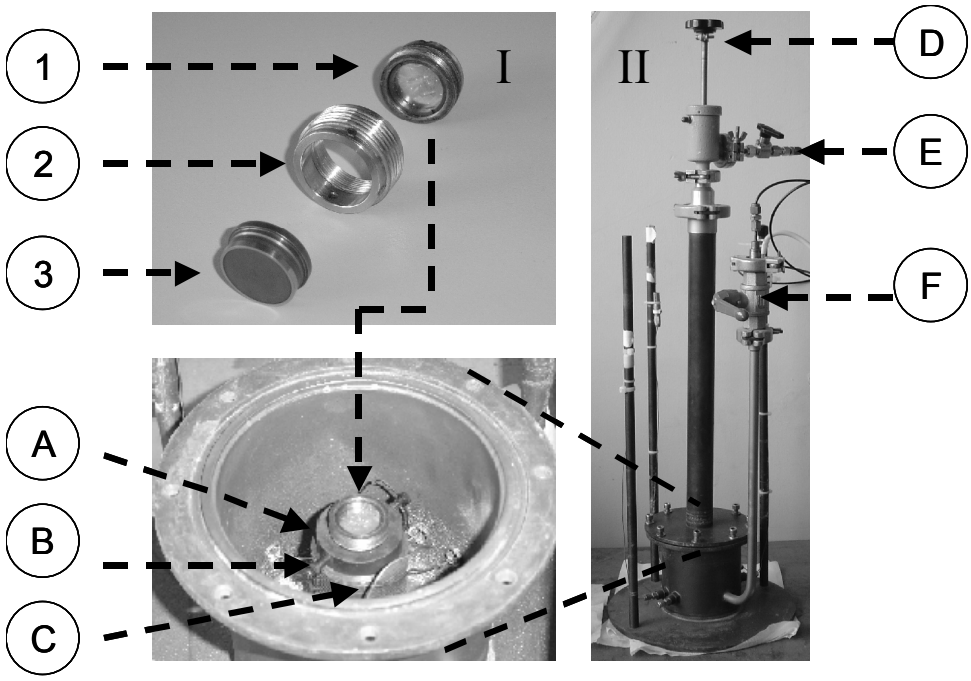

Figure 7.2. [I] *In situ cell: 1. sample holder (behind is a beryllium window), 2. cell cover, 3. beryllium window with an indium ring.* [II] *Reactor: A. heating mantel, B. cell clamps, C. thermocouple, D. cell cover holder, E. gas inlet, and F. gas outlet*

After each treatment, the *in situ* cell was cooled to room temperature, hermetically sealed, and then transferred to a cryostat for low temperature (i.e. 77 and 4.2 K) Mössbauer measurements. ^{57}Fe Mössbauer spectra were measured on a constant acceleration spectrometer in a triangular mode with a ^{57}Co:Rh source. The spectra were fitted with Lorentzian-shaped lines to obtain the Mössbauer parameters (i.e. isomer shift [IS], quadrupole splitting [QS], and hyperfine field [HF]). Isomer shift values are reported relative

to sodium nitroprusside. The broad magnetic features were fitted with several components, which simulate a distribution of hyperfine fields.

7.2.2. Catalyst treatments

7.2.2.1. Pretreatment in He

A sample of steam-treated [Fe,Al]MFI catalyst (ca. 160 mg) was placed in a sample holder (or cell) and mounted in the *in situ* reactor. Under a constant flow of He (30 ml/min), the reactor was heated to 823 K following a temperature ramp of 5 K/min. The pretreatment of the sample in He was kept at 823 K for about 2 h, similar to the pretreatment condition prior to the BTOP reaction (*see chapter 6*). The pre-treated sample was cooled down (in He) to room temperature (RT) and sealed. The *in situ* cell is equipped with an indium ring to avoid air exposure when sealed. It is then transferred to a cryostat for low temperature Mössbauer measurements at 77 K and 4.2 K.

7.2.2.2. N_2O oxidation

Following the heat treatment in He, the samples were oxidized by treatment with nitrous oxide (30 ml/min, 99.7% N_2O) and heated up to 623 K at a ramp rate of 5 K/min. The samples were treated for 1.5 h, and cooled down (in N_2O) to room temperature and sealed in the *in situ* cell. It is then transferred to a cryostat for low temperature Mössbauer measurements at 77 K and 4.2 K.

7.2.2.3. Benzene treatment

After N_2O treatment, the samples were subjected to a C_6H_6/He gas mixture (30 ml/min) at room temperature. Benzene was introduced in the gas mixture *via* an infusion pump (Harvard Apparatus PHD2000 programmable, equipped with 10 ml syringe) at a rate of 4.8 μL/min of liquid benzene and flushed with He to give a partial pressure of about 4% C_6H_6, rest He. After 1.5 h exposure in C_6H_6/He gas mixture at room temperature, the samples were hermetically sealed and transferred to a cryostat for low temperature Mössbauer measurements at 77 K and 4.2 K. The samples were then re-oxidized with nitrous oxide (30 ml/min) at 623 K for 1.5 h.

Following the re-oxidation in N_2O, the samples were mounted back in the *in situ* reactor and heated (temperature ramp of 5 K/min) to 473 K under a constant flow of C_6H_6/He gas mixture (30 ml/min; 4% C_6H_6, rest He). The reaction was kept at 473 K for 1.5 h. Before cooling down to room temperature, the reactor gas inlet and outlet were closed. Thus, the samples were cooled down to room temperature in a mixture of benzene and helium environment. The sample cell was then hermetically sealed and Mössbauer spectra were recorded at 77 K and 4.2 K.

7.2.2.4. BTOP reaction at 623 K

Following the benzene treatment at 473 K, the samples were treated with nitrous oxide (30 ml/min) at 623 K for 1.5 h. The re-oxidized samples were subjected to a reaction gas mixture of benzene in N_2O (30 ml/min; 4% C_6H_6, rest N_2O) and heated up to 623 K following a temperature ramp rate of 5 K/min. The reaction was kept at 623 K for 1.5 h. Afterwards, the reactor gas inlet and outlet were closed and the samples were allowed to cool down to room temperature in C_6H_6/N_2O environment. The samples were hermetically sealed in the *in situ* cell and transferred to a cryostat for low temperature Mössbauer measurements at 77 K and 4.2 K.

7.3. Results

7.3.1. *In situ* studies of [Fe,Al]MFI catalysts

For the [Fe,Al]MFI samples varying in iron concentration, the ^{57}Fe Mössbauer spectra taken ***directly*** after steam-treatment has been presented and discussed in chapter 4 (*see figure 4.9*). To recall, all spectra exhibit a predominant high-spin Fe^{2+} doublet with an isomer shift (IS) of 1.66 mm·s^{-1}, and a quadrupole splitting (QS) of 3.26 mm·s^{-1}. Based on spectral contribution, the divalent iron ions accounts to ca. 90% of the total iron in the samples. It seems therefore that the [Fe,Al]MFI samples in this study have iron that is predominantly in the ferrous state. Nevertheless, prior to performing any measurements under controlled environment, ^{57}Fe Mössbauer spectra of the steam-treated samples were again recorded at 77 and 4.2 K. This is to set a point of comparison before and after treatments, specifically since these catalysts are prone to aging effects – such as slow oxidation of the ferrous ions due to molecular oxygen uptake.[18]

^{57}Fe Mössbauer spectra of the steam-treated samples recorded at 77 K, prior to any treatments, are shown in figure 7.3. For [Fe,Al]MFI $(1{:}4)_{stm}$ and [Fe,Al]MFI $(0.5{:}4)_{stm}$, the samples with relatively high iron concentration, the spectra exhibit a high-spin Fe^{3+} doublet, **d(I),** with IS ~ 0.8 mm·s^{-1} and QS ~ 1.10 mm·s^{-1}. This component partially resolves into a sextuplet at 4.2 K (figure 7.4). Since the temperature window over which these transitions take place is small, it is likely that it is caused by superparamagnetic iron oxide nanoparticles (FeO_x) rather than paramagnetic ions. As this component is relaxed at 77 K and magnetically split at 4.2 K, we infer that these particles are small, ca. 2nm in diameter. Based on spectral contribution (tables 7.1-7.2), it is estimated that these superparamagnetic iron oxide nanoparticles are less than 10% of the total iron species formed. The fact that they were not observed in any transmission electron micrographs (*see chapter 4*) could be due to either the scarcity of the iron oxide phase or that they are highly disordered iron oxide particles, leading to an insufficient contrast in the TEM images. In addition to **d(I)**, [Fe,Al]MFI $(1{:}4)_{stm}$ and

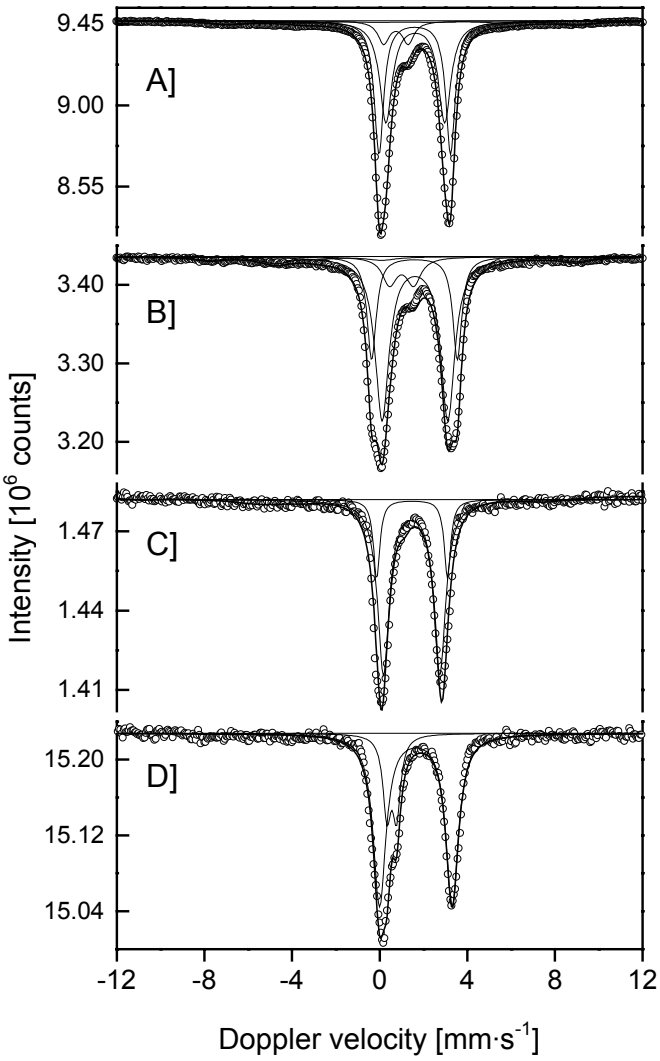

Figure 7.3. *^{57}Fe Mössbauer spectra recorded at 77 K in high vacuum (10^{-6} mbar) of* [Fe,Al]MFI *catalysts varying in iron content:* A] [Fe,Al]MFI (1:4)$_{stm}$, B] [Fe,Al]MFI (0.5:4)$_{stm}$, C] [Fe,Al]MFI (0.25:4)$_{stm}$, and D] [Fe,Al]MFI (0.12:4)$_{stm}$. *Open circles indicate measured values and solid lines show the fit and its sub-spectra.*

[Fe,Al]MFI (0.5:4)$_{stm}$ also exhibit a small contribution of a broad feature (± 10 mm·s^{-1}) in the Mössbauer spectra at 77 K. This is attributed to highly dispersed extra-framework iron species that show paramagnetic hyperfine splitting at 4.2 K. The presence of this additional magnetic behavior, also contributes to the broadening of the sextuplet linewidths.

Nevertheless, in all cases, the spectra still show a predominant contribution of the high-spin Fe^{2+} doublet, **d(II)**. However, compared to previous measurements,[19] the linewidths are observed to be rather broad (ca. 0.8 mm·s^{-1}), particularly the ones with relatively high iron concentration (i.e. for [Fe,Al]MFI (1:4)$_{stm}$ and [Fe,Al]MFI (0.5:4)$_{stm}$). These spectral changes can be attributed to the difference in measurement conditions. One important difference is the

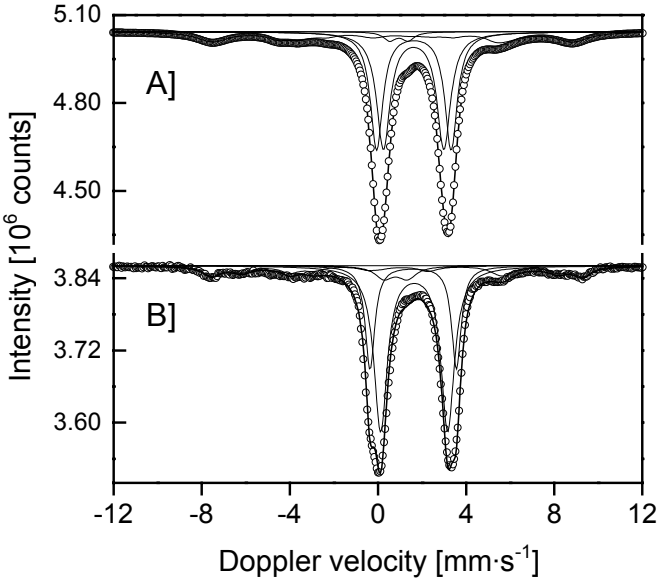

Figure 7.4. *^{57}Fe Mössbauer spectra recorded at 4.2 K in high vacuum (10^{-6} mbar) of steam-treated* [Fe,Al]MFI catalysts: A] [Fe,Al]MFI (1:4)$_{stm}$, and B] [Fe,Al]MFI (0.5:4)$_{stm}$. *Open circles indicate measured values and solid lines show the fit and its sub-spectra.*

fact that the current spectra were recorded under high vacuum condition, whereas, the previous ones were submerged in liquid He for 4.2 K measurements. In the current measurements, it is apparent that the predominant **d(II)** doublet is splitted into at least two high-spin Fe^{2+} sub-spectra – a doublet with a lower QS, *referred to as:* **d(II$^{-\delta}$)**, and another with a higher QS, *referred to as:* **d(II$^{+\delta}$)**. At low iron concentrations, however, most likely the splitting between these high-spin Fe^{2+} species overlaps into one single component.

Furthermore, for the sample with the lowest iron concentration, i.e. for [Fe,Al]MFI (0.12:4)$_{stm}$ (figure 7.3D), the spectrum recorded at 77 K exhibit an additional doublet (IS = 0.56 mm·s^{-1}; QS ~ 0.5 mm·s^{-1}). This component is also observed in [Fe,Al]MFI (0.17:4)$_{stm}$ (not shown for brevity). For discussion purposes, we refer to this component as **d(III)**. The IS of this doublet is characteristic of ferric ions, and is not observed in the ***freshly*** steamed state of the samples measured at 4.2 K.[11] The presence of this component could be a result of a chemical alteration (e.g. slow oxidation of the ferrous ions) that were incurred over a period of time (i.e. after several months). Nevertheless, since this component appears to be inactive under reduction/oxidation environments (*vide infra*), we infer that this component is just a spectator species in the BTOP reaction.

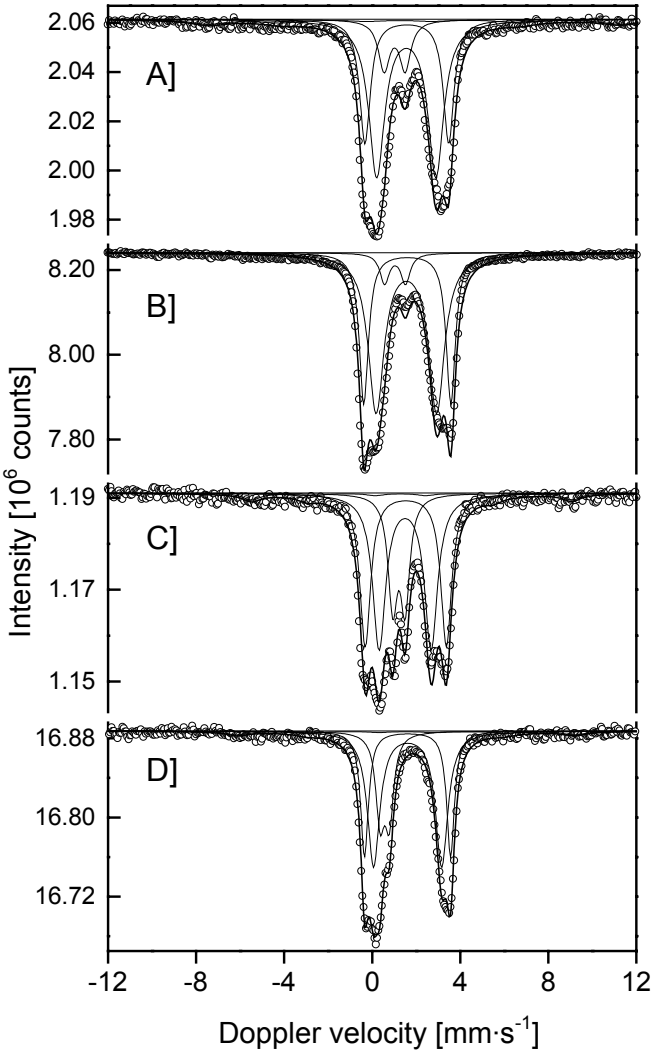

Figure 7.5. *^{57}Fe Mössbauer spectra recorded at 77 K of* [Fe,Al]MFI *catalysts varying in iron content after pretreatment in He at 823 K:* A] [Fe,Al]MFI $(1{:}4)_{stm}$, B] [Fe,Al]MFI $(0.5{:}4)_{stm}$, C] [Fe,Al]MFI $(0.25{:}4)_{stm}$, and D] [Fe,Al]MFI $(0.12{:}4)_{stm}$. *Open circles indicate measured values and solid lines show the fit and its sub-spectra.*

7.3.1.1. Pretreatment stage

Prior to activity measurements in the direct oxidation of benzene to phenol reaction, as well as in the N_2O decomposition, heat treatment in inert gas is normally carried out on the steam-treated [Fe,Al]MFI catalysts to remove physisorbed substances such as loosely bound water, air and hydrocarbons. This basically opens up the zeolite pores, improving their accessibility to the reactants. As pretreatment conditions can cause the iron ions to undergo an autoreduction process (*see chapter 5*), ^{57}Fe Mossbauer spectra were recorded after *in situ* pre-treatment of the steam-treated samples.

^{57}Fe Mössbauer spectra at 77 K of the pretreated [Fe,Al]MFI catalysts varying in iron concentration are plotted in figure 7.5. All spectra exhibit a general characteristic in which a splitting of **d(II)** component into **d(II$^{-\delta}$)** and **d(II$^{+\delta}$)** doublets is observed. This phenomenon was also observed by Overweg *et al*.,[15] after heat treatment of steam-treated [Fe,Al]MFI samples in He or Ar. These results indicate that we are dealing with more than one type of high-spin Fe^{2+} species. Furthermore, for [Fe,Al]MFI $(0.25{:}4)_{stm}$, an additional spectral component is observed after pretreatment (figure 7.5C). This is manifested by the presence of an additional doublet (IS = 1.21 mm·s^{-1}; QS = 0.56 mm·s^{-1}), which is typical of low-spin Fe^{2+} ions. The formation of low-spin Fe^{2+} species in the [Fe,Al]MFI $(0.25{:}4)_{stm}$ sample alone after pretreatment is not well understood at the moment. Nevertheless, it is noted that the same type of low-spin Fe^{2+} doublet has been found by Ovanesyan *et al*.[20] in their [Fe,Al]MFI catalysts after high-temperature activation in vacuum. Dubkov *et al*.,[5] later revealed that the low-spin Fe^{2+} species transforms into a high-spin Fe^{2+} species of **d(II)** type upon exposure to wet air.

For samples with relatively high iron concentration, i.e. for [Fe,Al]MFI $(1{:}4)_{stm}$ and [Fe,Al]MFI $(0.5{:}4)_{stm}$, the **d(I)** doublet is unaffected by the heat treatment. In addition, the **d(III)** component present in the low iron concentration [Fe,Al]MFI $(0.12{:}4)_{stm}$ also remained unchanged. These results suggest that both **d(I)** and **d(III)** components do not exhibit autoreduction during heat treatment in He at 823 K. This further substantiates the attribution of **d(I)** doublet to superparamagnetic iron oxide nanoparticles, which are unlikely to undergo autoreduction processes.

7.3.1.2. Oxidation by N_2O

Mössbauer spectra taken at 77 K and 4.2 K of the samples with varying iron concentration after treatment with N_2O are shown in figures 7.6 and 7.7 (left column), respectively. The main characteristics of the spectra after N_2O treatment are (i) the disappearance of mostly all high-spin Fe^{2+} species, and (ii) the presence of different types of ferric species. These spectral changes are attributed to the oxidation of iron ions in the presence of N_2O at 623 K.

^{57}Fe Mossabuer spectra at 77 K exhibit a broad magnetic component, which is more prominent in samples with low iron concentration. This component is most likely due to the presence of paramagnetic ferric ions, exhibiting slow relaxation behavior, which resolves into a complicated magnetically split spectral feature at 4.2 K. The lineshape of the magnetic feature is very complex and it is clear from visual inspection that it cannot be fitted with a single sextuplet. The complexity of the magnetic feature in the Mössbauer spectra at 4.2 K is most likely caused by several factors, such as: (i) contributions of an unknown number of components, (ii) the probable presence of strong quadrupole contributions, and (iii) irregular

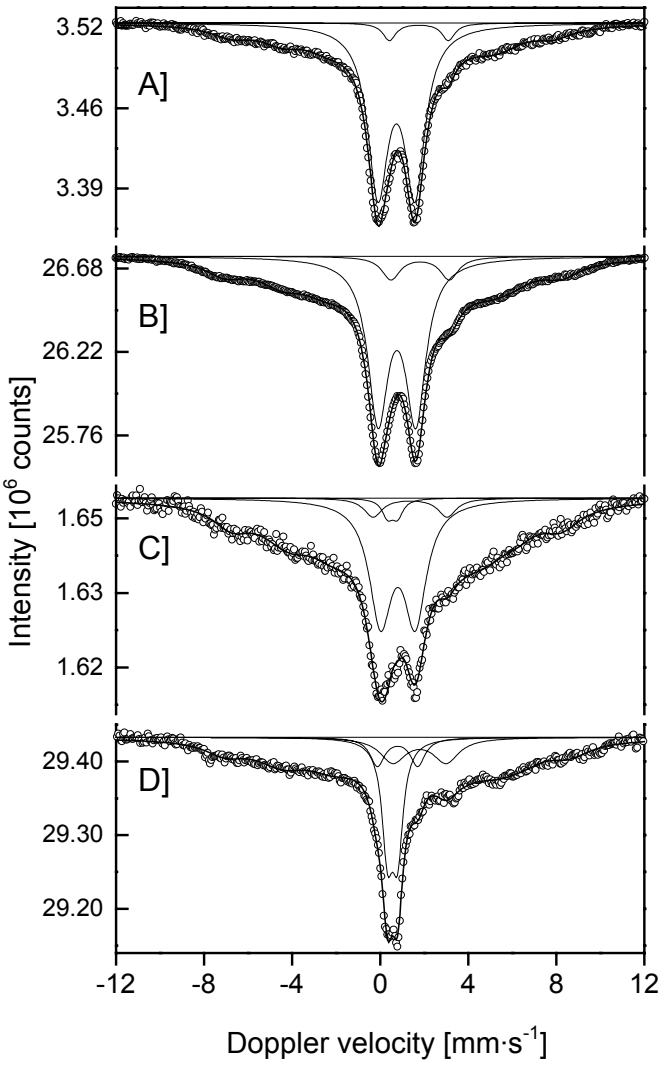

Figure 7.6. *^{57}Fe Mössbauer spectra recorded at 77 K of* [Fe,Al]MFI *catalysts varying in iron content after N_2O treatment 623 K:* A] [Fe,Al]MFI (1:4)$_{stm}$, B] [Fe,Al]MFI (0.5:4)$_{stm}$, C] [Fe,Al]MFI (0.25:4)$_{stm}$, and D] [Fe,Al]MFI (0.12:4)$_{stm}$. *Open circles indicate measured values and solid lines show the fit and its sub-spectra. Note: the broad magnetic feature in the spectra is deliberately excluded from figure for visual clarity.*

lineshapes, possibly due to relaxation behavior. Due to the complexity of the magnetic feature, we were not able to deconvolute the spectra into physically significant components.

Another component formed after N_2O treatment is a high-spin Fe^{3+} doublet (IS ~ 0.80 mm·s^{-1}; QS ~1.60 mm·s^{-1}), hereafter referred to as **d(IV)**, which exhibits a relatively high quadrupole splitting. The quadrupole splitting indicates that these ferric species have highly distorted/asymmetric coordination, which suggests that they are surface species. Therefore, this component is most likely due to small clusters of extra-framework ferric ions.

In [Fe,Al]MFI $(0.25{:}4)_{stm}$, the low-spin Fe^{2+} component formed upon heat treatment in He is not observed after N_2O treatment. This indicates that the low-spin Fe^{2+} ions are oxidized in the presence of N_2O. Furthermore, an additional doublet with a narrow quadrupole splitting is observed in the [Fe,Al]MFI $(0.25{:}4)_{stm}$ sample after N_2O treatment (figure 7.6C). The spectral parameters of this additional component are similar to that of **d(III)**, which shows no changes either under reduction or oxidation environments.

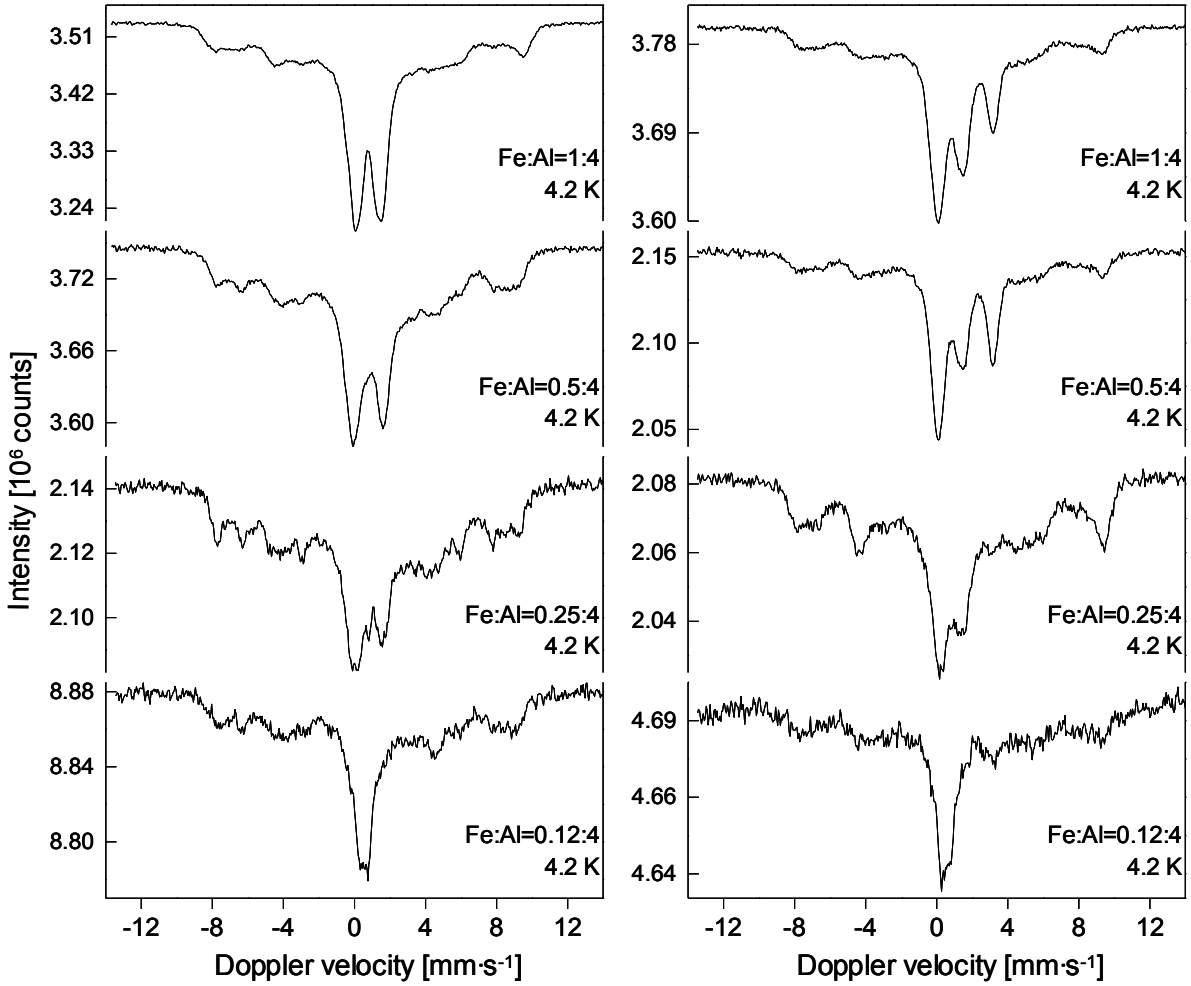

Figure 7.7. *^{57}Fe Mössbauer spectra recorded at 4.2 K of* [Fe,Al]MFI *catalysts varying in iron content after (a) N_2O treatment 623 K, left column, and (b) treatment in C_6H_6/He gas mixture at 300 K, right column.*

7.3.1.3. Reaction with benzene

As demonstrated by the Mössbauer spectra in the preceding section, almost all ferrous ions are oxidized to the ferric state in the presence of nitrous oxide. Therefore, it is essential to determine if these oxidized species contain the surface-active oxygen,[2,4,6] that is required to convert benzene into phenol. To investigate the iron species that reacts in the presence of

benzene, the samples after N_2O treatment were flushed with benzene (30 ml/min, 4% C_6H_6, rest He) at room temperature and at 473 K.

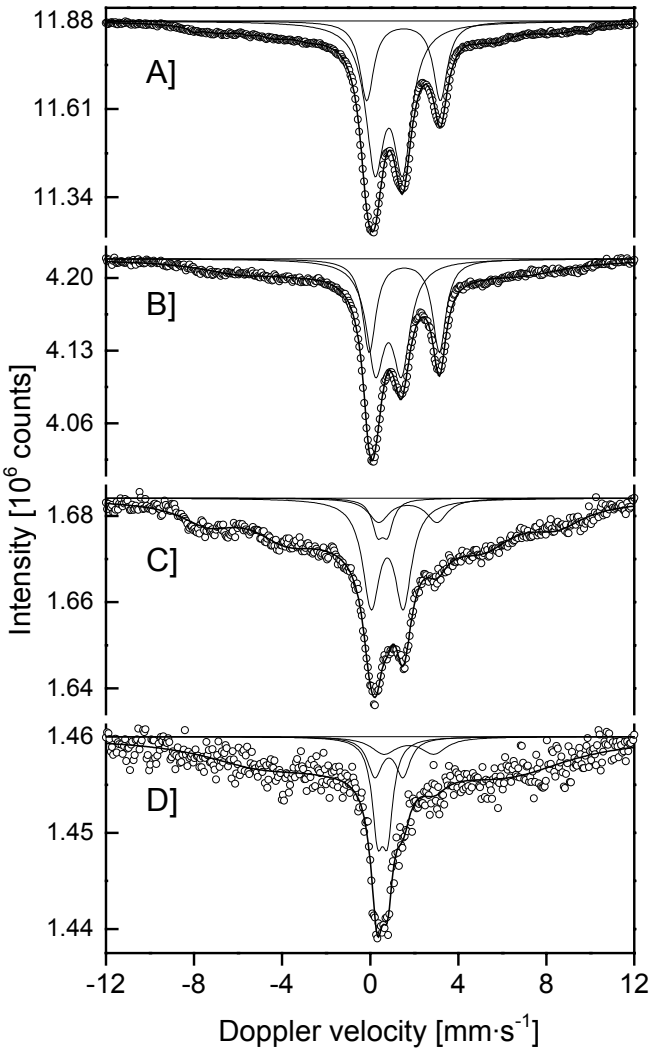

Figure 7.8. *^{57}Fe Mössbauer spectra recorded at 77 K of* [Fe,Al]MFI *catalysts varying in iron content after treatment in C_6H_6/He gas mixture at 300 K:* A] [Fe,Al]MFI $(1{:}4)_{stm}$, B] [Fe,Al]MFI $(0.5{:}4)_{stm}$, C] [Fe,Al]MFI $(0.25{:}4)_{stm}$, and D] [Fe,Al]MFI $(0.12{:}4)_{stm}$. *Open circles indicate measured values and solid lines show the fit and its sub-spectra. Note: the broad magnetic feature in the spectra is deliberately excluded from figure for visual clarity.*

7.3.1.3.a. Benzene reaction at 300 K

Mössbauer spectra collected at 77 K and 4.2 K after the samples were flushed with the C_6H_6/He mixture at room temperature are shown in figures 7.8 and 7.7 (right column), respectively. Remarkably, spectral changes can be observed even at room temperature after benzene treatment of the oxidized samples. To determine whether these changes are caused solely by the presence of benzene, the samples were flushed with He (30 ml/min) alone after

N_2O treatment. Subsequent Mössbauer spectra recorded at 77 K (not shown) exhibit no substantial changes and, thus, are comparable to the 77 K Mössbauer spectra (figure 7.6) of the N_2O treated samples. This confirms that the spectral changes observed in figure 7.8 are induced by the presence of benzene at room temperature. Two noticeable spectral changes observed are: (i) the presence of high-spin Fe^{2+} doublet, **d(II)**, and (ii) the decrease of the broad magnetic component, and, to some extent, also the high-spin Fe^{3+} doublet, **d(IV)**. This indicates a reduction of a fraction of two different ferric species to the ferrous state.

At 4.2 K (*figure 7.7, right column*), the broad magnetic component resolves into a complicated magnetically split spectral feature. Again, due to the complexity of the magnetic feature in the Mössbauer spectra at 4.2 K, fitting them with physically significant components proves to be difficult. However, compared to their corresponding spectra at 4.2 K prior to benzene treatment (*figure 7.7, left column*), the magnetic feature is observed to be less complex. This could indicate that part of the magnetic feature is reduced in the presence of benzene at room temperature.

7.3.1.3.b. Benzene reaction at 473 K

It has been shown in chapter 5 that considerable autoreduction can occur upon heat treatment in inert gas. Thus, prior to benzene treatment at 473 K, the samples after N_2O treatment were first subjected to heat treatment in He (30 ml/min) at 473 K (temperature ramp of 5 K/min) for 1.5 h to investigate its effect on the chemical state of the iron species. Mössbauer spectra taken at 77 K of the samples measured after heat treatment in He at 473 K are shown in figure 7.9. Significant changes are observed in the spectra recorded after heat treatment in He at 473 K, which is attributed to autoreduction processes. This is substantiated by the presence of the high-spin Fe^{2+} doublet, **d(II)**, in the Mössbauer spectra – i.e. the high energy shoulder observed in the spectrum of [Fe,Al]MFI $(1:4)_{stm}$ (figure 7.9A) and a well resolved doublet (IS ~ 1.60 $mm \cdot s^{-1}$; QS ~ 3.2 $mm \cdot s^{-1}$) for samples with low iron concentration. However, with regards to the spectral changes, no trend can be established as a function iron loading in the [Fe,Al]MFI catalysts.

The presence of **d(II)** component is accompanied mostly by the decrease in intensity of the broad magnetic feature in all samples. As the broad feature is most likely due to paramagnetic ferric ions with slow relaxation behavior, this suggests that highly dispersed iron species are likely to undergo an autoreduction process under the given conditions. However, in the case of [Fe,Al]MFI $(0.5:4)_{stm}$, both the magnetic feature (ca. 70%) and the **d(IV)** component (ca. 40%, based on 4.2 K spectral contribution) are reduced.

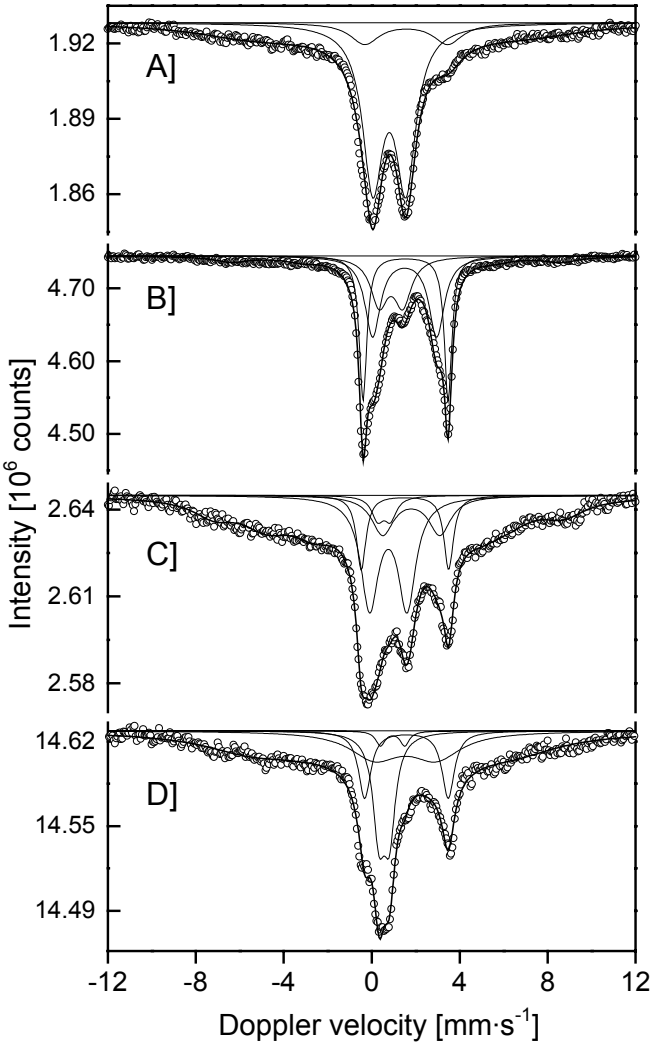

Figure 7.9. *^{57}Fe Mössbauer spectra recorded at 77 K of* [Fe,Al]MFI *catalysts varying in iron content after heat treatment in He at 473 K:* A] [Fe,Al]MFI (1:4)$_{stm}$, B] [Fe,Al]MFI (0.5:4)$_{stm}$, C] [Fe,Al]MFI (0.25:4)$_{stm}$, and D] [Fe,Al]MFI (0.12:4)$_{stm}$. *Open circles indicate measured values and solid lines show the fit and its sub-spectra. Note: the broad magnetic feature in the spectra is deliberately excluded from figure for visual clarity.*

After He treatment at 473 K, the samples were again oxidized following the procedure described in section 7.2.2.2 (*oxidation by N_2O*). Mössbauer spectra of the samples after N_2O treatment were recorded at 77 K. The spectra (not shown) are comparable to the 77 K spectra given in figure 7.6. This indicates that the reaction involving the autoreduction process and N_2O oxidation is reversible.

Following the re-oxidation in N_2O, the samples were treated with a C_6H_6/He gas mixture (30 ml/min; 4% C_6H_6, rest He) at 473 K for 1.5 h. The resulting ^{57}Fe Mössbauer spectra of the samples recorded at 77 K are shown in figure 7.10. Comparing the 77 K spectra of the

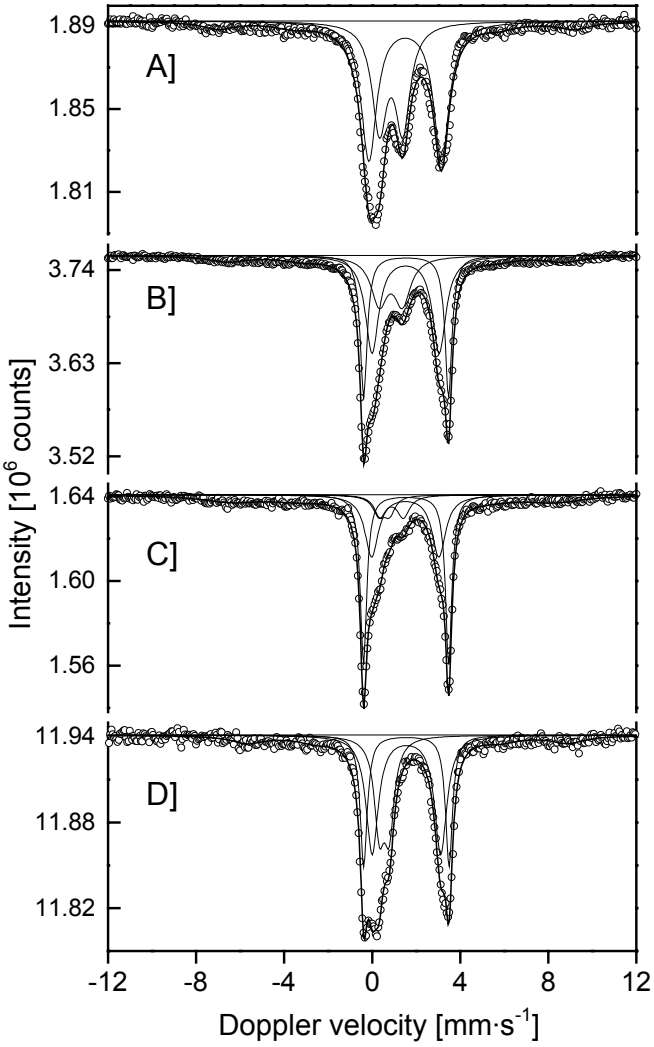

Figure 7.10. *^{57}Fe Mössbauer spectra recorded at 77 K of* [Fe,Al]MFI *catalysts varying in iron content after treatment in C_6H_6/He gas mixture at 473 K:* A] [Fe,Al]MFI $(1{:}4)_{stm}$, B] [Fe,Al]MFI $(0.5{:}4)_{stm}$, C] [Fe,Al]MFI $(0.25{:}4)_{stm}$, and D] [Fe,Al]MFI $(0.12{:}4)_{stm}$. *Open circles indicate measured values and solid lines show the fit and its sub-spectra.*

samples after C_6H_6/He treatment at 473 K to the results after heat treatment in He only at 473 K (figure 7.9), substantial spectral changes are observed. Most obvious amongst the spectral changes is the collapse of the broad component in all samples, accompanied by an increase in intensity of the high-spin Fe^{2+} doublet. Furthermore, a decrease in intensity of the high-spin Fe^{3+} doublet **d(IV)** is observed. This reduction appears to be more intense for samples with low iron concentration, particularly for the [Fe,Al]MFI $(0.25{:}4)_{stm}$ catalyst, compared to the samples with relatively high iron content at these conditions. Therefore, it is most likely that the extra-framework ferric complexes responsible for the **d(IV)** doublet in the Mössbauer spectra are larger in the case of steam-treated [Fe,Al]MFI samples with high iron concentrations.

Both, the collapse of the broad magnetic component and the decrease of the **d(IV)** doublet are attributed to the $Fe^{3+} \rightarrow Fe^{2+}$ transition in the presence of benzene at 473 K, except for the [Fe,Al]MFI $(0.5:4)_{stm}$ sample, where it is difficult to ascribed the changes to the presence of benzene alone as extensive autoreduction has been proven to take place at 473 K in He only. Nevertheless, it seems that the increase of the high-spin Fe^{2+} spectral contribution due to the presence of benzene alone is observed to be a function of iron concentration. The increase in high-spin Fe^{2+} contribution in the [Fe,Al]MFI $(1:4)_{stm}$, [Fe,Al]MFI $(0.25:4)_{stm}$, and [Fe,Al]MFI $(0.12:4)_{stm}$ samples is roughly by a factor of 4, 2, and 1, respectively. This shows that although a portion of extra-framework iron species, particularly in samples with high iron content, does not easily go through autoreduction, these species can still exhibit *redox* properties. The estimate was calculated by subtracting the spectral contribution of the high-spin Fe^{2+}components in the 77 K Mössbauer spectra after He treatment at 473 K to its corresponding spectral contribution after treatment in C_6H_6/He mixture at 473 K.

In addition, it is important to note that after the reduction of extra-framework iron species in the presence of benzene in helium mixture, both at room temperature and at 473 K, the Mössbauer spectra recorded at 77 K of the re-oxidized sample in N_2O at 623 K are comparable to that of figure 7.6. This is unequivocal proof of the reversibility of the *redox* transitions (i.e. $Fe^{3+} \rightarrow Fe^{2+} \rightarrow Fe^{3+}$) involving N_2O and benzene.

7.3.1.4. BTOP reaction at 623 K

To investigate the chemical state of iron after the direct oxidation of benzene to phenol reaction, the re-oxidized samples were subjected to a reaction gas mixture of 4 vol.% C_6H_6 in 96 vol.% N_2O at 623 K for 1.5 h. The resulting ^{57}Fe Mössbauer spectra of the samples recorded at 77 K after the BTOP reaction are shown in figure 7.11. Comparison of the 77 K Mössbauer spectra of the samples after BTOP reaction to that of the 77 K spectra of the samples in their oxidized state (figure 7.6) reveals a considerable reduction of ferric ions to the ferrous state. In excess N_2O, the broad magnetic component and the **d(IV)** doublet in the spectrum of the [Fe,Al]MFI $(0.5:4)_{stm}$ sample appear to have completely collapsed and a predominant high-spin Fe^{2+} doublet, **d(II)**, is observed after the BTOP reaction. Whereas for other samples, only a partial decrease in intensity, both the broad magnetic component and the **d(IV)** doublet, is observed. Note that x-ray near edge spectroscopy (XANES) shows that oxidation of extra-framework ferrous species in the presence of nitrous oxide commences only above 498 K (*see section 5.3.2, chapter 5*). The presence of a predominant high-spin Fe^{2+} species particularly in the [Fe,Al]MFI $(0.5:4)_{stm}$ zeolite, after a BTOP reaction in excess N_2O, could indicate that further reduction takes place upon cooling down in a C_6H_6/N_2O mixture. Most extra-framework iron species in this sample have been shown to be highly reactive towards benzene even at low temperatures (i.e. 300-473 K, *see section 7.3.1.3*).

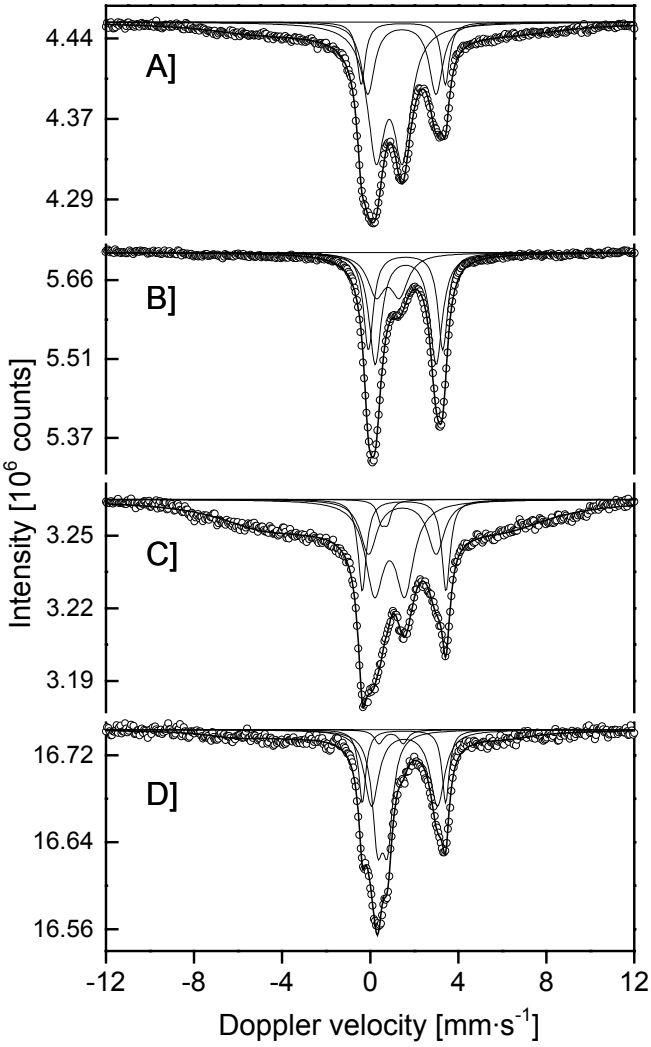

Figure 7.11. *^{57}Fe Mössbauer spectra recorded at 77 K of* [Fe,Al]MFI *catalysts varying in iron content after BTOP reaction in excess N_2O at 623 K:* A] [Fe,Al]MFI $(1:4)_{stm}$, B] [Fe,Al]MFI $(0.5:4)_{stm}$, C] [Fe,Al]MFI $(0.25:4)_{stm}$, and D] [Fe,Al]MFI $(0.12:4)_{stm}$. *Open circles indicate measured values and solid lines show the fit and its sub-spectra. Note: the broad magnetic feature in the spectra is deliberately excluded from figure for visual clarity.*

7.3.2. *In situ* studies of Al-free [Fe,Al]MFI catalyst

One of the interesting aspects of the aluminum free [Fe]MFI catalyst (i.e. [Fe,Al]MFI $(1:0)_{stm}$) is the fact that it exhibits different spectral properties compared to the samples with aluminum, as discussed in chapter 4. Since this material has been shown in the previous chapter to be active in the BTOP reaction, which is contrary to some reports,[3,13] its study should provide further insight into the nature of the active iron species.

7.3.2.1. Steam-treated sample

^{57}Fe Mössbauer spectrum of the [Fe,Al]MFI $(1:0)_{stm}$ recorded at 77 K, shown in figure 7.12 A, reveals a broad magnetically split feature together with a couple of high-spin Fe^{2+}

doublets and a high-spin Fe^{3+} doublet that exhibits a large quadrupole splitting. The high-spin Fe^{3+} doublet has spectral parameters that are comparable to the **d(IV)** component that is observed in the samples with aluminium only after N_2O treatment. The broad magnetic feature and the high-spin Fe^{2+} doublets in the Mössbauer spectrum at 77 K are replaced by a broad multiple-line magnetic feature at 4.2 K, figure 7.15(A2). Again, due to the complexity of the Mössbauer spectrum taken at 4.2 K, which is presumably composed of several magnetic contributions, it is difficult to deconvolute the spectra into physically significant components. This is also the reason why, for the rest of the series of treatments, we were not able to fit the corresponding Mössbauer spectra recorded at 4.2 K.

7.3.2.2. Pretreatment in He at 823 K

Pretreatment of the [Fe,Al]MFI $(1:0)_{stm}$ in He at 823 K, results in minor spectral shifts in the Mössbauer spectrum taken at 77 K (figure 7.12 B). The high-spin Fe^{2+} doublets appears to overlap into one high-spin Fe^{2+} doublet of **d(II)** type after pre-treatment. However, since there is no significant increase in the spectral contribution of the ferrous species, this indicates that hardly any autoreduction processes of iron ions took place. Furthermore, the high-spin Fe^{2+} doublet at 77 K is not observed in the 4.2 K spectrum (not shown for brevity). The only possible explanation for this phenomenon could be that extra-framework Fe^{2+} species in the steam-treated [Fe,Al]MFI $(1:0)_{stm}$ sample are magnetically coupled at 4.2 K.

7.3.2.3. N_2O oxidation

Oxidation of the pretreated samples in N_2O, shown in figure 7.12 C, results in the disappearance of the high-spin Fe^{2+} doublet. This indicates that the ferrous species present in the aluminum-free MFI were oxidized to the ferric state upon N_2O treatment. This is substantiated by the spectral changes incurred in the high-spin Fe^{3+} doublet, in which a splitting is observed, indicating the presence of an additional high-spin Fe^{3+} doublet. Based on spectral fitting, the additional high-spin Fe^{3+} doublet exhibits a very broad quadrupole splitting (IS ~ 0.60 $mm \cdot s^{-1}$; QS ~ 2.17 $mm \cdot s^{-1}$). This could be evidence for the formation of small extra-framework iron complexes.

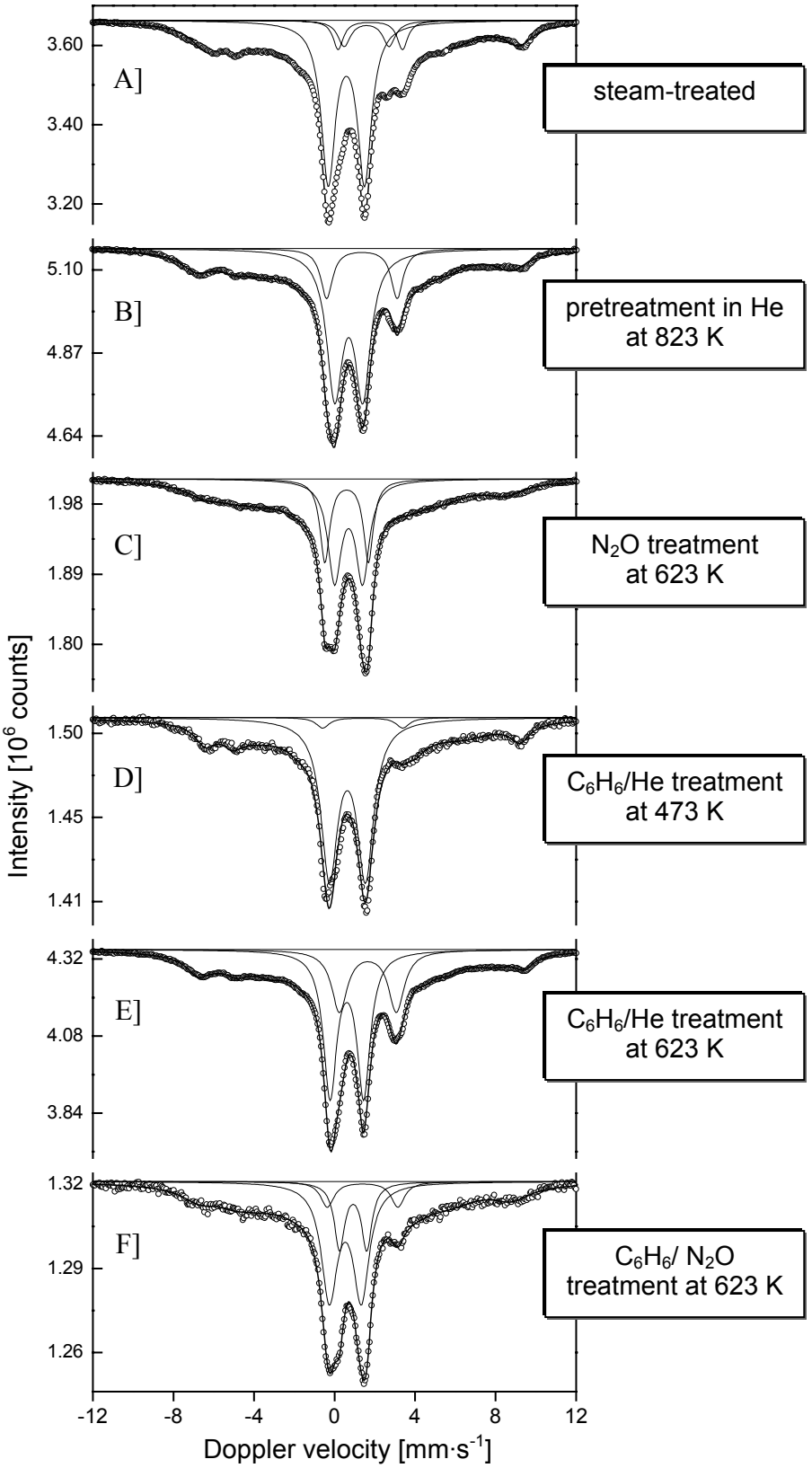

Figure 7.12. *^{57}Fe Mössbauer spectra recorded at 77 K of the Al-free* [Fe,Al]MFI (1:0)$_{stm}$ *catalyst after different treatment. Open circles indicate measured values and solid lines show the fit and its sub-spectra. Note: the broad magnetic feature in the spectra is deliberately excluded from figure for visual clarity.*

7.3.2.4. Reaction with benzene

After treatment with nitrous oxide, the [Fe,Al]MFI $(1:0)_{stm}$ sample was subjected to benzene treatment at room temperature and 473 K, as described in section 7.2.2.3. Mössbauer results reveal that no changes occurred after the treatment at room temperature and hardly any reduction is observed after treatment at 473 K (figure 7.12 D). Nevertheless, some changes in the magnetic feature are noted, but this could be due to relaxation effects. However, at higher reaction temperature (i.e. at 623 K), figure 7.12 E, further spectral changes are observed particularly the appearance of a high-spin Fe^{2+} doublet. The measured spectrum after benzene treatment at 623 K is comparable to the spectrum recorded after pretreatment in He at 823 K, in the 77 K (figure 7.12 B). This suggests that the chemical state of the iron species in the [Fe,Al]MFI $(1:0)_{stm}$ sample is reverted to its corresponding state prior to undergoing an oxidation process in the presence of N_2O. This provides further proof of the reversibility of the *redox* cycle (i.e. $Fe^{2+} \rightarrow Fe^{3+} \rightarrow Fe^{2+}$) involving N_2O and benzene.

7.3.2.5. After BTOP reaction

In a reaction gas mixture of benzene and N_2O at 623 K, the Mössbauer spectra recorded at 77 K (figure 7.12 F) exhibits subtle spectral changes compared to that after treatment in a C_6H_6/He mixture at 623 K. Apart from a small contribution from the high-spin Fe^{2+} doublet, most spectral characteristics at 77 K indicate iron species in the oxidized Fe^{3+} state. The presence of *redox* active species mostly in the oxidized state is attributed to the fact that the BTOP reaction was performed in the presence of excess N_2O. Nonetheless, these spectral changes further substantiates that the BTOP reaction involves a $Fe^{3+} \rightarrow Fe^{2+}$ transition.

Table 7.1. ^{57}Fe Mössbauer hyperfine parameters and relative intensities recorded at 77 K of the [Fe,Al]MFI (1:4)$_{stm}$ catalyst after different *in situ* treatments.

in-situ treatment	spectrum number	assignation	IS (mm·s^{-1})	QS (mm·s^{-1})	RI (%)	oxidation state
untreated	7.3 A	**d(I)**	0.74	1.12	8	Fe^{3+}
		d(II$^{-\delta}$)	1.63	2.68	42	Fe^{2+}
		d(II$^{+\delta}$)	1.60	3.27	42	Fe^{2+}
			1.11†		8	Fe^{3+}
	*7.4 A		0.95	0.84	3	Fe^{3+}
		d(II$^{-\delta}$)	1.62	2.74	40	Fe^{2+}
		d(II$^{+\delta}$)	1.63	3.38	37	Fe^{2+}
			0.85‡		20	Fe^{3+}
He treatment	7.5 A	**d(I)**	1.02	0.95	12	Fe^{3+}
at 823 K		**d(II$^{-\delta}$)**	1.55	2.69	52	Fe^{2+}
		d(II$^{+\delta}$)	1.57	3.80	28	Fe^{2+}
			1.58†		8	Fe^{3+}
N2O treatment	7.6 A	**d(IV)**	0.75	1.67	60	Fe^{3+}
at 623 K		**d(II)**	1.75	2.70	4	Fe^{2+}
			0.71†		36	Fe^{3+}
C_6H_6/He	7.8 A	**d(IV)**	0.80	1.33	50	Fe^{3+}
at 300 K		**d(II)**	1.50	3.34	22	Fe^{2+}
			0.79†		28	Fe^{3+}
He treatment	7.9 A	**d(IV)**	0.80	1.50	58	Fe^{3+}
at 473 K		**d(II)**	1.57	3.78	11	Fe^{2+}
			0.60†		31	Fe^{3+}
C_6H_6/He	7.10 A	**d(IV)**	0.86	1.06	37	Fe^{3+}
at 473 K		**d(II)**	1.50	3.29	52	Fe^{2+}
			1.09†		11	Fe^{3+}
C_6H_6/N_2O	7.11 A	**d(IV)**	0.87	1.20	45	Fe^{3+}
at 623 K		**d(II$^{-\delta}$)**	1.44	3.10	20	Fe^{2+}
		d(II$^{+\delta}$)	1.50	3.38	10	Fe^{2+}
			0.64†		25	Fe^{3+}

IS(isomer shift), QS(quadrupole splitting), RI(relative intensity);
all IS values are relative to SNP.
† *characterized by a broad magnetic component.*
* *^{57}Fe Mössbauer hyperfine parameters recorded at 4.2 K;*
‡ *Hyperfine field of 51.1 T.*

Table 7.2. ^{57}Fe Mössbauer hyperfine parameters and relative intensities recorded at 77 K of the [Fe,Al]MFI (0.5:4)$_{stm}$ catalyst after different *in situ* treatments.

in-situ treatment	spectrum number	assignation	IS (mm·s^{-1})	QS (mm·s^{-1})	RI (%)	oxidation state
untreated	7.3 B	**d(I)**	0.80	1.10	10	Fe^{3+}
		d(II$^{-\delta}$)	1.61	3.00	59	Fe^{2+}
		d(II$^{+\delta}$)	1.59	3.91	24	Fe^{2+}
			0.85†		7	Fe^{3+}
	*7.4 B		0.80	1.06	6	Fe^{3+}
		d(II$^{-\delta}$)	1.65	3.06	24	Fe^{2+}
		d(II$^{+\delta}$)	1.60	3.90	55	Fe^{2+}
			0.90‡		15	Fe^{3+}
He treatment	7.5 B	**d(I)**	1.04	0.95	7	Fe^{3+}
at 823 K		**d(II$^{-\delta}$)**	1.55	2.75	60	Fe^{2+}
		d(II$^{+\delta}$)	1.59	3.95	33	Fe^{2+}
			1.11	1.23	3.4	Fe^{3+}
N2O treatment	7.6 B	**d(IV)**	0.76	1.71	48	Fe^{3+}
at 623 K		**d(II)**	1.80	2.65	6	Fe^{2+}
			0.70†		46	Fe^{3+}
C_6H_6/He	7.8 B	**d(IV)**	0.83	1.18	39	Fe^{3+}
at 300 K		**d(II)**	1.55	3.18	27	Fe^{2+}
			0.59†		34	Fe^{3+}
He treatment	7.9 B	**d(IV)**	0.88	1.07	23	Fe^{3+}
at 473 K		**d(II$^{-\delta}$)**	1.50	2.91	36	Fe^{2+}
		d(II$^{+\delta}$)	1.54	3.87	31	Fe^{2+}
			1.15†		10	Fe^{3+}
C_6H_6/He	7.10 B	**d(IV)**	0.85	1.05	22	Fe^{3+}
at 473 K		**d(II$^{-\delta}$)**	1.52	3.05	38	Fe^{2+}
		d(II$^{+\delta}$)	1.54	3.86	29	Fe^{2+}
			1.14†		11	Fe^{3+}
C_6H_6/N_2O	7.11 B	**d(IV)**	0.80	1.06	22	Fe^{3+}
at 623 K		**d(II$^{-\delta}$)**	1.61	2.77	46	Fe^{2+}
		d(II$^{+\delta}$)	1.61	3.38	32	Fe^{2+}

IS(isomer shift), QS(quadrupole splitting), RI(relative intensity);
all IS values are relative to SNP.

† *characterized by a broad magnetic component.*

* *^{57}Fe Mössbauer hyperfine parameters recorded at 4.2 K;*

‡ *Hyperfine field of 52.0 T.*

Table 7.3. ^{57}Fe Mössbauer hyperfine parameters and relative Intensities recorded at 77 K of the [Fe,Al]MFI (0.25:4)$_{stm}$ catalyst after different *in situ* treatments.

in-situ treatment	spectrum number	assignation	IS (mm·s^{-1})	QS (mm·s^{-1})	RI (%)	oxidation state
untreated	7.3 C	**d(II$^{-\delta}$)**	1.46	2.57	80	Fe^{2+}
		d(II$^{+\delta}$)	1.48	3.23	20	Fe^{2+}
He treatment	7.5 C		1.21	0.56	20	Fe^{3+}
at 823 K		**d(II$^{-\delta}$)**	1.49	2.36	41	Fe^{2+}
		d(II$^{+\delta}$)	1.52	3.68	34	Fe^{2+}
			1.10†		5	Fe^{3+}
N2O treatment	7.6 C	**d(III)**	0.56	0.45	3	Fe^{3+}
at 623 K		**d(IV)**	0.80	1.60	32	Fe^{3+}
		d(II)	1.40	3.3	4	Fe^{2+}
			0.82†		61	Fe^{3+}
C_6H_6/He	7.8 C	**d(III)**	0.56	0.45	4	Fe^{3+}
at 300 K		**d(IV)**	0.77	1.46	24	Fe^{3+}
		d(II)	1.71	2.65	7	Fe^{2+}
			0.67†		65	Fe^{3+}
He treatment	7.9 C	**d(III)**	0.56	0.58	4	Fe^{3+}
at 473 K		**d(IV)**	0.75	1.70	26	Fe^{3+}
		d(II$^{-\delta}$)	1.51	3.98	10	Fe^{2+}
		d(II$^{+\delta}$)	1.80	2.60	11	Fe^{2+}
			1.27†		49	Fe^{3+}
C_6H_6/He	7.10 C	**d(III)**	0.56	0.45	5	Fe^{3+}
at 473 K		**d(IV)**	0.90	1.33	6	Fe^{3+}
		d(II$^{-\delta}$)	1.55	3.15	28	Fe^{2+}
		d(II$^{+\delta}$)	1.56	3.92	33	Fe^{2+}
			1.01†		28	Fe^{3+}
C_6H_6/N_2O	7.11 C	**d(III)**	0.56	0.45	8	Fe^{3+}
at 623 K		**d(IV)**	0.79	1.62	19	Fe^{3+}
		d(II$^{-\delta}$)	1.67	2.60	15	Fe^{2+}
		d(II$^{+\delta}$)	1.54	3.80	12	Fe^{2+}
			0.68†		46	Fe^{3+}

IS(isomer shift), QS(quadrupole splitting), RI(relative intensity);
all IS values are relative to SNP.
† *characterized by a broad magnetic component.*

Table 7.4. ^{57}Fe Mössbauer hyperfine parameters and relative intensities recorded at 77 K of the [Fe,Al]MFI (0.12:4)$_{stm}$ catalyst after different *in situ* treatments.

in-situ treatment	spectrum number	assignation	IS (mm·s^{-1})	QS (mm·s^{-1})	RI (%)	oxidation state
untreated	7.3 D	**d(III)**	0.55	0.44	22	Fe^{3+}
		d(II)	1.65	3.31	78	Fe^{2+}
He treatment	7.5 D	**d(I)**	0.57	0.41	20	Fe^{3+}
at 823 K		**d(II$^{-\delta}$)**	1.61	3.09	47	Fe^{2+}
		d(II$^{+\delta}$)	1.61	3.91	28	Fe^{2+}
			1.10†		5	Fe^{3+}
N2O treatment	7.6 D	**d(III)**	0.56	0.45	22	Fe^{3+}
at 623 K		**d(IV)**	0.79	1.80	8	Fe^{3+}
		d(II)	1.78	2.42	11	Fe^{2+}
			0.98†		59	Fe^{3+}
C_6H_6/He	7.8 D	**d(III)**	0.56	0.45	23	Fe^{3+}
at 300 K		**d(IV)**	0.78	1.69	9	Fe^{3+}
		d(II)	1.67	2.87	14	Fe^{2+}
			1.22†		54	Fe^{3+}
He treatment	7.9 D	**d(III)**	0.56	0.47	20	Fe^{3+}
at 473 K		**d(IV)**	0.95	1.10	3	Fe^{3+}
		d(II$^{-\delta}$)	1.53	2.80	20	Fe^{2+}
		d(II$^{+\delta}$)	1.58	3.80	14	Fe^{2+}
			0.60†		43	Fe^{3+}
C_6H_6/He	7.10 D	**d(III)**	0.55	0.44	24	Fe^{3+}
at 473 K		**d(II$^{-\delta}$)**	1.55	3.11	39	Fe^{2+}
		d(II$^{+\delta}$)	1.55	3.87	25	Fe^{2+}
			1.10†		12	Fe^{3+}
C_6H_6/N_2O	7.11 D	**d(III)**	0.56	0.43	23	Fe^{3+}
at 623 K		**d(IV)**	1.10	0.97	33	Fe^{3+}
		d(II$^{-\delta}$)	1.59	3.02	16	Fe^{2+}
		d(II$^{+\delta}$)	1.56	3.84	4	Fe^{2+}
			0.87†		24	Fe^{3+}

IS(isomer shift), QS(quadrupole splitting), RI(relative intensity);
all IS values are relative to SNP.
† *characterized by a broad magnetic component.*

Table 7.5. ^{57}Fe Mössbauer hyperfine parameters and relative intensities recorded at 77 K of the aluminum-free [Fe,Al]MFI (1:0)$_{stm}$ catalyst after different *in situ* treatments.

in-situ treatment	spectrum number	assignation	IS (mm·s^{-1})	QS (mm·s^{-1})	RI (%)	oxidation state
untreated	7.12 A	**d(IV)**	0.60	1.80	40	Fe^{3+}
			1.60	2.23	6	Fe^{2+}
			1.78	3.20	6	Fe^{2+}
			0.75†		48	Fe^{3+}
He treatment	7.12 B	**d(IV)**	0.70	1.40	44	Fe^{3+}
at 823 K		**d(II)**	1.36	3.50	12	Fe^{2+}
			0.64†		44	Fe^{3+}
N2O treatment	7.12 C	**d(IV)**	0.67	1.6	33	Fe^{3+}
at 623 K			0.65	2.17	23	Fe^{2+}
			0.70†		46	Fe^{3+}
C_6H_6/He	7.12 D	**d(IV)**	0.64	1.79	52	Fe^{3+}
at 473 K		**d(II)**	1.40	3.90	3	Fe^{2+}
			0.89†		45	Fe^{3+}
C_6H_6/He	7.12 E	**d(IV)**	0.61	1.67	38	Fe^{3+}
at 623 K		**d(II)**	1.65	2.83	19	Fe^{2+}
			0.55†		43	Fe^{3+}
C_6H_6/N_2O	7.12 F	**d(IV)**	0.92	1.35	13	Fe^{3+}
at 623 K			0.54	1.60	34	Fe^{3+}
		d(II)	1.40	3.50	6	Fe^{2+}
			0.65†		47	Fe^{3+}
Spent catalyst	7.16 B1	**d(IV)**	0.71	1.10	45	
		d(II)	1.63	3.24	12	
			0.52†		43	

IS(isomer shift), QS(quadrupole splitting), RI(relative intensity);
all IS values are relative to SNP.
† characterized by a broad magnetic component.

7.4. Discussion

7.4.1. Identification of extra-framework iron species

It has been described in chapter 4 that steam-treatment of the [Fe,Al]MFI samples in this study with varying iron concentration, leads to extra-framework iron species that are predominantly in the ferrous state. This is evident from the Mössbauer data, which demonstrate the presence of a high-spin Fe^{2+} doublet, ca. 90% based on spectral parameters. This high-spin Fe^{2+} doublet has Mössbauer parameters that are very similar to the high-spin Fe^{2+} component observed by Panov *et al*.,[5,20] which they have attributed to binuclear iron complexes with a structure similar to those present in the enzyme methane monooxygenase (MMO). MMO is known to activate dioxygen for incorporation into a wide variety of hydrocarbons.[21,22] However, although the spectral parameters of the high-spin ferrous species are close to that of MMO,[23] there are evidences that strongly indicate that the high-spin Fe^{2+} component is composed of several ferrous species.

The activity data (*see chapter 6*) show that most extra-framework iron species are capable of catalysing the N_2O decomposition reaction – assumed to be a vital step to create active oxygen species for benzene to phenol reaction. However, from the phenol productivity profile per gram of catalyst, it is apparent that only a fraction of the iron species participates in the BTOP reaction. It is therefore clear that we are dealing with various extra-framework divalent iron species. In addition, the Mössbauer spectra of the steam-treated samples recorded after pretreatment in He at 823 K for about 2 h, show a splitting of the high-spin Fe^{2+} doublet into two components, i.e. of **d(II$^{-\delta}$)** and **d(II$^{+\delta}$)** doublets, respectively. This suggests that more than one type of high-spin Fe^{2+} species is present in the steam-treated [Fe,Al]MFI catalysts.

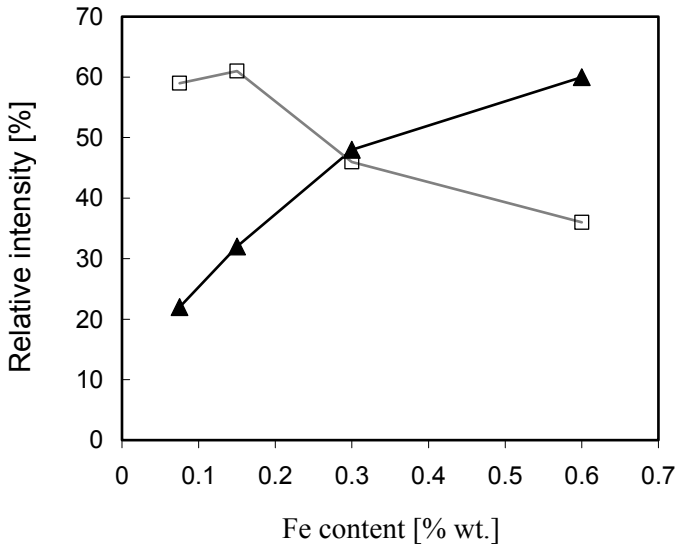

Figure 7.13. *Plot of the relative intensities of the* (▲) *high-spin doublet,* **d(IV)***, and* (□) *broad magnetic feature, based on 77 K spectra, as a function of iron loading.*

The different extra-framework iron species are discriminated though Mössbauer spectroscopy upon further treatment of the pretreated [Fe,Al]MFI samples by nitrous oxide at 623 K (*see figure 7.6*). Comparing the intensities of the sub-spectra of the samples after N_2O treatment, it seems that the broad magnetic feature and the high-spin Fe^{3+} doublet, **d(IV)**, are associated with the **d($II^{+\delta}$)** and **d($II^{-\delta}$)** doublets, respectively. Furthermore, the formation of different types of extra-framework iron species (i.e. the broad magnetic feature and the high-spin Fe^{3+} doublet, **d(IV)**) is observed to be a function of iron loading (figure 7.13). A general trend in the Mössbauer spectra shows that for samples with high iron concentration (e.g. [Fe,Al]MFI $(1:4)_{stm}$), most extra-framework iron species form oligonuclear clusters. This is characterized by the presence of a high-spin Fe^{3+} doublet, **d(IV)**. Whereas in samples where the iron loading is low, the broad magnetic feature is more prominent and indicates that most extra-framework iron species are highly dispersed, exhibiting PHS.

7.4.1.1. Iron transition in mononuclear and multinuclear species

As mentioned earlier, the broad magnetic component at 77 K in the Mössbauer spectrum that resolves into a complicated magnetically split feature at 4.2 K can be attributed to several contributions. A likely factor that is responsible for this magnetic feature is the presence of paramagnetic hyperfine splitting (PHS). The presence of PHS indicates that ferric ions in the sample possess slow electron relaxation rate, which is typical for ferric ions in dilute concentrations (*see chapter 2*). This is in agreement to the results presented in figure 7.13, where an increase in the broad magnetic feature is observed for samples with decreasing iron concentration.

In previous chapters, the presence of PHS has been attributed to paramagnetic isolated ferric species with Fe-Fe ion distances greater than 15 Å. These highly dispersed species have been shown through *in situ* treatments to be sensitive to reduction in the presence of benzene, as well as in the autoreduction conditions, and are easily oxidized in the presence of N_2O. If these iron species are ***mononuclear*** complexes, the following oxidation of ferrous ion is likely to occur:

$$Fe^{2+} \rightarrow Fe^{4+} + 2e^- \qquad (7.1)$$

Here, the oxidation of Fe^{2+} by an oxygen atom entails a two-electron transfer (O^{2-}). This reaction, however, has not been observed in this study, and only the reversible *redox* reaction involving the Fe^{2+} to Fe^{3+} transition is detected. One possibility of this transition to occur in a *redox* active mononuclear species is that the electron is delocalised (*see reaction below*).

$$Fe^{2+} + N_2O \rightarrow Fe^{4+}{=}O + N_2 \qquad (7.2)$$
$$\downarrow\uparrow$$
$$Fe^{3+}\text{-}O^{\bullet}$$

Nonetheless, Mössbauer data of the various steam-treated [Fe,Al]MFI catalysts after oxidation in N_2O have not shown any evidence of the presence of Fe^{4+} species, even with the measurements that are carried out at 4.2 K, in which electrons are expected to be localized on atoms. Although it can be argued that the complicated magnetic feature of the samples after N_2O treatment (*figure 7.7, left column*) may contain traces of Fe^{4+} species that are embedded amongst a distribution of broad magnetic components, this is unlikely since the 77 K measurements did not reveal any spectral contribution that can be attributed to an intermediate ferric and ferryl valence state. The isomer shift of Fe^{4+} (ca. 0.3 mm·s^{-1}, relative to SNP) is much lower than that of Fe^{3+}.[24] Therefore, for the steam-treated samples in this study, it appears that the presence of active mononuclear extra-framework iron center, which has been a subject of recent discussions,[25-28] is highly unlikely.

On the other hand, if these iron species are ***binuclear*** complexes, or an even number of iron atoms embedded in larger clusters, the *redox* reaction is envisaged to proceed as follows:

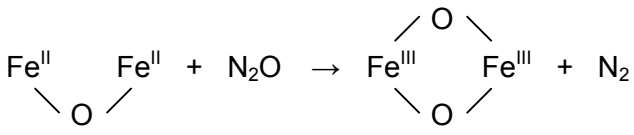

(7.3)

The presence of at least two neighboring Fe^{2+} atoms in the form of (for instance) a dimeric complex, similar to a structure proposed by Prins *et al.*[29], is a more convenient oxidation pathway of a two-electron (O^{2-}) transfer in a reversible $Fe^{2+} \leftrightarrow Fe^{3+}$ *redox* transition. To understand the Mössbauer spectra generated by these iron complexes, analysis would have to be based on enzymatic systems where these complexes are most commonly found, and their dynamic interactions and Mössbauer spectral interpretations are well documented.[30-32]

7.4.1.2. Magnetic behavior of isolated Fe-clusters

For dimeric iron complexes with localized valences, the Hamiltonian of the system for the analysis of the Mössbauer spectra is dependent on the isotropic exchange between the spins S_A and S_B of the iron sites (*A*) and (*B*) and is described by:

$$H = -J \cdot S_A \cdot S_B \tag{7.4}$$

The sign of the exchange coupling *J* can be positive or negative and this determines whether the exchange interaction is ferromagnetic or antiferromagnetic. Thus, for dimeric complexes, in principle both antiferromagnetic and ferromagnetic behavior can occur (although the latter has not been observed). Furthermore, the strength of the exchange coupling in both

antiferromagnetic and ferromagnetic behavior can either be strong or weak, which is indicated by the size of the coupling constant.

In the case of a strong antiferromagnetic limit, the ground state has a well-defined net spin $S = 0$. This exchange interaction would result in spin moments that are anti-parallel. The spins are, thus, antiferromagnetically coupled to a diamagnetic ground state, and would therefore lack a magnetic hyperfine splitting at low temperatures. Dimeric high-spin Fe^{3+} – Fe^{3+} complexes typically exhibit a lack of magnetic hyperfine splitting at low temperatures, instead, these Fe^{3+} – Fe^{3+} complexes would generate a doublet in the Mössbauer spectrum. Therefore, the **d(IV)** component found after exposure of the [Fe,Al]MFI samples to oxidizing N_2O environment can be attributed in general to diamagnetic ferric species. These species could be dimeric in nature, or composed of even numbered multiple atoms.

On the other hand, if the antiferromagnetic exchange spin interaction between two iron sites (*A**) and (*B**) is in the weak coupling limit, applying a magnetic field (internal or external) would cause the complex to change from a diamagnetic to a paramagnetic complex. This indicates that spin moments of the two iron sites would be aligned, which results to a paramagnetic ground state. This would cause a doublet to resolve into a magnetically split feature in the Mössbauer spectrum.

Thus, for systems with an even number of Fe-atoms, the magnetic behavior can either have a diamagnetic or paramagnetic a ground state. However, for Fe-complexes with uneven number of Fe-atoms, the magnetic behavior is always paramagnetic. In dilute systems where paramagnetic species are highly dispersed, PHS is generally observed and a broad magnetic feature is exhibited in the Mössbauer spectrum. If the cluster size increases, a state is reached in which the Mössbauer lineshape is determined by the relaxed limit. Upon further growth, the cluster eventually shows superparamagnetic behavior, where the relaxation behavior is strongly dependent on the temperature. Finally, extensive agglomeration of Fe-clusters will result in the formation of large iron oxide particles exhibiting either bulk ferromagnetic or antiferromagnetic behavior.

7.4.1.3. Summary of extra-framework iron species observed

From the variation of iron loading in the [Fe,Al]MFI catalysts, a general trend in the Mössbauer spectra can be extracted upon which a model for describing the preferred formation of extra-framework iron species is derived. This model, which strongly depends on the concentration of iron in the sample, is illustrated in figure 7.14.

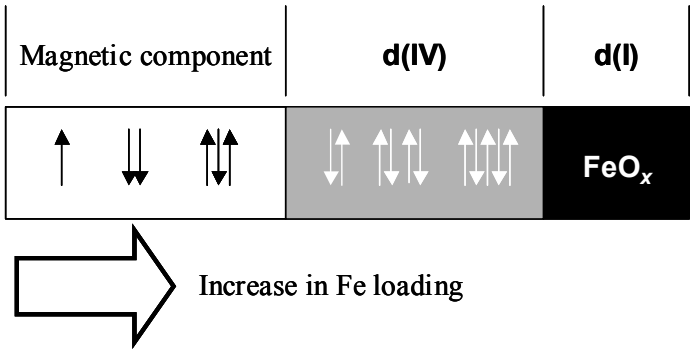

Figure 7.14. *A model of the distribution of iron species present in the* [Fe,Al]MFI *catalysts derived from* ^{57}*Fe Mössbauer spectra after a series of in situ treatments. The various extra-framework iron species are differentiated into regions according to the type of spectra they exhibit, i.e.* (i) *the broad magnetic component,* (ii) *the high-spin* Fe^{3+} *doublet,* **d(IV)**, *and* (iii) *the superparamagnetic iron oxide particles,* **d(I)**. *Nomenclature*: (↑) *isolated ferric ions;* (↑↓) *even numbered atoms with strong antiferromagnetic orientation;* (↑↑) *even numbered atoms with paramagnetic behavior;* (↑↓↑) *cluster of paramagnetic species;* (↑↓↑↓) *large clusters of diamagnetic species, and* (↑↓↑↓↑) *large clusters of paramagnetic species*.

Steam-treated [Fe,Al]MFI catalysts with low iron loading (ca. 1500 ppm, or less) generally contain highly dispersed paramagnetic extra-framework iron species, which exhibit a prominent broad magnetic feature in the Mössbauer spectra. Since these species are formed preferably in samples with dilute iron concentration, the distances between iron species are relatively far apart (i.e. > 15 Å). A gradual increase in iron concentration results in an increase in intensity of the iron species of **d(IV)** and **d(I)** type, successively. Thus, the higher the iron loading is in the [Fe,Al]MFI catalysts, the more intense is the spectral contribution of the iron species to the right of the model shown above.

For highly dispersed extra-framework iron species that exhibit PHS at 4.2 K, there are indications that support the earlier assessment that chemically different iron species comprise the broad magnetic feature in the Mössbauer spectra. First, the complicated magnetic splitting at 4.2 K suggests several contributions presumably from unknown iron species with distinct hyperfine fields. This indicates that more than one type of iron species exhibits magnetic splitting at 4.2 K. Second, the broad magnetic feature in different samples does not show the same response upon different *in situ* treatments.

For [Fe,Al]MFI $(1{:}4)_{stm}$, which has twice the amount of iron loading compared to [Fe,Al]MFI $(0.5{:}4)_{stm}$, most of the extra-framework iron species exhibit a high-spin ferric doublet, **d(IV)**, in the Mössbauer spectra. These iron species, which are probably composed of diamagnetic high-spin $Fe^{3+} - Fe^{3+}$ complexes with strong antiferromagnetic coupling, have been detected in all samples. Its intensity is observed to increase with the iron concentration. This

phenomenon is attributed to an enhanced spin electron relaxation rate, which is most likely due to an increase in the number of neighboring Fe-ions. Nevertheless, since **d(IV)** exhibits an unusually large quadrupole splitting, it suggests that most of these ferric clusters are surface species, which are highly distorted. This is further supported by the result after N_2O treatment, which indicates that these iron species are accessible and confirms that they are not embedded in bulk agglomerates.

In addition, the presence of superparamagnetic iron oxide nanoparticles could be shown in the samples with high iron concentration (e.g. [Fe,Al]MFI (1:4)$_{stm}$ and [Fe,Al]MFI (0.5:4)$_{stm}$). The formation of these iron oxide nanoparticles is brought about by further agglomeration of extra-framework iron species, which apparently is dependent on the iron concentration. However, Mössbauer spectra of the samples taken after subsequent treatments in N_2O have also shown an increase in spectral contribution of the superparamagnetic iron oxide particles. This is significant since it implies that iron oxide particles, which are known to be inactive in N_2O decomposition,[33] are further produced over prolonged treatment in N_2O. This could potentially cause catalyst deactivation both in N_2O decomposition and the direct oxidation of benzene to phenol reaction – since N_2O dissociation is a vital step in this catalytic reaction. Mössbauer spectra of the spent [Fe,Al]MFI (1:0)$_{stm}$ catalyst reveal a substantial spectral contribution of superparamagnetic iron oxide nanoparticles. The formation of these iron oxide particles could partially explain the slow deactivation of the [Fe,Al]MFI (1:0)$_{stm}$ catalyst during the BTOP reaction.

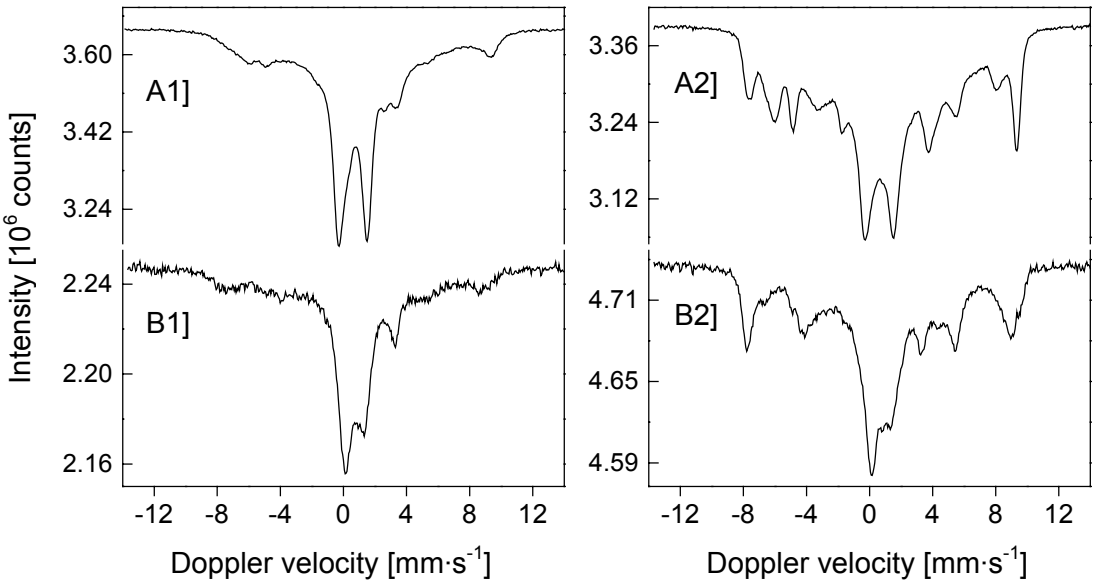

Figure 7.15. *^{57}Fe Mössbauer spectra of the fresh* [Fe,Al]MFI (1:0)$_{stm}$ *catalyst recorded at* A1] *77 K, and* A2] *4.2 K, together with the spectra of spent* [Fe,Al]MFI (1:0)$_{stm}$ *catalyst taken at* B1] *77 K, and* B2] *4.2 K*

In the spent [Fe,Al]MFI $(1:0)_{stm}$ catalyst used in the direct oxidation of benzene to phenol reaction (i.e. after 5 h BTOP reaction, described in chapter 6) ^{57}Fe Mössbauer spectra recorded at 77 and 4.2 K shows evidence of the growth of superparamagnetic iron oxide particles. The 77 K spectra (figure 7.15B1) of the spent catalyst exhibits a 'relaxed' high-spin Fe^{3+} doublet with a reduced quadrupole splitting compared to the fresh catalyst (figure 7.15A1). The lowering of the quadrupole splitting indicates that iron atoms are in a more symmetric environment. This could be brought about by the presence of large iron oxide particles, since iron ions in a bulk particle are likely to be symmetric than the surface iron species. The formation of large iron oxide particles is further substantiated by the 4.2 K spectra. By comparison of the hyperfine fields of both the fresh and spent catalysts, it seems that several magnetic components, most likely caused by small clusters of extra-framework iron species, agglomerate to large superparamagnetic iron oxide particles (figure 7.16 B2). This proves that catalyst deactivation particularly in the [Fe,Al]MFI $(1:0)_{stm}$ catalyst is caused by the formation of inactive iron oxide particles. Thus, regeneration is not possible, such as in the case of coke formation where it is possible to burn off the coke.

7.4.2. Reactivity to benzene

As mentioned in section 7.3.2, most ferrous ions were oxidized to ferric ions in the presence of nitrous oxide. However, it is apparent from the activity data that only a fraction of these ferric species are catalytically active in transferring atomic oxygen – generated from the dissociation of N_2O to benzene for the formation of phenol (*see chapter 6*). Thus, to determine amongst which of the iron species in the [Fe,Al]MFI catalysts are catalytically active, the N_2O-loaded samples were flushed with benzene (30 ml/min, 4% C_6H_6, rest He) at different temperatures.

Remarkably, even at room temperature benzene reaction, Mössbauer spectral changes are observed. These changes, which suggest a reduction of ferric to ferrous ions, can only be caused by the presence of benzene. Flushing the N_2O-loaded samples with He only at room temperature leaves the samples unchanged. The presence of benzene induces the reduction of ferric to ferrous ions most likely *via* a transfer of atomic oxygen. Since activity data, especially for the N_2O-loaded [Fe,Al]MFI $(0.5:4)_{stm}$ sample, show a high selectivity towards phenol, thus, it can be inferred that the active iron species for the BTOP reaction are in the ferric state following a N_2O dissociation step. In addition, the spectra revert to its oxidized form upon N_2O treatment. This shows further evidence that the *redox* transition in the BTOP reaction involves a reversible $Fe^{3+} \leftrightarrow Fe^{2+}$, which is contrary to that proposed for mononuclear centers,[27,28,34] which would involve a $Fe^{4+} \leftrightarrow Fe^{2+}$cycle.

Mössbauer results have shown that mostly the broad magnetic feature is affected by the presence of benzene, which is coupled by the appearance of a high-spin Fe^{2+} doublet. However, for samples with high iron concentration, also a fraction of the **d(IV)** component changed (figure 7.5). This suggests that most likely more than one type of iron species exhibit similar *redox* characteristics.

Mössbauer spectra recorded after the N_2O-loaded samples were flushed with benzene at 473 K reveal a substantial reduction of ferric to ferrous ions (figure 7.10). However, preceding experiments involving heat treatment in He alone of the N_2O-loaded samples at the same temperature already show a considerable reduction of ferric to ferrous ions. However, after subtracting the contribution resulting from heat-treatment-induced reduction, the spectral difference of the high-spin Fe^{2+} doublet (except for the [Fe,Al]MFI $(0.5{:}4)_{stm}$ sample) increases with the samples with high iron concentration. This suggests that at high temperatures, the presence of benzene stimulates further reduction of almost all Fe-species responsible for the broad magnetic feature and a substantial portion of the **d(IV)** component. For the [Fe,Al]MFI $(0.5{:}4)_{stm}$ sample, most of the iron species already exhibit high sensitivity towards an autoreduction process. Thus, it is difficult to discriminate the extent upon which the iron species are reduced in the presence of benzene only. However, there is reason to believe that the iron species that undergo an autoreduction process are also the same iron species reduced in the presence of benzene. This is because after subjecting the [Fe,Al]MFI catalysts in BTOP reaction gases (i.e. reaction with 4% benzene in N_2O at 623 K), a similar *redox* behavior amongst the iron species was observed. Since different types of iron species exhibit similar *redox* characteristics, this might also imply that probably more than one iron species is responsible for the catalytic oxidation of benzene to phenol, with N_2O as oxidant.

7.4.3. Active Fe-species in Al-free catalyst

Although the Al-free [Fe,Al]MFI $(1{:}0)_{stm}$ catalyst exhibit different spectral characteristics particularly in the magnetic features, *in situ* ^{57}Fe Mössbauer studies prove that the active extra-framework iron species are similar to that in the Al-containing [Fe,Al]MFI catalysts. This is illustrated by the changes in the Mössbauer spectra, where an almost reversible **d(IV)** to **d(II)** transition is observed during *redox* reactions. Moreover, it is noted that some of the species exhibited in the broad magnetic feature also changed. However, due to the complexity of the magnetic feature, which most likely exhibits a magnetic coupling of Fe^{3+} and Fe^{2+} species, it is difficult to quantify the extent of reduction in the presence of benzene. It is therefore proposed that redox-active extra-framework iron species in [Fe]MFI catalysts are most likely stabilized on tetrahedral framework iron.

7.5. Conclusion

There are several conclusions that can be deduced from the analysis of the *in situ* studies presented in this study. These can be summarized as follows:

- One of the underlying motivations why we systematically varied the iron concentration down to ppm levels was to start from a homogeneous and well-defined structure of extra-framework iron species. This was initially the understanding upon steam-treatment of the [Fe,Al]MFI samples with varying iron concentration, which generates a predominant high-spin ferrous ions. However, upon *in situ* studies in different reducing/oxidizing environments, it is confirmed that there is a distribution of several extra-framework species, even at ppm levels. Thus, this heterogeneous catalyst is simply heterogeneous in terms of the types iron species formed after steam-treatment. This makes it further difficult to establish a direct relationship between structure and activity in the BTOP reaction.
- Pretreatment of the catalyst exposes two chemically different Fe^{2+} species, which makes the assignment of the high-spin ferrous doublet with a structure similar to that of MMO highly doubtful.
- Mononuclear iron species, which is a subject of recent discussions as a probable active site, apparently is not observed in the current batch of samples.
- Reaction with benzene at room temperature provides unequivocal proof that the active catalyst in the BTOP reaction is in the ferric state (after oxidation of ferrous species in N_2O).
- Finally, reaction with benzene at high temperature indicates that probably more than one type/form of extra-framework iron species is active in the catalytic oxidation of benzene to phenol using N_2O as oxidant.

REFERENCES

1. G.I. Panov, *Cattech*, 4 (2000) 18.
2. P.P. Notté, *Top. Catal.*, 13 (2000) 387.
3. A. Ribera, I.W.C.E. Arends, S. de Vries, J. Pérez-Ramírez, and R.A. Sheldon, *J. Catal.*, 195 (2000) 287.
4. J.B. Taboada, E.M.J. Hensen, I.W.C.E. Arends, G. Mul, and A.R. Overweg, *Catal. Today*, 110 (2005) 221.
5. K.A. Dubkov, N.S. Ovanesyan, A.A. Shteinman, E.V. Starokon, and G.I. Panov, *J. Catal*., 207 (2002) 341.
6. A.M. Ferretti, C. Oliva, L. Forni, G. Berlier, A. Zecchina, and C. Lamberti, *J. Catal*., 208 (2002) 83.
7. J.A. Ryder, A.K. Chakraborty, and A.T. Bell, *J. Catal*., 220 (2003) 84.
8. J. Pérez-Ramírez, F. Kapteijn, and A. Brückner, *J. Catal*., 218 (2003) 234.
9. P.K. Roy and G.D. Pirngruber, *J. Catal*., 227 (2004) 164.
10. J. Jia, K.S. Pillai, and W.M.H. Sachtler, *J. Catal*., 221 (2004) 119.
11. J.B. Taboada, A.R. Overweg, P.J. Kooyman, I.W.C.E. Arends, and G. Mul, *J. Catal*. 231 (2005) 56.
12. G.I. Panov, A.K. Uriarte, M.A. Rodkin, and V.I. Sobolev, *Catal. Today*, 41 (1998) 365.
13. E.J.M Hensen, Q. Zhu, and R.A. van Santen, *J. Catal*., 233 (2005) 136.
14. P. Fejes, J.B. Nagy, K. Lázár, and J. Halász, *Appl. Catal. A*, 190 (2000) 117.
15. A.R. Overweg, M.W.J. Crajé, A.M. van der Kraan, I.W.C.E. Arends, A. Ribera, and R.A. Sheldon, *J. Catal*., 223 (2004) 262.
16. G.I. Panov, V.I. Sobolev, K.A. Dubkov, V.N. Parmon, N.S. Ovanesyan, A.E. Shilov, and A.A. Shteinman, *React. Kinet. Catal. Lett.*, 61 (1997) No.2, p.251.
17. J.W. Niemantsverdriet, C.F.J. Flipse, A.M. van der Kraan, and J.J. van Loef, *Appl. Surf. Sci.*, 10 (1982) 302.
18. Q. Zhu, R.M. van Teeffelen, R.A. van Santen, and E.J.M. Hensen, *J. Catal.*, 221 (2004) 575.
19. J. Pérez-Ramírez, G. Mul, F. Kapteijn, J.A. Moulijn, A.R. Overweg, A. Doménech, A. Ribera, and I.W.C.E. Arends, *J. Catal*., 207 (2002) 113.
20. N.S. Ovanesyan, A.A. Shteinman, K.A. Dubkov, V.I. Sobolev, G.I. Panov, *Kinet. Catal*., 39 (1998) 792.
21. J.G. DeWitt, J.G. Bentsen, A.C. Rosenzweig, B. Hedman, J. Green, S. Pilkington, G.C. Papaeftymiou, H. Datlton, K.O. Hodgson, S.J. Lippard, *J. Am. Chem. Soc.*, 113 (1991) 9219.
22. J. Green, and H. Dalton, *J. Biol. Chem*., 264 (1989) 17698.

23. B.G. Fox, J.G. Borneman, L.P. Wackett, and J.D. Lipscomb, *Biochemistry*, 29 (1990) 6419.
24. N.N. Greenwood and T.C. Gibb, Mössbauer Spectroscopy, Chapman and Hall Ltd., London, 1971, chap. 10.
25. A. Heyden, B. Peters, A.T. Bell and F.J. Keil, *J. Phys. Chem. B*, 109 (2005) 1857.
26. J. Pérez-Ramírez, F. Kapteijn, J.C. Groen, A. Doménech, G. Mul, and J.A. Moulijn, *J. Catal*,. 214 (2003) 33.
27. J. Jia, K.S. Pillai, and W.M.H. Sachtler, *J. Catal*,. 221 (2004) 119.
28. P. Kubánek, B. Wichterlová, and Z. Sobalík, *J. Catal*,. 211 (2002) 109.
29. P. Marturano, L. Drozdova, A. Kogelbauer, and R. Prins, *J. Catal.*, 192 (2000) 236.
30. V. Schünemann and H. Winkler, *Rep. Prog. Phys*. 63 (2000) 263.
31. P.G. Debrunner, *Hyperfine Interactions*, 53 (1990) 21.
32. D.M. Kurts Jr., *Chem. Rev.*, 90 (1990) 585.
33. F. Kapteijn, J. Rodriguez-Mirasol, J.A. and Moulijn, *Appl. Catal. B*, 9 (1996) 25.
34. J.A. Ryder, A.K. Chakraborty, and A.T. Bell, *J. Catal.*, 220 (2003) 84.

Chapter 8

Concluding Remarks

"*True sciences are those which have penetrated through the senses as a result of experience and thus silencing the tongues of disputants, not feeding investigators on dreams but always proceeding successively from primary truths and established principles, in a proper order towards the conclusion.*"
– Leonardo da Vinci, *Codex* ***Urbinas Latinus***

Elucidating the active iron species in [Fe,Al]MFI catalysts for the direct oxidation of benzene to phenol

On the active iron species in the direct oxidation of benzene to phenol

The investigation of the catalytically active sites in steam-treated [Fe,Al]MFI zeolites for the direct oxidation of benzene to phenol (BTOP), using N_2O as the oxidant, started out with the notion of elucidating the structure of a single iron species that is responsible for the catalysis.[1] [Fe,Al]MFI catalysts varying in iron concentration were prepared. From 0.6 wt.% Fe, which is found normally in commercial [Fe,Al]MFI zeolites, or FeZSM-5, the iron concentration was systematically varied down to ppm levels.[2,3] The presence of almost all iron in the [Fe,Al]MFI catalysts in the ferrous state after steam-treatment regardless of iron concentration has provided an interesting starting point for establishing the structure-activity relationship.[4,5] However, although a predominant high-spin Fe^{2+} doublet was attained after steam-treatment, further ^{57}Fe Mössbauer studies on these samples after subjecting them to different reduction/oxidation gases involved in the BTOP reaction strongly indicate that we are dealing with several types of extra-framework iron species.[6] This is substantiated by the activity results,[7,8] which prove that only a fraction of these iron species is active in the direct oxidation of benzene to phenol.

The heterogeneous mixture of extra-framework iron species, as deduced from the *in situ* ^{57}Fe Mossbauer experiments, encompasses the following: (*a*) diamagnetic clusters – i.e. dimeric complexes to large clusters with a few even number of iron atoms; (*b*) paramagnetic species – i.e. complexes with uneven number of iron atoms ranging from isolated to large clusters in the 'relaxed' limit; and to some extent, (*c*) large iron oxide nanoparticles specifically in samples with high iron concentration. Except for large iron oxide nanoparticles, which are known to be inactive in both N_2O decomposition[9] and benzene to phenol reactions,[10] most of these species, especially small extra-framework iron complexes, exhibit *redox* properties.

It is therefore not surprising that a straightforward relationship is found for the set of catalysts with varying iron concentration and their corresponding activity in the decomposition of nitrous oxide.[7] That is because most extra-framework iron species formed on steam-treatment at the given conditions,[4,5] show high affinity towards N_2O. This is confirmed in the ^{57}Fe Mössbauer data in which most, if not all, high-spin Fe^{2+} species are oxidized in the presence of N_2O at 623 K.[6] Furthermore, these species exhibit high sensitivity towards autoreduction, even at relatively low temperatures.[6,11]

Although, the presence of Fe^{2+} species can be associated to the formation of surface active oxygen *via* the dissociation of N_2O,[12-14] it is rather premature to ascribe these species as active centers, such as *α-sites*,[12] in the direct oxidation of benzene to phenol. It is clear from the BTOP activity data[7,8] that selectivity plays a major role in determining whether an extra-framework iron *redox* site is catalytically active in the direct oxidation of benzene to phenol. Thus, a linear correlation between the presence of Fe^{2+} species and the amount of active sites is highly doubtful, especially in [Fe,Al]MFI catalysts with relatively high iron concentration. At steady-state condition, only a fraction of Fe^{2+} species remains active in the BTOP reaction. This faction evidently increases as the iron concentration is deceased, which indicates that most likely the active species are highly dispersed extra-framework complexes (e.g. enzyme-like system) composed of a few number of iron atoms.

Based on the observed valences as derived from the obtained isomer shifts in the ^{57}Fe Mössbauer spectra recorded after different reduction/oxidation treatments,[6] it is most likely that an ensemble of at least two neighboring Fe-atoms participate in the BTOP catalysis, which leads to a two-electron *redox* transfer (O-transfer). However, from *in situ* studies,[6] there is no definitive proof of a single structure of extra-framework iron species that is responsible for the catalytic oxidation of benzene to phenol, using N_2O as oxidant. Rather it is proposed that most likely several types of extra-framework Fe-species in the [Fe,Al]MFI catalysts are active in the BTOP reaction. Therefore, this makes it difficult to establish a direct correlation between the structure of the active iron species and catalytic activity in the benzene to phenol oxidation reaction.

On the role of aluminum

In the presence of a substantial amount of aluminum, most extra-framework iron species in [Fe,Al]MFI catalysts have been illustrated in this study to go through an autoreduction process, i.e. the reduction of ferric to ferrous ions during heat treatment in inert (He) gas.[11] In addition, Mössbauer data reveals that hardly any autoreduction process takes place in the aluminum-free [Fe,Al]MFI $(1:0)_{stm}$ catalyst after heat treatment in He at 823 K.[6] This result implies that aluminum plays an important role, at least, in the autoreduction process, and, therefore in the eventual formation of *redox* active Fe^{2+} species.

The formation of Fe^{2+} *redox* center is deemed crucial in both N_2O decomposition and benzene to phenol reactions since it denotes the presence of and empty catalytic site. However, although aluminum enhances the formation of ferrous species,[11] activity data in both N_2O decomposition and benzene to phenol reactions give different impressions.[7] The decomposition of N_2O over [Fe,Al]MFI catalysts shows an increase in activity with increasing aluminum concentration. On the other hand, BTOP reaction data reveals that

aluminum ***does not*** play a role in the BTOP catalysis at all.[7] In fact, phenol productivity even decreases with increasing aluminum concentration.

Although the formation of active-oxygen species is a vital step in the reaction pathway of the benzene to phenol reaction, it does not warrant a direct correlation in the benzene to phenol activity. This indicates that other factors affecting the catalyst performance have to be considered. From the activity data, the decrease in phenol productivity as a function of aluminum content is apparently caused by a decrease in catalyst selectivity towards phenol. A competing reaction of N_2O decomposition was ruled out since molecular oxygen was not observed in the mass spectroscopy data, and besides activity data for N_2O decomposition did not show any conversion at 623 K in all samples. Nevertheless, the presence of coke formation leading to combustion (CO_2 and H_2O) is proven to be responsible for the decline in catalyst selectivity. Since coke formation is hardly observed in the aluminum-free sample,[6] the presence of aluminum could be the cause of unwanted reactions, leading to poor selectivity and eventually to catalyst deactivation.

REFERENCES

1. Chapter 1, *this thesis*.
2. Chapter 3, *this thesis*.
3. J.B. Taboada, A.R. Overweg , M.W.J. Crajé, I.W.C.E. Arends, G. Mul, and A.M. van der Kraan, *Microporous Mesoporous Mater.,* 75 (2004) 237.
4. Chapter 4, *this thesis*.
5. J.B. Taboada, A.R. Overweg , P.J. Kooyman, I.W.C.E. Arends, and G. Mul, *J. Catal.,* 231 (2005) 56.
6. Chapter 7, *this thesis*.
7. Chapter 6, *this thesis*.
8. J.B. Taboada, E.J.M. Hensen, I.W.C.E. Arends, G. Mul, and A.R. Overweg, *Catal. Today,* 110 (2205) 221.
9. F. Kapteijn, J. Rodriguez-Mirasol, J.A. and Moulijn, *Appl. Catal. B*, 9 (1996) 25.
10. G.I. Panov, A.K. Uriarte, M.A. Rodkin, and V.I. Sobolev, *Catal. Today,* 41 (1998) 365.
11. Chapter 5, *this thesis*.
12. G.I. Panov, *Cattech*, 4 (2000) 18.
13. G.I. Panov, A.K. Uriarte, M.A. Rodkin, and V.I. Sobolev, *Catal. Today*, 41 (1998) 365.
14. K.A. Dubkov, N.S. Ovanesyan, A.A. Shteinman, E.V. Starokon, and G.I. Panov, *J. Catal.*, 207 (2002) 341.

Summary

Direct Oxidation of Benzene to Phenol

Investigation of the active iron species in [Fe,Al]MFI catalysts by ^{57}Fe Mössbauer spectroscopy

PhD Thesis by Jerome B. Taboada

Fe-containing ZSM-5 zeolite, or [Fe,Al]MFI, is known to catalyse various chemical reactions. Recently, it has gained increasing attention for its catalytic performance in the direct oxidation of benzene to phenol, using N_2O as oxidant (BTOP). However, despite extensive efforts, the nature of the active sites in the [Fe,Al]MFI catalyst for the BTOP reaction is still largely unknown. This is mainly due to various synthesis and activation methods of [Fe,Al]MFI catalysts that have led to different interpretations. Nevertheless, there seems to be a consensus in open literature that steam-treatment of isomorphously substituted [Fe,Al]MFI zeolite forms a particular extra-framework iron species that is catalytically active in the BTOP reaction.

To elucidate the active sites, this study investigates the relationship between the structure and activity of [Fe,Al]MFI catalysts in the BTOP reaction. Several isomorphously substituted [Fe,Al]MFI zeolites were prepared *via* hydrothermal treatment. In one set of zeolite samples, the iron concentration was systematically varied down from 0.6 wt.% Fe, which is normally found in commercial [Fe,Al]MFI zeolites, to 0.075 wt.% Fe. In this set of zeolites, the aluminum content was kept constant at 1.1 wt.%. The rationale behind the variation of iron are as follows: (i) prevent the formation of large iron oxide nanoparticles, which are known to be inactive in the BTOP reaction; (ii) simulate the iron impurity concentrations in commercial ZSM-5 zeolites; and (iii) form highly dispersed iron species, which many authors regard as the catalytically active species in the direct oxidation of benzene to phenol. Another set of [Fe,Al]MFI zeolites, varying in aluminum concentration (0.0-1.1 wt.% Al) while keeping the iron content constant at 0.6 wt.%, were also prepared to study the role and importance of aluminum in the BTOP oxidation. Furthermore, all [Fe,Al]MFI samples were enriched with ^{57}Fe isotope to enhance the Mössbauer effect, and thus providing an excellent signal-to-noise ratio.

^{57}Fe Mössbauer spectroscopy was used as the principal characterization tool in this study. It is an ideal method to characterize iron-containing solids, such as the various iron species present in the steam-treated [Fe,Al]MFI catalysts. Unlike electron paramagnetic resonance

(EPR), there is no form of iron that is Mössbauer-silent. Moreover, it provides richer information compared to bulk-averaging techniques such as magnetic susceptibility.

Isomorphously substituted [Fe,Al]MFI zeolites with varying iron and aluminum concentrations were successfully prepared by hydrothermal synthesis as described in this thesis. Because all samples were enriched with ^{57}Fe isotope, the synthesis method had to be improved to prevent phase segregation and heterogeneity of the trivalent (iron and aluminum) ion distribution in the [Fe,Al]MFI zeolite. This was achieved by rotating the autoclave during hydrothermal treatment to enhance the homogeneity of the solution gel.

^{57}Fe Mössbauer data reveals that iron in the *as*-synthesized [Fe,Al]MFI zeolites is present as isolated paramagnetic Fe^{3+} ions that are tetrahedrally coordinated in the MFI framework regardless of iron and aluminum concentrations. Calcination of the *as*-synthesized [Fe,Al]MFI zeolites at 823 K for 10 h causes part of the framework iron to migrate into extra-framework positions. Transformation of the calcined [Fe,Al]MFI zeolites to H-form (by three consecutive overnight exchanges with 0.1 M ammonium nitrate and subsequent calcination at 823 K for 5 h) induces further migration of iron from framework to extra-framework positions. [Fe,Al]MFI samples with low iron content (< 0.6 wt%) forms highly dispersed extra-framework Fe^{3+} species, which easily undergo autoreduction to its divalent state. Steam-treatment of [Fe,Al]MFI zeolites at 873 K (300 mbar H_2O) leads to the removal of almost all iron from framework to extra-framework positions. This results to a predominant presence of high-spin Fe^{2+} species (ca. 90%), particularly in the samples with 1.1 wt% aluminum. However in the steam-treated [Fe,Al]MFI samples with low aluminum concentration, the quantity of the trivalent iron increases.

In situ Fe *K*-edge XANES measurements performed on three [Fe,Al]MFI zeolites varying in aluminum concentration reveal that the presence of aluminum enhances the formation of *redox*-active extra-framework iron species. These types of extra-framework iron easily undergo autoreduction upon thermal treatment in N_2 at 623 K. The autoreduction process is shown to occur even at low heat-treatment temperatures (i.e. between 300 K and 398 K) in N_2. On the other hand, ferrous species can only be oxidized by N_2O above 498 K. This perfectly illustrates the need to measure in a controlled environment, as the state of extra-framework iron easily changes with different conditions.

Steam-treated [Fe,Al]MFI zeolites, with varying iron and aluminum concentrations, were evaluated for their catalytic performance in the direct oxidation of benzene to phenol, using N_2O as oxidant. Moreover, as the dissociation of N_2O is directly related to the BTOP reaction, the catalysts were also tested separately for their activity in the decomposition of

N_2O. For [Fe,Al]MFI catalysts with increasing iron content (i.e. 0.075-0.6 wt.% Fe), a decrease in the phenol productivity per gram of iron was observed. This indicates that not all extra-framework iron species formed after steam-treatment of the [Fe,Al]MFI zeolites are active in the BTOP reaction. It also shows that active iron species are preferably formed in samples with low iron concentration. However, in the N_2O decomposition reaction, higher N_2O conversions were achieved for [Fe,Al]MFI catalysts with increasing iron loading. This illustrates that most extra-framework iron species formed after steam-treatment are catalytically active in the decomposition of N_2O.

For the set of [Fe,Al]MFI catalysts with varying aluminum concentration (0.0-1.1 wt.% Al), BTOP activity after 1h time on stream is observed to decrease significantly for catalysts with higher aluminum loading. This implies that the occurrence of catalyst deactivation, most likely due to coke formation, is more favorable in the presence of aluminum. On the other hand, N_2O decomposition data reveals that catalysts with higher aluminum concentration exhibit superior performance compared to the samples with lower or without aluminum. These results show that although aluminum appears to enhance the formation of active sites for the catalytic decomposition of N_2O, it nevertheless deters the selectivity towards phenol in the BTOP reaction. Furthermore BTOP activity data specifically for the Al-free sample strongly indicates that aluminum does not play a role in the BTOP catalysis.

Finally, *in situ* ^{57}Fe Mössbauer studies show that there are several active sites for the direct oxidation of benzene to phenol. These active sites are most likely small clusters of iron species with low nuclearity (e.g. enzyme-like systems). Subjecting the [Fe,Al]MFI catalysts to several controlled treatments confirms that there is a distribution of several extra-framework iron species, even at ppm levels. Thus, this heterogeneous catalyst is simply heterogeneous in terms of the extra-framework iron species formed after steam-treatment, which makes it difficult to establish a direct relationship between structure and activity in the BTOP reaction.

Samenvatting

Directe Oxidatie van Benzeen naar Fenol

Onderzoek van actieve ijzer-vormen in [Fe,Al]MFI katalysatoren met ^{57}Fe Mössbauer spectroscopy

PhD Thesis door Jerome B. Taboada

Van Fe-bevattend ZSM-5 zeoliet, ook wel [Fe,Al]MFI genaamd, is bekend dat het diverse chemische reacties katalyseert. Recentelijk is er stijgende belangstelling voor de katalytische prestaties in de directe oxidatie van benzeen naar fenol met gebruik van N_2O als oxidatiemiddel (BTOP). Ondanks uitgebreide inspanningen is echter de aard van de actieve plaatsen in de [Fe,Al]MFI katalysator voor de BTOP reactie nog grotendeels onbekend. Dit is hoofdzakelijk toe te schrijven aan de diversiteit van gebruikte synthese- en activeringsmethodes die tot verschillende interpretaties heeft geleid. Toch lijkt er in de literatuur een consensus te zijn dat een stoombehandeling van isomorf gesubstitueerd [Fe,Al]MFI zeoliet een speciaal *extra-framework* ijzer-type vormt dat katalytisch actief is in de BTOP reactie.

Om de actieve plaatsen nader te belichten, wordt in deze studie het verband tussen de structuur en de activiteit van [Fe,Al]MFI katalysatoren in de BTOP reactie onderzocht. Gesubstitueerde isomorfe [Fe,Al]MFI zeolieten werden bereid via een hydrothermische behandeling. In c set van zeoliet monsters werd de ijzerconcentratie systematisch gevarieerd van 0.6 gew.%, hetgeen gewoon is in commerciële [Fe,Al]MFI zeolieten, tot 0.075 gew.%. In deze set werd de aluminiumconcentratie constant gehouden op 1.1 gew.%. De redenen van deze variatie in de ijzerconcentratie zijn: (i) verhindering van de vorming van grote ijzeroxide nanodeeltjes, welke inactief zijn in zowel N_2O decompositie als de reactie van benzeen naar fenol; (ii) simulatie van de concentraties van de ijzeronzuiverheid in commerciële ZSM-5 zeolieten; en (iii) vorming van hoog gedispergeerde ijzer-vormen, door veel auteurs beschouwd als de katalytisch actieve vorm voor de directe oxidatie van benzeen naar fenol. Een andere set van [Fe,Al]MFI zeolieten, met een systematisch gevarieerde aluminiumconcentratie van 0.0 gew.% tot 1.1 gew.% bij een gelijkblijvende ijzerconcentratie van 0.6 gew.%, werd bereid om de rol en het belang van aluminium in de directe BTOP oxidatie te bestuderen. Verder werden alle [Fe,Al]MFI monsters verrijkt met het ^{57}Fe isotoop om het Mössbauer effect te verbeteren, waardoor een uitstekende signaal-ruisverhouding werd bereikt.

^{57}Fe Mössbauer spectroscopie werd gebruikt als de belangrijkste karakteriseringstechniek in deze studie. Het is een ideale methode om ijzer-bevattende vaste stoffen te kenmerken, zoals de verschillende aanwezige ijzersoorten in stoombehandelde [Fe,Al]MFI katalysatoren. In tegenstelling tot elektron paramagnetische resonantie (EPR) is er geen vorm van ijzer die *Mössbauer-stil* is. Voorts verstrekt het meer informatie dan bulk-middelende technieken, zoals magnetische susceptibiliteit.

Isomorfe gesubstitueerde [Fe,Al]MFI zeolieten met variërende ijzer- en aluminium-concentraties werden met succes bereid via een hydrothermische synthese, zoals in dit proefschrift wordt beschreven. Om alle monsters met ^{57}Fe isotoop te verrijken, moest de synthese methode verbeterd worden om fasescheiding en heterogeniteit van de driewaardige (ijzer en aluminium) ionendistributie in het [Fe,Al]MFI zeoliet te verhinderen. Dit werd bereikt door de autoclaaf te roteren tijdens de hydrothermische behandeling om zodoende de homogeniteit van de oplossing te verbeteren.

^{57}Fe Mössbauer data laaten zien dat ijzer in de *as-synthesized* [Fe,Al]MFI zeolieten aanwezig is als geïsoleerde paramagnetische Fe^{3+}-ionen die tetrahedrisch in het MFI rooster worden gecoördineerd, ongeacht ijzer- en aluminiumconcentraties. Calcinering van de *as-synthesized* [Fe,Al]MFI zeolieten bij 823 K gedurende 10 uur veroorzaakt een migratie van een deel van het roosterijzer naar de *extra-framework* positie. Transformatie van gecalcineerd [Fe,Al]MFI zeolieten naar de *H-form* (door drie opeenvolgende uitwisselingen met ammoniumnitraat van 0.1 M gedurende een nacht en verder calcineren bij 823 K gedurende 5 uur) veroorzaakt verdere ijzermigratie van het rooster naar de *extra-framework* posities. [Fe,Al]MFI monsters met laag ijzergehalte (< 0.6 % gew.) vormen hoog gedispergeerd *extra-framework* Fe^{3+}-deeltjes, die gemakkelijk autoreductie naar tweewaardig ijzer ondergaan. Stoombehandeling van [Fe,Al]MFI zeolieten bij 873 K (300 mbar H_2O) leidt tot de verwijdering van bijna al het ijzer van het rooster naar de *extra-framework* posities. Dit leidt tot een overheersende aanwezigheid van high-spin Fe^{2+}-deeltjes (circa 90%), in het bijzonder in de monsters met 1.1 gewichtsprocent aluminium. Daarentegen stijgt in stoombehandelde [Fe,Al]MFI monsters met lage aluminiumgehaltes de hoeveelheid van het driewaardige ijzer.

In situ Fe *K*-edge XANES metingen die uitgevoerd werden op drie [Fe,Al]MFI zeolieten met variërende aluminiumconcentratie, laten zien dat de aanwezigheid van aluminium de vorming van redox-actief *extra-framework* ijzer verbetert. Deze vormen van *extra-framework* ijzer ondergaan gemakkelijk autoreductie bij een thermische behandeling in N_2 bij 623 K. Het autoreductie proces blijkt zelfs bij lage thermische behandelingstemperaturen voor te komen (tussen 300 K en 398 K) in N_2. Anderzijds kunnen ijzerhoudende deeltjes door N_2O alleen geoxideerd worden boven 498 K. Dit illustreert de noodzaak om in een gecontroleerde

omgeving te meten, aangezien de toestand van *extra-framework* ijzer gemakkelijk verandert bij verschillende condities.

De katalytische prestaties van stoombehandelde [Fe,Al]MFI zeolieten, met variërende ijzer- en aluminiumconcentraties, werden geëvalueerd in de directe oxidatie van benzeen naar fenol met N_2O als oxidant. Aangezien de ontleding van N_2O direct verwant is aan de BTOP reactie, werd de activiteit van de katalysatoren ook afzonderlijk getest voor de ontleding van N_2O. Voor [Fe,Al]MFI katalysatoren met een stijgend ijzergehalte (i.e. 0.075-0.6 % gew.) werd een daling van de fenolproductiviteit per gram ijzer waargenomen. Dit wijst erop dat niet alle vormen van het *extra-framework* ijzer, die zich na stoombehandeling van [Fe,Al]MFI zeolieten vormden, actief zijn in de BTOP reactie. Het toont ook aan dat de actieve ijzersoorten voornamelijk in monsters met lage ijzerconcentratie worden gevormd. Daarentegen werden in de N_2O decompositiereactie hogere N_2O omzettingen bereikt voor [Fe,Al]MFI katalysatoren met stijgend ijzergehalte. Dit illustreert dat de meeste vormen van het *extra-framework* ijzer die na stoombehandeling worden gevormd katalytisch actief zijn in de ontleding van N_2O.

Voor de reeks van [Fe,Al]MFI katalysatoren met variërende aluminiumconcentratie (0.0 - 1.1 % gew.) neemt de BTOP activiteit na één uur significant af voor katalysatoren met hogere aluminiumconcentratie. Dit impliceert dat het voorkomen van deactivering, hoogstwaarschijnlijk door vorming van roet, toeneemt met de aanwezigheid van aluminium. Aan de andere kant laten de N_2O-ontledings-gegevens zien dat de katalysatoren met hogere aluminiumconcentraties superieure prestaties kennen in vergelijking met de monsters met een lager gehalte aan of zonder aluminium. Deze resultaten tonen aan dat, hoewel het aluminium de vorming van actieve plaatsen voor de katalytische ontleding van N_2O lijkt te verbeteren, het de selectiviteit naar fenol in de BTOP reactie vermindert. Verder wijzen de BTOP-activiteitsgegevens van met name de aluminium-vrije samples er sterk op dat het aluminium geen rol speelt in de BTOP reactie.

Tot slot tonen *in situ* ^{57}Fe Mössbauer studies aan dat er verscheidene actieve plaatsen voor de directe oxidatie van benzeen naar fenol zijn. Deze actieve plaatsen zijn hoogstwaarschijnlijk kleine clusters van ijzer met lage nucleariteit (e.g. enzym-achtige systemen). Het onderwerpen van [Fe,Al]MFI katalysatoren aan verschillende *in situ* behandelingen bevestigt dat er een distributie van verscheidene *extra-framework* ijzervormen is, zelfs op ppm-niveau. Aldus is deze heterogene katalysator heterogeen in de zin van de *extra-framework* ijzervormen die na stoombehandeling worden gevormd, waardoor het moeilijk is om een direct verband te leggen tussen structuur en activiteit in de BTOP-reactie.

Publications and presentations

Publications:

J.B. Taboada, E.J.M. Hensen, I.W.C.E. Arends, G. Mul, and A.R. Overweg, Reactivity of generated oxygen species from nitrous oxide over [Fe,Al]MFI catalysts for the direct oxidation of benzene to phenol, *Catalysis Today,* 110 (2005) 221-227.

J.B. Taboada, A.R. Overweg, and P.J. Kooyman, Direct synthesis of mesoporous Fe-MFI zeolite, *Studies in Surface Science and Catalysis,* 158 (2005) 27-34.

J.B. Taboada, A.R. Overweg, P.J. Kooyman, I.W.C.E. Arends, and G. Mul, Following the evolution of iron from framework to extra-framework positions in isomorphously substituted [Fe,Al]MFI with ^{57}Fe Mössbauer spectroscopy, *Journal of Catalysis,* 231 (2005) 56-66.

J.B. Taboada, A.R. Overweg, I.W.C.E. Arends, and G. Mul, Probing the redox states of iron in steam-treated isomorphously substituted [Fe,Al]MFI catalyst, *Industrial Applications of the Mössbauer Effect*, eds. M. Gracia, J.F. Marco, and F. Plazaola, American Institute of Physics (2005) 31-36.

J.B. Taboada, A.R. Overweg, M.W.J. Crajé, I.W.C.E. Arends, G. Mul, A.M. van der Kraan, Systematic variation of ^{57}Fe and Al content in isomorphously substituted ^{57}FeZSM-5 zeolites: Preparation and Characterization. *Microporous and Mesoporous Materials,* 75 (2004) 237-246.

M. Pérez-Cabero, J.B. Taboada, I. Rodríguez-Ramos, A.R. Overweg, and A. Guerrero-Ruiz, The role of alpha-iron and cementite phases in the growing mechanism of carbon nanotubes: a ^{57}Fe Mössbauer spectroscopy study, *Phys. Chem. Chem. Phys.*, 8 (2006) 1230-1235.

J. Pérez-Ramírez, G. Mul, J.B. Taboada, F. Kapteijn and J.A. Moulijn, Thermal decomposition of layered Co-Al hydrotalcite: An in situ study. *Proceedings of the 12th International Clay Conference*, eds. E. Dominguez, G.R. Mas, and F. Cravero, Elsevier Science, Amsterdam (2001) 631-638.

Articles in Preparation:

J.B. Taboada, I.W.C.E. Arends, G. Mul, and A.R. Overweg, Investigating the active iron sites in the direct oxidation of benzene to phenol through *in situ* ^{57}Fe Mössbauer studies of steam-treated [Fe,Al]MFI zeolites.

J.B. Taboada, E.J.M. Hensen, I.W.C.E. Arends, G. Mul, and A.R. Overweg, Catalytic performance of [Fe,Al]MFI catalysts in the direct oxidation of benzene to phenol: effect of iron and aluminum concentrations.

Oral Presentations (*presenter underlined*)**:**

J.B. Taboada, G. Mul, I.W.C.E. Arends, and A.R. Overweg, *In situ* studies of [Fe,Al]MFI catalyzed oxidation of benzene to phenol, *American Institute of Chemical Engineers (AIChE) Annual Meeting* , Cincinnati, OH, U.S.A., October 30-November 4, 2005.

P.J. Kooyman, J.B. Taboada, and A.R. Overweg, Direct synthesis of mesoporous Fe-MFI zeolite, *3rd Federation of the European Zeolite Association (FEZA) Conference*, Prague, Czech Republic, August 23-26, 2005.

J.B. Taboada, E.J.M. Hensen, A.R. Overweg, I.W.C.E. Arends, and G. Mul, Elucidating the active iron-sites by in-situ 57Fe Mössbauer spectroscopy of steam-treated [Fe,Al]MFI for the direct oxidation of benzene to phenol, *Netherlands Catalysis and Chemistry Conference (NCCC) VI*, Noordvijkerhout, the Netherlands, March 7-9, 2005

J.B. Taboada, E.J.M. Hensen, A.R. Overweg, I.W.C.E. Arends, and G. Mul, Elucidating the active iron-sites by *in situ* 57Fe Mössbauer spectroscopy of steam-treated [Fe,Al]MFI for the direct oxidation of benzene to phenol, *International Workshop on Microporous and Mesoporous Materials as Catalytic Hosts for Fe, Co, Cu*, Scheveningen, the Netherlands, March 1-4, 2005.

P.J. Kooyman, J.B. Taboada, and A.R. Overweg, Direct synthesis of mesoporous Fe-MFI zeolite, *Nederlandse Vereniging voor Microscopie (NVvM) Symposium Papendal 2004*, Arnhem, the Netherlands, November 30-December 1, 2004.

A.R. Overweg, J.B. Taboada, I.W.C.E. Arends, and G. Mul, Probing the *redox* behavior of FeMFI catalysts through ^{57}Fe Mössbauer Spectroscopy, *Catalysis Society of South Africa (CATSA) Conference 2004*, Potchefstroom, South Africa, November 14-17, 2004

J.B. Taboada, A.R. Overweg , I.W.C.E. Arends, and G. Mul, Probing the *redox* behavior of FeMFI catalysts through ^{57}Fe Mössbauer Spectroscopy, *International Symposium on the Industrial Application of the Mössbauer Effect*, Madrid, Spain, October 4-9, 2004.

J.B. Taboada, G. Mul, I.W.C.E. Arends, M.W.J. Crajé, and A.R. Overweg, Following the tracks of iron in FeZSM-5 during preparation and catalysis, *Netherlands Catalysis and Chemistry Conference (NCCC) V*, Noordvijkerhout, the Netherlands, March 8-10, 2004.

Poster Presentations (*presenter underlined*)**:**

J.B. Taboada, A.R. Overweg , M.W.J. Crajé, I.W.C.E. Arends, and G. Mul, and A.M. v.d. Kraan, Systematic variation of ^{57}Fe and Al content in isomorphously substituted ^{57}FeZSM-5 zeolites, *Netherlands Catalysis and Chemistry Conference (NCCC) IV*, Noordvijkerhout, the Netherlands, March 10-12, 2003.

M. Pérez-Cabero, J.B. Taboada, I. Rodríguez-Ramos, A.R. Overweg, and A. Guerrero-Ruiz, Estudio por espectroscopia Mössbauer del papel del la cementita en el mecanismo de crecimiento de los nanotubos de carbono, *Sociedad Española de Catálisis (SECAT) 2005*, Madrid, Spain, June 27-29, 2005.

Acknowledgements

Although it takes dedication, hard work and sacrifice to conduct a scientific research, it is also equally impossible to finish this thesis without the direct and indirect contributions of people that I would like to acknowledge here. To all of them, I am truly indebted.

Foremost, I would like to gratefully acknowledge my indefatigable supervisors. First, I thank my supervisor Dr. Arian R. Overweg. I highly appreciate your continuous scientific guidance throughout the course of my PhD research. Your insights and good ideas, which opened an avenue to many of our stimulating discussions, have enabled me to have a clear direction of my work. Thanks also for the time you spent and for being conscientious in your effort to correct all chapters of my dissertation. Furthermore, I fully enjoyed working with you, most especially in exploring the possibilities of using sophisticated characterization techniques (e.g. ESRF and ISIS experiments). You have been supportive to my spectrum of endeavors that encompasses the intellectual, social, emotional, physical, and paternal aspects. For that I am grateful to have you as my mentor and friend. Second, I thank my *toegevoegd promotor* Dr. Isabel W.C.E. Arends. Without your unwavering support and contributions, it would have been difficult for me to come through the completion of this thesis. Thanks for the encouragement and for your continuous interest in my research. This gave me a boost in confidence that I really need to carry out this work, especially during the early stages of my PhD program. I truly appreciate all our interesting discussions and I value your suggestions in whatever form. Third, I thank Dr. Guido Mul. I am grateful for the time you allocated in your tight agenda for our discussions. Thanks for sharing your insightful ideas, and for giving me access and the necessary support to perform catalytic activity measurements.

To my professors, I express my gratitude. First, to Prof. dr. Gordon J. Kearley, thanks a lot for the motivation and guidance throughout my PhD research. Unfortunately you have to leave TUDelft after the beacon of ANSTO attracted you. I hope someday we can work together again to finish the neutron scattering work we did at ISIS. Second, thanks to Prof. dr. Ignatz M. de Schepper. Although we did not have a chance to work together at the department of Radiation, Radionuclides & Reactors, I highly appreciate that you accepted the responsibility to be my *promotor*. Thanks a lot for your time during the finalization of this dissertation.

I would like to gratefully acknowledge the persons whom I worked with and to those who were directly involved in the acquisition of valuable experimental data. Most of them are from TUDelft, unless otherwise mentioned. To Michel Steenvoorden, my *paranimf*, thank you my friend *voor alles*. I really appreciate your presence in the laboratory, be it in performing some of my experiments (i.e. Mössbauer, XAS, neutron scattering), or just simply discussing football and *gewoon dingen*. Thanks a lot for the Dutch version of the summary (*samenvatting*). Niek van der Pers is acknowledged for the high-resolution XRD results and Gerard de Vos for the SEM equipment training. Thanks to Dr. Jacobus C. Jansen and Dr. Leszek Góra for imparting the techniques in zeolite synthesis. For elemental analyses, my gratitude to Delia van Rij for doing ICP-OES and Mehmet Sarilar for doing INAA. Many thanks to Bart van der Linden for lending hand in the CRD and six-flow reactors. To Dr. ir. Emiel Hensen (TU/e), thanks for giving me the opportunity to use your dedicated benzene to phenol setup in Eindhoven. I am truly indebted to your kindness. Thanks also to Robert van

Teeffelen (TU/e) for the technical support. Dr. Sergey Nikitenko (ESRF) is appreciated for his time and help at the *dubble* station. Dr. Patricia Kooyman is gratefully acknowledged for acquiring the high-resolution TEM images, and for the time spent for fruitful scientific discussions. Thanks also for presenting our results to the 3rd FEZA conference.

I am thankful to former colleagues in the endangered Mössbauer group of TUDelft (and the Netherlands). To Adri van der Kraan, it has been a privilege to be my supervisor during the early stages of my PhD quest. To Menno Crajé, Anton Goossens, and Iulian Dugulan, thanks for your time and friendship. To all my colleagues and friends at IRI (lately Reactor Institute Delft), most especially to the people behind R^3, thank you for the memorable moments we had, and the laughter we shared together. I am truly grateful for your presence and for cultivating a healthy environment that is conducive to intellectual and social growth. Special mention is given to Marianne van Baaren; thanks a lot for the utmost administrative support, kindness and care, and for your sensitivity to our needs.

To my Filipino friends in the Netherlands, mostly the Filipino scholars in Delft (Rupert, Ram, Ric, Ruben, Patrick, Kadong, Jerry, Weng, Dang, and Mayang), thanks for sharing with me the joy and pain of being far and away. Many thanks to friends I met in the Netherlands, especially those who in some ways have contributed to my work (Arjen, Ben, Gijs, Mieke, Monica, Sander, Serdar, Peter, Piet, and Piotr). To my friends and classmates in college and high school, thanks for keeping in touch. Your often ludicrous emails somehow brighten up a dull day.

To *Mamá*, thank you very much for everything. For your love, sacrifice, generosity, and (physical, mental, moral, and spiritual) nourishment, I am sincerely indebted to you. To *inday* Ann, thank you for your support and prayers. To my relatives, especially to uncle Ben and mommy Bren, I am truly grateful for your thoughts and prayers. I also would like to express my appreciation to Eve's family, particularly to Abeth and Ricky for being there to take care of my love ones, and to Vangie for looking after Venise at Cebu International School. For all your selflessness, thank you!

To my beloved wife Eve and to our utterly adorable children, Venise and Nico, you are the wellspring of my inspiration. You bring real meaning and joy to my life. Words will never be enough to express how much I cherish You in my life. You are all the reasons I reach for my dreams, including this one. I am forever grateful for your gift of unconditional love and affection. You are truly manna from heaven.

Above all, I give thanks and praise to God almighty for all the blessings He has given me.
I am but an instrument; may this simple offering glorify Him.

Jerome

Delft, the Netherlands November 6, 2006

About the author

Jerome Bolabola Taboada was born in Cebu City, Philippines on December 19, 1974. He graduated high school from Don Bosco Technology Center, Cebu City, Philippines in 1992 with specializations in electro-mechanics and pneumatics. In that same year, he took up B. S. in Chemical Engineering at the University of San Carlos (USC), Cebu City, Philippines and graduated in 1997. During his university education, he was a recipient of USC's Presidential Award (1994) and Certificate of Merit (1995) for giving honor and recognition to the university with his accomplishments as member of the USC swimming varsity.

After acquiring his license as a professional chemical engineer, he joined the Department of Chemical Engineering at USC as staff member doing teaching and research work. In 1998, he received a scholarship grant from the University Fellowship Programme of Nuffic (Netherlands organization for international cooperation in higher education) to pursue graduate studies at Delft University of Technology (TUDelft) and completed his M. S. in Chemical Engineering in 2000. His master's thesis entitled 'Multi-component catalysts based on hydrotalcites for the decomposition of N_2O' was supervised by Prof. dr. J. Pérez-Ramírez and Prof. dr. F. Kapteijn. He also worked with Dr. ir. A.W. Gerritsen for a two-month course development in Chemical Reactor Engineering at DelftChemTech, Delft University of Technology in 2001, which was funded by the MHO-USC-DUT Project in Chemical Engineering.

In 2002, he left USC to start his PhD studies at the section Fundamental Aspects of Materials and Energy, Department of Radiation, Radionuclides & Reactors, Faculty of Applied Sciences, Delft University of Technology. His PhD project was the result of a collaboration of three departments at TUDelft supervised by Dr. A.R. Overweg, Dr. I.W.C.E. Arends, Dr. G. Mul, Prof. dr. G.J. Kearley, and (lately) Prof. dr. I.M. de Schepper. The significant results of his PhD research are described in this thesis. Most results have been published in refereed scientific journals and presented in both local (in the Netherlands) and international conferences.

Currently, he is working as a post-doctoral fellow at the section Catalysis Engineering, DelftChemTech, Delft University of Technology. His post-doctoral research is funded by the ASPECT (Advanced Sustainable Processes by Engaging Catalytic Technologies) programme of NWO (Netherlands Organization for Scientific Research) under the supervision of Dr. Guido Mul.

He is married to Evelyn Montajes Buque and the father of Venise Alexandria and Xavier Dominic.

November 6, 2006